LCH Laboratoire de Constructions Hydrauliques
Laboratory of Hydraulic Constructions

ÉCOLE POLYTECHNIQUE
FÉDÉRALE DE LAUSANNE

Communication 71

Hydro-morphological processes through permeable sediment traps at mountain rivers

Sebastian Schwindt

Editeur : Prof. Dr A. Schleiss

Lausanne, 2017

Communications du Laboratoire de Constructions Hydrauliques ISSN 1661-1179
Ecole Polytechnique Fédérale de Lausanne
Editeur: Prof. Dr A. Schleiss

Preface

In alpine regions villages are often situated near alluvial fans which are fed by mountain rivers transporting high sediment load during floods. In the past, these mountain rivers on the alluvial fans have often been channelized near urbanized areas, where the bed and banks were lined with large sawed granite or gneiss blocks laid into concrete layer. Some of these channels have still a mobile bed which is fixed with transversal sills against erosion. These channels have a high discharge and sediment transport capacity as long as no sediment deposits occur. The latter may be triggered by constrictions as they occur at bridges or by backwater effect when the channel enters the main river in the plain. In order to avoid sediment deposits in the channel, which can create dangerous overtopping with catastrophic consequences in the nearby urbanized areas, sediment traps have been installed upstream of the alluvial fans with the purpose to retain bed load during such critical floods. Practical experience with most of these sediment traps have shown that they retain already sediments for quite low and not yet dangerous floods. Thus, for such conditions the morphology of the river downstream becomes impoverished since traveling bed load creating gravel bars during frequent floods is missing. Furthermore, it has been observed in many cases that unwanted flushing of sediment traps occurred during the flood where they should safely retain sediments.

In his research Dr. Sebastian Schwindt developed a new concept of sediment traps which are permeable for bed load transport up to floods which are frequent and not yet dangerous for the downstream reach, but which retain safely sediment for hazardous floods. With systematic laboratory experiments it could be revealed that a guiding channel implemented across the deposition area upstream of the barrier, having a combination of mechanical and hydraulic control structures, provides a reliably working concept for permeable sediment traps. Combined mechanical-hydraulic control is achieved by an appropriate orifice or slot in the barrier which is equipped with an especially designed bar screen in front of it. Smaller bed load-laden discharges, which correspond to the bank-full discharge of the guiding channel, can pass unhindered through such combined barriers. For higher discharges, the hydraulic control at the orifice or slot provokes a backwater which reduces flow velocities in the upstream guiding channel, causing of the channel banks followed by bedload deposition. The latter, especially in the presence of large boulders, lead to a mechanical blocking of the bar screen which can then prevent unwanted sediment flushing with increasing filling of the deposition area.

As a basis for the new sediment trap concept, Dr. Schwindt could give design recommendations about the required bottom clearance of the bar screen and the spacing between the vertical bars, as well as the size of the orifice or slot in the barrier and the function of the guiding channel capacity.

We would like to thank the members of PhD committee Dr. Volker Weitbrecht from VAW-ETH Zürich, Switzerland; Prof. Alain Recking from IRSTEA Université Grenoble Alpes, France and Prof.

Stuart Lane from University of Lausanne, Switzerland. Finally, we also thank gratefully the Swiss Federal Office of Environment for their financial support under project “Sediment and habitat dynamics”.

Prof. Dr. Anton Schleiss and Dr. Mário Franca

That which exercises reason is more excellent than
that which does not exercise reason;

there is nothing more excellent than the universe,
therefore the universe exercises reason.

Zeno of Citium (334 BC - 262 BC)
quoted by Cicero: De Natura Deorum.

Acknowledgments

This research was funded by the Swiss Federal Office for the Environment within the Sediment and Habitat Dynamics project.

A huge word of gratitude goes to my supervisors Prof. Anton J. Schleiss and Mário J. Franca who accompanied patiently my research and guided me toward the right, target-oriented direction. I want to thank Giovanni De Cesare who was always available for sharing his vast knowledge with an appreciable bright smile on his face.

Special thanks goes to Guillaume Piton (Irstea Grenoble, France). The fruitful discussions with Guillaume and his enthusiasm were an incentive for me, more than once.

I would also like to thank Alain Recking (Irstea Grenoble, France), Marwan Hassan (University of British Columbia, Canada), Rui M. L. Ferreira (University of Lisbon, Portugal) and Markus Moser (die.wildbach, Austria) for sharing their expertise and discussing the analysis of the experiments. Further thanks goes to the Master students Aïdatou Sakho and Alessandro Reffo. Their contributions to the experimental work were a great support.

My marvelous LCH colleagues with all their colorful, diversified characters were a precious enrichment of everyday life – thank you all for the amazing time! This gratitude addresses equally and especially the many room-mates and friends who varicolored my life in Lausanne. I want to thank also my friends at home, in particular the Maître d'acier, and abroad for the good time, diversification and relativizing professional stress.

Beyond the professional work, my family, including Wolfgang, Michael and Bärbel, was a warm-hearted support which allowed me to relax and to get down from the intense work. My special gratitude goes to my mother, sister and grandparents who unconditionally supported me everywhere at any time. Particular thanks goes to my father for all the good time and discussions we had.

Besides the professional life, family and friends, the sage and bright presence of Adélaïde became the most important wind in my sails of life during the last four years. Every minute spent with Adélaïde gives me the safe feeling to be at the right place, at the right time. This perception is regularly reinforced by the affectionate reception of the Chopard family in the chilly French Doubs. Un grand merci.

Lausanne, July 2017 S. S.

Abstract

Sediment traps are used for the protection of urban settlements at rivers in mountainous regions. These structures aim at the retention of sediment in the case of hazardous floods, but existing sediment traps tend to retain sediment also when the discharge is not hazardous to the downstream urban regions. This excessive retention of sediment causes an interruption of the river continuum that may lead to channel incision and the morphological depletion of downstream reaches. Another problem is the remobilization of formerly deposited sediments during a flood, which is addressed in terms of the unwanted flushing of sediment traps. This research project aims at the development of sediment traps which are permeable up to a certain flood, but not susceptible to unwanted sediment flushing.

Typical sediment traps consist of a retention area upstream of a barrier or check dam equipped with openings. The barrier can trigger the retention of sediment in the deposition area either by hydraulic control or by mechanical control.

The hydraulic control leading to deposition is achieved by check dams with one or more openings constricting the flow vertically and/or laterally. Improved formulae for the estimation of the discharge capacity of such constrictions have been experimentally obtained for rough, turbulent upstream flow conditions with bed load under varying channel slopes. The constriction-induced head loss and reduction in the bed load transport capacity based on the bed shear stress are analyzed as a function of the upstream flow depth and discharge. The experiments show that the flushing of upstream sediment deposits may occur at open-crested slit check dams or close-crested slot check dams, but only when the latter are overtopped.

The mechanical control leading to sediment retention is achieved by screens with vertical bars. The horizontal space between the bars corresponds to the characteristic grain size of traveling bed load. The required bottom clearance under such screens was optimized here in view of the possibility of bed load transfer for small (flood) discharges on the one hand, and the ensured clogging of the screen for high (flood) discharges on the other hand. This optimum bottom clearance height was found to be 1.75 times the D_{84}, which represents the characteristic grain size that is transported during floods. Once the bar screen was clogged, the unwanted sediment flushing could not occur anymore. However, the clogging depends on the estimation of the characteristic grain size.

The experimental study shows that the combination of mechanical and hydraulic control structures provides a reliably working solution for permeable sediment traps. Smaller bed load-laden discharges can pass unhindered through such combined barriers. For higher discharges, the hydraulic control causes backwater which reduces the influence of the characteristic grain size on the clogging of the bar screen. Moreover, the bar screen prevents unwanted sediment flushing through the hydraulic control.

The implementation of a guiding channel across the retention area is introduced and was exper-

imentally verified as being a pertinent structural tool for improving the eco-morphological flow continuum.
Finally, the design of a permeable sediment trap is described based on an optimal interaction between a guiding channel and a barrier combining the mechanical control by a bar screen and hydraulic control by a slot check dam.

Keywords: *Bed load, Check dams, Flood protection, Hazard mitigation, Morphodynamics, Mountain rivers, Sediment control structures, Sediment retention, Sediment transport, Sediment traps.*

Résumé

Les pièges à graviers sont utilisés pour la protection des zones urbaines situées à proximité de rivières dans des régions montagneuses. Ces structures visent à retenir les sédiments en cas de crues dangereuses. Néanmoins, les pièges à graviers existants ont tendance à conserver les sédiments également lorsque le débit n'est pas dangereux pour les régions urbaines en aval. Cette rétention excessive de sédiments provoque une interruption de la continuité de la rivière, qui peut mener à une incision des lits et à une précarisation morphologique en aval. De plus, ces installations présentent le risque de s'auto-curer de manière indésirable pendant les crues. Ce projet de recherche vise le développement de pièges à graviers qui soient perméables jusqu'à ce qu'un certain débit soit franchi, tout en limitant le risque de purges indésirables.

Les pièges à graviers typiques sont constitués d'une zone de dépôt en amont d'un barrage filtrant équipé d'ouvertures. Le barrage filtrant peut déclencher la rétention des sédiments dans la zone de dépôt, soit par un contrôle hydraulique, soit par un contrôle mécanique.

Le contrôle hydraulique menant au remblaiement des sédiments est obtenu par des barrages filtrants avec une ou plusieurs ouvertures contractant le débit verticalement et/ou latéralement. Des formules corrigées pour l'estimation de la capacité de débit de ces contractions ont été obtenues expérimentalement pour des conditions d'écoulement turbulentes en amont avec charriage et en considérant des pentes de lit variables. La perte de charge entraînée par la contraction et la réduction de la capacité de transporter des sédiments par charriage, selon la contrainte de cisaillement, sont analysées en fonction de la profondeur d'eau en amont et du débit. Les expériences montrent que la purge des dépôts de sédiments dans la zone de dépôt peut se produire à travers des barrages à fentes ouvertes ou des barrages filtrants à crêtes fermées, mais seulement lorsque la section de déversement du barrage est active.

Le contrôle mécanique menant au remblaiement des sédiments est obtenu par des grilles avec barreaux verticaux. L'écart horizontal entre les barreaux correspond au diamètre caractéristique du charriage. L'écart vertical entre le lit et la pointe inférieure des barreaux a été optimisé au niveau de la possibilité du transfert du charriage des petits débits (de crue) d'une part, et le blocage définitif de la grille pour les débits (de crue) élevés d'autre part. Cet écart vertical optimal a été trouvé par 1,75 fois le D_{84}, qui représente le diamètre caractéristique du charriage pendant les crues. Lorsque la grille est obstruée mécaniquement, la purge des sédiments indésirables ne peut plus se produire. Cependant, l'obstruction dépend de l'estimation du diamètre des grains caractéristiques charriés pendant les crues.

L'étude expérimentale montre que la combinaison de structures de contrôle mécaniques et hydrauliques représente une solution fiable pour des pièges à graviers perméables. Des petites crues avec charriage peuvent traverser ces structures combinées sans entrave. Pour des débits de crues plus élevés, le contrôle hydraulique provoque un remous, ce qui réduit l'importance du diamètre

caractéristique des grains pour l'obstruction de la grille. De plus, la grille empêche les purges des sédiments indésirables à travers du contrôle hydraulique.
Un chenal de direction a été mis en place dans la zone de dépôt. Les expériences ont prouvé que le chenal était un outil pertinent pour améliorer la continuité éco-morphologique de la rivière.
En fin de compte, la conception d'un piège à graviers perméable est décrite en fonction d'une interaction optimale entre un chenal de direction et un barrage filtrant combinant le contrôle mécanique, par une grille à barreaux verticaux, et un contrôle hydraulique par un barrage filtrant avec un seul orifice et crête fermée.

Mots clefs : *Structures de contrôle des sédiments, Barrages filtrants, Charriage, Transport solide, Rétention des sédiments, Canaux raides, Pièges à graviers.*

Zusammenfassung

Geschiebesammler werden zum Schutz von Siedlungen vor Wildbachgefahren in Gebirgsregionen eingesetzt. Diese Strukturen zielen auf den Geschieberückhalt bei grossen Hochwassern ab. Bestehende Geschiebesammler neigen jedoch dazu, auch dann Geschiebe zurückzuhalten, wenn keine Gefahrensituation besteht. Dies führt zu übermässigem Geschieberückhalt und verursacht die Unterbrechung des natürlichen Fliesskontinuums. Der entstehende Geschiebemangel kann im Unterlauf zu Gerinneeintiefungen und morphologischer Verarmung führen. Ein weiteres Problem bestehender Geschiebesammler sind unerwünschte selbsttätige Entleerungen während Hochwassern. Dieses Forschungsprojekt bezweckt die Entwicklung von Geschiebesammlern, die für kleine, ungefährliche Hochwasser durchgängig sind und gleichzeitig Geschiebe sicher zurückhalten bei grossen Hochwassern.

Klassische Geschiebesammler bestehen aus einem Rückhalteraum und einem offenen Abschlussbauwerk. Das Abschlussbauwerk kann den Geschieberückhalt im Rückhalteraum entweder hydraulisch oder mechanisch bedingt auslösen.

Der hydraulisch bedingte Geschieberückhalt wird durch Wildbachsperren mit einer oder mehreren Öffnungen erreicht, die den Abfluss vertikal und / oder seitlich einschnüren. Formeln für die Abschätzung der Abflusskapazität solcher Öffnungen wurden hier experimentell verbessert, hinsichtlich rauen und turbulenten Abflusses mit Geschiebe. Zusätzlich wurden variierende Gerinneneigungen betrachtet. Die einschnürungsbedingten Energieverluste und die Verringerung der Geschiebetransportkapazität wurden in Funktion der Abflussbedingungen des Oberlaufs bestimmt. Die Versuche zeigen, dass selbsttätige Entleerungen durch Abschlussbauwerke mit einem Schlitz (offene Krone des Abschlussbauwerks) oder einer Dole (geschlossene Krone des Abschlussbauwerks) auftreten können. Die selbsttätige Entleerung durch Dolen wurde jedoch nur beobachtet, wenn das Abschlussbauwerk gleichzeitig überströmt wurde.

Der mechanisch bedingte Geschieberückhalt wurde hier durch einen Stabrechen mit einer Grundöffnung erreicht. Der horizontale Abstand zwischen den Stäben entspricht der charakteristischen Korngröße D_{84} des mobilen Geschiebes. Die erforderliche Höhe der Grundöffnung unter dem Stabrechen wurde optimiert bezüglich der Geschiebedurchgängigkeit während kleiner Hochwasser einerseits und des sicheren Verlegens des Rechens bei grossen Hochwassern andererseits. Diese optimale Höhe der Grundöffnung entspricht dem 1,75-fachen des D_{84} des mobilen Geschiebes. Sobald der Stabrechen verlegt war, wurden selbsttätige Entleerungen nicht mehr beobachtet. Die Verlegung des Rechens hängt in der Praxis jedoch stark vom Schätzwert des D_{84} ab.

Die Experimente zeigen, dass eine Kombination eines vorgeschalteten Stabrechens für den mechanisch bedingten Rückhalt und einer Dolensperre für den hydraulisch bedingten Rückhalt eine zuverlässig funktionierende Lösung für teildurchgängige Abschlussbauwerke bietet. Abflüsse mit geringerer Geschiebeintensität können solche kombinierten Barrieren ungehindert passieren. Bei

höheren Geschiebefrachten bewirkt das hydraulische Kontrollorgan einen Rückstau, in dem sich die Verlegungssensibilität des Stabrechens bezüglich des D_{84} verringert. Im Gegenzug verhindert der Stabrechen unerwünschte selbsttätige Entleerungen durch die Dole.
Die Implementierung eines Leitgerinnes im Rückhalteraum wurde als zusätzliche Verbesserungsmassnahme für die Geschiebedurchgängigkeit experimentell getestet. Es zeigte sich, dass ein solches Leitgerinne eine sinnvolle Massnahme darstellt, um die Kontinuität des Geschiebetransports zu verbessern.
Abschliessend wurde ein ganzheitliches Konzept für teildurchgängige Geschiebesammler experimentell überprüft. Das Konzept beruht auf dem zuvor eingeführten Leitgerinne im Rückhalteraum und mit einem kombinierten Abschlussbauwerk, bestehend aus einem vorgeschalteten Stabrechen mit anschliessender Dolensperre.

Stichwörter: *Geschiebe, Wildbachsperren, Hochwasserschutz, Gefahrenprävention, Auendynamik, Wildbäche, Sedimentkontrollstrukturen, Sedimentrückhalt, Sedimenttransport, Geschiebesammler.*

Contents

List of Figures

List of Tables

Notation

Roman letters

Letter	Unit	Description
A	m^2	flow cross section
a	m	constriction height
a_*	–	relative constriction height
a_{*cr}	–	relative constriction height (critical flow conditions)
a_{*D}	–	grain-related relative constriction height
a_i	m	clearance height between individual elements
B	m	total barrier width
b	m	constriction width
b_*	–	relative constriction width
b_{*cr}	–	relative constriction width (critical flow conditions)
b_{*D}	–	grain related relative constriction width
b_i	m	clearance width between individual elements
C	$m^{1/2}\ s^{-1}$	Chézy flow resistance coefficient
c_c	–	coefficient of curvature (sediment grain size distribution)
c_u	–	coefficient of uniformity (sediment grain size distribution)
c_K	–	coefficient of discharge according to Kindsvater et al. (1953)
c_{KQ}	–	adapted coefficient of discharge
c'_{KQ}	–	slope corrected, adapted coefficient of discharge
c_Q	–	correction factor for discharge capacity of later flow constrictions
D	m	grain diameter
D_m	m	mean grain diameter of the sediment mixture
D_{max}	m	diameter of the largest grain of the sediment mixture
D_{pq}	m	grain diameter of which pq % of the mixture are finer
D_w	m	characteristic diameter of driftwood
E	m	total energy per unit force
Err_Q	–	error in discharge capacity calculation
F_*	–	grain-related flow velocity
Fr	–	Froude number
Fr_0	–	Froude number upstream of flow constriction
$f()$	var.	function of quantities
f_c	–	empirical factor for the drawdown length

f_f	–	Darcy-Weisbach friction factor
f_m	–	factor for clearance under mechanical barrier
g	m s^{-2}	gravitational acceleration
H	m	energy head
h	m	flow depth
h_*	–	relative upstream flow depth
h_{*cr}	–	relative upstream flow depth referring to critical flow conditions
h_{*D}	–	grain-related relative upstream flow depth
h_0	m	flow depth upstream of flow constrictions
h_1	m	flow depth downstream of flow constrictions
h_c	m	flow depth, constricted channel
h_{cr}	m	critical flow depth
h_{nc}	m	flow depth, non-constricted channel
k_{st}	m$^{1/3}$ s^{-1}	Strickler roughness coefficient
L_{dep}	m	deposit length
L_{fish}	m	length of fish
L_w	m	backwater drawdown length
m	–	channel bank slope
m_{bar}	–	bar inclination of vertical racks
n	m$^{-1/3}$ s	Manning's roughness coefficient
P	m	wetted perimeter
$p1/p2/p3$	–	coefficients of regression curves
Q	m^3 s^{-1}	water discharge
Q_*	–	discharge relative to bank-full channel capacity
Q_{30}	m^3 s^{-1}	discharge that is not exceeded over 30 days per year
Q_{330}	m^3 s^{-1}	discharge that is not exceeded over 330 days per year
Q_c	m^3 s^{-1}	discharge capacity of openings
q	m^2 s^{-1}	unitary water discharge
Q_b	kg s^{-1}	bed load transport capacity
Q_{b*cr}	kg s^{-1}	dimensionless bed load transport capacity (critical flow conditions)
$Q_{b,i}$	kg s^{-1}	bed load supply rate
$Q_{b,o}$	kg s^{-1}	bed load outflow rate
q_b	kg s^{-1} m^{-1}	unitary bed load transport capacity
Q_{bf}	m^3 s^{-1}	bank-full discharge
Q_c	m^3 s^{-1}	water discharge capacity of flow constrictions
R^2	–	coefficient of determination
Re	–	Reynolds number
Re_*	–	particle Reynolds number
R_h	m	hydraulic radius
S_0	–	channel slope
S_{dep}	–	deposit slope
S_e	–	energy slope
S_{eq}	–	equilibrium bed slope
S_f	–	deposit front slope

s	–	ratio of sediment grain and water density
t	s	time, duration
t_+	s	duration of rising hydrograph limb
t_-	s	duration of falling hydrograph limb
t_*	–	duration, relative to the rising hydrograph limb
u	m s^{-1}	cross-section-averaged flow velocity
u_{max}	m s^{-1}	maximum admissible flow velocity in the guiding channel
V_*	%	percentaged deposit volume, relative to hydrograph supply
V_{dep}	m^3	volume of sediment deposits
V_Σ	m^3	sediment supply volume during hydrograph
We	–	Weber number
w	m	channel bottom width
w_m	m	mean flow width
X_*	–	dimensionless streamwise coordinate
X_{data}	var.	generic data
x	m	streamwise coordinate, pointing in the upstream direction
Y_*	–	dimensionless spanwise coordinate
Y_{data}	var.	generic data, derived from X_{data}
y	m	spanwise coordinate, pointing toward the right bank
Z_*	–	relative deposit height (dimensionless vertical coordinate)
z	m	vertical coordinate, pointing against gravity acceleration vector
ΔE	m	head loss
Δx	m	horizontal distance between flow cross sections
Δz	m	difference in height
Δz_{dam}	m	barrier / dam height
Δz_{dep}	m	maximum deposit height along the channel axis

Greek letters

Letter	Unit	Description
α	–	first test run
β	–	second test run (repetitive, redundant)
Δ	var.	difference of quantities
ϵ	var.	error values
ϵ_V	%	percentaged error of the volume measurements
η	–	critical bed shear stress reduction
μ_f	–	discharge coefficient for free-surface-flow-orifices
μ_p	–	discharge coefficient for pressurized orifices
ν	m^2 s^{-1}	kinematic viscosity
Φ	–	bed load transport intensity
Φ_i	–	bed load supply intensity
Φ_o	–	bed load outflow intensity
Φ_{mpm}	–	bed load transport intensity according to Meyer-Peter and Müller (1948)

$\Phi_{\text{mpm,c}}$	–	corrected bed load transport intensity (Wong and Parker, 2006)
Φ_{sj}	–	bed load transport intensity according to Smart (1984)
Φ_{ric}	–	bed load transport intensity according to Rickenmann (1991)
ϕ_{u}	deg	angle of repose of undrained cohesionless grains
ρ_f	kg m^{-3}	water density
ρ_s	kg m^{-3}	sediment grain density
ρ'_s	kg m^{-3}	sediment deposit density
σ	N m^{-1}	surface tension (tensile force per unit length)
τ	N m^{-2}	bed shear stress
τ_*	–	dimensionless bed shear stress
τ_{*b}	–	sidewall corrected dimensionless bed shear stress
τ_{*cr}	–	critical dimensionless bed shear stress (Shields parameter)
$\tau_{*,m}$	–	site-specific grain mobility parameter
θ	–	relative reduction of the bed load transport capacity
ζ_c	–	constriction loss coefficient

Acronyms, abbreviations and subscripts

Chpt	Chapter
Eawag	Federal Institute of Aquatic Science and Technology
EPFL	École polytechnique fédérale de Lausanne
ETHZ	Swiss Federal Institute of Technology in Zürich
FOEN	Federal Office for the Environment (Switzerland)
Hy	Hydraulic
LCH	Laboratory of Hydraulic Constructions of EPFL
Mec	Mechanical
no	non-overflown
o	overflown
VAW	Laboratory of Hydraulics, Hydrology and Glaciology of ETHZ
WSL	Federal Institute for Forest, Snow and Landscape research

1 Introduction

1.1 Context

Sediment traps on mountain rivers are protection measures with the purpose to retain solid material that potentially represents a threat to downstream urban areas. The bed load transport capacity of channelized downstream river sections may be reduced at bridges or due to shallower channel slopes. During floods, mountain rivers can transport important amounts of sediment and driftwood. This transported matter can deposit or entangle in urban areas with reduced transport capacity, with the consequence of dangerous flooding. Therefore, sediment traps are built upstream of urban areas to retain debris or sediment that can potentially cause flooding in downstream reaches (Fig. 1.1). These flood protection measures consist typically of a reservoir or deposition area with a downstream torrential barrier equipped with openings (Armanini and Larcher, 2001). This concept for sediment traps has been applied at mountain rivers for centuries (Piton et al., 2016), but two basic problems have often been observed: (1) sediment traps retain too much sediment or (2) sediment traps retain sediment insufficiently. The excessive retention of sediment already during ordinary, non-hazardous floods interrupts the solid transport continuity with negative effects on

Figure 1.1 – *A typical sediment trap with torrential barrier (left) for flow control, with upstream deposition area (Jenbach, Germany). © S. Schwindt.*

the downstream river eco-morphology and causes the need for dredging works in the deposition area. Such disturbances of the sediment transport involve an interruption of the supply of minerals which are also an important source of life for biota in downstream alluvial zones (e.g., Everett and Ruiz, 1993; Johnson et al., 2005). Moreover, the retained sediment is missing in the downstream river reaches, where the river bed and banks can be consequently endangered by erosion (Kondolf, 1997b; Brandt, 2000; Schleiss et al., 2014).
The insufficient retention of sediment, i.e., a bad functioning of the sediment trap, can even generate hazards due to self-emptying, i.e., unwanted flushing of former sediment deposits in the deposition area (Bergmeister et al., 2009; Sodnik et al., 2015). Such failure events have been reported, e.g., at the Schächen Torrent in Switzerland or at the Schnannerbach Torrent in Austria during a major flood event in 2005 (Hübl et al., 2006; Bezzola, 2008). The minimization of the dimensions of openings in torrential barriers reduces the risk of unwanted sediment flushing and increases sediment retention. However, too small openings lead again to excessive sediment retention with negative effects on the eco-morphological variety of downstream river reaches and the need for reservoir dredging.

1.2 Research objectives

The poor environmental status of many rivers in Switzerland called for adaptations of the legal framework (Swiss Confederation, 1991). In this context, the Swiss Federal Office for the Environment (FOEN) launched the research program *River Basin Management* (Hostmann, 2005; Schleiss et al., 2008). Within this research program, the focus of the 2013–2017 phase was on the problematic of *Sediment and Habitat Dynamics* (Schleiss et al., 2014). The accordingly named Sediment and Habitat Dynamics project links environmental sciences and river engineering issues, with contributions from four leading Swiss research institutions, notably the Federal Institute of Aquatic Science and Technology (Eawag), the Federal Institute for Forest, Snow and Landscape research (WSL), the Laboratory of Hydraulics, Hydrology and Glaciology (VAW) of the Swiss Federal Institute of Technology in Zurich (ETHZ) and the Laboratory of Hydraulic Constructions (LCH) of the École polytechnique fédérale de Lausanne (EPFL). The fundamental research in the framework of the Sediment and Habitat Dynamics project has the goal to establish guidelines for eco-morphologically sustainable river training works. An essential criterion for such river training works is the undisturbed, continuous sediment transfer across hydraulic structures. In this context, the review and improvement of contemporary concepts for the design of sediment traps is crucial, as many sediment traps currently work insufficiently, i.e., the traps are either idle or retain too much sediment. The retention of bed load by sediment traps was previously studied with respect to morphological implications, already at the beginning of the 20th century and between the 1960s and the 1980s (e.g., Wang, 1901, 1903; Hampel, 1968; Kronfellner-Krauss, 1972; Leys, 1976; Zollinger, 1983). Following a period with only a few scientific studies on the topic, the research on the hydraulic behavior of torrential barriers became more important after 2000, which is reflected in several substantial contributions (e.g., Frey and Tannou, 2000; Armanini and Larcher, 2001; Wehrmann et al., 2006; Osanai et al., 2010; Conesa Garcia and Lenzi, 2011). The current knowledge on working principles and design criteria for sediment trapping using torrential barriers were summarized exhaustively in Piton and Recking (2016a,b). However, research gaps persist in the essential knowledge about the artificial sediment deposition control due to hydraulic constrictions imposed by torrential barriers.

Furthermore, systematic studies of innovative concepts for sediment traps with low impact on the eco-morphological river continuum are missing.
This research study intends to fill these gaps by a systematic analysis of concepts for sediment traps that are only permeable up to small, morphologically effective floods and fail-safe in the case of exceptional, hazardous floods. A particular research question is the design of openings in torrential barriers and their effects on the bed load transport. The working principles of such barriers must be distinguished between the mechanically and the hydraulically controlled sediment deposition. The triggering of sediment deposition due to mechanical control was analyzed in previous studies. The hydraulic sediment deposition control can be achieved by barriers with an opening that represents a flow constriction. The effect of such flow constrictions on the bed load transport is part of this study which addresses the following research questions:

1. How do openings in barriers affect the bed load transport capacity of rough and steep streams?
2. What effects has the channel slope on the bed load transport capacity upstream of such permeable barriers?
3. How can flow barriers be designed for transferring fluvial bed load during small non-hazardous floods and retaining fluvial bed load reliably during hazardous floods?
4. How can sediment traps, including deposition areas, be improved to promote bed load transport during small non-hazardous floods and to reduce maintenance works?

The research questions 1 and 2 contribute to the understanding of the hydraulic sediment deposition control. These findings are essential for answering the research questions 3 and 4.

1.3 Report structure

The research report is divided into 9 interconnected chapters which refer to the elements of sediment traps in a geomorphological framework as illustrated in Fig. 1.2.

Chapter 2 represents a review on fluvial morphology, including the hydraulic and fluvial solid transport processes in mountain rivers. The relevant natural hazards and corresponding mitigation measures are summarized. The existing literature about sediment traps, as part of alpine flood protection measures, is analyzed in detail. This literature review allows to define the detailed research needs at the end of Chapter 2.
Chapter 3 describes the experimental set-up with technical explanations of the water and sediment supply, as well as measuring devices. The experimental set-up was adapted in the following chapters with respect to the considered research questions. The set-up adaptations are separately explained in the particular chapters.
Chapter 4 contains an analysis of the hydraulics of torrential barriers in the shape of flow constrictions, which affect the upstream bed load transport capacity.
Chapter 5 analyzes the hydraulic behavior of flow constrictions and related effects on the bed load transport capacity with respect to changing channel slopes.
Chapter 6 serves for the study of the problematic of the control (triggering) of sediment deposition when hazardous floods occur. This is achieved using barriers with an opening and measures against

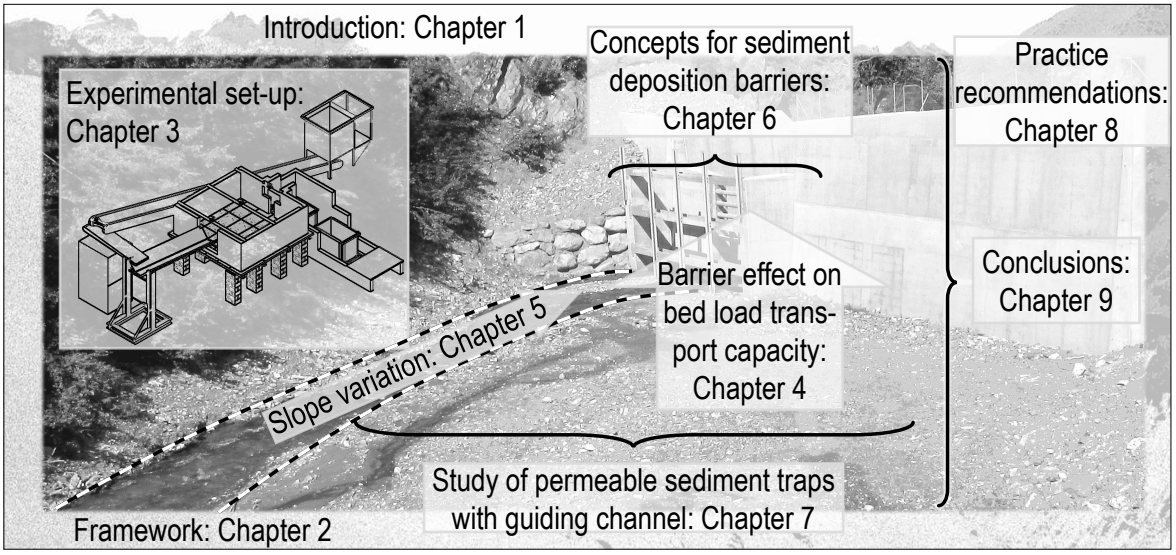

Figure 1.2 – *A representative view of the report structure (background: sediment trap upstream of Riddes, Switzerland).*

the unwanted flushing of the deposition area by combining hydraulic and mechanical controls. The study of such flow barriers with combined control is extended in Chapter 7 by the additional consideration of an upstream deposition area with an artificial guiding channel.
Chapter 7 introduces the guiding channel to enable the sediment transfer up to flood discharges that are non-hazardous. In this context, sediment deposition patterns and volumes, as well as flushing of the deposition area equipped with the guiding channel are studied using a standardized hydrograph. In addition, eco-morphologically important aspects of rivers are considered in view of the design of sediment traps.
Chapter 8 includes practical recommendations for the design of permeable sediment traps with a guiding channel.
Chapter 9 states the main conclusions and requirements for future research.
Supplementary data tables that are not shown in the main document, such as input data for the design of the experimental set-up or additional graphs and pictures, are enclosed in the Appendix.

2 State-of-the-art

2.1 Geomorphological framework

2.1.1 Terrain descriptions

Mountain rivers are by definition rivers located in steep terrains and have generally channel gradients of more than 0.2 % (Jarrett, 1992; Wohl, 2000). The morphology of such streams can be influenced by torrential barriers, defined as transverse structures across mountain rivers (DIN 19663-1985:6), 1985). Such torrential barriers may affect the sediment transport, leading to sediment retention upstream and channel erosion downstream (Brandt, 2000; Conesa Garcia and Lenzi, 2011; Castillo et al., 2014; Norman and Niraula, 2016; Piton and Recking, 2016c). Therefore, the study and implementation of torrential barriers requires a holistic assessment of the geomorphological environment of mountain rivers.
The morphological classification of mountain rivers depends on the application field and requires the consideration of different spatial and temporal scales (Kondolf, 1995; Montgomery, 1999; Hassan et al., 2008). Torrential barriers represent local anthropogenic morphological controls on small temporal and catchment scales. These anthropogenic interventions on the small scales may also have implications for larger spatial and temporal scales, i.e., the long-term landscape evolution (Lane and Richards, 1997). The (scale-related) processes which are relevant to this research are subsequently outlined, coming from the larger, general to small-scale aspects.
The catchment area of mountain rivers are characterized by steep slopes with high, intermittent sediment production (Leopold et al., 2012). The discharge from the catchment area passes subsequently in typical steep canyon stretches which open finally into an alluvial fan (Wang, 1901; Parker et al., 1998; Romang, 2004; Bergmeister et al., 2009). Fig. 2.1 illustrates a typical geomorphological environment of mountain rivers. Moreover, hazard mitigation structures are represented in the shape of:

① Solid barriers for terrain consolidation;
② Net or lattice barriers for the stabilization of hill slopes;
③ Sectional barriers for the energy dissipation of debris flow;
④ Sediment traps with permeable, open barrier; and
⑤ Lateral deviation structures.

The types of barriers and their functioning are introduced subsequently in Chpt. 2.6.2 (page 22 ff.).

2.1.2 Morphological features of mountain rivers

The intermittent convexity and concavities of mountainous terrains are the result of surface erosion and deposition processes, respectively (Yamada, 1999). The alluvial fan has a smoother slope than the headwaters and is sometimes populated or crossed by infrastructures (Wang, 1903; Bull, 1977). The balance between sediment supply from headwaters and the capacity of the flow to transport sediment plays a key role for the morphological pattern of downstream reaches (Dietrich et al., 1989; Powell, 1998; Wohl, 2000).
Low sediment supply and high transport capacity lead to “threshold” or “stable” channel reaches with limited exchange between the traveling sediment and the channel boundaries. Their shape is governed by the discharge, longitudinal channel slope and the median grain size of the bed material (Howard, 1980; Ikeda et al., 1988). The channel bed is characterized by structured, armored surfaces in “underloose” conditions (Church, 1977; Hassan et al., 2008).
High sediment supply may lead to the development of “alluvial” streams with high exchange rates between the transported sediment and the boundary material. The channel width, slope and cross section geometry respond directly to changes in discharge and sediment supply (Wolman and Miller, 1960). Alluvial channel beds consist of “overloose” packed sediments (Church, 1977).
The spatial and temporal variability of discharge and sediment supply causes transitions between non-alluvial and alluvial stream types (Hassan and Zimmermann, 2012). Non-alluvial streams can turn into alluvial streams in downstream reaches or with increasing discharge (Copeland et al., 2001).
Rivers are constantly responding to the varying hydraulics and sediment supply. Therefore, many rivers are globally in a semi-alluvial or “colluvial” state with punctual sediment storages in the bed or sources along the channel. In such colluvial channels, the punctually supplied, alluvial pulses are transported in the downstream direction (Recking, 2009; Ferguson, 2012; Hassan et al., 2014). The local sediment supply can also be influenced by driftwood-induced log-jams. These wood accumulations, i.e., driftwood logs, decrease punctually the channel slope, thus, causing local deposits upstream and scour downstream of the logs (Hogan et al., 1998; Buffington and Montgomery, 1999).
Moreover, the displacement of sediment entails longitudinal and vertical grain sorting (Blom and Parker, 2004; Hassan, 2005; Blom et al., 2006). A refinement of the bed material can be routed with increasing distance from the source and decreasing channel slope due to cumulative effects from local sorting and changing hydraulics (Lane, 1955; Deigaard and Fredsøe, 1978; Knighton, 1980; Powell, 1998). Local, vertical grain sorting is differentiated between static and kinetic sorting (Bacchi et al., 2014). Static sorting results from spontaneous percolation of finer particles in void spheres of the soil (Bridgwater et al., 1969). Simple criteria for the probability of spontaneous percolation were established for uniform spheres, but in mountain rivers, variably large and non-uniform grains cause higher complexity (Beschta and Jackson, 1979; Troadec and Dodds, 1993; Luchnikov et al., 1999; Gibson et al., 2009, 2010). This static sorting generates stratified, poorly mobile bed armoring (Pitlick et al., 2008; Bacchi et al., 2014). Kinetic sorting (also: sieving) produces periodical armoring with a quasi-static layer beneath the active transport layer. If the supply of fine sediment is inferior to the transport capacity and both spontaneous percolation and kinetic sorting co-occur,

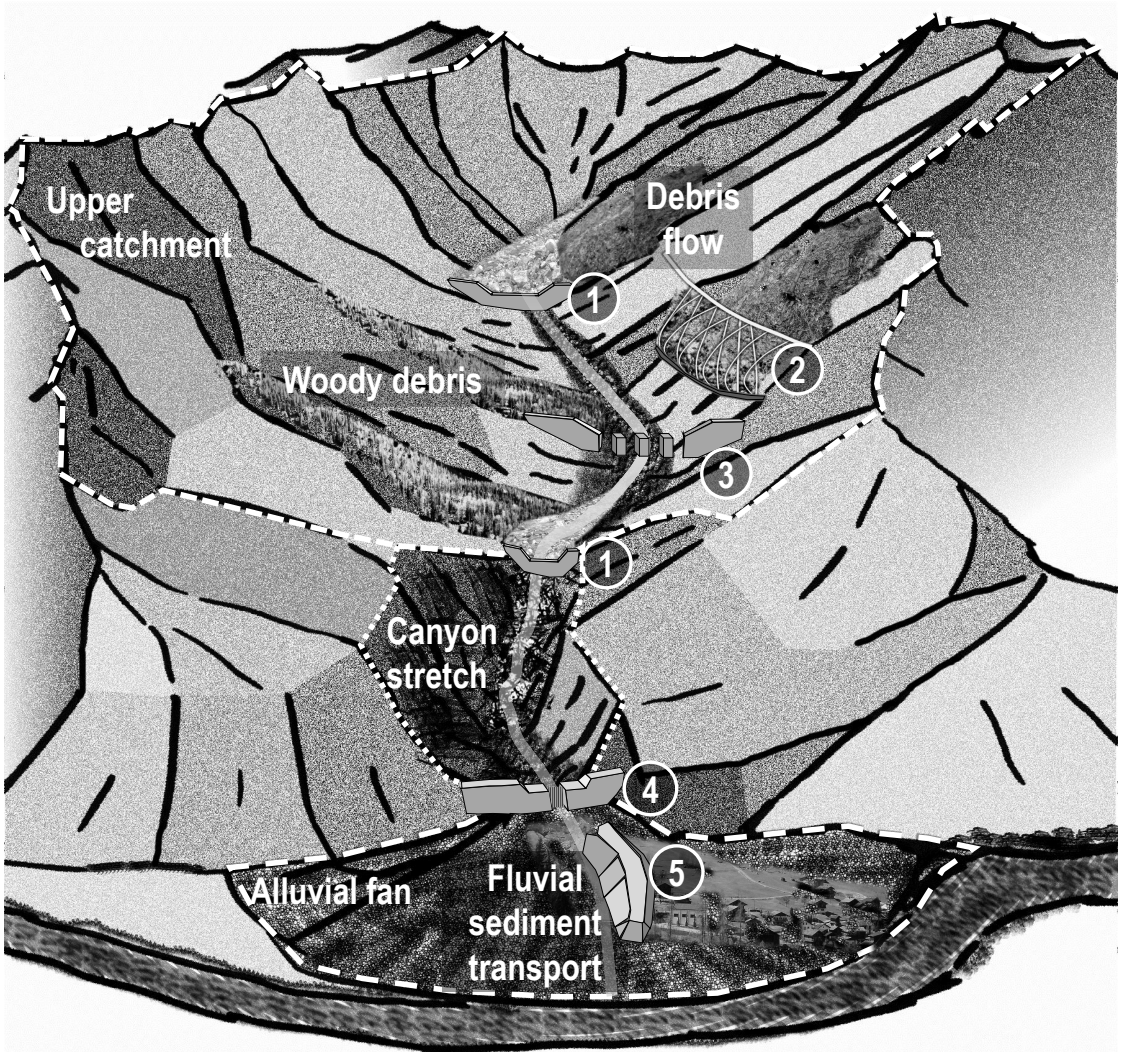

Figure 2.1 – *The typical geomorphological environment of mountain rivers with steep catchments, hill terraces and alluvial fan in the valley where urban structures may be situated. The structural elements for hazard mitigation introduced in Chpt. 2.6.2) are indicated: ① closed barriers (sills); ② net / lattice barrier; ③ sectional barrier; ④ sediment trap with partially open barrier; and ⑤ lateral deviation structure.*

the total sediment transport increases, leading to channel degradation. If the fine sediment supply exceeds the transport capacity or spontaneous percolation is geometrically not possible, channel aggradation occurs, which leads to an increase in the channel slope (Dudill et al., 2016).

2.1.3 Stream types and characteristics

The interplay between river morphology and sediment transport is also linked to natural hazards and ecological aspects (Pitlick and Van Steeter, 1998; Arnaud-Fassetta et al., 2009; Maynard et al., 2012; Church and Ferguson, 2015). Therefore, every intervention in a river system requires an assessment of the morphological river state to identify governing processes and sensitive planning criteria (USACE, 1997). The differentiation between the following channel types is essential for the design of structural interventions in mountain rivers (Montgomery and Buffington, 1997; Bisson et al., 2007; Recking et al., 2016):

- **Colluvial** - Ephemeral streams situated at the tip of headwaters and directly supplied by loose unpacked (colluvial) material from neighboring hill slopes (Dietrich et al., 1982).
- **Cascade** - Individual chutes over boulder clast, confined by the valley slopes.
- **Bedrock** - Non-alluvial channels with some sediment-filled pockets and generally confined by the valley walls (Montgomery et al., 1996).
- **Step-pool** - Elevation drops over discrete steps stretching over the river width and strong confinement by the valley (Whittaker and Jaeggi, 1982; Molnar et al., 2010).
- **Plane-bed** - Irregular bedforms with distant, varying confinement, often in transition between transport capacity and limited sediment supply.
- **Braided streams** - Subdivided streams, characterized by bars and islands; sediment transport requires the differentiation between individual sub-streams (Dey, 2014).
- **Riffle-pool** - Channel beds characterized by alternating sequences of bars, pools and riffles (Leopold et al., 2012).

The stream types can be associated with sediment supply conditions, dominating transport processes and roughness elements, as well as morphological characteristics according to Tab. 2.1, with the representation of typical streams in Fig. 2.2.
In addition, woody debris obstructions cause local pool formations which lead to the development of naturally “forced reaches” with effects on sediment transport (Buffington et al., 2002; Bisson et al., 2007). Further channel types related to finer sediment and smoother slopes can be observed farther downstream, beyond the study field of this research.
Every anthropogenic intervention can cause changes of the upstream and downstream stream morphology which should be assessed to avoid negative ecological implications (Williams and Wolman, 1984; Wohl, 2000; Bernhardt et al., 2005; Schleiss et al., 2014).

Table 2.1 – *Channel types with morphological characteristic and relevant features for sediment transport in intermittent to steep-sloped rivers, adapted from Montgomery and Buffington (1997) and Bisson et al. (2007), with consideration of complementary data (Lisle, 1982; Sawada et al., 1983; Abrahams et al., 1995; Buffington et al., 2003; Molnar et al., 2010; Dey, 2014; Hassan et al., 2014; Recking et al., 2016).*

Zone (typical, cf. Fig. 2.1)	CATCH-MENT	CATCHMENT / CANYON			CANYON	ALLUVIAL FAN	
Type	Colluvial	Cascade	Bedrock	Step-pool	Plane-bed	Braided	Riffle-pool
Transport limiting factor	Trans-port capacity	Sedi-ment supply	Sedi-ment supply	Sedi-ment supply	Transi-tional	Trans-port capacity	Trans-port capacity
Dominant transport process	Debris flow	Debris flow & fluvial	Debris flow	Fluvial & debris flow	Fluvial & debris flow	Fluvial & debris flow	Fluvial
Frequency of morphologi-cal event	<annual	50-100 yrs	unde-fined	30-80 yrs	1-2 yrs	1-2 yrs	<annual
Slope	>20 %	4-25 %	variable	2-8 %	1.5-4 %	<3 %	0.1-2 %
Bed material	Loose, unconsoli-dated	Boulders	Rock out-crops	Cobbles, boulders	Gravel, cobbles	Cobbles, boulders, gravel, sand	Gravel
Sediment storage & sources	Hill-slopes, bed	Accumula-tions at flow obstruc-tions	Hill-slopes, pockets	Bed-forms, hill slopes	Channel banks	Channel banks, bed-forms	Channel banks
Dominant roughness elements	Grains	Grains, banks	Bed, banks	Bed-forms, banks, grains	Grains, banks	Bed-forms (pools), boulders, cobbles	Bed-forms (sinuos-ity), banks, grains
Channel armoring	None	None	Rock	Locally varying	Variable	Little	Variable
Confinement	Terrain	Valley	Valley walls	Moder-ate, valley	Variable	Variable	Little
Reference in Fig. 2.2	a)	b)	c)	d)	e)	g)	f)

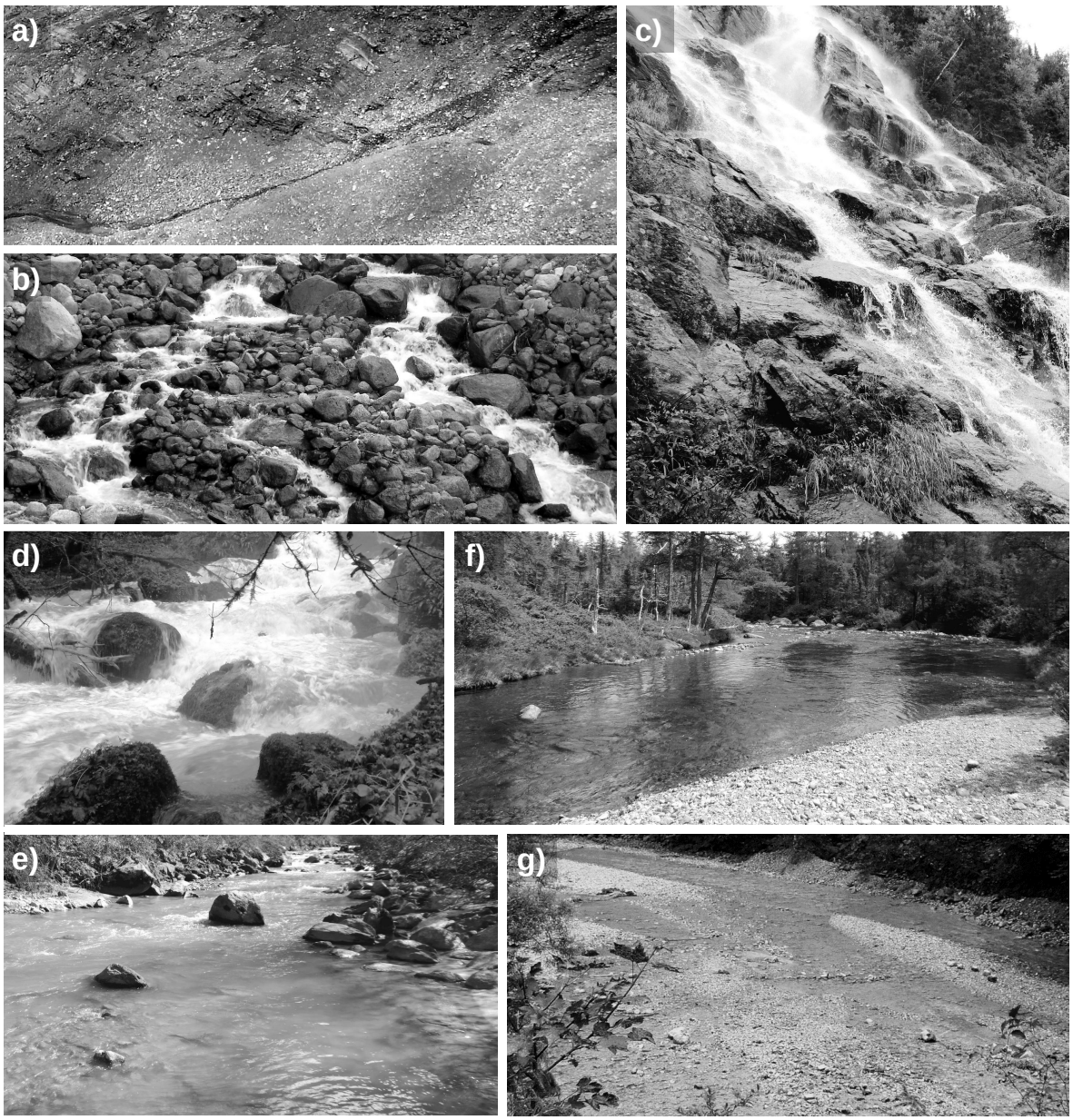

Figure 2.2 – *a) A colluvial headwater stream (Furtschaglbach, Austria), b) a cascade stream (Torrent des Favrands, France), c) a bedrock stream (Anse St-Jean, Québec, Canada), d) a step-pool stream (Dessoubre, France), e) a plane-bed stream (Dranse, Switzerland), f) a riffle-pool stream (Le diable, Québec, Canada), g) a braided stream (Jenbach, Germany). © S. Schwindt.*

2.2 Hydraulics of steep and rough channels

2.2.1 Geometric description

The flow in rough and steep channels is described by the dimensional variables of discharge Q, flow depth h, representative particle size D_{pq} (where pq % of the particle mixture is finer), channel slope S_0 and channel geometry (Wohl, 2000). All variables (Fig. 2.3) mutually interact with each other, but may be bounded due to natural or artificial flow barriers, or morphological limits in the shape of rocks or channel reinforcement.
The transversal channel geometry depends on the stream type (Fig. 2.2), but a general approximation can often be made by assuming a trapezoidal cross section with bottom width w and dimensionless bank inclination m. Thus, the mean flow width is given by $w_m = w + h\ m$. The corresponding surface is $A = h \cdot w_m$ and the wetted perimeter is $P = w + 2\ h\ \sqrt{m^2+1}$. The ratio of the flow cross section surface and the wetted perimeter is the hydraulic radius R_h. The cross-section-averaged flow velocity in the stream direction can be computed by $u = Q\ /\ A$ (Henderson, 1966). The channel slope between two sections i and i+1 is the ratio of the elevation difference of the channel bottom Δz and the horizontal distance Δx.

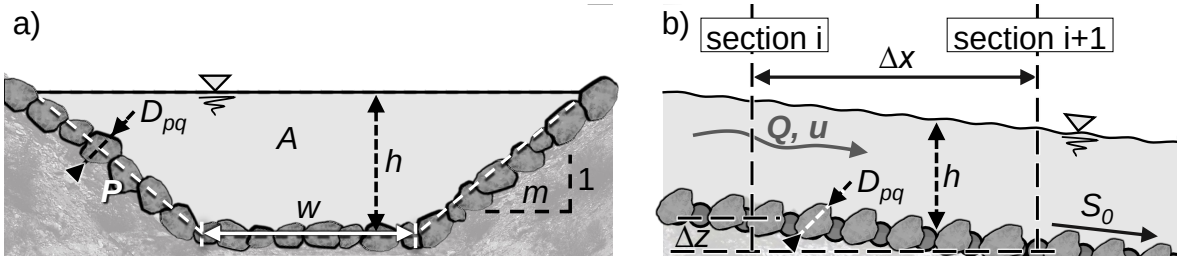

Figure 2.3 – *The hydraulic parameters describing the flow in rough and steep channels; a) transversal cross section; and b) longitudinal profile between two sections i and i+1.*

2.2.2 Flow properties

The balance of the total energy per unit force E, which applies for a 1D uniform distribution of flow velocity across the sections i and i+1, is given by:

$$E_i = E_{i+1} + \Delta\ E_r + \Delta\ E_{Q_b} + \Delta\ E_{add} \tag{2.1}$$

where $E_i = z_i + h_i + \frac{u_i^2}{2\ g}$; $E_{i+1} = z_{i+1} + h_{i+1} + \frac{u_{i+1}^2}{2\ g}$; and g denotes the gravitational acceleration (9.81 m s^2). The terms $\Delta\ E_r$, $\Delta\ E_{Q_b}$ and $\Delta\ E_{add}$ denote energy losses due to roughness, solid transport and tertiary sources, respectively.
Roughness losses and the corresponding energy slope S_e can be assessed by a friction law such as the Chézy flow resistance C:

$$\Delta E_r = \Delta x \cdot S_e = \Delta x \cdot u_i^2 \cdot C^{-2} \cdot R_{h_i}^{-1} \tag{2.2}$$

For steady and uniform flow conditions the energy slope S_e is equal to the channel bottom slope S_0 (Henderson, 1966). In this case, the "Gauckler–Manning–Strickler" formula relating the channel geometry, roughness, slope and flow depth to the flow velocity can be applied:

$$u = k_{st} R_h^{2/3} S_0^{1/2} \tag{2.3}$$

where k_{st} is the Strickler coefficient, which accounts for the channel roughness. The roughness can be alternatively expressed by the Chézy coefficient C, the Darcy-Weisbach friction factor f_f or Manning's n (Chézy, 1776; Weisbach, 1845; Darcy, 1857; Manning, 1891; Strickler, 1923; Ferguson, 2007). These approaches can be related to each other as follows (e.g., Ferguson, 2007):

$$k_{st} R_h^{1/6} = C = \sqrt{\frac{8\,g}{f_f}} = \frac{1}{n} R_h^{1/6} \tag{2.4}$$

For high values of the relative submergence, defined as the ratio between the flow depth and roughness length (h / D_{pq}), the roughness can be derived using D_{50} (in m) as representative grain size: k_{st} = 21.1 / $\sqrt[6]{D_{50}}$ $\mathrm{m}^{1/3}$ s^{-1} (Strickler, 1923), and in fully turbulent flow using D_{90}, i.e., k_{st} = 26 / $\sqrt[6]{D_{90}}$ $\mathrm{m}^{1/3}$ s^{-1} (Meyer-Peter and Müller, 1948). This approach hypothesizes the application of the representative grain size D_{pq} to the roughness length. Equivalent tables can be found for Manning's n, ranging from values of $n \approx 0.1$ for very irregular surfaces to $n \approx 0.015$ for very smooth surface (Chow, 1959). These approaches consider skin friction based on grain roughness, which works well in deep rivers with low slopes (Ferguson, 2010). However, the assessment of flow resistance, in particular in a mountain river environment, requires a more holistic approach, with consideration of form drag (Powell, 2014). The consideration of the channel slope for estimating additional roughness, especially in step-pool streams, was proposed and analyzed (e.g., Whittaker and Jaeggi, 1982; Smart et al., 2002; Aberle and Smart, 2003; Nitsche et al., 2012), but evidence for the influence of the channel slope is not generally confirmed (Comiti et al., 2007). Typical equations for the quantification of roughness are either based on a Manning–Strickler–like skin friction approach or a logarithmic-law approach (Keulegan, 1938) and refer to some calibration with a particular dataset. The combination of both roughness laws (skin friction and logarithmic law) with respect to the relative submergence of relevant roughness objects in terms of h / D_{pq} into a "Variable Power Equation" (VPE) was found to be generally more accurate (Ferguson, 2007). An optimization of this approach, using a large set of field data and the D_{84} as representative grain size, results in the following substitution for the Darcy-Weisbach friction (Rickenmann and Recking, 2011):

$$\sqrt{\frac{8}{f_f}} = 4.416 \left(\frac{h}{D_{84}}\right)^{1.904} \left[1 + \left(\frac{h}{1.283 D_{84}}\right)^{1.618}\right]^{-1.083} \tag{2.5}$$

The application of Eq. 2.5 is limited to h / D_{84} > 0.5 (Ferguson, 2007; Rickenmann and Recking, 2011). The solutions to Eqs. 2.3 and 2.5 are implicit and a better accuracy can be obtained by using the discharge Q instead of h / D_{84}, when data are available (Rickenmann and Recking, 2011). Multilayer roughness models include additional drag from the roughness element form, dispersive stresses, as well as viscous drag (Nikora et al., 2001, 2007). However, from a practical point of view, roughness predicted by the VPE according to Ferguson (2007), in combination with the

comprehensive data set from Rickenmann and Recking (2011), based on the D_{84} of the bed material as representative roughness length, represents a well-elaborated and adequate approach (Powell, 2014).
Spill resistance in step-pool streams (Fig. 2.2 d) may occur due to the presence of boulders. The additional roughness can be assessed, e.g., by engineering approaches for stepped spillways (Church and Zimmermann, 2007; Comiti et al., 2009; Dust and Wohl, 2012) or by correcting the slope (Whittaker and Jaeggi, 1986).
Further flow resistance in mountain rivers may occur due to solid transport in the shape of bed load, which increases the water depth due to its additional volume and induces energy losses (Recking et al., 2008a; Piton and Recking, 2016a). The corresponding flow resistance is considered by ΔE_{Q_b} which is (Uchiogi et al., 1996; Frey et al., 1999):

$$\Delta E_{Q_b} \in [1.0\ D_{max}, 1.5\ D_{max}] \tag{2.6}$$

where D_{max} is substituted by the D_{75} or D_{84} (Piton and Recking, 2016a). According to Recking et al. (2008a), the difference in roughness due to bed load can be accounted by a difference in roughness of $\Delta\sqrt{8/f_f}$ = -2.93. This validation of ΔE_{Q_b} is based on a small dataset with low statistical evidence. Therefore, in this study, bed-load-induced flow resistance is considered by the application of two different stage-discharge relations, i.e., one for clear-water flow and another for flow with bed load.
Additional sources of flow resistance $\Delta\ E_{add}$ may occur due to vegetation. Plants on banks that are washed out in the case of floods (floodplains) represent flexible roughness elements that can be considered by sectional calculations (Järvelä, 2002; Indlekofer, 2004). Such sources of flow resistance are not considered in this study, but have to be accounted in practice when necessary.

2.2.3 Characteristic numbers

The flow of mountain rivers can be characterized by the dimensionless Reynolds number Re and the Froude number Fr. The Reynolds number relates viscous forces to inertia and is a key parameter for flow turbulence (Chow, 1959; Jansen et al., 1994):

$$Re = \frac{u\ h}{\nu} \begin{cases} < 800 \rightarrow \text{ laminar flow} \\ \geq 800 \text{ and } \leq 2\,000 \rightarrow \text{ transitional flow} \\ > 10\,000 \rightarrow \text{ turbulent flow} \end{cases} \tag{2.7}$$

Where ν denotes the kinematic viscosity (10^{-6} m^2 s^{-1} for water at 20°C). In mountain rivers, inertia forces are dominant compared with viscous forces; therefore Re is generally larger than 2 000 and the flow is turbulent (Chow, 1959; Wohl, 2000).
The Froude number is the ratio between inertia and gravity forces; it is a key number of wave propagation, i.e., states whether information can be transmitted in upstream direction or not (Chow, 1959; Hager and Schleiss, 2009; Hager, 2010):

$$Fr^2 = \frac{Q^2}{A^3\ g}\ \frac{\partial A}{\partial h} \begin{cases} < 1 \rightarrow \text{ subcritical flow (upstream and downstream wave propagation)} \\ = 1 \rightarrow \text{critical flow (standing waves in upstream direction)} \\ > 1 \rightarrow \text{ supercritical flow (downstream wave propagation only)} \end{cases} \tag{2.8}$$

The transition from supercritical flow to subcritical flow is called “hydraulic jump”. For a trapezoidal cross section A, the Froude number becomes:

$$Fr = Q \left(\frac{w + 2\,h\,m}{A^3 \cdot g} \right)^{0.5} \tag{2.9}$$

Further key figures for the flow description can be found in the literature (Chow, 1959; Henderson, 1966). However, the Reynolds number and in particular the Froude number are most relevant to the analysis of sediment transport in open channel flow (Yalin, 1971, 1977).

2.3 Sediment transport in steep channels

2.3.1 Principles of sediment transport

Transport modes and key drivers

Fluvial sediment transport is a function of local hydraulics, sediment characteristics, as well as sediment availability and is differentiated between (Einstein, 1950):

- **Bed load**, i.e., particles rolling, sliding and jumping on the channel bed;
- **Suspended load**, i.e., particles with a weight that is carried by the fluid; and
- **Wash load**, i.e., transport of sediment that is finer than the bed particle size.

This study focuses on bed load and a particular type of bed load transport, similar to wash load without suspended load, corresponding to the concept of “traveling bed load” according to Yu et al. (2009) and Piton (2016). This type of bed load transport that is supplied by channel-external sources during floods and is more detailed described in the following section. These descriptions require the differentiation of two limiting factors for bed load transport, namely, (1) the flow-driven transport capacity and (2) the sediment supply (Church and Ferguson, 2015).
The hydraulic transport capacity (1) results from the bed shear stress τ of the flow (Du Boys, 1879; Yalin, 1977; Carson and Griffiths, 1987):

$$\tau = \rho_f \cdot g \cdot R_h \cdot S_e \tag{2.10}$$

where ρ_f denotes the fluid density (1000 kg m^{-3}). The dimensionless expression of the bed shear stress is τ_*, which refers to the particle density ρ_s (2680 kg m^{-3}) and the representative grain diameter D_{pq} (Von Karmàn, 1930; Kramer, 1932):

$$\tau_* = \frac{R_h \cdot S_e}{(s-1) \cdot D_{pq}} \tag{2.11}$$

where the ratio of solid and water density is here considered as $s = 2.68$. Bed particles are moved by the flow when a threshold value of τ_* is exceeded. This threshold value is referred as critical dimensionless shear stress τ_{*cr}, or also known as the “Shields parameter”, which in literature is sometimes also assigned by the Greek letter θ_{cr} (Shields, 1936). The grain mobility can be interpreted as some function of τ_{*cr} and the dimensionless particle diameter D_* or the particle

Reynolds number Re_* (Einstein, 1950; Guo, 2002):

$$D_* = \left[\frac{(s-1)\cdot g}{\nu^2}\right]^{1/3} \cdot D \tag{2.12}$$

$$Re_* = \frac{u_* \cdot D}{\nu} \tag{2.13}$$

This results in the grain mobility threshold curve shown in Fig. 2.4, where τ_{*cr} is nearby constant for $Re_* > 500$. More recent research has shown that τ_{*cr} is also a function of channel roughness and slope, relative submergence and bed load transport intensity (Wilcock, 1993; Gregoretti, 2008; Lamb et al., 2008; Recking et al., 2008a,b; Ferguson, 2012).

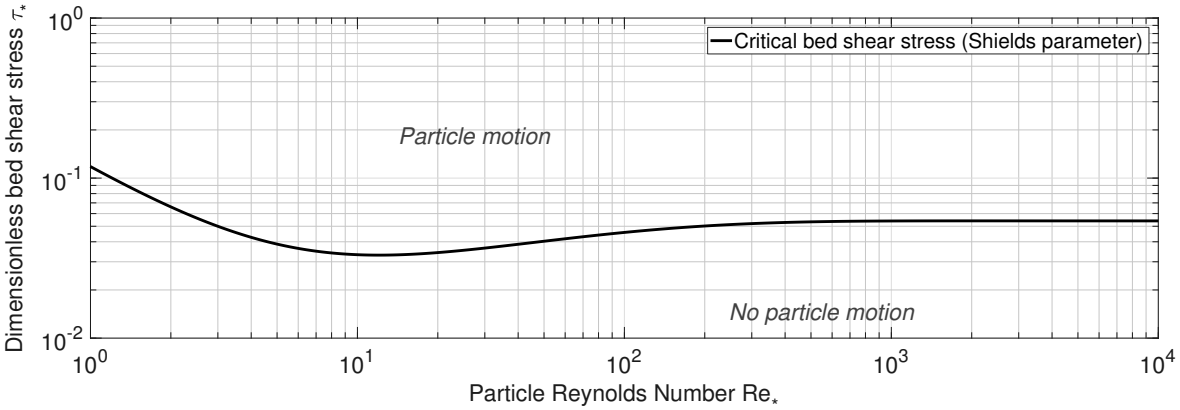

Figure 2.4 – *Critical dimensionless bed shear stress (Shields parameter) for grain mobility as a function of the particle Reynolds number Re_* (Eq. 2.13), according to Guo (2002).*

For the application in mountain rivers, Lamb et al. (2008) established a function for τ_{*cr}, based on the channel slope. Recking (2009) found that a reliable estimate for τ_{*cr} is obtained by considering the grain size distribution in addition to the channel slope:

$$\tau_{*cr} = (1.32\ S_0\ +\ 0.037)\ \cdot \left(\frac{D_{84}}{D_{50}}\right)^{-0.93} \tag{2.14}$$

The computation of the hydraulic bed load transport capacity was analyzed in several (semi-) empirical studies, as a function of the difference between a site-specific grain mobility parameter $\tau_{*,m}$ and its critical value τ_{*cr} (Meyer-Peter and Müller, 1948). In simple linear flow cross sections, $\tau_{*,m} = \tau_*$ (Eq. 2.11). However, stream morphologies are often complex with non-linear distribution of bed shear stresses (Recking, 2013a). Recking et al. (2016) propose a formulation to estimate $\tau_{*,m}$ in plane-bed streams (Fig. 2.2 e) with such a non-linear distribution of bed shear stress:

$$\tau_{*,m} = (5.0\ S_0\ +\ 0.06)\ \cdot \left(\frac{D_{84}}{D_{50}}\right)^{4.4\ \sqrt{S_0}\ -\ 1.5} \tag{2.15}$$

This expression also applies for step-pool, riffle-pool and braided stream types, but with lower statistical evidence. The application limits of Eq. 2.15 refer to the Recking (2013b) formula according to the figures in Tab. 2.2 (page 18).

Morphological interaction and traveling bed load

The complexity of driving hydraulic forces of bed load transport incorporates some uncertainty in each parameter involved. Another source of uncertainty is the source and type of sediment supply, which determines the characteristics of transported sediments as, for instance, the grain size distribution.
The term "traveling bed load" refers to the difference between the bed grain size and the efficient grain size of the transported bed load, mainly supplied by external sources during floods (Piton, 2016). Traveling bed load has no or limited exchange with the river bed. Its grain size distribution can be determined by looking at "silent witnesses" (Kaitna and Hübl, 2013), i.e., deposits on the floodplain or the alluvial fan from former flood events.
The transported bed load that interacts with the bed, i.e., that has some morphological effect on the river, is referred as "structural bed load" (Yu et al., 2009; Piton, 2016). Sediment, which is mobilized in the catchment during floods, can pass steep headwaters in the shape of traveling bed load and may deposit in less steep downstream reaches (Sutherland et al., 2002; Hassan et al., 2005). The lower-gradient-reaches can be associated with alluvial fans (Fig. 2.1) that often require flood protection measures due to urbanization. For this reason, it is essential for flood protection measures in mountainous regions to distinguish between (semi-) alluvial and non-alluvial channels. Bed load in (semi-) alluvial channels is mainly supplied by the stream bed and the hydraulic bed load transport capacity determines the sediment flux; (traveling) bed load of non-alluvial streams is governed by periodical, external sediment supply. (Semi-) alluvial channels can be associated with riffle-pool and braided streams (Fig. 2.2 f, g); non-alluvial channels are typically associated with bedrock, step-pool or cascade streams (Fig. 2.2 b, c, d). Non- or semi-alluvial channels, such as plane-bed streams (Fig. 2.2 e), can turn into alluvial streams during floods due to armor breaking (Lisle, 1986; Montgomery et al., 1996; Montgomery and Buffington, 1997; Hassan and Woodsmith, 2004; Hassan et al., 2008). Supply-limited channels can also be linked to the concept of "equal mobility", i.e., the simultaneous mobilization of all grain sizes constituting the channel bed (Parker et al., 1982; Montgomery, 1999). Alluvial channels with high sediment supply can be related to "selective entrainment", i.e., the likelihood of mobilization of equally-sized grain clasts (Wilcock, 1993; Montgomery, 1999).
External sediment supply underlies flexible periodical events which increase the local sediment storage punctually (Beschta, 1979; Benda, 1990). In function of the sediment concentration, these events are differentiated between hyperconcentrated flow, debris or mud flow and debris floods occurring essentially in the upper catchment and the canyon section (Iverson, 2005; Pierson, 2005).

2.3.2 Formulae for bed load transport estimation

One of the earliest concepts for the estimation of bed load transport in steep streams was introduced by Meyer-Peter and Müller (1948) and can be written in a dimensionless way, assuming that the

critical dimensionless bed shear stress for incipient motion of grains is $\tau_{*cr} = 0.047$ (Smart, 1984):

$$\Phi_{\text{mpm}} = 8 \cdot \left[\left(\frac{k_s}{k_r} \right)^{1.5} \tau_* - \tau_{*cr} \right]^{1.5} \tag{2.16}$$

where $\Phi = Q_b \,/\, [w_m \sqrt{(s-1)\, g\, D^3}]$ denotes the dimensionless bed load transport intensity (Einstein, 1942; Smart, 1984); k_s refers to the Strickler (1923) coefficient of roughness for the bed region; and k_r is the Strickler (1923) coefficient of bed roughness associated with skin friction only (Wong and Parker, 2006). The ratio of both roughness coefficients accounts for the presence of bed forms. Accordingly, $k_s \,/\, k_r$ is unity if there are no bed forms and decreases to 0.5 if bed forms are present (Raudkivi, 1976). Since the development of the Meyer-Peter and Müller (1948) formula, the consideration of flow resistance has been revised by several authors (e.g., Wong and Parker, 2006; Ferguson, 2007; Rickenmann and Recking, 2011). Moreover, Eq. 2.16 is based on the assumption of equal grain mobility, which leads to an overprediction of bed load transport (Hunziker and Jaeggi, 2002). A re-analysis of the data from Meyer-Peter and Müller (1948) has shown that the form drag correction ratio can be omitted in plane-bed streams (cf. Fig. 2.2 e, page 10) and that the overestimation can be corrected (Wong and Parker, 2006):

$$\Phi_{\text{mpm,c}} = 4.93 \cdot (\tau_{*b} - \tau_{*cr})^{1.6} \tag{2.17}$$

where τ_{*b} is the sidewall corrected dimensionless bed shear stress acting on the active bed region (Vanoni, 1975), which is computed by applying the hydraulic radius on the bed region and $D_{pq} = D_m$ (Eq. 2.11).

The formulae from Meyer-Peter and Müller (1948) formula and its correction (Eqs. 2.16 and 2.17) apply for channel slopes $S_0 \in [0.04, 2.0]$. The formula was extended to steeper slopes up to 20 % and for non-uniform sediment distributions (Smart and Jaeggi, 1983; Smart, 1984):

$$\Phi_{\text{sj}} = 4 \left(\frac{D_{90}}{D_{30}} \right)^{0.2} S_0^{0.6} \frac{C}{g^{0.5}} \tau_*^{0.5} (\tau_* - \tau_{*cr}) \tag{2.18}$$

In this case, the flow resistance in terms of the Chézy coefficient C can be computed by an iterative solution to Eq. 2.3. Rickenmann (1991) extended the former work with regard to high concentration of fine sediment originating from debris flow:

$$\Phi_{\text{ric}} = \frac{3.1}{(s-1)^{0.5}} \left(\frac{D_{90}}{D_{30}} \right)^{0.2} \tau_{*b}^{0.5} (\tau_{*b} - \tau_{*cr}) \; Fr^{1.1} \tag{2.19}$$

Several other approaches can be found in literature, e.g., approaches accounting for the non-linearity of bed shear stresses (Recking, 2013b,a) or approaches considering the volume fractions of the grain size distribution (Wilcock, 2008). An overview of relevant approaches for mountain rivers and their application limits is listed in Tab. 2.2. However, only Eqs. 2.18 (Smart and Jaeggi, 1983) and 2.19 (Rickenmann, 1991) are used in the later analyses of a flume with little non-linearity in the flow cross section. Therefore, the (Smart and Jaeggi, 1983) and (Rickenmann, 1991) formulae are considered to be most suitable for the application to the laboratory environment, as shown in previous studies (Jordan et al., 2003; Kaitna et al., 2011; Frey and Tannou, 2000).

Table 2.2 – *A list of some approaches for estimating the bed load transport in mountain rivers, with indication of application limits.*

Author(s)	**Year**	**Grain diameter** [10^{-3} m]	**Froude** Fr [-]	**Slope** S_0 [%]	**Flow depth** [m]
Bagnold	1980	$0.25 < D_{50}$ $D_{50} < 70$		$0.009 < S_0$ $S_0 < 3.5$	
Barry et al.	2005	$5.0 < D_{50}$ $D_{50} < 204$		$0.07 < S_0$ $S_0 < 5.1$	
Einstein	1950	$0.8 < D_{35}$ $D_{35} < 28.6$			
Meyer-Peter and Müller	1948	$0.4 < D_{pq}$ $D_{pq} < 29.0$	$10^{-4} < Fr$ $Fr < 639$	$0.04 < S_0$ $S_0 < 2.0$	$0.01 < h$ $h < 1.2$
Parker	1990	$0.54 < D_{pq}$ $D_{pq} < 28.6$	$Fr < 0.8$		
Recking	2013a 2013b	$0.25 < D_{50}$ $0.3 < D_{84}$ $D_{50} < 220$ $D_{84} < 558$		$0.004 < S_0$ $S_0 < 8.5$	$0.04 < h$ $h < 7.5$
Rickenmann	1991	$0.4 < D_m$ $D_{90}/D_{30} < 8.8$		$0.1 < S_0$ $S_0 < 20.0$	$0.01 < h$ $h < 1.2$
Smart and Jaeggi	1983	$0.4 < D_m$ $D_{90}/D_{30} < 8.8$		$0.2 < S_0$ $S_0 < 20.0$	$0.01 < h$ $h < 1.2$
Wilcock	2008	*variable*			

2.4 Driftwood

Wood in mountain rivers originates from steep tributaries, avalanches and landslides, or vegetated (over-) bank, as well as from wood industries (Hartlieb and Bezzola, 2000; Piton and Recking, 2016b). With respect to the relevance of driftwood transport, the following differentiation of wood in rivers is made (Rimböck, 2003; Lange and Bezzola, 2006):

- **Deadwood** ≙ Woody debris in the shape of dead trees and branches, originating from snow damage, windfall, avalanches, landslides or forestry.
- **Green wood** ≙ Fresh wood that is mobilized solely by floods through bank erosion and hang slides.
- **Industrial wood** ≙ Anthropologically caused woody debris, originating from wood yards or structural elements such as wood bridges or wooden sills.

The size of woody debris depends on its transport length, as it is shredded into approximately 1 to 5-m-long pieces during the transport (Zollinger, 1983). The driftwood quantities can be estimated based on empirical formulae, which refer to the analysis of former events or the catchment area, as well as flood discharge or sediment transport volumes (Uchiogi et al., 1996; Rickenmann, 1997; Hartlieb and Bezzola, 2000; Lange and Bezzola, 2006; Schmocker and Weitbrecht, 2013).
Incipient motion of driftwood was identified as some function of the relation between the Froude number Fr and the ratio of the flow depth h and wood diameter D_w (Braudrick and Grant, 2000; Lange and Bezzola, 2006):

$Fr \approx 0.75 \rightarrow$ incipient motion of driftwood if $h > 0.75\ D_w$
$Fr \approx 1.25 \rightarrow$ incipient motion of driftwood if $h > 1.25\ D_w$

Bezzola et al. (2002) analyzed the mobilization of driftwood as function of its texture:

$h > 1.0\ D_w \rightarrow$ mobilization of smooth trunks
$h > 1.2\ D_w \rightarrow$ mobilization of trunks with branches
$h > 1.7\ D_w \rightarrow$ mobilization of trunks with branches and root stocks

In the presence of bed load, the threshold value of the flow depth for driftwood mobilization reduces by approximately 20 to 30 % (Lange and Bezzola, 2006). Thus, the mobilization of important volumes of driftwood can be associated with exceptional flood events and related phenomena such as side erosion or landslides (Ruiz-Villanueva et al., 2013; Schmocker and Hager, 2013).
Wood can have important effects on a reach-scale morphology by creating local channel obstructions, thus forcing step-pool morphologies (Montgomery and Buffington, 1997; Hassan et al., 2005; Wilcox et al., 2006; Church and Zimmermann, 2007).

2.5 Eco-morphological considerations and requirements

2.5.1 Links between ecology and morphology

The morphological diversity of mountain rivers is essential to the dynamics of ecosystems. Anthropogenic disturbances to the connectivity of flowing waters and natural flow variability have a direct

impact on the eco-morphological state of rivers (Allan and Castillo, 2007; Sponseller et al., 2013). Naturally, the state of rivers is a multidisciplinary concern to understand the role of anthropogenic interventions. This requires the consideration of ecological and morphological site evaluations (Bain et al., 1999).
Existing evaluation methods refer either to morphological (cf. Chpt. 2.1 and Leopold and Maddock, 1953; Leopold and Wolman, 1957; Howard, 1980; Rosgen, 1994; Buffington and Montgomery, 1999; Church and Ferguson, 2015) or biologic (e.g., Cummins, 1962; Hamilton, 1984; Hankin and Reeves, 1988; Modde et al., 1991; Auble et al., 1994; Jensen and Bourgeron, 2012) site characteristics.
Further methods exist for the evaluation of the success of stream restoration projects with regard to reach-scale hydro-morphodynamics (Gostner et al., 2013) or fish abundance (e.g., Pretty et al., 2003; Woolsey et al., 2007). Some of these methods are complex as they require considerable efforts such as the assessment of local livestock.
With respect to the applicability in practice, significant site characteristic parameters resulting from ad hoc observations are of particular importance for the assessment of the eco-morphological river state (Bernhardt et al., 2005). Such parameters refer to commonly immobile objects that are only dislocated or reshaped by the consequences of exceptional meteorological events or geotechnical activity. Therefore, the application of all-time visually perceptual parameters such as typical plants (e.g., Demars et al., 2014; White et al., 2014; Kondo and Sakai, 2015), sediment characteristics (e.g., Kondolf, 1997a) and morphological pattern (e.g., Wolman and Miller, 1960; Montgomery and Buffington, 1997) is preferable. Correlations between such parameters and human activity were analyzed in a large number of studies (e.g., Catford and Jansson, 2014; Kuglerová et al., 2015).
Also links between the presence of woody debris and the morphological pattern of rivers as habitats for the aquatic livestock were identified (Everett and Ruiz, 1993; Johnson et al., 2005; Hassan et al., 2008). For instance, it was found that driftwood is important as substrate for macroinvertebrates (Haden et al., 1999) or fish abundance (Montgomery and Piégay, 2003). Therefore, the artificial retention of wood should be generally limited to important floods only for avoiding negative effects on the ecological abundance of downstream river reaches (Ruiz-Villanueva et al., 2016).
The morphological processes (Chpt. 2.1) and the sediment supplied by headwaters are equally important to the quality of aquatic habitats at downstream reaches (Milhous, 1998; Gomi et al., 2002; Hassan et al., 2005; Denic and Geist, 2015; Recking et al., 2016). Criteria for the evaluation of the natural state of sediment transport-related morphological patterns of a river are eligible for rating the quality of aquatic habitats and biodiversity. Therefore, criteria related to sediment transport can also be designated as “eco-morphological” river characteristics (Moyle and Mount, 2007).

2.5.2 Eco-morphological assessment

Due to the interaction between the ecological and morphological diversity of rivers, sediment transport-related criteria may be assessed by a certain discharge which alters and rearranges the channel bed. This discharge can be either defined by the bank-full discharge (Williams, 1978) or the dominant, morphologically effective discharge (Wolman and Leopold, 1957a,b; Wolman and Miller, 1960).
The bank-full discharge fills the channel to the level of the flood plain (Andrews, 1980), but the re-shaping of the channel is often associated with already smaller discharges (Harvey, 1969; Pickup

and Warner, 1976). Therefore, the concept of the bank-full discharge is not considerable for the eco-morphological assessment of rivers.
The dominant, morphologically effective discharge corresponds to the discharge that is responsible for the displacement of the biggest part of sediment and varies from river to river (Wolman and Miller, 1960; Benson and Thomas, 1966). Some authors linked the effective discharge also to specific return periods, typically in the order of 1–3 years (Wohl, 2000; Crowder and Knapp, 2005). But, in the case of mountain rivers with strong bed armoring or bed-rock-type channels, the return period of the effective discharge can be up to 50 years (Hassan et al., 2014). The assessment of the dominant discharge requires flow and sediment rating curves (Biedenharn et al., 2000; Klonsky and Vogel, 2008), which should refer to the traveling bed load (Chpt. 2.3.1) in mountain rivers.
A direct relationship between the dominant, morphologically effective discharge and the transport of organic matter was identified by Doyle et al. (2005). Similar dependencies between the morphologically and environmentally effective discharges were observed in other studies (e.g., Ensign et al., 2013; Goñi et al., 2013; Meitzen et al., 2013). Hence, the eco-morphological state of downstream river reaches can be related to the capacity of mountain rivers to convey sediment during floods corresponding to the dominant/effective discharge.

2.5.3 Effects of anthropogenic interventions on rivers

The undisturbed sediment transport in river networks is essential for the eco-morphological diversity of rivers. Anthropogenic interventions may disturb the sediment transport capacity of rivers in the form of longitudinal and transversal river training structures for purposes of hydro power generation, derivation of drinking water or flood protection (Williams and Wolman, 1984; Kondolf, 1997b; Lane et al., 2014). These interventions may cause downstream river bed incision and amplified erosion of channel banks (e.g., Slattery and Phillips, 2011; Ji et al., 2014).
A major negative implication in the ecological connectivity is represented by the disruption of fish migration. Approaches and design criteria for enabling the migration of the aquatic livestock through hydraulic structures were found in terms of, e.g., replacing sills by block ramps, installing fish passage facilities and studying hydraulic requirements for fish migration.
The design of stable and fish friendly block ramps has been exhaustively studied (e.g., Pagliara and Chiavaccini, 2006; Pagliara and Palermo, 2008; DWA, 2009; Tamagni, 2013; Weitbrecht et al., 2016) and the criteria established are generally applicable for interventions in mountain rivers.
The design of fish passes is described in, e.g., FAO and DVWK (2002) [in English] and more in detail in DWA (2014) [in German]. The migration of fish is deemed to be related to hydraulic characteristics in terms of seasonal discharges, maximum admissible flow velocities and minimum flow depths required. The seasonal discharges which are relevant to fish migration can be commonly designated to river-specific discharges between Q_{30} and Q_{330}, i.e., the discharges which are statistically not exceeded during 30 and 330 days per year, respectively (DWA, 2005; Tamagni, 2013). The maximum flow velocities and minimum flow depths required for fish migration vary among the species (Bainbridge, 1958; Beamish, 1978; Pavlov, 1989; Geitner and Drewes, 1990; Jensen and Aass, 1995). A summary of species-related migration velocities and flow depths is provided in Tamagni (2013).
The conflict between the eco-morphological permeability and sediment retention in mountain rivers for flood protection is addressed in Chpts. 6, 7 and 8.

2.6 Floods and hazard mitigation measures in Alpine environments

2.6.1 Assessment hazard processes related to floods

Flood-driven natural hazards in mountainous Alpine environments are summarized in Tab. 2.3 (Hübl, 2006; Romang, 2004; Bergmeister et al., 2009). In this research, hazards related to fluvial bed load transport are considered, where Newtonian fluid laws apply. The identification of a

Table 2.3 – *Hazard processes in mountain rivers, adapted from Hübl (2006) and Bergmeister et al. (2009).*

Process terminology	Flood (clear water)	Fluvial bed load transport	Debris flood	Debris flow
Flow type	Newtonian	Newtonian	Almost Newtonian	Non-Newtonian
Solid concentration	< 0.1 %	0–20 %	20–40 %	> 40 %
Maximum grain diameter	$< 10^{-1}$ m	$< 10^{0}$ m	$> 10^{0}$ m	$> 10^{0}$ m
Driving forces	Turbulence, bed shear stress	Turbulence, bed shear stress	Buoyancy, turbulence, bed shear stress, dispersive pressure	Buoyancy, turbulence, bed shear stress, viscous & friction forces
Grain sorting	Yes	Yes	Rather non-existing	Non-existing
Damages arising from	Water and suspended load	Water, suspended and bed load	Solid matter and water	Solid matter (and water)

stream bed (re-)shaping flood discharge is of essential interest for the design of hydraulic structures for minimizing negative effects on the eco-morphological pattern of mountain rivers. Such a "morphological flood" can be assessed by the above-introduced concept of dominant/effective discharge (Wolman and Leopold, 1957a,b; Wolman and Miller, 1960), which is relevant to the eco-morphological diversity of downstream reaches (Chpt. 2.5). Therefore, hydraulic structures should not affect the flow until the dominant/effective discharge is exceeded.

2.6.2 Classification of torrential hazard mitigation structures

The physical aspects of torrential hazards (Tab. 2.3) require a functional distinction of the following protection measures (Mizuyama, 1993, 2008; ONR 24800, 2014):

- **Deviation** of (debris) floods and debris flow serves for bypassing sensitive urban areas;
- **Drainage** for the selective retention of coarse material;
- **Stabilization** of the river bed and banks to avoid erosion;

- **Consolidation** to foster the stability of the channel by reducing the channel bottom slope locally;
- **Retention** of water and/or solid material (sediment and driftwood) that cannot pass downstream river reaches without endangering riverine urban areas;
- **Energy dissipation** of debris flow.

Deviation and drainage of debris flow can be achieved by the combination of transversal torrential barriers with longitudinal structural elements (Bergmeister et al., 2009). The retention function can be selectively improved in terms of dosing or sorting. Dosing aims at the temporal retention of water and fluvial sediment transport during flood peaks, with a partial release of the retained material when the flood has passed (Üblagger, 1973; Jaeggi, 1992; Bergmeister et al., 2009). Sorting of large solid matter, transported as fluvial sediment or as hyperconcentrated debris flood/flow, is considered to filter boulders or driftwood that cannot pass sensitive downstream reaches, such as culverts or bridges (Kettl, 1973; Hübl et al., 2003; D'Agostino, 2013).
The protection functions can be achieved by different types of torrential barriers (check dams), which can be classified according to Fig. 2.5. The application of particular barrier types in the terrain is illustrated in Fig. 2.1; the related target protection functions are specified in Tab. 2.4 (Leys, 1973, 1976; Hübl et al., 2003; Wehrmann et al., 2006).
The combination of structural aspects, e.g., solid or slot barriers with sectional barriers on top, is labeled "compound" barrier in the literature (Hübl et al., 2003; Wehrmann et al., 2006). Typical construction materials are wood, stone blocks, (reinforced) concrete and steel (ONR 24800, 2014).
The separation of sediment and driftwood retention is desirable, as the according characteristic

Table 2.4 – *Attribution of protection functions to torrential control barriers (Fig. 2.5), adapted from Hübl et al. (2003) and Bergmeister et al. (2009).*

TYPE	Solid body barriers	Partially open barriers			
		Slot	Slit	Sectional	Lattice + Net
CONSOLIDATION	Yes	Yes	No	No	No
RETENTION (water)	Limited	Yes (small slots)	Limited	No	No
RETENTION (sediment)	Yes	Yes (small slots)	Yes	Limited	Limited
SORTING	No	Yes (large slots)	Yes	Yes	Yes
DOSING	No	Yes (large slots)	Yes	Yes	Yes
ENERGY DISSIPATION	No	No	Limited	Yes	Limited
WOOD RETENTION	No	No	Yes	Yes	Yes

diameters for triggering retention may differ significantly. However, the characteristic diameter plays an important role in the design of open barriers and important variations may result from

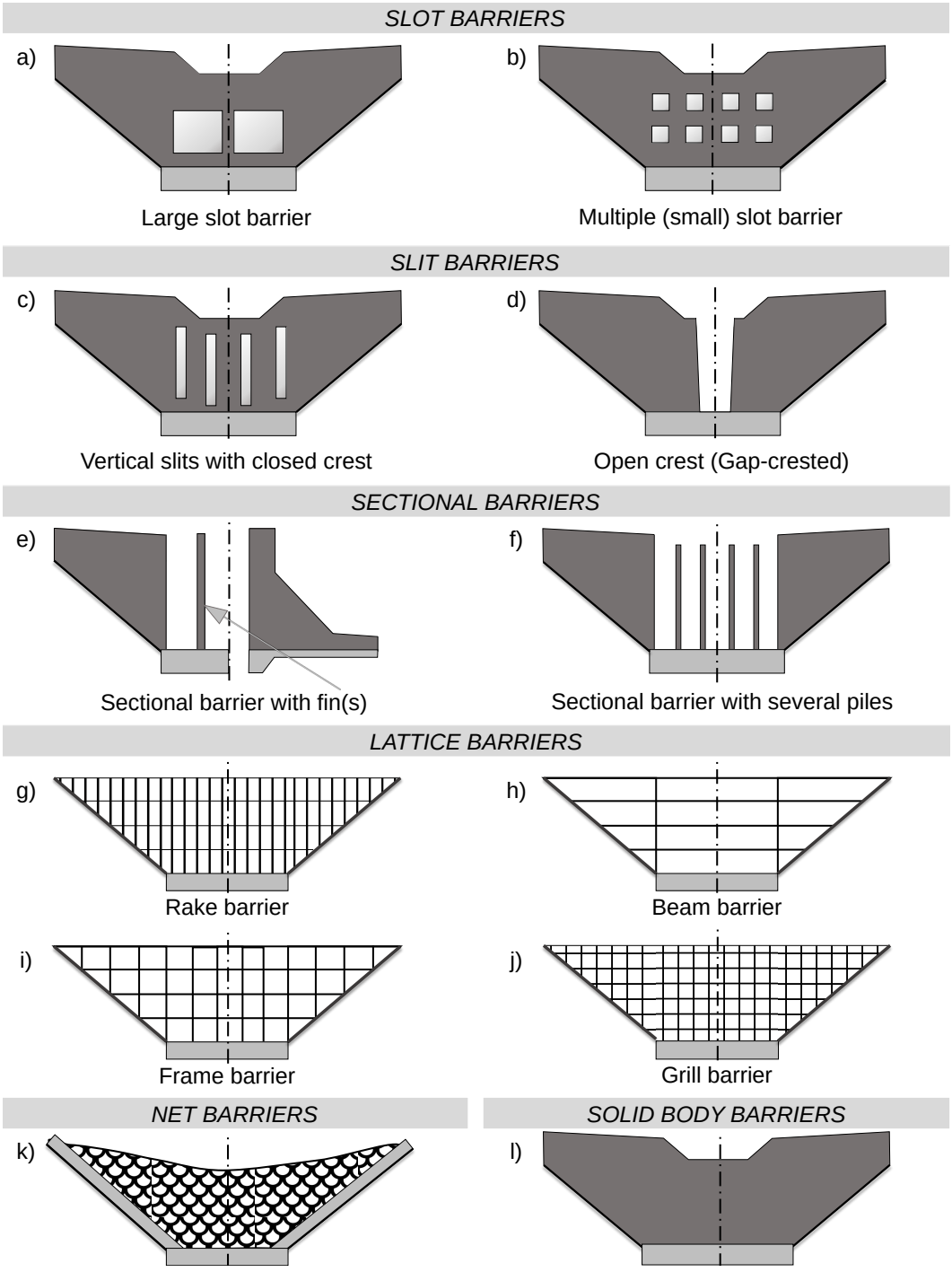

Figure 2.5 – *Classification of torrential barriers; adapted from Hübl et al. (2003, 2005).*

competing design criteria (Jordan et al., 2003; Böll et al., 2008; Comiti et al., 2012). For instance, the clearance widths or heights of open barriers differ for the design of a driftwood or a sediment retention structure. The combined retention of driftwood and sediment is only possible by two different structures, as one barrier needed to have clearance dimensions satisfying the characteristic diameters of driftwood and sediment simultaneously.
Structures aiming at solely driftwood retention consist in sectional, lattice or net barriers. A lateral arrangement of vertical pillars at the outer extremity of river bends can be considered as an effective measure for driftwood retention when the morphological conditions are suitable (Schmocker and Weitbrecht, 2013). In addition, the implementation of downflow baffles (German: *Tauchwand*) in combination with slot barriers may be considered in combination with sediment trapping (Bezzola et al., 2004). However, the decoupling of driftwood retention and sediment deposition is nearby impossible in practice (Bezzola et al., 2004; Lange and Bezzola, 2006). For increasing the eco-morphological diversity of downstream reaches, the transfer of acceptable amounts of driftwood is advantageous (Hauenstein, 2003; Comiti et al., 2012; Ruiz-Villanueva et al., 2016).
The selective retention, dosing or sorting of sediments can be forced by open barriers and enhanced by river widenings (Hunzinger et al., 1995; Rohde et al., 2005; Leite Ribeiro et al., 2016). The combination of such widenings with a downstream partially open barrier is labeled “sediment trap” (Fig. 2.1 ④). The working principles and the design of sediment traps are in the focus of this research and detailed descriptions are given in the following (Chpt. 2.7).

2.7 Sediment traps

2.7.1 Constructive elements

Sediment traps can (partially) retain solid material that represents a hazard to urban downstream reaches during fluvial floods. The concept of a conventional sediment trap is shown in Fig. 2.6, including the following elements (Zollinger, 1983, 1984):

① Inlet structure;
② Downstream scour protection downstream of the inlet structure;
③ Deposition area (or retention basin/reservoir);
④ Lateral dykes confining the deposition area;
⑤ Maintenance access;
⑥ Torrential barrier with opening(s) (open check dam);
⑦ Controlled overflow crest of the torrential barrier;
⑧ Downstream abutments (stabilization buttress); with
⑨ Counter dam.

The functional design of these elements is described in detail in Chpt. 8 regarding the establishment of a permeable sediment trap. In the terrain, sediment traps are typically located downstream of a knick-point in the channel axis and upstream of urban areas (cf. Fig. 2.1 and Wang, 1901, 1903; Hampel, 1968; Kronfellner-Krauss, 1972). At such knick-points, the channel slope decreases, and therefore, the natural bed load transport capacity decreases also. Channel knick-points can be observed, e.g., at the apex of alluvial fans (Fig. 2.1 ④).

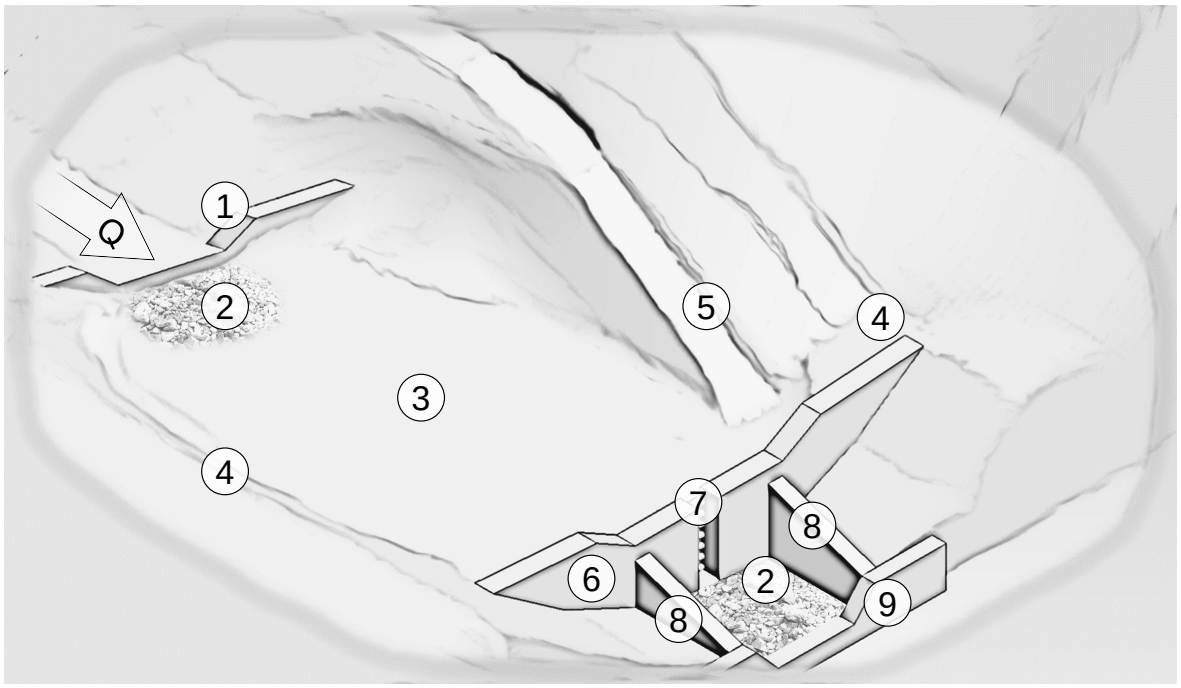

Figure 2.6 – *Concept of a typical sediment trap consisting of ① an inlet structure with ② scour protection; ③ a deposition area (or retention basin/reservoir) confined by ④ lateral dykes; ⑤ a maintenance access; ⑥ a torrential barrier with opening(s) (open check dam) and ⑦ a controlled overflow dam crest; ⑧ downstream abutments, i.e., stabilization buttress, with ⑨ a counter dam (ground sill). According to Zollinger (1983), Bergmeister et al. (2009) and Piton and Recking (2016a).*

The channel bed may be laterally widened and the banks degraded in the upstream direction to increase the storage volume of the retention basin (Fig. 2.6 ③). Degrading the channel and the banks in the upstream direction results in a drop between the initial channel bed and the retention basin, which requires an inlet structure with scour protection. Regarding the maintenance of the longitudinal river connectivity and for reducing the extent of scour protection, it is beneficial to use (structured) block ramps instead of high sills for the inlet structure, e.g., as proposed by Tamagni (2013) and Weitbrecht et al. (2016). However, this application is only meaningful when the downstream river reaches are also free from barriers interrupting the longitudinal connectivity.

2.7.2 Working principle

The river discharge passes the retention basin and the opening(s) of the open barrier without interaction, unless a certain flood discharge for triggering bed load retention is exceeded. This triggering flood discharge is determined as a function of the conveyance capacity of downstream bottlenecks such as bridges or low-graded reaches in urban areas. For higher discharges, sediment traps shall retain the sediments that are expected to deposit at the downstream bottlenecks (Leys, 1976; Zollinger, 1984; Armanini et al., 1991; Armanini and Larcher, 2001; Mizuyama, 2008). The bed load retention can be induced either hydraulically, due to a local reduction in the energy slope,

or mechanically, i.e., due to entangled blocks or boulders. These mechanisms can be achieved in sediment traps as follows (modified from Piton and Recking, 2016a):

- Hydraulic control due to a reduction in the energy slope in the backwater of a torrential barrier (Fig. 2.7 a);
- Mechanical control (obstruction) (Fig. 2.7 b) of the open barrier (Chpt. 2.7.4);
- Reduction of the energy slope due to the widening in the retention basin, i.e., deposition area, and the resulting spread of the flow (Chpt. 2.7.6).

The hydraulic control by the open barrier occurs when it causes backwater by confining the flow laterally or vertically in the opening. The flow decelerates in the backwater, where the energy slope reduces consequently, thus, promoting sediment deposition. The hydraulic control and the mechanical clogging of open barriers are illustrated in Fig. 2.7. The deposition pattern in the retention basin depends on the basin geometry, barrier features (barrier height, opening geometry and size) and flood characteristics (amount and size of sediment, flood duration and intensity, discharge variations). The deposition dynamics and pattern related to the basin geometry and varying flood characteristics have been previously studied, e.g., by Zollinger (1983) or Piton (2016). The barrier-related bed load retention controls are studied in Chpts. 6 and 7.

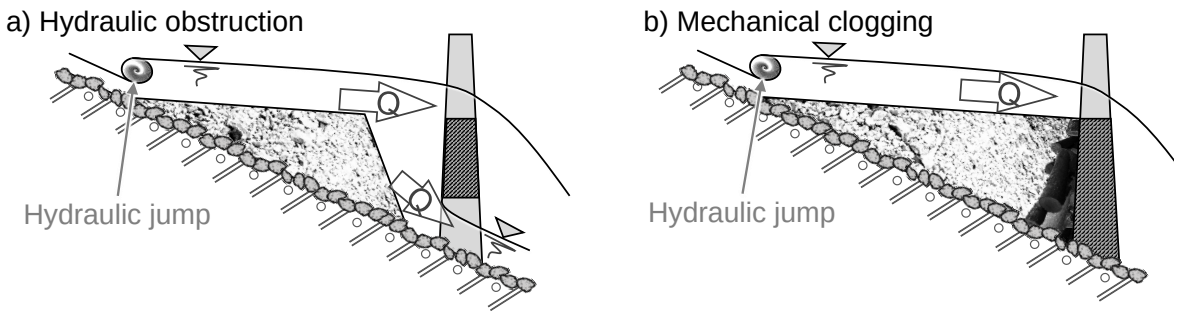

Figure 2.7 – *Obstruction mechanisms of torrential barriers with opening; a) hydraulic obstruction, occurring when a flood exceeds the discharge capacity of the opening in the barrier; and b) mechanical clogging by coarse sediment or wood with a diameter that exceeds the clearance of the opening in the barrier (Piton and Recking, 2016a).*

When a barrier is hydraulically or mechanically obstructed, the discharge is spilled over the barrier crest. The overflow section of the barrier crest needs to be confined to avoid lateral spill and erosion besides the barrier. Therefore, the lateral wings require a safe foundation in the hill slopes and their crest should be beveled toward the channel axis for centering the flow.

2.7.3 Hydraulic control of bed load retention

Permeable barriers in terms of open check dams are hydraulically characterized by their opening (constriction) height a and width b, as well as by the dam (barrier) height Δz_{dam} shown in Fig. 2.8. A further differentiation is made between check dams with (1) closed and (2) open crest (Leys, 1976; Zollinger, 1983; D'Agostino, 2013):

Case 1 corresponds to "Slot check dams" (Fig. 2.5), where the opening (orifice) is impounded. The flow in the opening is governed by pressurized flow conditions during floods. Such openings are denominated in the following as "vertical flow constriction".

Case 2 corresponds to "Slit check dams" (Fig. 2.5), where the opening height corresponds to the full barrier height ($a = \Delta z_{dam}$) and the barrier represents an abrupt narrowing. The flow in the opening is characterized by free surface flow conditions. Such openings are denominated in the following as "lateral flow constriction".

The opening of the barrier results in both cases in a constriction of the flow cross section, which is related to the discharge capacity of the flow constriction. When the river discharge exceeds the capacity of the constriction, backwater occurs upstream. The latter reduces the energy slope upstream of the constriction, and therefore, also the bed shear stress (Eq. 2.10) along with the bed load transport capacity. Then the hydraulically controlled bed load retention occurs in the backwater of the barrier (Frey and Tannou, 2000; Armanini and Larcher, 2001; Frey, 2014; Piton and Recking, 2016a).
The reduction of the bed load transport capacity upstream of the barrier due to hydraulic control by the backwater of flow constrictions is studied experimentally in Chpts. 4 and 5.

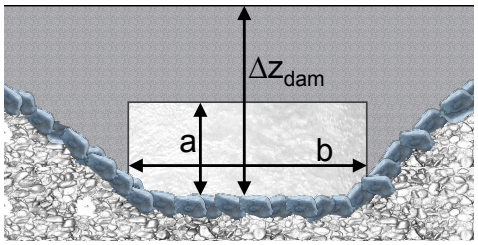

Figure 2.8 – *Relevant geometric parameters of an partially open barrier (open check dam) for primarily hydraulic control; indicating the opening height a, opening width b and the barrier height* Δz_{dam}.

2.7.4 Mechanical control of bed load retention

Torrential barriers with opening(s) are obstructed mechanically when the characteristic size of the transported sediment is too large to pass the opening(s). Mechanical control is typically achieved with sectional, lattice or net barriers (cf. Fig. 2.5 e-k). The vertical clearance a_i or horizontal clearance b_i of the mesh or between the individual fins / piles / bars is decisive for the initiation of mechanical clogging and subsequent bed load retention. The threshold values for the vertical and horizontal clearance, which induce clogging are listed in Tab. 2.5, based on the characteristic diameter, here taken as D_{84} (in line with D'Agostino, 2013). Some studies underline the necessity to differentiate between threshold values for the vertical and horizontal clearance, as vertical confinements are more prone to sediment flushing (Takahashi, 2014; Piton, 2016).

Sediment traps have to function also in the presence of driftwood, which can be improved by inclined rakes connected to a downstream torrential barrier for sediment deposition control (Lange and Bezzola, 2006; Bergmeister et al., 2009; Wallerstein et al., 2013). Rake barriers for the mechanical control of sediment deposition in combination with slot check dams for the hydraulic control are studied in Chpt. 6.

Table 2.5 – *Threshold values for the initiation of mechanical clogging with indication of the source, based on the representative grain diameter D_{pq}. The probability of mechanical clogging is close to unity for smaller values than listed here.*

Author	(year)	Relative clearance height a_i / D_{84}	width b_i / D_{84}
Zollinger	(1983)	1.2	1.6
Uchiogi et al.	(1996)	1.5	
SABO Division	(2000)	2.0	
Lien	(2003)	2.0	
Ono et al.	(2004)	1.0–1.5	
Mizuyama	(2008)	1.5	
Takahashi	(2014)	< 0.5	> 0.6
Canelas et al.	(2015)	–	1.49
Piton	(2016)	1.0	1.5–2.0
Shima et al.	(2016)	1.5–2.0	

2.7.5 Discharge capacity of torrential barriers

Hydraulic control of slot check dams

A slot in a check dam corresponds to a pressurized orifice in the barrier. Therefore, the derivation of the discharge capacity of such submerged orifices is based on the definition of the flow velocity $u = \sqrt{2\,g\,h}$, according to *Evangelista Torricelli* (1608–1647). This expression is valid for flow through pressurized openings, with some submergence cover depth h. The pressure due to the submergence cover increases linearly with increasing distance to the water surface, along the z–axis indicated in Fig. 2.9. In the case of non-negligible stream-wise flow velocity in the backwater of flow constriction, the additional pressure by the velocity head u_0 / (2 g) has to be considered. Therefore, the origin of the z–axis is defined here corresponding to the upstream energy grade line (dashed white line in Fig. 2.9). According to this, the flow velocity at any z position in the opening is:

$$u_z = \sqrt{2\,g\,z} \tag{2.20}$$

The discharge through an infinitesimally high rectangular partial area dA in an opening of width b is $dQ = u_z \cdot dA$, given that the focal point of dA lies in some height z. The discharge through the total opening area is derived based on the Leibniz' integral of the flow velocity over the opening height. This approach neglects local losses due to flow contraction and the opening edge shape, among others. These losses are accounted by a discharge coefficient μ_p, as described by Leys (1976). Thus, the discharge capacity Q_c of submerged orifices is:

$$Q_c = \mu_p \int_{H_0-a}^{H_0} u_z\,dA = \sqrt{2\,g}\,\mu_p \int_{H_0}^{H_0-a} z\,dA \tag{2.21}$$

For rectangular-shaped openings, the partial area is defined by $dA = dz \cdot b$. Trapezoidal openings with decreasing width in z–direction (Fig. 2.9), imposed by the channel bank slope m, are subsequently considered based on the beginning of the narrowing in z–direction in terms of H_t; i.e., the height of trapezoidal openings is defined by H_0 - H_t. Obviously, this coincides with the opening height a in the case of pure trapezoidal shapes. Pressurized openings that consist of an

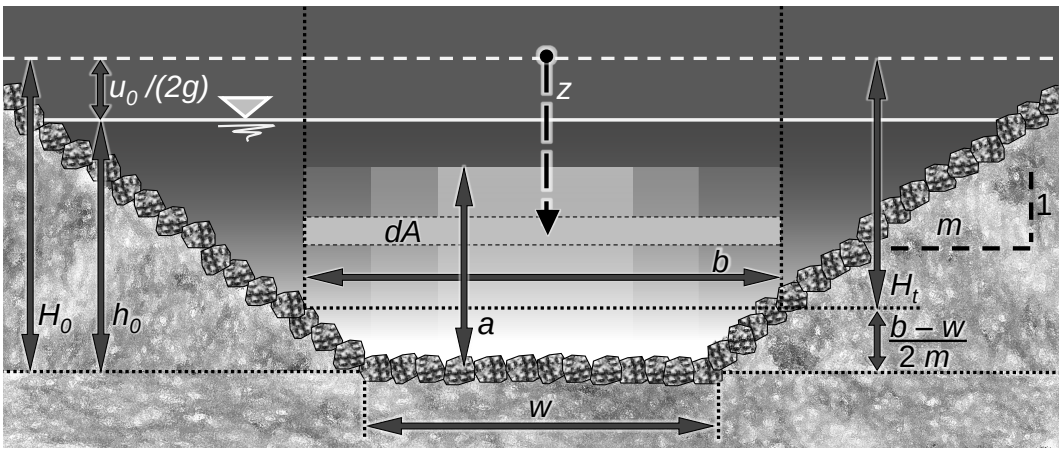

Figure 2.9 – *A schematic view of the flow cross section immediately upstream of a pressurized flow constriction; with indication of the energy head H_0; the flow depth h_0; the velocity head u_0 / (2 g); the constriction height a and width b; the channel bottom width w; the bank slope m; the energy grade line (dashed, white horizontal line); and an infinitesimal integration surface d A. z is the generic integration direction, with respect to the flow pressure in the orifice. Some variations of the opening width b are indicated in the background.*

upper rectangular part, due to lateral flow constriction, and a lower trapezoidal part require a differentiated consideration of the term H_0 - H_t. According to the notations in Figs. 2.9 and 2.10, it applies that:

$$\frac{H_0 - H_t}{\frac{b-w}{2}} = \frac{1}{m} \iff H_0 - H_t = \frac{b-w}{2\,m} \tag{2.22}$$

The width b_z of some infinitesimally high partial surface $d\,A$ in a trapezoidal opening can be derived relative to the height of the trapezoid H_0 - H_t:

$$b_z = w + (H_0 - z) \cdot \frac{b-w}{H_0 - H_t} \tag{2.23}$$

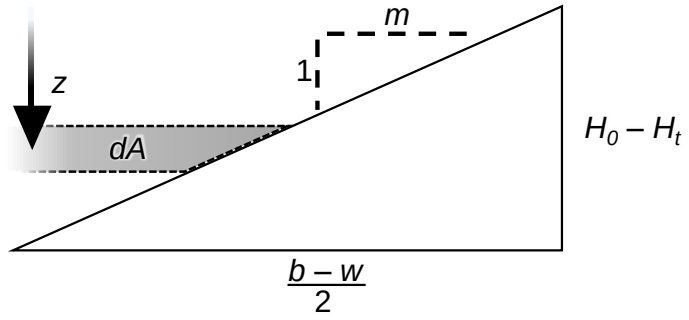

Figure 2.10 – *Detailed view of the right channel bank with its inclination m. This is considered here for the definition of the trapezium angle at the bottom of pressurized openings.*

With respect to the integral in Eq. 2.21, the discharge capacity of trapezoidal openings and / or their

combination with an upper rectangular part is generally given by:

$$Q_c = \mu_p \, (\overbrace{\int_{H_0-a}^{H_t} u_z \, dA}^{\text{Rectangle}} + \overbrace{\int_{H_0}^{H_t} u_z \, dA}^{\text{Trapezoid}}) \tag{2.24}$$

The stepwise solution to these integrals is illustrated in the following, with consideration of the integral definitions of the flow velocity u_z(Eq. 2.20) and the opening width b_z (Eq. 2.23).

$$Q_c = \mu_p \sqrt{2\,g} \, \{ \overbrace{\int_{H_0-a}^{H_t} b \, z^{1/2} \, dz}^{\text{Rectangle}} + \overbrace{\int_{H_0}^{H_t} b_z \, z^{1/2} \, dz}^{\text{Trapezoid}} \}$$

$$= \mu_p \, b \sqrt{2\,g} \int_{H_0-a}^{H_0-H_t} z^{1/2} \, dz + \mu_p \sqrt{2\,g} \int_{H_0}^{H_t} \left[w \, z^{1/2} + \frac{H_0 \, (b-w)}{H_0 - H_t} \, z^{1/2} + \frac{b-w}{H_0 - H_t} \, z^{3/2} \right] dz$$

$$= \mu_p \sqrt{2g} \cdot \left[\overbrace{\frac{2}{3} b \left(H_t^{\frac{3}{2}} - (H_0 - a)^{\frac{3}{2}} \right)}^{\text{Top rectangle}} + \overbrace{\frac{2}{3} w \left(H_0^{\frac{3}{2}} - H_t^{\frac{3}{2}} \right)}^{\text{Center of trapezoid}} \quad \ldots \right.$$

$$\left. + \overbrace{\frac{2}{3} \cdot \frac{H_0}{H_0 - H_t} (b-w) \cdot \left(H_0^{\frac{3}{2}} - H_t^{\frac{3}{2}} \right) - \frac{2}{5} \cdot \frac{b-w}{H_0 - H_t} \left(H_0^{\frac{5}{2}} - H_t^{\frac{5}{2}} \right)}^{\text{Wings of trapezoid}} \right]$$

For purely trapezoidal cross sections, i.e. $H_t = H_0 - a$, the expression becomes:

$$\begin{aligned} Q_{c\,\bigtriangledown} = \mu_p \sqrt{8\,g} \, \Bigg[& \frac{w}{3} \left(H_0^{\frac{3}{2}} - (H_0 - a)^{\frac{3}{2}} \right) \ldots \\ & + \frac{H_0}{3\,a} \, (b-w) \left(H_0^{\frac{3}{2}} - (H_0 - a)^{\frac{3}{2}} \right) - \frac{b-w}{5\,a} \left(H_0^{\frac{5}{2}} - (H_0 - a)^{\frac{5}{2}} \right) \Bigg] \end{aligned} \tag{2.25}$$

For purely rectangular cross sections, i.e. $H_t = H_0$, the expression simplifies to:

$$Q_{c\,\square} = \mu_p \sqrt{2\,g} \, \frac{2}{3} \, b \left[H_0^{\frac{3}{2}} - (H_0 - a)^{\frac{3}{2}} \right] \tag{2.26}$$

For composed rectangular cross sections, i.e. $H_t = H_0\text{-}(b - w\ /\ (2\ m)$, the discharge capacity is:

$$Q_{c} = \mu_p \sqrt{8\,g}\left[\frac{w}{3}\left(H_0^{\frac{3}{2}} - \left(H_0 - \frac{b-w}{2\,m}\right)^{\frac{3}{2}}\right) + \frac{2\,H_0\,m}{3}\left(H_0^{\frac{3}{2}} - \left(H_0 - \frac{b-w}{2\,m}\right)^{\frac{3}{2}}\right)\ldots\right.$$
$$\left. - \frac{2\,m}{5}\left(H_0^{\frac{5}{2}} - \left(H_0 - \frac{b-w}{2\,m}\right)^{\frac{5}{2}}\right) + \frac{b}{3}\left(\left(H_0 - \frac{b-w}{2\,m}\right)^{\frac{3}{2}} - (H_0 - a)^{\frac{3}{2}}\right)\right] \qquad (2.27)$$

An analysis of μ_p as a function of the upstream flow conditions (backwater) is performed in Chpts. 4 and 5. Analogous derivations of the discharge capacity and hydraulic design concepts can be found in (D'Agostino, 2013).

Hydraulic control of slit check dams

The flow through check dams with a slit is characterized by free surface flow conditions in the slit which represents a control section given that the flow of mountain rivers is generally supercritical. Therefore, the discharge capacity of slit check dams can be derived by solving the cross-section-averaged energy per unit force between a section immediately upstream of the slit and in the slit (according to Eq. 2.1) for the discharge (Armanini and Larcher, 2001; Armanini et al., 2006; Piton and Recking, 2016a):

$$Q_{c\,||} = \sqrt{2\,g}\,\frac{2}{3^{\frac{3}{2}}}\,b\,H_0^{\frac{3}{2}} \qquad (2.28)$$

The application of this expression (Eq. 2.28) is examined in Chpts. 4 and 5.

Mechanical control with rakes

The discharge capacity of sectional rake (screen) barriers with vertically inclined bars (cf. Fig. 2.5 e-g) depends on the total width of the barrier B, including vertical beams, the void ratio $\sum b_i\ /\ B$ and the dimensionless vertical rake inclination m_{bar}. Thus, the discharge capacity of inclined sectional rakes Q_{rake} can be estimated based on the following empirical equation (Di Stefano and Ferro, 2013, 2014; Piton and Recking, 2016a):

$$Q_{c\ \text{rake}} = B \cdot \sqrt{g} \cdot \left[\frac{h_0}{0.957 + \left(m_{bar}^2 + 1\right)^{-1.833/2}}\right]^{\frac{3}{2}} \cdot \left(\frac{B}{\sum b_i}\right)^{1.35 - 2.25\left(m_{bar}^2 + 1\right)^{-0.055}} \qquad (2.29)$$

The inclination m_{bar} is the arctangent of the rake inclination angle; i.e., $m_{bar} = 0$ for vertical rakes and $m_{bar} = 1$ for rakes with an inclination of 45°. Also the retention of driftwood can be achieved by such mechanical barriers. In this case, the relevant clogging criteria are related to the characteristic length of the woody debris (Uchiogi et al., 1996; SABO Division, 2000; Bezzola et al., 2004; Wallerstein et al., 2013; Piton and Recking, 2016b).

2.7.6 Deposition pattern and sediment flushing

The combined morphological effects of the reservoir, i.e., deposition area, and the barrier with openings were analyzed qualitatively and quantitatively in several studies (Leys, 1976; Zollinger, 1983; Hunzinger et al., 1995; Piton and Recking, 2016a). During floods, the flow conditions in mountain rivers can be considered as generally supercritical. Therefore, a hydraulic jump (transition from supercritical to subcritical flow) occurs at the upstream end of the backwater caused by the barrier. Sediment deposition occurs downstream of the hydraulic jump, where a delta-like deposit forms that evolves further downstream towards the barrier (Zollinger, 1983; Hunzinger and Zarn, 1996; Jordan et al., 2003). However, the deposit may lead to a spatial dispersion and relocate the position of the hydraulic jump (Armanini and Larcher, 2001; Busnelli et al., 2001; Campisano et al., 2014). Thus, the position of the hydraulic jump and the tail of the sediment deposit influence each other mutually. In the case of only small backwater, or mechanical blockage of the barrier, the formation of the deposit is initiated immediately upstream of the barrier. Such deposits evolve in upstream direction in a succession of quasi-equilibrium states (Armanini and Larcher, 2001; Campisano et al., 2014).
The deposit geometry can generally be quantified by its length L_{dep} and maximum height Δz_{dep}, as well as its deposition slope S_{dep} and front slope S_f, as shown in Fig. 2.11.

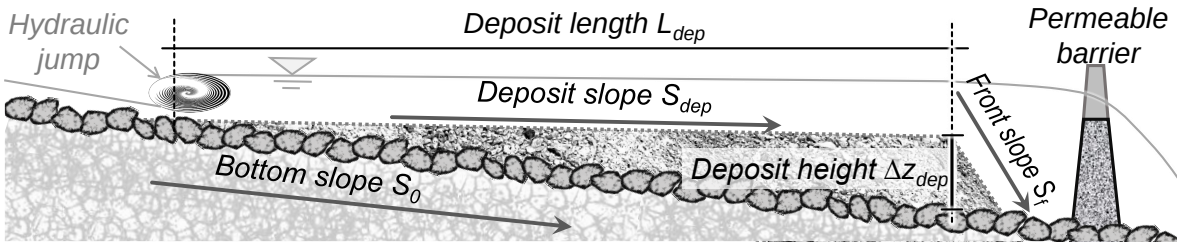

Figure 2.11 – *Longitudinal section of a filled sediment trap with indication of geometric characteristics of a deposit.*

The deposit length complies approximately with the length of the backwater induced by the permeable barrier. In the case of mechanical obstruction, the maximum deposit height Δz_{dep} can be estimated based on the height of the permeable barrier Δz_{dam}, the ratio between the opening width b (Fig. 2.8, page 28) and the upstream channel width w, as well as the flow depth h_0 (Fig. 2.3, page 11) upstream of the barrier. The estimation of Δz_{dep} can be obtained using the upstream Froude number Fr_0 in the case of hydraulically controlled bed load retention. Thus, the following expression can be applied for estimating an envelop curve of the maximum deposit height Δz_{dep} (Armanini and Larcher, 2001; Piton and Recking, 2016a):

$$\frac{\Delta z_{dep}}{h_0} = \frac{3}{2}\left(Fr_0 \frac{w_m}{b}\right)^{2/3} - 1 - \frac{Fr_0}{2}\left[1 - \left[1 - \frac{2}{3}\left(Fr_0 \frac{w_m}{b}\right)^{-2/3}\right]^2\right] \tag{2.30}$$

This expression allows also to assess the quantities of sediment that can be flushed by a certain discharge. Armanini et al. (2006) revised (Eq. 2.30) regarding debris flow. The upstream energy head and the flood duration for appraising the sediment deposit height may also be taken into account (Jordan et al., 2003).
The deposit slope S_{dep} can be described as a function of the initial channel slope, which corresponds

to S_0 if the channel bed has not been modified. In addition, S_{dep} is influenced by the flood intensity (D'Agostino, 2013; Osti and Egashira, 2013; Piton and Recking, 2016a):

$$S_{dep} \approx \begin{cases} 1\ /\ 2\ S_0 & \text{for small floods} \rightarrow \text{initial disaster conditions} \\ 2\ /\ 3\ S_0 & \text{for extreme floods \& high sediment concentration} \end{cases} \tag{2.31}$$

Alternatively, the deposit slope can be obtained by the equilibrium slope S_{eq} based on the solution to Eq. 2.18 (Smart and Jaeggi, 1983) for zero-transport conditions ($\Phi_{sj} = 0$), i.e., the equilibrium state of sediment in- and outflow. This results in the equilibrium channel slope S_{eq} as follows (Zollinger, 1983):

$$S_{eq} = \frac{D_{pq}}{h} \cdot \tau_{*cr} \cdot (s-1) \tag{2.32}$$

The equilibrium channel slope S_{eq} is considered in the analysis of the experimentally observed sediment deposits in Chpt. 7. The front slope S_f (Fig. 2.11) can be estimated based on the undrained angle of repose of cohesionless grains ϕ_u (typically about 45° for gravel) and the volumetric mass density of sediment ρ'_s (Jordan et al., 2003; Goris and Schneider, 2012; DIN 18127, 2012):

$$S_f = \tan\left(\phi_u\right) \cdot \frac{\rho_f}{\rho'_s} \tag{2.33}$$

Thus, the range of the front slope S_f is typically between 45° and 60° according to the friction angle of the sediment material.

The performance of a sediment trap, in terms of its actively used storage volume, can be evaluated by the trapping efficiency, which is defined by the ratio of the trapped and the inflowing sediment (Brown, 1939, 1943; Brune, 1953). The trapping efficiency is substantially influenced by the geometry of the retention basin. The sediment deposition effects reduce when the basin width is equal to or smaller than the basin length. However, the probability of sediment flushing increases with decreasing basin width and increasing basin length. A high trapping efficiency with a simultaneously low risk of sediment flushing can be obtained by a length to width ratio of 4:3 of the deposition area (reservoir). Accordingly, advantageous shapes were found in drop (also: pear)-shaped deposition areas, with the narrow part pointing in upstream direction (Zeller, 1973; Hampel, 1974; Leys, 1976; Zollinger, 1983; Piton and Recking, 2016a). With the drop-shaped basin, the deposit evolves similarly to natural alluvial fans, which can be described by its opening angle and bottom width. Therefore, the opening angle of the retention basin should be oriented at alluvial deposition cones, which is approximately 30° (Wang, 1901; Parker et al., 1998).

2.8 Concluding remarks and need for research

General concepts and targets of sediment traps are currently well defined (e.g. Piton and Recking, 2016a). However, the triggering of bed load retention during fluvial floods is not yet accurately understood; i.e., either bed load is excessively retained, already during non-hazardous flow situation, with the consequence of unnecessary and eco-morphologically problematic retention of bed load; or the bed load retention is insufficient with hazardous consequences for dwellers at downstream

reaches.
The design criteria for mechanically controlled bed load retention are sufficiently described by several studies (Tab. 2.5). But the design criteria for hydraulically controlled bed load retention are only partially understood (Chpt. 2.7.3). In particular, the reduction of the bed load transport capacity due to the reduction of the energy slope upstream of constriction-like permeable barriers has not yet been systematically analyzed. The hydraulic effects of vertical pressurized flow constrictions and free surface flow in lateral flow constrictions in the presence of bed load constitute an important element in the design of torrential barriers. Thus, the first goal of this research is a systematic parameter study of the influence of such flow constrictions on the bed load transport capacity of mountain-river-like channels, with rough and turbulent flow conditions. This analysis serves also for the identification of relevant approaches for deriving stage-discharge relations, head loss and the constriction-induced reduction in bed shear stress.
The channel bottom slope contributes to the energy head and is a key parameter for estimating bed load transport (e.g., using Eqs. 2.16, 2.18 or 2.19). Therefore, the second objective of this research is to analyze the effect of the channel slope on the hydraulics and bed load transport capacity of vertical and lateral flow constrictions.
Unwanted sediment flushing of sediment traps poses a permanent problem in practice. Consequently, undersized barrier openings are often designed to overcome the risk of sediment flushing during hazardous floods. Expensive technical solutions in the shape of movable weirs were realized, e.g., at the Schnannerbach torrent in Austria or the Schächen torrent in Switzerland (die.wildbach, 2016; Kanton Uri, 2016). The effects of flow constrictions for the hydraulic control of bed load retention and a bar screen (inclined rake) for the mechanically controlled bed load retention can be considered as a passive solution to such unwanted sediment flushing. Therefore, the third objective of this research is to analyze combinations of hydraulic and mechanical controls of bed load retention.
The development of permeable sediment traps, based on an experimental study of sediment transfer and deposition under varying discharges, is the final objective of this research. Therefore, a novel element in terms of a guiding channel for the flow control in the deposition area is analyzed in combination with permeable barriers aiming at hydraulically and mechanically induced bed load retention.

3 Experimental methods

3.1 Parameters involved and dimensional analyses

A set of potentially relevant parameters Λ is established based on the literature review (Chpt. 2, Figs. 2.3, 2.8 and 2.11):

$$\begin{aligned}\Lambda = f\big(&A,\ a,\ a_i,\ b,\ b_i,\ B,\ C,\ D_{pq},\ E,\ f_f,\ g,\ H,\ h,\ n,\ m,\ m_{bar},\ P,\ Q,\ Q_b,\ R_h,\ S_0,\ \dots\\ &S_{dep},\ S_e,\ S_{eq},\ S_f,\ t,\ u,\ w,\ w_m,\ z,\ \Delta z_{dam},\ \Delta z_{dep},\ \nu,\ \rho_f,\ \rho_s,\ \rho'_s,\ \tau\big)\end{aligned} \tag{3.1}$$

This parameter set contains additionally the time variable t (in s). The representative grain diameter D_{pq} is subsequently substituted by D_{84}, according to literature findings (Ferguson, 2007; Zimmermann, 2010; Rickenmann and Recking, 2011; Recking, 2013b; Ghilardi et al., 2014). The following parameters can be defined as a function of other variables:

- Cross section surface A;
- Total barrier width B;
- Total energy head per unit force E;
- Roughness coefficients f_f, k_{st} and n;
- Wetted perimeter P;
- Hydraulic radius R_h;
- Longitudinal slopes of deposits S_{dep}, energy S_e and transport equilibrium S_{eq};
- Flow velocity u;
- Mean channel width w_m; and
- Bed shear stress τ.

Replacing these parameters in the above set of parameters, Λ reduces to:

$$\begin{aligned}\Lambda = f\big(&a,\ a_i,\ b,\ b_i,\ C,\ D_{84},\ g,\ h,\ m,\ m_{bar},\ Q,\ Q_b,\ \dots\\ &S_0,\ S_f,\ t,\ w,\ z,\ \Delta z_{dam},\ \Delta z_{dep},\ \nu,\ \rho_f,\ \rho_s,\ \rho'_s\big)\end{aligned} \tag{3.2}$$

where the following variables are considered:

- Constriction height a and the clearance height between individual elements a_i;
- Constriction width b and the clearance width between individual elements b_i;

- Chézy coefficient C;
- Representative grain diameter D_{84};
- Gravitational acceleration g;
- Flow depth h;
- Inclinations of the channel bank m and bar screen m_{bar};
- Discharge Q;
- Bed load transport Q_b;
- Slopes of the channel bottom S_0 and the deposit front S_f;
- Time t;
- Vertical elevation z;
- Barrier height Δz_{dam};
- Deposit thickness Δz_{dep};
- Kinematic viscosity ν; and
- Densities of water ρ_f, sediment grains ρ_s and deposits ρ'_s.

The application of the experimental results beyond the laboratory requires the consideration of appropriate prototype conditions. A river inventory was established, based on 132 observations of mountain rivers that are partially equipped with torrential barriers. A complete list of these river datasets is included in Appendix A.1. The design of the experimental set-up was based on this river inventory regarding:

- Ratio of the channel base width w and the D_{84} of the grain size distribution;
- Channel slope S_0;
- River bank slope m; and
- Stage-discharge relations.

These values were used for a pilot study and do not represent a prior application limit. Hence, the experimental set-up is not related to some distinct prototype and model scale. Even though, the geometric relation between the characteristic grain size D_{84} used in the model and the field observations can be attributed to a range between 1:5 and approximately 1:98. However, in the case of sediment transport it is only reasonable to apply the experiments to prototype problems where the geometric scale is larger than 1:40 due to scale effects. The same holds regarding the tested range of channel slopes, i.e., in practice it has to be ensured that S_0>0.020 and S_0<0.055. Further scaling constraints regarding the Froude number and the Reynolds number due to scaling are introduced in the following.
The applicability of the scaled random natural environment to particular real cases can be achieved by respecting geometric length scales, as well as kinematic and dynamic relations. Jansen et al. (1994) list two methods for scaling:

(1) The dimensional analysis, i.e., the derivation of dimensionless Π-groups (Buckingham, 1915) resulting in characteristic figures such as Froude or Reynolds number;
(2) The mathematical description of relevant physical phenomena, i.e., the derivation of scale relations from hydrodynamic equations.

A detailed description of the dimensional analysis based on the Buckingham Π theorem is included in Appendix A.2.1 (according to Yalin, 1971; Barenblatt, 1987; Kundu and Cohen, 2008). The detailed

derivation of scales based on the mathematical description of considered phenomena is included in Appendix A.2.2.
With respect to the similarity of the experimental set-up and to a prototype application, the geometric, kinematic and dynamic scales are coherent in an ideal case. This criterion is only true in the trivial case of all scales being unity, i.e., the model and prototype dimensions are equal. The geometric similarity implies a constant length scale of all object dimensions. The kinematic similarity refers to constant scales of time dependent quantities, such as the flow velocity or discharge. The dynamic similarity implies the geometric and kinematic similarities and requires similar ratios of forces acting on the fluid, for instance, the Froude or Reynolds numbers (Kundu and Cohen, 2008). The similarity in terms of the Froude number refers to a constant ratio of inertia and gravity forces, which is essential for open channel flow. The Reynolds number represents the ratio of inertia and viscous forces, which is important to pipe flow (Kobus and Abraham, 1978).
Thus, Froude similarity is more relevant to this research, underlying that viscous forces can be neglected in turbulent flows, i.e., $Re > 10^5$ (Eq. 2.7). In addition, the similarity of sediment transport, in terms of the critical dimensionless bed shear stress, is of particular importance for the interpretation of this research (Jansen et al., 1994; Barenblatt, 1996; Kundu and Cohen, 2008). The similarity concepts are always respected subsequently, based on the explanations in Appendix A.2.3.
The relevant phenomena vary between the chapters. Thus, different sets of repeating variables apply for the derivation of dimensionless variables (according to Appendix A.2.1 and Yalin, 1977). The dimensional analyses in Chpts. 4 and 5 refer to the repeating variables of h, g and ρ_f; while Chpts. 6 and 7 refer to the repeating variables of D_{84}, g and ρ_f. Comprehensive explanations recall the dimensional considerations in each Chapter, within the framework describing the particular experimental methods.
Further scaling effects may occur due to surface tension which can be assessed through the Weber number (Peakall and Warburton, 1996; Peakall et al., 1996):

$$We = \frac{\rho_f \, u^2 \, h}{\sigma} \tag{3.3}$$

where σ denotes surface tension, i.e., the tensile force per unit length, which is for water at 20° $\sigma = 0.07274$ N m^{-1} (Wagner and Kretzschmar, 2008). The herein applied similitude of the Froude number and sediment transport is in conflict with correct scaling of the Weber number. However, it can be assumed that beyond critical values of $We \approx 10$ to 10^2, scaling effects due to surface tension are negligible. This is ensured in the experiments as the minimum flow depth is larger than 0.03 m, which represents a critical value for the physical modeling of sediment deposition and mobilization (Novák and Cabelka, 1981; Nazari-Giglou et al., 2016).

3.2 Experimental set-up

3.2.1 Installation and working principle

The conception of the experimental set-up is shown in Fig. 3.1. Sediments were stored in a pyramidal vessel, with a rotating rough bottom cylinder to release grains to a system of conveyor belts. Water was supplied by the laboratory pump system. Sediment and water were intermixed in an upstream,

2.5-m-long adaptation reach. The adaptation reach was followed by the 3.0-m-long observation reach, which had a rough trapezoidal section and a variable longitudinal slope between 2 and 5.5 %. The observation reach was framed by an elevated reservoir, with a length and width of 2.5 m × 2.5 m, and a 0.5-m-long outlet. The reservoir geometry was adjusted using an interior timber frame in the last experimental phase, according to the descriptions in Chpt. 7. The flow barriers in terms of constrictions for hydraulic deposition control or rake structures for mechanical deposition control were introduced in the lower third of the observation reach (Fig. 3.1). The outflowing sediment was filtered downstream of the observation reach in a water-permeable basket. Particular adaptations of the model are illustrated in the corresponding chapters (Chpts. 4–7). Pictures of the experimental set-up are included in Appendix A.3.1 (page X.12).

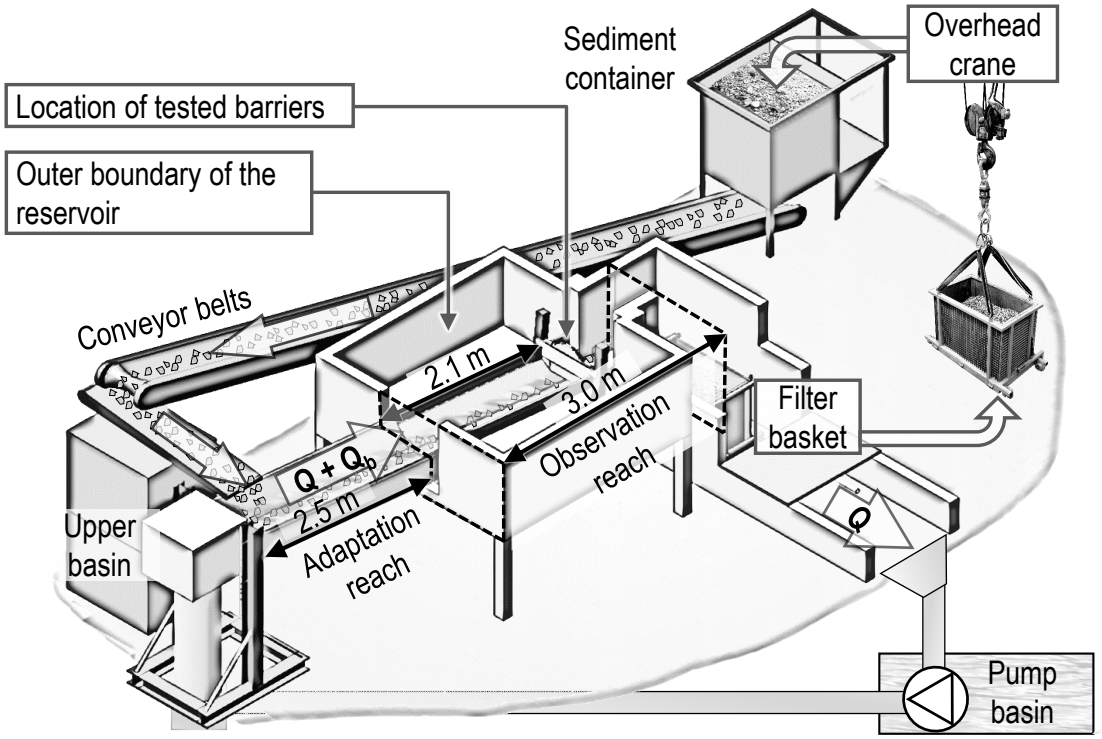

Figure 3.1 – *Conceptual 3D–view of the experimental set-up.*

3.2.2 Sediment characteristics and supply

The dimensionless characteristic grain size distribution of the sediment mixture for the experiments was established based on the river inventory (Chpt. 3.1 and Appendix A.1). Former studies of typical grain size distributions in Alpine rivers were also considered (Hersberger, 2002). Further constraints were:

- The similarity of sediment transport, i.e., the grains needed to be large enough that the characteristic length (D_{84}) is in the plateau of the Shields curve ($\tau_{*cr} \approx 0.047$), i.e., $D_* > 10^2$ (Fig. 2.4, page 15) to allow for up-scaling with invariant critical dimensionless bed shear stress;
- The applicability in the laboratory, i.e., the smallest grains needed to be filterable; this requires that $D_{min} > 0.002$ m.

The delivered, admixed sediment mixture of several gravel classes was verified based on three samples of about 10 kg. The characteristics of the resulting grain size distribution (Fig. 3.2) are listed in Tab. 3.1, including the dimensionless coefficients of curvature $c_u = D_{60} \,/\, D_{10}$ and uniformity $c_c = D_{30}^2 \,/\, (D_{10} \cdot D_{60})$. According to the standards (e.g., ASTM D2487-11, 2011), the sediment mixture is at the limit between the classifications of "well-graded" and "poorly graded" gravel. The mass related mean grain diameter is calculated by $D_m = \sum (D_{pq}\, M_{pq\pm5}) \,/\, \sum M_{pq\pm5}$, where $M_{pq\pm5}$ denotes the weight fraction of the grain size $D_{pq} \pm 5\%$.
The main elements of the sediment supply system are shown in Fig. 3.3. The sediments were stored

Table 3.1 – *Characteristic grain sizes of the sediment mixture used for the experiments, where pq percent of the mixture are finer than D_{pq} (in 10^{-3} m).*

Parameter	D_m	D_{10}	D_{16}	D_{30}	D_{50}	D_{60}	D_{84}	D_{90}	D_{100}	c_u	c_c
Value	10.13	6.71	7.27	8.39	9.65	10.45	13.68	14.78	20.00	1.56	1.00

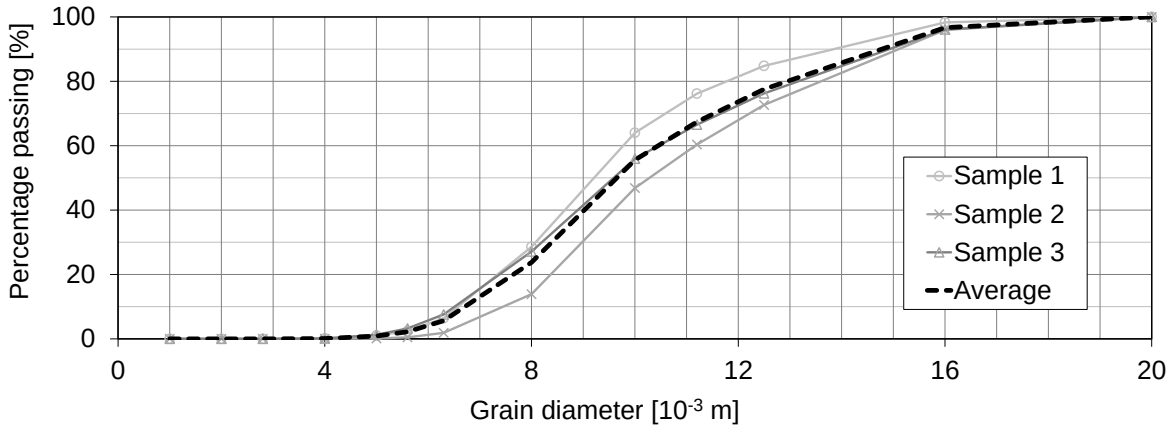

Figure 3.2 – *Sieving curve of the sediment mixture used for the experiments.*

in a pyramidal vessel ①, indicated by the white dashed lines. An electric motor ② drove a cylinder with opening sluices ③ at the bottom of the the pyramidal vessel. The rotation speed of the cylinder was controlled by a mechanical step-down gear ④ and a frequency modulator ⑤ for the fine adjustment. The frequency modulator enabled regular breaks, with a maximum duration of 16 s, to reduce the sediment supply below the minimum of the mechanical step-down gear. A mechanical gate ⑥ was used to enable adjustments of the opening gap at the bottom of the pyramidal vessel. This opening gap was additionally furnished with rubber lips, to prevent a continuous sediment flux through the gap. When the sluiced cylinder turned, the sediment was released in a controlled manner through the gap on a system of conveyor belts ⑧ (cf. Fig. 3.1). A guiding structure below the gap, consisting of wood planks and a rubber lip ⑦ was installed to avoid grain scattering besides the conveyor belt.

The sediments were wetted by an external water source before every experiment to ensure similar initial conditions for every experiment. Pictures of the sediment supply system are shown in Appendix A.3.1 (page X.14).

The system was calibrated in terms of the rotation speed control by the mechanical step-down gear, related to the solid discharge. The sediment release reduction due to the breaks imposed by the frequency modulator were measured subsequently. For the calibration, the gear system was run three times for five minutes. The three single measurements were used to establish a mean value of solid discharge per second, based on the rotation speed and frequency modulation. Thus, the sediment supply rates could be controlled by sediment release rating curves (cf. Appendix A.3.2).

The sediment was collected at the downstream end of the model in a filter basket, with a mesh aperture of 2 mm and mobile bottom. An overhead crane was used to return the collected sediment back to the sediment vessel, by releasing the sediment through the mobile bottom of the filter

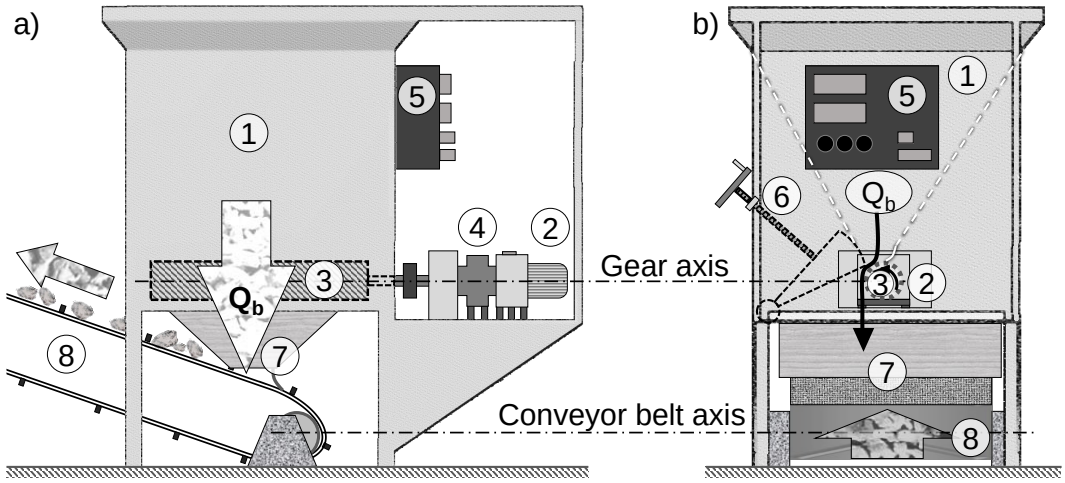

Figure 3.3 – *The sediment supply system, a) side view and b) front view: ① pyramidal sediment vessel; ② electric motor; ③ rotating cylinder with opening sluices; ④ mechanical step-down gear; ⑤ control unit for gear system, with frequency modulator for fine adjustment, and fuses; ⑥ mechanical gate for controlling the sediment release opening clearance; ⑦ sediment guiding structure; ⑧ conveyor belt with lamellae; adapted from Hersberger (2002) and Ghilardi (2014).*

basket (cf. Fig. 3.1). The moving of the sediments is also illustrated by the pictures in Appendix A.3.1 (pages X.13 and X.15).

3.2.3 Rough channel

The trapezoidal 3.0-m-long mountain-river-like, rough channel in the observation reach (applies for Chpt. 4, 5 and 6) had a bottom width of $w \approx 0.11$ m and a bank inclination of $m \approx 2.25 : 1$ (cf. Fig. 2.3, page 11). The channel shape was constituted by a wooden frame. Grains, with a minimum diameter of the D_{84} of the supply mixture, were cast in a concrete bed on a wooden frame, to establish the bed roughness. Two longitudinal steel pipes and cobble filling were used beneath the trapezoidal frame to increase the longitudinal stiffness of the channel (Fig. 3.4). The channel was colored in red, to enable a clear differentiation between the channel bed and sediment deposits based on camera observations.

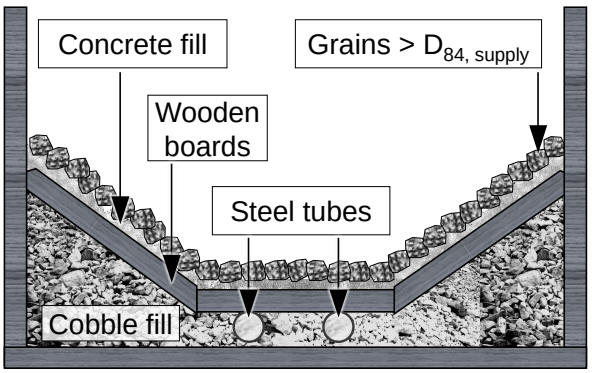

Figure 3.4 – *Conceptual illustration of the cross section of the mountain-river-like channel in the observation reach, with roughness elements (grains larger than the D_{84} of the supply mixture, cast in concrete), wooden boards for the base shape of the channel and stabilization elements (cobble filling and steel tubes).*

3.2.4 Flow constriction

The flow constrictions for the analysis of hydraulic control of bed load retention were introduced in the observation reach approximately 2.1 m downstream of the upper boundary of the observation reach (Fig. 3.1). The constrictions were constituted by mobile PVC elements, which allowed to adjust the height *a* by the mm (Fig. 3.5 a). The width of the PVC elements varied between 0.0025 m, 0.025 m and 0.04 m. Thus, the constriction width could be adjusted by minimum increments of 0.05 m (Fig. 3.5 b). The bottom of the PVC elements over the banks were miter-milled, according to the channel bank slope. The maximum constriction height was conform to the height of the central PVC elements of 0.40 m. The thickness of the PVC elements, i.e., the constriction length in flow direction, was 0.03 m.

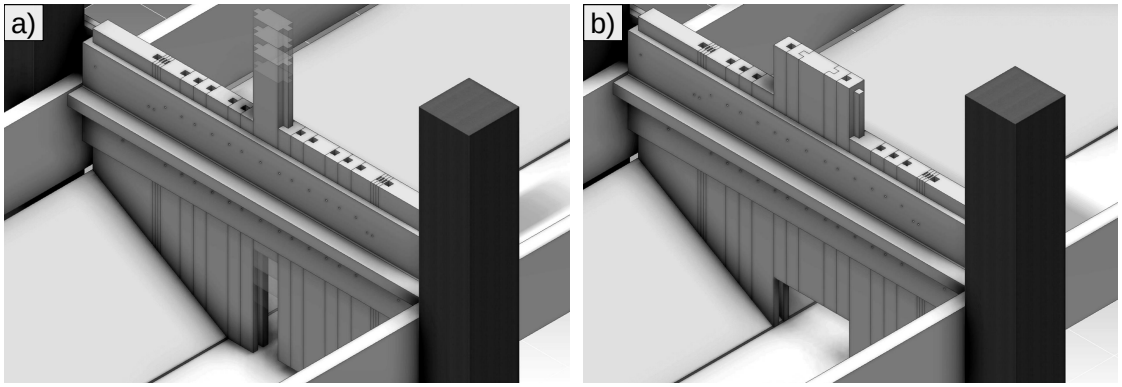

Figure 3.5 – *Illustration of the usage of PVC elements for adjusting the hydraulic constriction height (a) and width (b).*

Pictures of the installation of the channel and the flow constriction are shown in Appendix A.3.1 (page X.13).

3.2.5 Measurement equipment

Channel geometry

The geometric shape of the channel was determined by laser measurements (using a laser of type Leica DISTO D410) below ultrasonic sensors, which were installed for determining the flow depth. An example application is shown in Fig. 3.6 for a channel slope of 5.5 %. These measurements allowed for the precise determination of the flow cross section surface A and hydraulic radius R_h, based on the flow depth measurements.

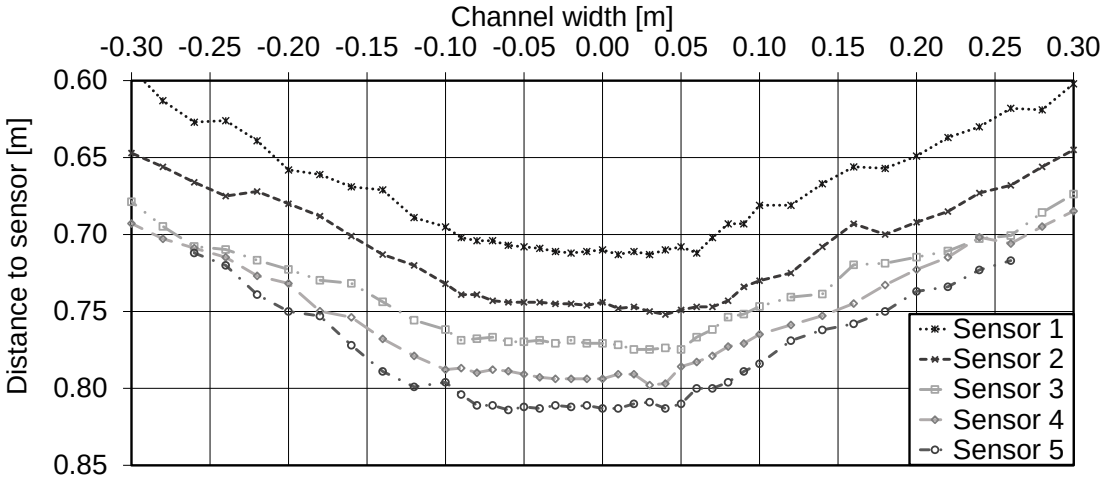

Figure 3.6 – *Example of laser-profile measurements at the ultrasonic probes, for a longitudinal channel slope of S_0 = 5.5 %. The positions of the sensors along the channel are indicated in Fig. 3.8.*

Flow depth

Five ultrasonic sensors (type Baumer UNAM 30, Fig. 3.7) were installed over the longitudinal channel axis, four of them upstream and one downstream of the flow constriction. These sensors emit a conical-shaped ultrasonic signal that is reflected by the water surface and received back by the sensor. The time of flight that the signal takes for coming and going is interpreted by the sensor in terms of voltage variations. The distance (in m) between the sensor and the reflecting object, i.e., here the water surface, can be evaluated by a linear function of the voltage. Thus, the flow depth measurements represent the average of an elliptic surface with a diameter of approximately 0.05 m. The upstream sensor that was closest to the constriction had to be installed empirically, so that the signal did just not interfere with the flow constriction itself. The further three upstream sensors were installed in distances of 0.36 m, 0.91 m and 1.50 m from the constriction-closest probe in the upstream, respectively (Fig. 3.8). The fifth probe was installed 0.24 m downstream of the constriction. Also this position was empirically defined, according to the closest position to the constriction, where no influence of water splashes was observed. The accuracy of the ultrasonic sensors is given in Tab. 3.2.

Figure 3.7 – *Ultrasonic sensor; source: Baumer (2010).*

Discharge

An electromagnetic flow meter (type ABB FXE4000) in the laboratory circuit was used for registering

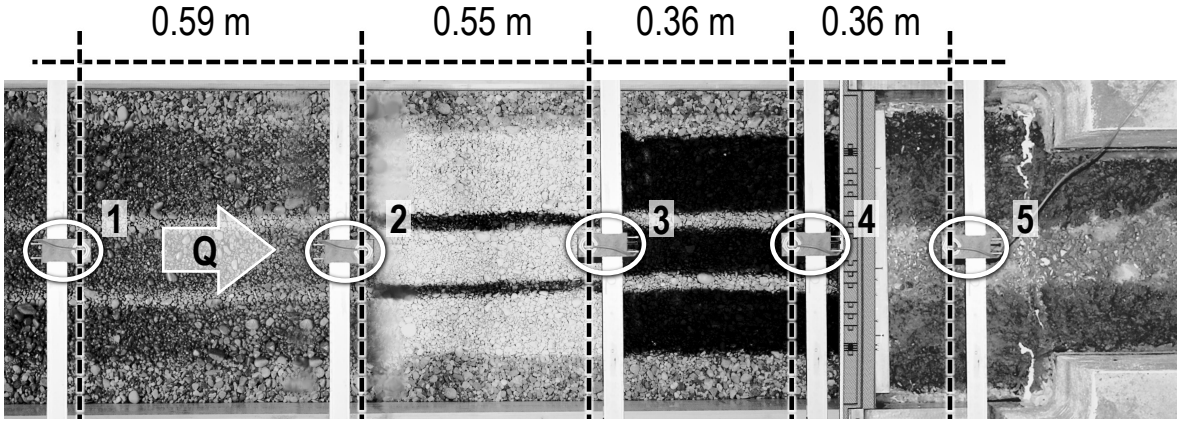

Figure 3.8 – *The positions of the ultrasonic sensors 1 to 5 (highlighted by the white circles), illustrated by a plan view picture of the observation reach.*

the pump discharge (in l/s) every three seconds, with a precision of 0.1 % (Tab. 3.2).

Solid discharge

The solid discharge was evaluated in terms of the outflowing sediment, by minute-wise weight measurements. For intense solid discharges (> 10 kg/min), the sediment weight was measured by a wireless industrial scale (type Dynafor MWXL-5, precision of ± 0.1 %), directly attached between the filter basket and the laboratory overhead crane (Fig. 3.1). As these weight measurements implied the tax weight of the filter basket (207 kg), smaller solid discharges (< 10 kg/min) could be affected by considerable imprecision. Therefore, a dynamometer (precision of ± 1 %) and a small scale (type Kern 440 51N, precision of ± 2 g), with an intermediate sieve in the filter basket, were used for measuring smaller solid discharges. As the usage of the dynamometer is cumbersome in practice, the small scale was preferably used. However, the metering range of the small scale was restricted to 5 kg. Thus, the usage of the three different scales depended on the expected solid discharge:

< 5 kg/min → small scale (type Kern 440 51N);
> 5 kg/min and < 10 kg/min → dynamometer; and
> 10 kg/min → industrial, wireless scale (type Dynafor MWXL-5).

The outflowing water had a significant influence on the weight measurements in the filter basket, which varied depending on the discharge. Therefore, the wet sediment was weighed outside of the flowing water.

Sediment deposits

The volume and pattern of sediment deposits (Chpt. 7) were measured using a motion sensing camera (Microsoft Kinect V2). This application has been shown to be promising, but the results were still affected by uncertainties (Lachat et al., 2015). For this reason, complementary reference measurements were made using the laser. This reference mesh was produced by centimeter-wise measurements along 16 cross sections with an interspace of 0.10 m, which corresponds to approximately 650 point measurements. A technical application of the Kinect V2 is included in

the Appendix (A.3.3). The comparison of both measurement techniques is part of the analysis in Chpt. 7. Moreover, a GoPro Hero4 Silver (2016) camera was used for the observation of the evolution of sediment deposits during relevant experiments.

3.2.6 Error analysis and propagation

The accuracy of the measuring instrumentation was verified by reference test runs with steady flow conditions. Thus, calibration measurements, subsequently denoted by X_{data}, were obtained. These X_{data}-data can be statistically described by its mean value $\langle X_{data} \rangle$ and variance VAR $\langle X_{data} \rangle$, based on the assumption of normally distributed data spreading. The measuring inaccuracies are subsequently considered by the standard error, which is the square root of the variance: $\epsilon = \sqrt{\text{VAR } \langle X_{data} \rangle}$. The comparison between manufacturer's indications and observed errors ϵ_i are listed in Tab. 3.2. The empirically determined values are equal or larger than the instrument errors, as these comprise also other influences such as surface waves of the flow or minute-wise fluctuations of the pump discharge. The combination of quantities, such as the flow depth and the discharge for the dimen-

Table 3.2 – *Accuracy of the measuring instrumentation.*

Device	Unit	Standard error ϵ_i	
		Manufacturer	Measured
Ultrasonic sensors	mm	± 1.0	± 1.0
Laser	mm	± 1.0	
Pump discharge	%	± 0.1	± 1.0
Industrial scale	%	± 0.1	In terms of solid
Dynamometer	%	± 1.0	discharge Q_b:
Small scale	g	± 2.0	± 0.2 %
Kinect V2	mm	< 1.0	cf. Chpt. 7

sionless description of flow characteristics in terms of the Froude number (Eq. 2.8), implies also the combination of singular standard errors ϵ_i. These are subsequently evaluated based on the Gaußian error propagation method, in which singular measured quantities X_i are expressed by a model $f(X_1, X_2, \ldots, X_n)$. Then, the standard error of the model of normally distributed quantities X_i, with singular standard errors $\epsilon_i(X_i)$, based on a 68 % confidence interval is (DIN 1319-3, 1996; Hartung et al., 2005):

$$\epsilon\left[f(X_1, X_2, \ldots, X_i, \ldots, X_n)\right] \cong \sqrt{\sum_{i=1}^{n} \left[\left. \frac{\partial f(X_i)}{\partial X_i} \right|_{X_i = \langle X_{data} \rangle} \right]^2 \cdot \epsilon_i^2(X_i)} \tag{3.4}$$

The model uncertainties related to the measurements are represented in the graphs showing the results: by error bars in the case of little amounts of data; and by dashed confidence-interval-lines of interpolation curves according to the trends in large data sets with significant trends. The quality of these interpolation curves is subsequently assessed by the coefficient of determination R^2, based on a data pair X_{data} and Y_{data} (Hartung et al., 2005):

$$R^2_{Y,X} = \frac{\sum_{i=1}^{n} \left(\hat{Y}_i - \langle Y_{data} \rangle \right)^2}{\sum_{i=1}^{n} \left(Y_i - \langle Y_{data} \rangle \right)^2} \tag{3.5}$$

where Y_i are singular observations (data points); $\langle Y_{data} \rangle$ is the average of the observations; and $\hat{Y}_i$ are estimated observations, resulting from the model $f(X_{data})$.
It always applies that $0 \leq R^2_{Y,X} \leq 1$, which is a measure of the goodness of the model $f(X_{data})$ (curve fitting) derived from measurements X_{data} and Y_{data}. The variation in Y_{data} is perfectly explained by a (interpolated) function of X_{data}, when $R^2_{Y,X} = 1$. Lower values, such as for example $R^2_{Y,X} = 0.38$, can be interpreted as "38 percent of the variance in Y_{data} can be explained by the model" $f(X_{data})$ (Box et al., 2005). R^2 is not a measure of statistical significance (Hartung et al., 2005) and it is used in the following only for the evaluation of the goodness of fit of interpolation curves between variables of interest.

3.3 Experimental campaigns and procedures

3.3.1 Hydraulic control of flow constrictions

The hydraulically induced sediment deposition in rough channels with bed load is experimentally analyzed as follows:

1. Reference tests: determination of the changes in the channel hydraulics and the bed load transport capacity of the non-constricted channel for steady flow, within a range of discrete discharges $Q \in [5.5, 10.0]$ l/s.
2. Introduction of flow constrictions: determination of the channel hydraulics and the bed load transport capacity compared with the flow conditions of the reference tests.
3. Variation of constriction types: vertical flow constrictions with pressurized flow and lateral flow constrictions with free surface flow conditions.
4. Variation of the channel slope: $S_0 \in [0.020, 0.035, 0.055]$ and repetition of the above steps 1–3.

The study procedure is used for the analysis in Chpts. 4 and 5 and it is additionally illustrated in Fig. 3.9. The stage-discharge relations in the non-constricted channel were measured as reference without and with bed load. The corresponding channel roughness was evaluated using the Chézy coefficient. The hydraulic conditions correspond to steady flow, according to a distinct discharge, within a range of $Q \in [5.5, 10.0]$ l/s by increments of about 0.2–0.3 l/s.
The analysis of the hydraulic effects of vertical flow constrictions, with pressurized flow conditions, and lateral flow constrictions, with free surface flow conditions, complete the first fundamental experimental test series.

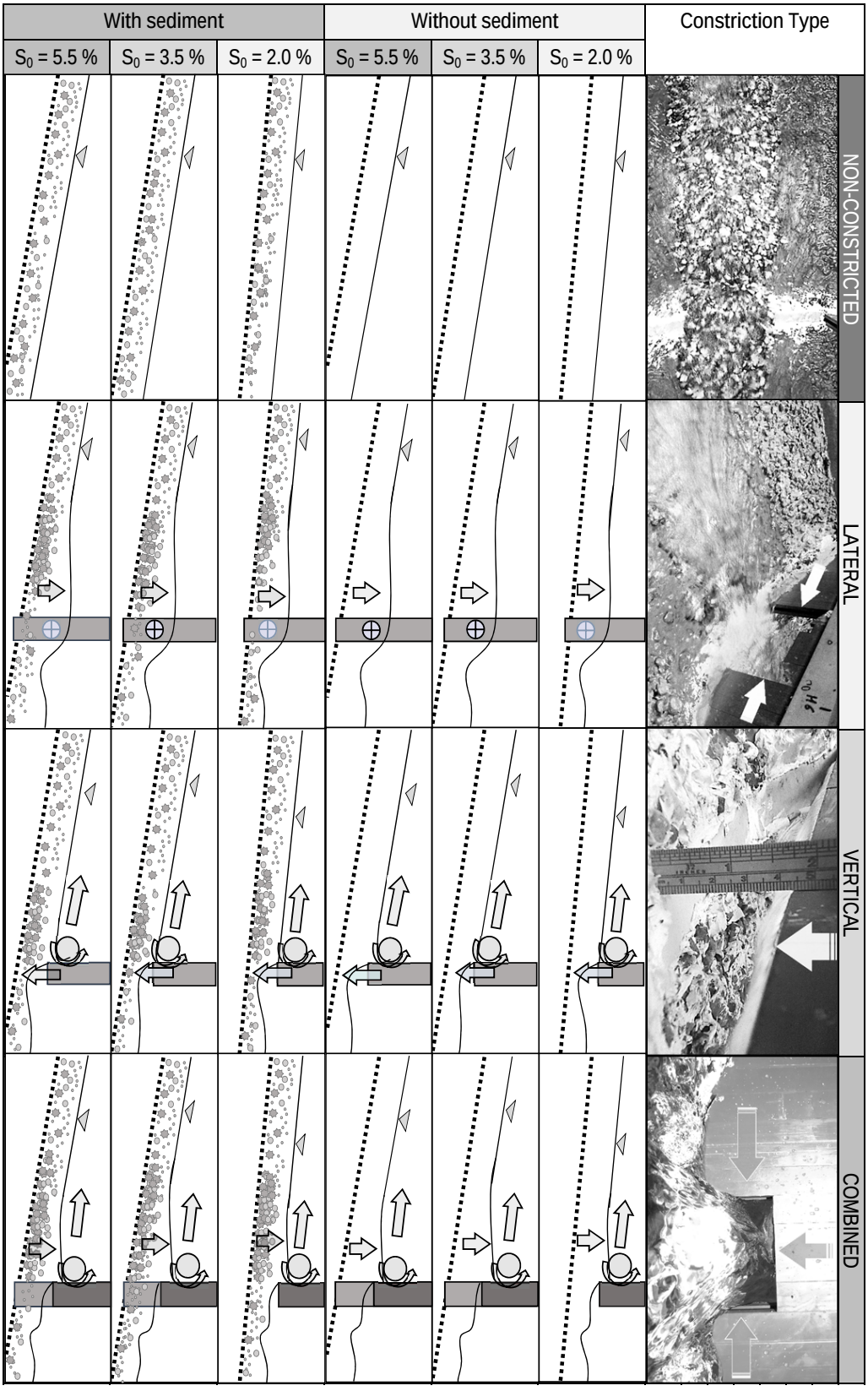

Figure 3.9 – *Experimental campaigns for the analysis of hydraulically induced sediment deposition due to lateral, vertical and combined flow constrictions compared with the non-constricted channel, without and with sediment supply. Varying channel slopes S_0 were applied.*

3.3.2 Sediment deposition and re-mobilization upstream of open barriers

The sediment deposition and re-mobilization upstream of mechanical barriers, flow constrictions for hydraulic control and their combination are studied using a channel slope of $S_0 = 0.055$ (Chpt. 6):

1. Verification and optimization of the obstruction of the mechanical barrier designed based on literature findings.
2. Influence of structure overflow the on sediment transfer through flow constrictions for the hydraulic controlled onset of bed load retention.
3. Effects of mechanical barriers combined with hydraulic flow constrictions on sediment deposition and flushing.

The permeability of sediment traps is preferable for small floods, but it is problematic regarding unwanted sediment flushing. Thus, the occurrence of sediment flushing is studied based on tests with flow constrictions and a mechanical barrier. Obstruction criteria and the design of mechanical barriers were previously studied (cf. Tab. 2.5, page 29). For this research, a mechanical barrier is designed based on state-of-the-art-criteria and optimized with respect to the wanted permeability of sediment traps for small, non-hazardous floods. The possibilities of flow and control of bed load retention with mechanical barriers and hydraulically effective flow constrictions is analyzed in Chpt. 6.

3.3.3 Quasi unsteady flow through permeable sediment traps

Based on the previous findings, *quasi* unsteady flow through permeable sediment traps was studied as follows (Chpt. 7):

1. Consideration of river widenings upstream of sediment and flow control barriers.
2. Analysis of appropriate measures for hydraulic flow control with regard to sediment transfer.
3. Observation of sediment deposition and flushing pattern for quasi unsteady flow, according to some generic flood hydrograph.

The findings from the previous experimental series are applied to establish a concept for permeable sediment traps. The upstream channel is widened in the observation reach to a retention reservoir, with a geometry corresponding to literature findings. The relevance of constructive elements and their application were tested by experiments with *quasi* unsteady flow, based on a generic flood hydrograph. The hydrograph is operated by incremental changes of discrete pump discharges and sediment supply. The duration and amplitude of the rising and falling limbs of the hydrograph are determined according to general hydrological characteristics of mountain rivers. Sediment deposits in the observation reach are analyzed after every hydrograph test. The possibilities and pattern of sediment flushing are examined in particular cases. The detailed experimental modalities and observations are described and discussed in Chpt. 7.

4 Effects of lateral and vertical constrictions on flow in rough steep channels with bed load [1]

Notation hint: The subscripts *nc* and *c* denote "*related to the non-constricted channel*" and "*related to the constricted channel*", respectively. The subscripts 0 and 1 indicate variables related to section 0, upstream of the constriction and section 1, downstream of the constriction. Variables related to roughness are indicated by the subscript *r*.

Abstract

The two-phase flow found at bridges or open check dams is complex, especially when rivers are steep and bed load is present. Undesirable bed load deposition and backwater effects may occur in steep mountain rivers at bridges. In contrast sediment deposition is desirable at open check dams combined with sediment traps. For design purposes, it is necessary to know the discharge and bed load transport capacity across these flow constrictions. Here, the energy losses, discharge and bed load transport capacity of vertical and lateral flow constrictions are experimentally studied in a rough, 2.0-%-inclined, trapezoidal channel. Both free surface and pressurized flow conditions, as caused by lateral and vertical flow constrictions, respectively, were analyzed since both may occur at bridges and open check dams. The discharge capacity is analyzed in detail, with respect to the flow conditions in the constriction. The experiments demonstrate that the vertical flow constrictions cause a faster increase in the backwater depth with increasing discharge than lateral constrictions. The resulting upstream flow conditions on the backwater can be determined by the upstream Froude number, defined as a function of the constriction dimensions. The bed load transport capacity reduces as the upstream Froude number decreases. The practical relevance of the findings is illustrated by a design example of flow constrictions at open check dams.

[1] This chapter is based on the technical paper draft "Effects of lateral and vertical constrictions on flow in rough steep channels with bedload" by S. Schwindt, M.J. Franca and A.J. Schleiss (Schwindt et al., 2017c). The experiments and analyses hereafter are original and were developed by the author.

4.1 Introduction

At open check dams with free surface flow, a lateral flow constriction provokes a critical section (Armanini and Larcher, 2001; Piton and Recking, 2016a). Similar lateral flow constrictions can also be observed at bridges as long as the water level is lower than the vertical clearance height underneath the bridge. Open check dams with a closed crest represent a vertical flow constriction resulting in pressurized orifice flow (Piton and Recking, 2016a). Pressurized flow may also occur during floods at bridges, which may cause unwanted overtopping of the bridge and its abutments (McEnroe, 2009). In addition, open check dams or bridges may comprise combined lateral and vertical constrictions.
To the best of the authors' knowledge, systematic studies of the hydrodynamics coupled with the bed load transport at such flow constrictions are lacking. Therefore, the energy losses, discharge capacity and bed load transport capacity of vertical, lateral and combined flow constrictions are systematically analyzed in this chapter. A moderately steep, rough channel with a 2 % bottom slope was used (cf. Chpt. 3.2.3), which reproduces typical conditions of channels on alluvial fans formed by constant sediment supply (Montgomery et al., 1996; Parker et al., 1998, and Chpt. 2.1). The effects of flow constrictions on the bed load transport capacity of this type of channel are analyzed in terms of the critical bed shear stress and considering the sediment supply at equilibrium transport capacity. With a fixed bed, morphological channel adjustments upstream of check dams are not considered. The problem of the combined trapping of floating objects and bed load, studied by Uchiogi et al. (1996), Lange and Bezzola (2006) and Piton and Recking (2016b) among others, is not considered here.

4.2 Theoretical discharge capacity of flow constrictions

4.2.1 Orifice flow conditions

To estimate the discharge capacity of the flow constrictions, two flow situations are considered at the constriction, given that the constriction imposes a hydraulic jump upstream (transition from super- to subcritical flow, cf. descriptions on page 14):

- Orifice discharge under pressurized flow conditions (vertical and combined constriction) and
- Free surface critical flow (lateral constriction).

The flow situations at vertical, lateral and combined flow constrictions are illustrated in Fig. 4.1, recalling that a denotes the constriction height; b denotes the constriction width; w denotes the bottom width of the channel; m is the channel bank slope; h_0 and H_0 denote the upstream uniform flow depth and energy head, respectively; u_0^2 / (2 g) is the upstream velocity head; h_{cr} is the critical flow depth; u denotes the cross-averaged flow velocity (in m s^{-1}); and g denotes the gravity acceleration (in m s^{-2}). The discharge capacity needs to be evaluated separately for pressurized and free surface flow conditions, which are introduced subsequently.

4.2.2 Pressurized orifice flow

The discharge capacity of pressurized flow constrictions is based on a Torricelli-type formulation for the calculation of the velocity, i.e., $u = \sqrt{2\,g\,h}$, where h denotes the flow depth at the cross section considered. It is thus assumed that the pressure distribution is hydrostatic over the opening height. The approaching flow velocity is non-negligible; hence the kinematic energy head is also non-negligible in the total energy balance. Therefore, the flow depth h is substituted by the energy head H (Chow, 1959).
The pressure flow in combined constrictions requires the decomposition of the cross section geometry in a trapezoidal bottom part and an upper rectangular part (Fig. 4.1 b). For vertical flow constrictions, only the trapezoidal part is relevant (Fig. 4.1 a). The parameter H_t accounts for the head above the trapezoidal part of the opening. In the case of solely vertical constriction, $H_t = H_0$ - a. For composed cross sections (the trapezoidal and rectangular part), $H_t = H_0$ - $(b\text{-}w)/(2\ m)$ (Fig. 4.1 b, c).

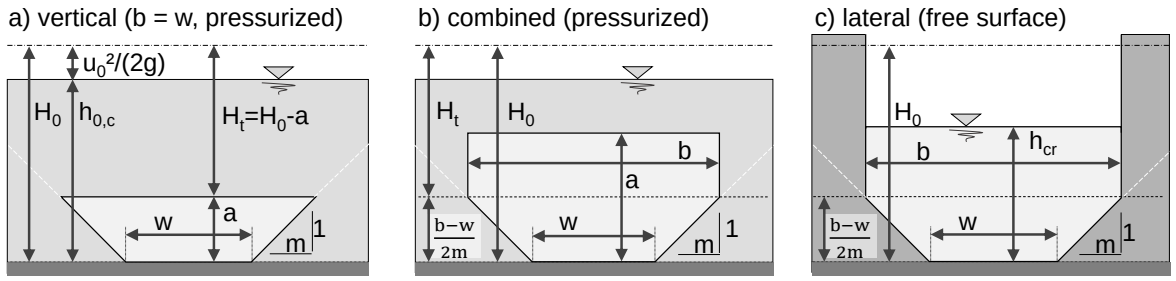

Figure 4.1 – *Flow cross sections of the constriction types considered: a) vertical, i.e., trapezoidal with pressurized flow conditions; b) combination of vertical and lateral with pressurized flow conditions; and c) lateral only with free surface flow.*

Integrating the flow velocity over the opening surface, according to Torricelli's velocity distribution, results in the following expression which is only valid for pressurized flow constrictions (h_0 - $a > 0$):

$$Q_c = \mu_p \sqrt{2g} \cdot \left[\overbrace{\frac{2}{3} w \left(H_0^{\frac{3}{2}} - H_t^{\frac{3}{2}} \right)}^{\text{Center of trapezoid}} + \overbrace{\frac{2}{3} \cdot \frac{H_0}{H_0 - H_t} (b-w) \cdot \left(H_0^{\frac{3}{2}} - H_t^{\frac{3}{2}} \right)}^{\text{Wings of trapezoid}} + \right.$$
$$\left. \overbrace{-\frac{2}{5} \cdot \frac{b-w}{H_0 - H_t} \left(H_0^{\frac{5}{2}} - H_t^{\frac{5}{2}} \right)}^{\text{Wings of trapezoid}} + \overbrace{\frac{2}{3} b \left(H_t^{\frac{3}{2}} - (H_0 - a)^{\frac{3}{2}} \right)}^{\text{Top rectangle}} \right] \tag{4.1}$$

The stepwise derivation of Eq. 4.1 is explained in detail in Chpt. 2.7.5. The discharge coefficient μ_p was introduced in Eq. 4.1 to account for local energy losses and the effects of the vena contracta (Leys, 1976). Von Mises (1917) and Werner (1963) developed a theoretical approach based

on streamlines to evaluate the losses due to the vena contracta as a function of the upstream flow depth, the downstream flow depth and the opening height. The experiments conducted by (Brooke Benjamin, 1955) show that this procedure is accurate for smooth wall conditions. This approach is not suitable for rough flow with bed load such as in the application considered herein. According to Leys (1976), the corresponding inaccuracies are typically accounted for as $\mu_p \in [0.6, 0.7]$. The experimental data from Mejean et al. (2015) confirm this interval. The evaluation of the discharge coefficient μ_p is further developed in this paper for turbulent and rough flow with bed load.
A simplification of Eq. 4.1 applies for purely rectangular flow cross sections ($H_t = H_0$ and $w = b$, cf. Chpt. 2.7.5):

$$Q_{c\,\square} = 2/3 \cdot \mu_p \cdot b \cdot \sqrt{2\,g} \cdot \left[H_0^{\frac{3}{2}} - (H_0 - a)^{\frac{3}{2}} \right] \tag{4.2}$$

Leys (1976) and Zollinger (1983) also applied Eq. 4.1 for free surface flow in lateral flow constrictions. This is questionable because Eq. 4.1 is based on the assumption of a hydrostatic flow velocity distribution, which is an approximation that is only acceptable for pressurized flow conditions.

4.2.3 Free surface flow in the orifice

In the case of free surface flow (lateral constrictions, Fig. 4.1 c), the energy balance according to Armanini and Larcher (2001) can be applied for the derivation of the discharge capacity. These authors equate the total energy per unit force upstream of the constriction and in the constriction. Since the constriction is a control section, the Froude number equals unity here, and the equation can be solved for the discharge. This approach neglects the upstream flow velocity, which needs to be considered here, as mentioned above. The application of the energy balance upstream of the constriction and the control section in a constriction with trapezoidal or composed flow cross section, with consideration of the approach velocity, results in the following:

$$Q_c = \sqrt{2g \cdot (h_{cr} - h_0) \cdot \left(\frac{1}{A_0^2} - \frac{1}{A_c^2} \right)^{-1}} \tag{4.3}$$

The trapezoidal cross section is computed by $A = w\,h + h^2\,m$. For the cross sections of the upstream channel A_0 and the flow constriction, h is substituted by h_0 and h_{cr}, respectively. The approach neglects several local losses at the flow constriction due to three-dimensional flow effects as well as the geometry of the constriction walls. The required correction of Eq. 4.3 is subsequently considered by a factor c_Q, defined as the ratio of observed and calculated discharge:

$$c_Q = \frac{Q_{obs.}}{Q_c\,(\text{Eq. 4.3})} \tag{4.4}$$

The critical flow depth h_{cr} in the constriction is calculated using the Froude number, according to Eq. 2.9 (page 14). The solution to Eqs. 4.3 and 2.9 is iterative, given that the computation of the discharge and the critical flow depth is implicit. For rectangular lateral constrictions, the required

upstream head $H_0 = h_0 + u_0^2/2g$ equals $1.5 \cdot h_{cr}$, and Eq. 4.3 simplifies to (Armanini and Larcher, 2001)

$$Q_c = \frac{2}{3^{3/2}} \cdot c_Q \cdot b \cdot \sqrt{2\,g} \cdot H_0^{\frac{3}{2}} \tag{4.5}$$

A further solution to the discharge capacity of lateral flow constrictions has been introduced by (Kindsvater et al., 1953), as a function of the flow depth upstream and downstream of the constriction, head losses and the approach velocity (Kindsvater et al., 1953):

$$Q_c = c_K \cdot A_1 \cdot \sqrt{2\,g \cdot \left[(h_0 - h_1) + \frac{u_0^2}{2\,g}\,(1 - \zeta_c) \right]} \tag{4.6}$$

A_1 (in m^2) and h_1 (in m) denote the flow cross section surface and the flow depth at the constriction outlet (Fig. 4.2). These quantities are substituted in this chapter by the measurements from the ultrasonic sensor downstream of the flow constriction (sensor positions according to Fig. 3.8 on page 46). c_K is the "*coefficient of discharge*" according to Kindsvater et al. (1953) and is evaluated here analogous to c_Q (Eq. 4.4). The constriction-induced head losses ζ_c are part of the analysis in this chapter.

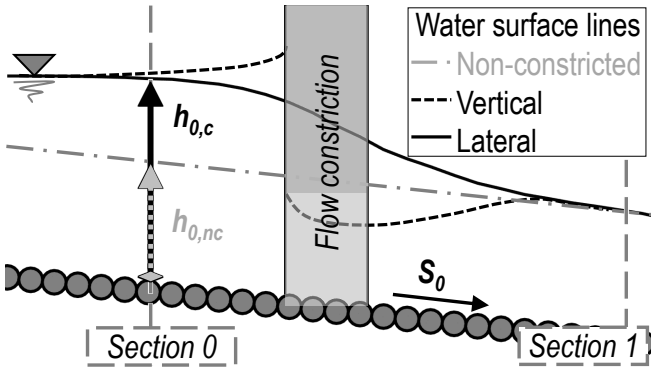

Figure 4.2 – *Sketch of the longitudinal section at the flow constriction with the reference sections 0 (upstream) and 1 (downstream); the water levels and the flow depths $h_{0,nc}$ (non-constricted channel) and $h_{0,c}$ (constricted channel) are qualitatively indicated. S_0 is the channel slope.*

4.3 Methodology

4.3.1 Adjustment of the experimental set-up

The adjustment of the experimental set-up for the tests in this chapter is illustrated in the conceptual sketch of the longitudinal section of the model in Fig. 4.3. The constructive elements are specified in Chpt. 3.2 (page 39 ff.).
The PVC elements were used to adjust the constriction height and width, with a quasi-infinite height (Fig. 4.4); i.e., structure overflow was not possible.
The relevant measurements for this chapter are the flow depth (ultrasonic sensors), pump discharge (electromagnetic flow meter) and solid discharge, according to the specifications in Chpt. 3.2.5.

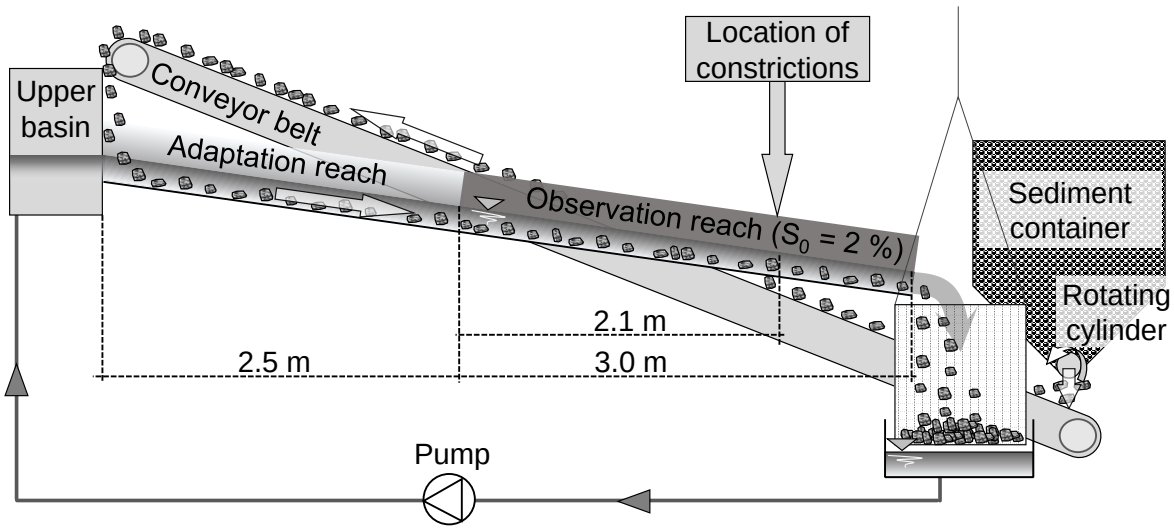

Figure 4.3 – *An illustration of the experimental set-up adjustment (longitudinal cross section) used in this chapter; with indication of the water supply by the laboratory pump system, the sediment supply structure, as well as the channel, with an upstream adaptation reach and a downstream observation reach.*

4.3.2 Experimental data evaluation and procedures

Head losses

For the evaluation of energy losses due to constriction, the energy balance is set in terms of the cross-section-averaged energy per unit force for a 1D uniform distribution of flow velocity across the section (Eq. 2.1, page 11). Where the additional energy losses are due to the flow constriction ($\Delta\ E_c$)between two cross sections. Section 0 is located just upstream of the flow constriction and section 1 downstream of the flow constriction (Fig. 4.2). Moreover, Fig. 4.2 shows qualitatively the flow depths in the non-constricted $h_{0,nc}$ and the constricted $h_{0,c}$ channels at section 0.
The total energy per unit force E consists of the sum of the geodetic height, the piezometric term (the flow depth in this case) h and the kinetic term $u^2/(2g)$ (cf. Eq. 2.1, page 11). The energy balance between sections 0 and 1 is therefore:

$$E_0 = E_1 + \Delta E_r + \Delta E_{Q_b} + \Delta E_c \tag{4.7}$$

The energy losses correspond to the sum of losses due to the channel roughness ΔE_r (Eq. 2.2, page 11), losses due to bed load movement ΔE_{Q_b} (if present, Eq. 2.6 on page 13) and losses due to flow constrictions ΔE_c (if present). The laboratory flume was rectilinear and the roughness losses were dominated by the bed grain friction because no relevant bed forms were allowed in the experiments. Thus, ΔE_r is evaluated in the non-constricted channel without sediment supply using the Chézy coefficient C (in $\mathrm{m}^{1/2}\ \mathrm{s}^{-1}$) according to Eq. 2.2.

C was estimated by applying a 1D numerical code that solves the 1D cross-section-averaged shallow water equation for the flow depth based on a Newton-Raphson scheme. The calculation of the continuous head loss was based on the hypothesis of *quasi*-uniform flow conditions. The simulated values were compared with the data measured along the channel and a global Chézy roughness coefficient C was calibrated using a shooting method (Chapra and Canale, 2010).
According to the literature, the losses due to bed load are $\Delta E_{Q_b} = D_{84} \cdot 1.25 \pm 0.25$ (Eq. 2.6, page 13). The constriction losses ΔE_c depend on the constriction dimension (a, b) and were evaluated in terms of the local loss coefficient ζ_c:

$$\Delta E_c = \zeta_c \cdot \frac{Q^2}{2\ g\ A_0^2} \tag{4.8}$$

Further energy losses, as listed by Piton and Recking (2016a), may occur due to the deposition height in front of the constriction or due to woody debris. Both sediment deposition and driftwood were not considered.

Discharge capacity

The discharge capacity was evaluated according to Eqs. 4.1 (pressurized), 4.3 (free surface) and 4.6 (free surface) using the discharge coefficient μ_p, the correction factor c_Q and the coefficient of discharge c_K, respectively. These coefficients were evaluated in the range of the discharges tested without and with bed load.

Bed load transport capacity

The bed load transport capacity Q_b is the maximum solid discharge that can be conveyed through the non-constricted or the constricted channel for a given discharge (cf. Chpt. 3.2.5, page 46). This capacity corresponds to the outflowing sediment weight measured with the suspended basket. The wet, non-submerged sediment was weighed every minute, outside of the outflowing water jet. The evaluation procedure was repeated for the non-constricted and constricted channels for each geometric configuration of the constriction and for the discharge range considered (Chpt. 3.2.5). The procedure began with a low sediment supply, which was incrementally increased until the first deposits occurred in the channel. The highest sediment supply without sediment deposition in the channel was considered subsequently as the hydraulic bed load transport capacity $Q_b(Q)$ for the discharge in question. A total of 368 data sets were obtained, as listed in Tab. 4.1. The bed shear stress τ corresponding to the bed load transport capacity was derived from the flow depth and discharge measurements. τ was determined first for the non-constricted channel and then for each set-up of lateral, vertical and combined flow constrictions by (cf. Eq. 2.10):

$$\tau = \rho_f \cdot g \cdot S_e \cdot R_h \tag{4.9}$$

where ρ_f denotes the fluid density (1 000 kg m^{-3}). The energy slope was computed by $S_e = u/(C^2 \cdot R_h)$, where R_h denotes the hydraulic radius (in m), based on the water depth h, the channel bottom width w and the bank slope m (Fig. 4.1).

Table 4.1 – *Number of measurements from the non-constricted and constricted channel without and with bed load (Σ = 368).*

Constriction type	Without bed load	With bed load
None	63	34
Vertical only	37	30
Lateral only	74	32
Combined	49	49

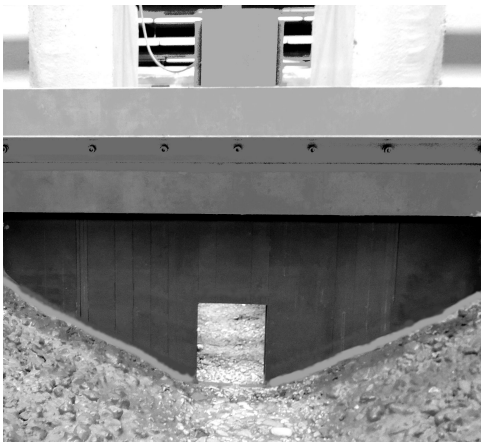

Figure 4.4 – *A picture of the channel with constriction composed of multiple PVC elements (view from upstream to downstream).*

4.3.3 Parameters and dimensional analysis

The hydraulic conditions at the flow constriction can be assessed by the energy balance (Eq. 4.7), which implies the following 17 parameters (here defined generically by the set of variables Λ):

$$\Lambda = f\left(a, b, D_m, g, H_0, h_{0,c}, h_{0,nc}, m, q, q_b, S_0, S_e, w, \nu, \rho_f, \rho_s, \tau\right) \tag{4.10}$$

where it is recalled that S_0 is the channel slope (dimensionless); ν is the kinematic viscosity of water (in $m^2 s^{-1}$); and ρ_s is the grain density (2 680 kg m^{-3}). The flow depth is differentiated between the non-constricted channel $h_{0,nc}$ and the constricted channel $h_{0,c}$ (cf. Fig. 4.2). q and q_b are the discharge and bed load transport capacity per unit width. Since τ (Eq. 4.9) and H_0 are derived from the remaining variables, the system reduces to 15 parameters.
The dimensionless analysis is conducted according to the Π-theorem (Barenblatt, 1987). All parameters stated in Eq. 4.10 are defined by three dimensions: mass M, length L and time T. Therefore, a dimensional matrix of rank $\Re = 3$ is established for deriving $15 - 3 = 12$ Π-groups by applying $h = h_{0,nc}$, g and ρ_f as repeating and linearly independent variables. $h_{0,nc}$ is the discharge-related flow depth of the non-constricted flow at section 0. This leads to the following dimensionless expression (cf. Chpt. 3.1 and Appendix A.2.1):

$$\Pi_\Lambda = f\left(\frac{a}{h_{0,nc}}, \frac{b}{h_{0,nc}}, \frac{D_m}{h_{0,nc}}, \frac{h_{0,c}}{h_{0,nc}}, m, \frac{q}{h_{0,nc}^{\frac{3}{2}}\, g^{\frac{1}{2}}}, \frac{q_b}{h_{0,nc}^{\frac{3}{2}}\, g^{\frac{1}{2}}\, \rho_f}, S_0, S_e, \frac{w}{h_{0,nc}}, \frac{\nu}{h_{0,nc}^{\frac{3}{2}}\, g^{\frac{1}{2}}}, \frac{\rho_s}{\rho_f}\right) \tag{4.11}$$

Finally, the combination of the Π-numbers relevant for this chapter results in the following dimensionless numbers:

- Relative upstream flow depth $h_* = (h_{0,c}/h_{0,nc})^{-1}$, where $h_{0,nc}$ is the uniform flow depth (non-constricted channel) and $h_{0,c}$ is the backwater depth upstream of the constriction;
- Froude number $Fr = Q \cdot \sqrt{(w + 2h_0 m)/(A_0^3 \cdot g)}$;

- Relative constriction height $a_* = a / h_{0,nc}$;
- Relative constriction width $b_* = b \,/\, (w + 2h_{0,nc}m)$;
- Ratio of bed shear stress reduction $\eta = \tau_{0,c} \,/\, \tau_{0,nc} = R_{h,0,c} \cdot S_{e,0,c} \,/\, R_{h0,nc} \cdot S_{e,0,nc}$.

Combined vertical and lateral constrictions are represented by the product of the dimensionless numbers a_* and b_*. Variables related to the constricted and non-constricted channel are indexed with subscripts c and nc, respectively. The index 0 refers to the flow cross section immediately upstream of the constriction.
The reduction in the hydraulic bed load transport capacity η is analyzed with the ratio of the bed shear stress τ in the constricted and the non-constricted channels, at the same position immediately upstream of the constriction, $\eta = \tau_{0,c} \,/\, \tau_{0,nc}$.

4.4 Results and analysis

4.4.1 Energy losses in the non-constricted channel

The energy losses due to roughness were derived based on the cross-section-averaged flow velocity u, in terms of the Chézy roughness coefficient (Eq. 2.2, page 11). The resulting relationship between the discharge and Chézy coefficient C is shown in Fig. 4.5 for the flow without and with bed load. The computation of C is influenced by the error due to averaging along the channel. This results in a maximum error of approximately 23 % between the averaged channel value and the section-related value, mainly due to the averaging procedure. The roughness-induced energy

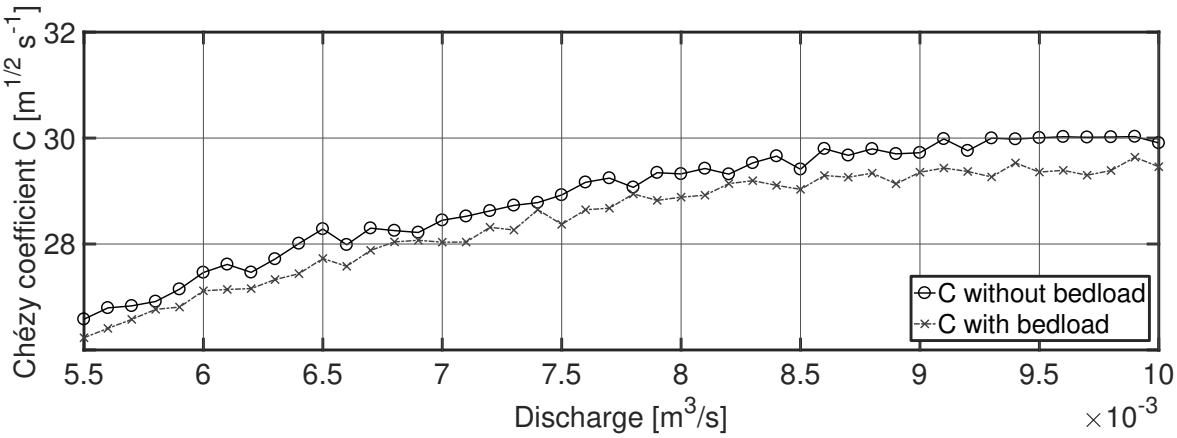

Figure 4.5 – *Evaluation of the Chézy coefficient C for roughness as a function of discharge, without and with bed load (considering the increased discharge volume).*

losses ΔE_r as introduced in Eq. 4.7, are determined subsequently according to Eq. 2.2, where Δx refers to the length between sections 0 and 1.
The effect of bed load was evaluated by comparing the energy losses in terms of roughness without and with bed load. When bed load is present, the average Chézy coefficient C is reduced by a factor of 0.985. This observation may be impacted by the fact that the bed load represents an additional volume that increases the flow depth. The additional flow depth due to bed load is only significant

in flumes steeper than 5 % (Smart and Jaeggi, 1983). However, the bed load transport capacity in the present experiments is only approximately 0.05 to 0.5 % of the total discharge and has no measurable effect on the flow depth. Therefore, compared to other studies where sediment deposits were considered (Uchiogi et al., 1996; Frey et al., 1999; Piton and Recking, 2016a), the influence of bed load is negligible here, i.e., $\Delta E_{Q_b} \approx 0$.

4.4.2 Effect of flow constrictions on the upstream flow

The relative upstream flow depth h_*, provided by the dimensional analysis, was defined by the ratio between the uniform flow depth $h_{0,nc}$ and the backwater depth $h_{0,c}$ immediately upstream of the constriction (Fig. 4.2). The measured relative upstream flow depth h_* is shown in Fig. 4.6 a) as a function of the constriction ratio for the three types of flow constrictions.
The flow conditions upstream are more adequately described by the upstream Froude number Fr_0 as shown in Fig. 4.6 b). Data sets without bed load are indicated by open symbols and those with bed load are indicated by filled symbols.

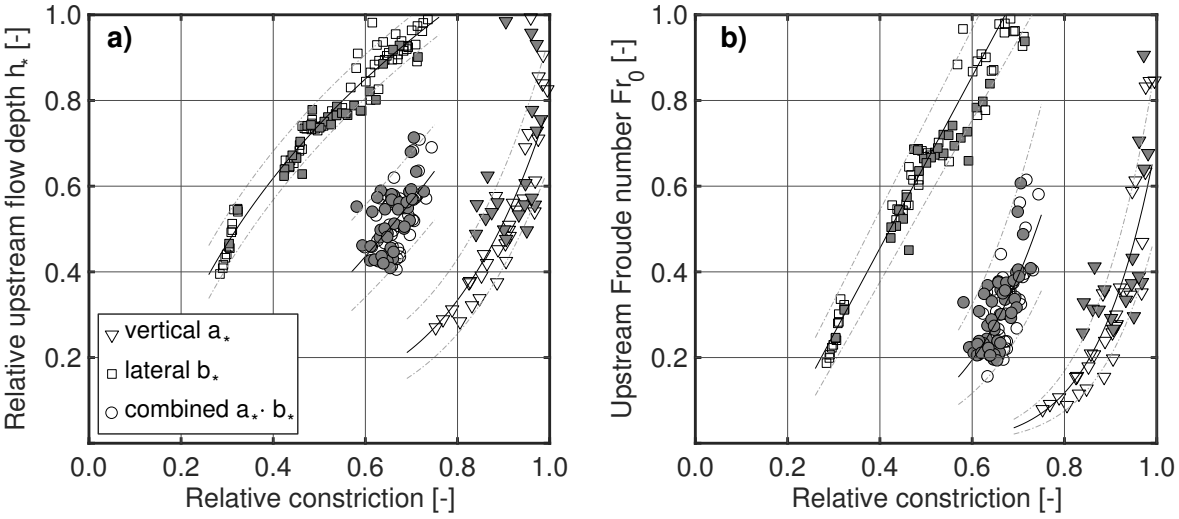

Figure 4.6 – *Experimental values of a) the relative upstream flow depth h_* and b) the Froude number Fr_0 as a function of the constriction ratio. The regression lines according to Eq. 4.12 and Tab. 4.2 are plotted; the dashed lines indicate the standard deviation (68 % confidence interval). The filled data points correspond to measurements with bed load.*

The data may be grouped according to the constriction type (vertical, lateral or combined). Then the relation between the constriction ratio and h_* or Fr_0 is clearly visible, as shown in Fig. 4.6. In the following, the distinction between the three constriction types is only based on how they affect the upstream flow conditions in terms of h_* and Fr_0. The regression curves (gray lines in Fig. 4.6) can be derived based on:

$$Y_{data} = p1 \cdot X_{data}^{p2} + p3 \tag{4.12}$$

For the regression curves indicated in Fig. 4.6, X is replaced by the constriction ratio (vertical a_*, lateral b_* or combined $a_* \cdot b_*$) and Y represents h_* or Fr_0. The coefficients $p1$, $p2$ and $p3$ are

empirical constants as defined in Tab. 4.2. Eq. 4.12 is the definition of a power law equation and is also applied here for the description of linear curves when $p2 = 1$. The goodness of fit of the regression curves is measured using the coefficient of determination R^2 (Eq. 3.5, page 47), which accounts for the variation in the data, as shown for the individual graphs in Tab. 4.2.
Analogous to the evaluation of the roughness coefficient, the results in Fig. 4.6 show that the presence of bed load has no significant influence on the flow conditions upstream of the constriction (relative upstream flow depth h_* and Froude number Fr_0).

4.4.3 Head loss

The energy balance (Eq. 4.7) can be rewritten by setting the head loss ΔE_c equal to the head difference between the reference sections 0 and 1, and by subtracting the continuous loss ΔE_r. The loss ΔE_{Q_b} due to bed load can be neglected, as mentioned above. Based on Eqs. 4.7, 2.2 and 4.8, the local loss coefficient ζ_c can be assessed with the experimental data:

$$\Delta E_c = E_0 - E_1 - \Delta E_r - \overbrace{\Delta E_{Q_b}}^{\approx 0} = \zeta_c \cdot \frac{Q^2}{2\,g\,A_0^2} \tag{4.13}$$

The loss coefficient ζ_c obtained is shown in Fig. 4.7 as a function of the relative upstream flow depth h_* and the Froude number upstream of the constriction Fr_0. The corresponding regression

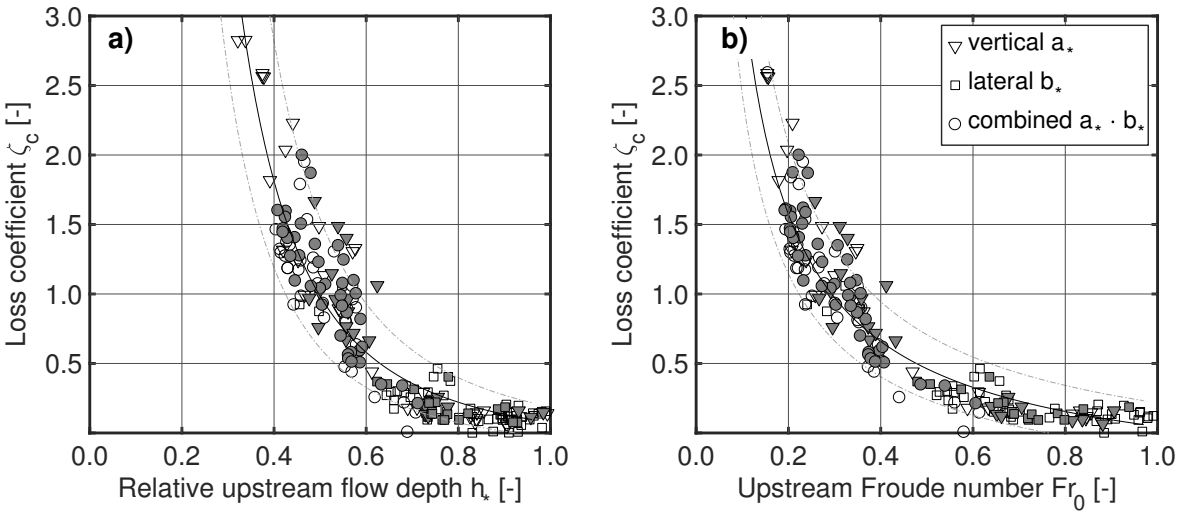

Figure 4.7 – *Experimental values of the loss coefficient ζ_c (Eq. 4.8) as a function of a) the relative upstream flow depth and b) the upstream Froude number. The regression curves are represented, with indication (dashed lines) of the standard deviation (68 % confidence interval). The filled data points correspond to measurements with bed load.*

curves are based on Eq. 4.12, with the coefficients according to Tab. 4.2. It can be noted in Fig. 4.7 that, within the application limits of the experiments, the bed load has no significant effect on ζ_c.

4.4.4 Discharge capacity

The discharge capacity of the vertical, pressurized flow constrictions (Eq. 4.1) knowing the discharge coefficient μ_p. According to the literature, this ranges from approximately 0.6 to 0.7 (Leys, 1976; Zollinger, 1983). Here, μ_p is calculated from the experimental data by substituting the geometrical and measured hydraulic quantities in Eq. 4.1. The values of μ_p obtained are represented in Fig. 4.8 as a function of the relative upstream flow depth and upstream Froude number. The figures show a linear increasing trend of μ_p for low Froude numbers ($Fr < 0.5$) with well-developed backwater ($h_* < 0.7$). The linear regression curves indicated in Fig. 4.8 are based on Eq. 4.12 with the coefficients listed in Tab. 4.2. For higher Froude numbers ($Fr > 0.5$) and relatively small backwater ($h_* > 0.7$), the average of the discharge coefficient μ_p is approximately 0.69 with a standard deviation of ±0.08.

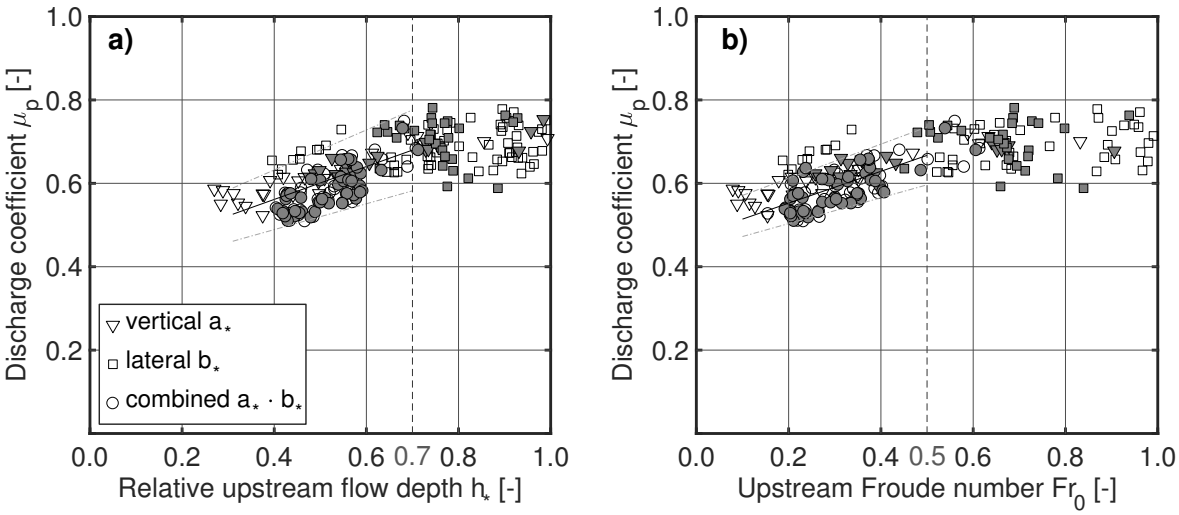

Figure 4.8 – *Experimental values of the discharge coefficient μ_p (Eq. 4.1) as a function of a) the relative upstream flow depth and b) the upstream Froude number. The regression curves, according to Eq. 4.12 and Tab. 4.2, for low Froude numbers ($Fr < 0.5$) with well-developed backwater ($h_* < 0.7$) are plotted; the dashed lines indicate the standard deviation (68 % confidence interval). The filled data points correspond to measurements with bed load.*

Eq. 4.3 can be applied for lateral flow constrictions (free surface flow) and is represented in Fig. 4.9 showing the correction factor c_Q.
Two cases can be clearly distinguished: (1) extensive backwater with rectangular cross sections, where b_* and Fr_0 are smaller than 0.4, and (2) limited backwater with trapezoidal cross sections. In case (1), c_Q increases linearly with rising backwater for both b_* and Fr_0. In case (2), c_Q decreases linearly with rising backwater. The coefficients for the linear regression curves depend on b_* and Fr_0 according to Eq. 4.12 and are given in Tab. 4.2.
The coefficient of discharge c_K in the Kindsvater et al. – formula (Eq. 4.6) for the discharge capacity of lateral flow constrictions, is shown in Fig. 4.10 as a function of the relative constriction width b_* and the upstream Froude number Fr_0.
The regression curves in Fig. 4.10 are based on the power law (Eq. 4.12). The corresponding regression coefficients are listed in Tab. 4.2.

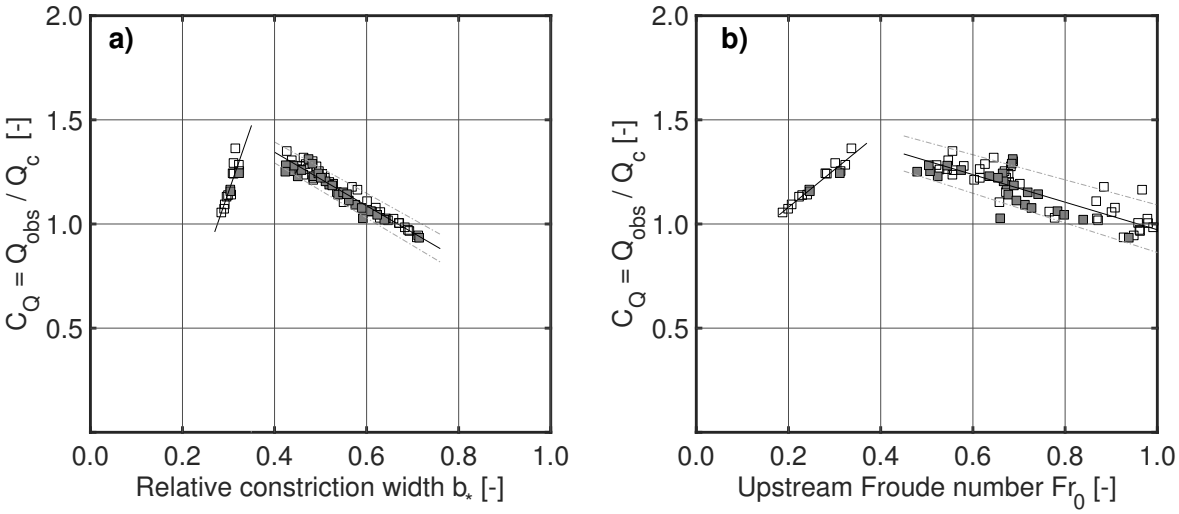

Figure 4.9 – *Correction factor c_Q of the observed and calculated discharge according to Eq. 4.3 as a function of a) the relative constriction width b_* and b) the upstream Froude number for lateral flow constrictions with free surface flow. The regression curves according to Eq. 4.12 and Tab. 4.2 are represented; the dashed lines indicate the standard deviation (68 % confidence interval). The filled data points correspond to measurements with bed load.*

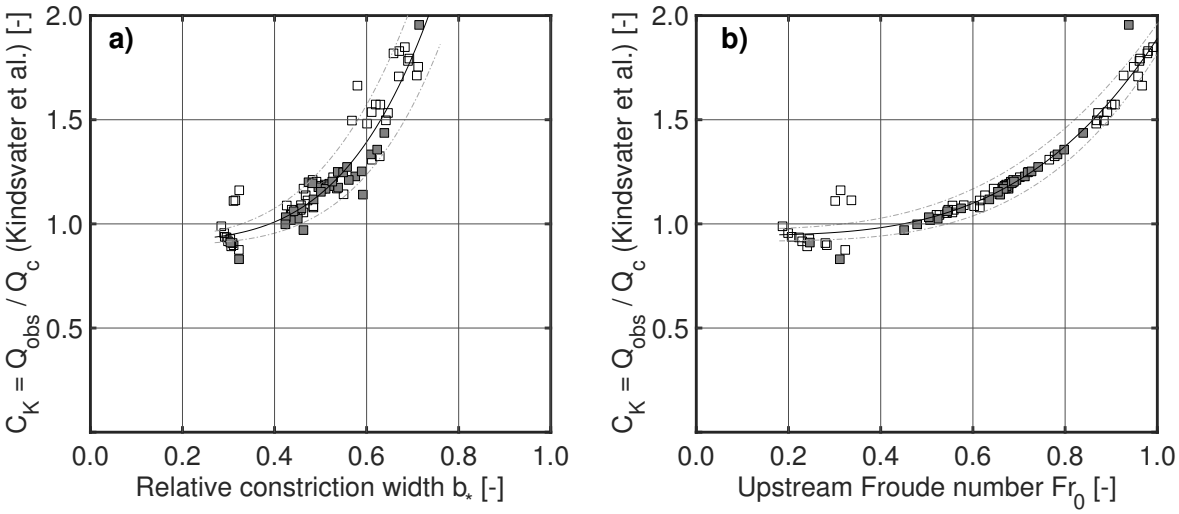

Figure 4.10 – *Coefficient of discharge c_K (Kindsvater et al., 1953) as a function of a) the relative constriction width b_* and b) the upstream Froude number Fr_0 for lateral flow constrictions with free surface flow. The regression curves according to Eq. 4.12 and Tab. 4.2 are represented; the dashed lines indicate the standard deviation (68 % confidence interval). The filled data points correspond to measurements with bed load.*

4.4.5 Effect of flow constrictions on bed shear stress

In the constricted channel, the flow conditions just before the initiation of sediment deposition define the bed load transport capacity, as described in the experimental procedure. Under bed load transport capacity conditions, the value of the bed shear stress corresponding to the constricted channel ($\tau_{0,c}$) is smaller than in the non-constricted channel ($\tau_{0,nc}$). This is shown in Fig. 4.11 using the ratio of bed shear stresses η as a function of the upstream Froude number Fr_0. The regression curve in Fig. 4.11 is described by Eq. 4.12 with the coefficients listed in Tab. 4.2. The corresponding coefficient of determination is close to unity, which demonstrates the good correlation between the upstream Froude number and η.

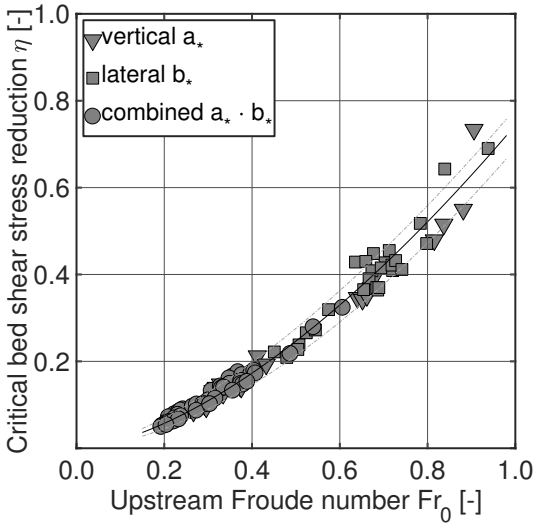

Figure 4.11 – *Ratio of the critical bed shear stress reduction η as a function of the upstream Froude number. The regression curve according to Eq. 4.12 and Tab. 4.2 is represented; the dashed lines indicate the standard deviation (68 % confidence interval).*

Table 4.2 – *The empirical coefficients $p1$, $p2$ and $p3$ of the regression curves shown in Figs. 4.6, 4.7, 4.8 and 4.11, according to Eq. 4.12; the observation ranges are indicated.*

Constriction type	Y	$X \in$ [observation]	$p1$	$p2$	$p3$	R^2
Relative upstream flow depth h_* (Fig. 4.6 a)						
Vertical	$h_*(a_*)$	$a_* \in [0.70, 0.99]$	0.70	4.77	0.09	0.72
Lateral	$h_*(b_*)$	$b_* \in [0.28, 0.76]$	3.18	0.21	-2.01	0.95
Combined	$h_*(a_*, b_*)$	$a_* \cdot b_* \in [0.53, 0.68]$	1.03	1.69	0	0.34
Upstream Froude number Fr_0 (Fig. 4.6 b)						
Vertical	$Fr_0(a_*)$	$a_* \in [0.70, 0.99]$	0.71	8.04	0	0.82
Lateral	$Fr_0(b_*)$	$b_* \in [0.28, 0.76]$	2.01	1.00	-0.35	0.92
Combined	$Fr_0(a_*, b_*)$	$a_* \cdot b_* \in [0.53, 0.68]$	1.96	4.52	0	0.48
Loss coefficient of constrictions ζ_c (Fig. 4.7)						
Relative upstream flow depth	$\zeta_c(h_*)$	$h_* \in [0.38, 0.99]$	0.20	-2.50	-0.12	0.65
Froude number	$\zeta_c(Fr_0)$	$Fr_0 \in [0.17, 0.96]$	0.51	-0.86	-0.46	0.95
Discharge coefficient μ_p (Fig. 4.8)						
Relative upstream flow depth	$\mu_p(h_*)$	$h_* \in [0.70, 0.99]$	0.39	1.00	0.40	0.64
Froude number	$\mu_p(Fr_0)$	$Fr_0 \in [0.50, 0.96]$	0.38	1.00	0.48	0.60
Correction factor c_Q (Fig. 4.9)						
Relative width	$c_Q(b_* < 0.35)$	$b_* \in [0.28, 0.35]$	6.39	1.00	-0.76	0.75
	$c_Q(b_* > 0.4)$	$b_* \in [0.40, 0.76]$	-1.23	1.00	1.86	0.93
Froude number	$c_Q(Fr_0 < 0.3)$	$Fr_0 \in [0.17, 0.30]$	1.81	1.00	0.72	0.95
	$c_Q(Fr_0 > 0.44)$	$Fr_0 \in [0.44, 0.96]$	-0.66	1.00	1.63	0.66
Coefficient of discharge c_K (Fig. 4.10)						
Relative width	$c_K(b_*)$	$b_* \in [0.28, 0.76]$	3.79	4.07	0.92	0.89
Froude number	$c_K(Fr_0)$	$Fr_0 \in [0.17, 0.96]$	0.95	3.56	0.95	0.96
Critical bed shear stress reduction η (Fig. 4.11)						
Froude number	$\eta(Fr_0)$	$Fr_0 \in [0.17, 0.96]$	0.74	1.59	0.0	0.98

4.5 Discussion

4.5.1 Roughness and constriction head losses

The continuous loss due to the roughness of the channel is determined using the Chézy equation (Eq. 2.2). For the present data, the Chézy coefficient increases slightly when bed load is supplied, which indicates an increase in the channel roughness. This increase seems to be related to the higher discharge due to bed load transport because the additional volume of the sediment increases the flow depth. The effect is small; however it is expected to be more significant for steeper channels with slopes greater than 5 % (Smart and Jaeggi, 1983). The total energy losses are then obtained by the sum of the losses due to roughness ΔE_r and due to the flow constriction ΔE_c according to Eq. 4.7, where the bed load-induced energy losses are negligible ($\Delta E_{Q_b} \approx 0$).
The constriction-induced loss coefficient ζ_c is shown in Fig. 4.7 a) as a function of the relative upstream flow depth and in Fig. 4.7 b) as a function of the upstream Froude number. The loss coefficient ζ_c depends more on the upstream Froude number than on the relative upstream flow depth, which is also reflected by the 0.95 and 0.65 coefficients of determination, respectively.

4.5.2 Flow conditions upstream of the constriction

The backwater effects as a function of the constriction ratios are analyzed in Fig. 4.6. On the one hand, a flow constriction causes deep backwater when the relative upstream flow depth h_* and upstream Froude number Fr_0 tend toward zero. On the other hand, the constriction-induced backwater effects are small when h_* and Fr_0 are close to unity.
In practice, the flow depth upstream of a constriction $h_{0,c}$ can be derived from Fig. 4.6 a) on the basis of the flow depth in the non-constricted channel $h_{0,nc}$ and the constriction dimensions a and b. For instance, the dimensionless constriction ratios a_* and b_* can be computed by dividing a and b by $h_{0,nc}$. Then the corresponding relative upstream flow depth h_* can be deduced from the regression lines shown in Fig. 4.6 a). The value of h_* obtained is defined as the ratio of the flow depths in the non-constricted $h_{0,nc}$ and the constricted $h_{0,c}$ channel. Thus, the flow depth in the constricted channel can be assessed by the known value of $h_{0,nc}$ and the estimated value of h_*: $h_{0,c} = h_{0,nc} / h_*$. A similar, discharge-based derivation of $h_{0,c}$ is possible using the upstream Froude number Fr_0, as shown in Fig. 4.6 b).
The minimum and maximum values of h_* and Fr_0 correspond to the maximum and minimum discharges tested: 10.0 l/s and 5.5 l/s, respectively. All constriction types were tested within this same range of discharges. Therefore, the sensitivity of the backwater caused by a certain constriction type can be assessed within the experimental range of h_* or Fr_0.
For vertical constrictions, the reduction in the relative constriction height a_* causes a sharp and prominent decrease in h_* (Fig. 4.6 a), where the minimum and maximum discharges correspond to a 0.72 decrease in h_*. The insertion of a lateral constriction causes a smaller 0.59 reduction in h_*. An analogous observation can be made based on the upstream Froude number Fr_0 (Fig. 4.6 b). Within the range of discharges tested, the vertical constrictions cause a substantial 0.91 decrease in Fr_0, while the lateral constrictions cause a smaller0.80 decrease in Fr_0. These numbers reveal that the development of backwater due to vertical flow constrictions is more rapid with increasing discharge than with lateral flow constrictions.

The experimental data from the combined vertical and lateral flow constrictions show an abrupt, but diffuse decrease in h_* and Fr_0, as a function of $a_* \cdot b_*$. The differences of 0.31 in h_* and 0.45 in Fr_0 indicate a lower sensitivity of $a_* \cdot b_*$ with respect to the discharge. The steepness suggests that the vertical constriction is the governing parameter of combined flow constrictions. However, the correlation between the measurement data from the combined constriction is low, which is also reflected in the low coefficients of determination (Tab. 4.2). An extension of the measurements with the combined constrictions was not possible due to the model limitations regarding the discharge.

4.5.3 Discharge capacity of flow constrictions

Application of a simplified formula for pressurized flow

The application of the general solution to Eq. 4.1 for pressurized constrictions with a trapezoidal bottom requires complex calculations in practice. Therefore, the simplified expression for the discharge capacity in terms of rectangular, pressurized flow constrictions (Eq. 4.2) is often applied. This results in an error relative to the ratio of the constriction width and the channel bottom width (b / w), as well as the ratio of the upstream energy head and constriction height (H_0 / a). The evaluation of this error Err_Q is shown in Fig. 4.12, based on the application of the mean width of the trapeze in the simplified Eq. 4.2: $b = (b + w)$ / 2. Err_Q is plotted in terms of Q_c ▽ (according to Eq. 4.1) and Q_c □ (according to Eq. 4.2):

$$Err_Q = \left(Q_c \square - Q_c \triangledown\right) / Q_c \triangledown \tag{4.14}$$

The set of error curves (Fig. 4.12) for ratios of b / w ranging from 1.5 to 10 indicate an increase in the error for increasing ratios b / w and decreasing ratios H_0 / a. Err_Q is generally smaller than 10 % for ratios of b / $w < 3.0$ or H_0 / $a < 1.3$. However, the field observations from the 132 datasets used for the design of the experimental set-up indicate no case where b / $w > 3.0$. The experiments (Fig. 4.6) show a rapid increase of the orifice submergence, which is proportional to an increase of H_0 / a. The according assumptions that H_0 / $a > 1.5$ and b / $w < 3.0$ are related to errors of $Err_Q \leq 5$ %.
The evaluation Err_Q of is independent of the channel bottom width w, bank slope m and the discharge coefficient μ_p, as these parameters are congruent in Eqs. 4.1 and 4.2. Thus, the application of the simplified expression Eq. 4.2, with the substitution of b by the mean trapeze width, i.e., $b = (b + w)$ / 2, instead of Eq. 4.1 is reasonable in practice.

Discharge coefficients

For the discharge coefficient μ_p, Leys (1976), Zollinger (1983) and Mejean et al. (2015) provide a constant value within the range of [0.60, 0.70]. These observations are confirmed by the present experimental data, but only when $h_* > 0.7$ and $Fr_0 > 0.5$, where $\mu_p = 0.69 \pm 0.08$. For important impounding, i.e., $h_* < 0.7$ and $Fr_0 < 0.5$, the upstream flow conditions significantly influence μ_p which should be considered for the design of flow constrictions based on the linear regression curves shown in Fig. 4.8.
As described above, Eq. 4.1 is inappropriate for free surface flow, which occurs for lateral flow constriction only. The approach used by Armanini and Larcher (2001) considers the constriction

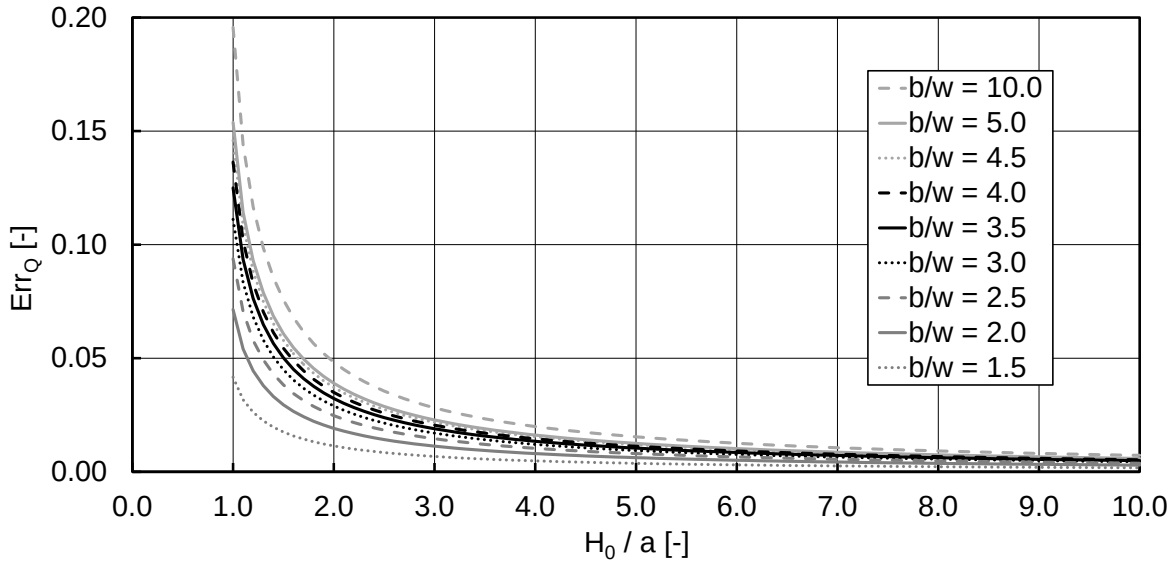

Figure 4.12 – *The relative error Err_Q (Eq. 4.14), when the simplified expression Eq. 4.2 for rectangular constriction shapes is used for (composed) trapezoidal shapes, instead of the correct application of Eq. 4.1.*

as a control section. This approach is further developed here for constrictions with a trapezoidal bottom according to Eq. 4.3 and replacing the flow depth with the energy head. The correction factor c_Q (Eq. 4.3) considers the losses neglected that occur in three-dimensional flow. By neglecting these losses, it can be expected that c_Q will be smaller than unity. However, Eq. 4.3 underestimates the discharge capacity ($c_Q > 1$). Fig. 4.9 also indicates a limit value of b_* and Fr_0, where c_Q has a local maximum. This limit value can be associated with ranges of $b_* = 0.37 \pm 0.03$ or $Fr_0 = 0.40 \pm 0.05$. The comparison of Eqs. 4.2 and 4.5 indicates that $\mu_p = c_Q / \sqrt{3}$. This analogy is only valid for rectangular cross sections with substantial backwater, which is confirmed by the data shown in Fig. 4.9. However, based on the data it is not possible to conclude whether substantial backwater or the constriction geometry (rectangular or trapezoidal) plays a more important role.

Mejean et al. (2015), as well as Piton and Recking (2016a) state that the discharge capacity is underestimated by approximately 11 % when the approach of Armanini and Larcher (2001) is applied for clear water flow. Therefore, Piton and Recking (2016a) recommend applying Eq. 4.1, simplified for rectangular cross sections as described above, also for free surface flow. Eq. 4.3 is physically correct for free surface flow, but the evaluation of the correction factor c_Q indicates unequivocal application limits of Eq. 4.3 for low and high values of b_* and Fr_0.

The expression for the discharge capacity of lateral flow constrictions with free surface flow from Kindsvater et al. (1953) is derived based on the flow depths upstream and downstream of the constriction. Local energy (friction) losses are considered by ζ_c, but further effects due to three-dimensional flow contraction are also not accounted by this approach. The resulting inaccuracies in Eq. 4.6 are considered by the coefficient of discharge c_K, which is best described in terms of a power law-regression curve depending on the upstream Froude number Fr_0 (Fig. 4.10). But, the application in practice is linked to higher uncertainties due to the requirement of estimating the flow conditions upstream and downstream of the constriction. In line with Fig. 4.10, Kindsvater

et al. (1953) and Chow (1959) derive c_K as a function of the relative contraction width. However, these authors state values of $c_K \in [0.87, 1.0]$, i.e., values that are generally smaller than unity. The new experimental data show values of $c_K > 1$. This corresponds to an underestimation of the discharge capacity, which can be attributed to the drawdown of the water surface at the constriction (cf. qualitative curves in Fig. 4.2). With respect to the physical uncertainties in the determination of the flow depth at the outflow section, the application of Eq. 4.3 is still preferable to Eq. 4.6.

4.5.4 Evaluation of the effect on the bed load transport capacity

Only data sets without sediment deposition upstream of the constriction are considered here. However, an effect on the backwater was observed in additional experiments with sediment deposition. Alternatively, the dimensionless bed shear stress related to the hydraulic bed load transport capacity can be derived using the representative sediment grain size D_{pq} instead of $h_{0,nc}$ in the dimensional analysis (Einstein, 1950). This results in the dimensionless critical bed shear stress τ_* (cf. Eq. 2.11, page 14) according to Shields (1936), where η remains unchanged. τ_* varies with the grain mixture, channel roughness and relative submergence (Wilcock, 1993; Recking et al., 2008b; Ferguson, 2012). τ_* increases with decreasing relative submergence of the grains (h/D) and with increasing bed load (Gregoretti, 2008; Recking et al., 2008a). The flow constriction slows down the flow and increases the relative submergence upstream. Consequently, the maximum sediment transport rate decreases. Applying D_m as the representative grain size, the experiments in the non-constricted channel result in $\tau_* \approx 0.07$. This value is significantly higher than suggested by Shields (1936) but reasonable for moderately steep and rough channels (Prancevic et al., 2014). With the introduction of flow constrictions, the energy slope decreases exponentially, and therefore, the dimensionless bed shear stress τ_* and its reduction factor η decrease as well. According to the value of τ_* in the non-constricted channel, bed load transport theoretically ceases when $\eta \leq 0.4$ ($\tau_* \approx 0.03$), which corresponds to $Fr_0 \approx 0.7$. Small amounts of sediment could still pass even when $Fr_0 << 0.7$. However, in the context of check dams, these transport rates are negligible. Therefore, the hydraulic obstruction of open check dams occurs for all types of constrictions when $Fr_0 \leq 0.7$.
Schwindt et al. (2016b) compare the decrease in the absolute bed load transport under capacity conditions as a function of lateral flow constrictions. The authors show that the bed load transport capacity is not influenced by lateral constrictions with relative width ratios larger than 0.9 and drops to zero for relative constriction widths smaller than one-third. These results are in good agreement with the analysis based on the bed shear stress reduction, as shown in Fig. 4.11.

4.6 Application

Piton and Recking (2016a) present a 13-step design approach for sediment traps, where the opening dimensions of the check dam are based on the upstream deposit height. However, the design of sediment traps in terms of flood protection measures is often based on a certain flood discharge and its related bed load transport capacity that endangers downstream dwellers. This requires hydraulically triggered sediment trapping, which is controlled by the size of the check dam opening. The following procedure illustrates the application of the results presented in this chapter to the design of a check dam opening for a certain flood discharge of 50 m^3/s at which the hydraulic sediment deposition triggering is targeted. In the following example, the reference channel is characterized by a trapezoidal cross section with an 8-m bottom width, a 2-% channel slope, a 28-$m^{1/2}/s$ Chézy coefficient and a bank inclination of $m = 2.4$:

- The hydraulics of the non-constricted channel can be determined using the Gauckler–Manning–Strickler formula (Eq. 2.3, page 12).
  For the above-mentioned reference channel, the uniform flow depth for a design discharge of $Q = 50\ m^3/s$ *is* $h_{0,nc} \approx 1.2\ m$.
- The hydraulic bed load transport capacity is close to zero when $\eta < 0.4$ and $Fr_0 \leq 0.7$. The iterative solution to Eq. 2.9 for $Fr_0 = 0.7$ results in $h_{0,c} \approx 1.7$ m. Thus, the relative upstream flow depth is $h_* \approx 0.7$.
- Three different constriction types can be applied to attain a relative upstream flow depth of $h_* \approx 0.7$. Depending on the constriction type, the required dimensions (constriction ratio) can be determined according to Fig. 4.6 a):
  - For a vertical flow constriction, the corresponding relative constriction height is $a_* \approx 0.9$.
    Following the above-introduced example, this results in constriction height of $a = 0.9 \cdot h_{0,nc} \approx 1.1\ m$.
  - For a lateral flow constriction, the corresponding relative constriction width is $b_* \approx 0.5$.
    For the uniform flow depth of 1.2 m, the surface flow width is approximately 13.8 m. Then, the required constriction width becomes $b = 0.5 \cdot w + 2h_{0,c}m \approx 7\ m$.
  - A combined constriction is not considered here because of the low correlation between the measurements with combined flow constrictions.

For the computation of backwater curves or for the design of downstream structures such as scour protection, the constriction-induced local energy losses and backwater are also of interest for higher flood discharges. Computing this requires a boundary condition at the constriction considered. According to the findings in this chapter, the relative upstream water depth h_* or Froude number Fr_0 in close vicinity to the constriction can serve to assess the boundary condition. Based on the above-mentioned design example of a vertical flow constriction for a discharge of 50 m^3/s, the evaluation of the boundary conditions just upstream of a flow constriction and the derivation of related local energy losses for a 10 % higher discharge of 55 m^3/s can be assessed as follows:

- A stage-discharge relation can be established based on the discharge capacity of the constriction.

Considering the sensitive effects of vertical flow constrictions, substantial backwater is already assumed for a discharge of 55 m^3/s, i.e., the upstream Froude number is smaller than 0.5. Therefore, the discharge coefficient μ_p is a linear function of the upstream Froude number. This requires an iterative solution for Eq. 4.1, and the discharge coefficient μ_p according to Fig. 4.8 with Eq. 4.12 and coefficients according to Tab. 4.2. Here, this results in μ_p(55 m^3/s) = 0.50 and Fr_0(55 m^3/s) = 0.06.

- Based on the upstream Froude number Fr_0, the local energy losses can be derived according to Eq. 4.12 and Tab. 4.2, i.e., $\zeta_c(Fr_0 = 0.06) = 0.51 \cdot Fr_0^{-0.86}$ - 0.46 ≈ 5.
- The related reduction of the bed load transport capacity can be computed according to Fig. 4.11.
  In the example, the bed load transport capacity is close to zero ($\eta \approx 0.10$).

The values are based on the assumption that no overflow of the open check dam occurs. As this requires a considerable dam height, in practice, overflow needs to be considered, e.g., according to Khatsuria (2005).

4.7 Conclusions

Flow constrictions in open channel flows, by lateral, vertical or combined constrictions, are experimentally studied in this chapter for hydraulically controlled obstructions in terms of local energy losses, discharge capacity and bed load transport capacity.
Vertical flow constrictions have a significant influence on the upstream Froude number Fr_0. The energy loss from the constriction can be deduced with an empirical function of the upstream Froude number.
The computation of the discharge capacity of flow constrictions requires a correction factor that is considered in terms of the discharge coefficient μ_p for pressurized orifice flow. For substantial backwater ($Fr_0 < 0.5$), μ_p is a linearly increasing function of the upstream Froude number. For less significant backwater ($Fr_0 > 0.5$), μ_p is approximately constant with values of 0.69 ±0.08. An approach for free surface flow conditions in the constriction is bound to some limit value of Fr_0.
Extensive equations for the discharge capacity of compound, trapezoidal constrictions can be substituted by simple expressions for rectangular constrictions. The amplitude of resulting computation errors is reasonable (< 5–10 %).
For the 2-% channel slope tested, the influence of bed load transport is negligible with regard to the hydraulic characteristics in terms of the flow depth of the non-constricted channel. Additionally, the local constriction-induced energy loss, the flow conditions upstream of the constriction and its discharge capacity present no significant sensitivity to the presence of bed load under the experimental conditions.
The constriction reduces the bed load transport capacity of the flow. This reduction can be assessed by the ratio of the critical bed shear stresses in the constricted and the non-constricted flow. The critical bed shear stress ratio can be empirically predicted when the upstream Froude number is known. In particular, the bed load transport capacity of the channel is very low when the Froude number upstream of the constriction is smaller than 0.7.

5 The influence of the channel slope in hydraulically constricted channels [1]

Abstract

Instream open check dams are essential for flood protection in mountainous regions. These structures comprise an opening acting as a lateral or vertical flow constriction to force sediment deposition when floods occur. Otherwise, the constriction should not affect the runoff. Design criteria for the discharge capacity referring to the size and geometry of the opening were previously established. This experimental study reviews the existing formulae for the discharge capacity and analyzes the beginning of sediment deposition, with varying channel slopes. The effects of the channel slope on backwater, sediment deposition and local head losses are relevant when free surface flow conditions persist in the opening. A channel slope-sensitive correction factor is introduced for calculating the discharge capacity. The sediment transfer rate through the constriction decreases with increasing backwater and is most sensitive in transcritical flow conditions. The findings are validated against a case study in the Swiss Alps.

[1] This chapter is based on the scientific article draft "Bottom slope influence on flow and bedload transfer through contractions" by S. Schwindt, M.J. Franca and A.J. Schleiss (Schwindt et al., 2017b). The experiments and analyses hereafter are original and were developed by the author. The measurement data are included in the Appendix (A.4.1).

5.1 Introduction

The discharge capacity in the presence of bed load transport and the evolution of critical bed shear stresses at flow constrictions as encountered at open check dams or bridges were studied in the previous chapter (Schwindt et al., 2017c), for a single channel slope.
Popular bed load transport formulae suggest a non-linear relation between bed load transport and the channel slope (Smart, 1984; Rickenmann, 1991; Recking, 2013b). Therefore, it can be assumed that there is a direct link between the channel slope and the sediment deposition due to open check dams. In this chapter, the discharge and the bed load transport capacity are studied for hydraulically controlled openings under steady state conditions for varying channel slope.
The tests were performed in the previously introduced rough trapezoidal channel for three different channel slopes, taking into account that open check dams are characterized either by free surface or pressurized flow conditions. The results allow the formulae for the discharge capacity to be modified to account for the channel slope. The slope-dependent reduction in the bed load transport capacity and the energy head losses are analyzed as functions of the flow conditions upstream of the flow constriction.

5.2 Methodology

5.2.1 Adjustment of the experimental set-up

Similar to the first test series (Chpt. 4), openings of check dams were tested in terms of barriers with a slit, i.e., lateral constrictions with free surface flow, and barriers with a slot orifice, i.e., vertical flow constrictions with pressurized flow conditions in the case of flooding. The constriction types and the corresponding dimensions of height a (in m) and width b (in m) are recalled in Fig. 5.1.

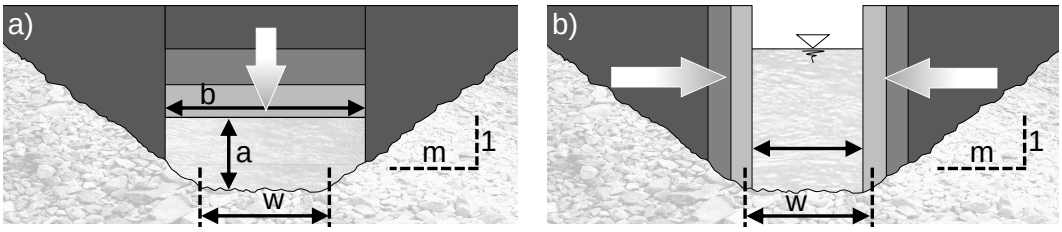

Figure 5.1 – *The constriction types analyzed in this chapter: a) pressurized flow conditions in vertical constrictions with height* a *and b) free surface flow conditions in lateral constrictions with width* b*; placed in the trapezoidal channel with bank slope* m ≈ *2.25 and bottom width* w ≈ *0.11 m.*

The sediment supply mixture remained unchanged, with the characteristic parameters listed in Tab. 3.1 (page 42). Also the channel roughness and its trapezoidal cross section, characterized by the bank slope m of approximately 2.25 and the base width w of approximately 0.11 m, correspond to the previous test series (Chpt. 4). This chapter is focused on the effects of the channel slope S_0 which was consecutively varied between values of 2.0 %, 3.5 % and 5.5 %, as indicated in Fig. 5.2.
The local head losses caused by the flow constrictions are considered by the previously introduced loss coefficient ζ_c (Eq. 4.13, page 61), based on the cross-section-averaged energy balance defined per unit force (Eq. 4.7, page 56).

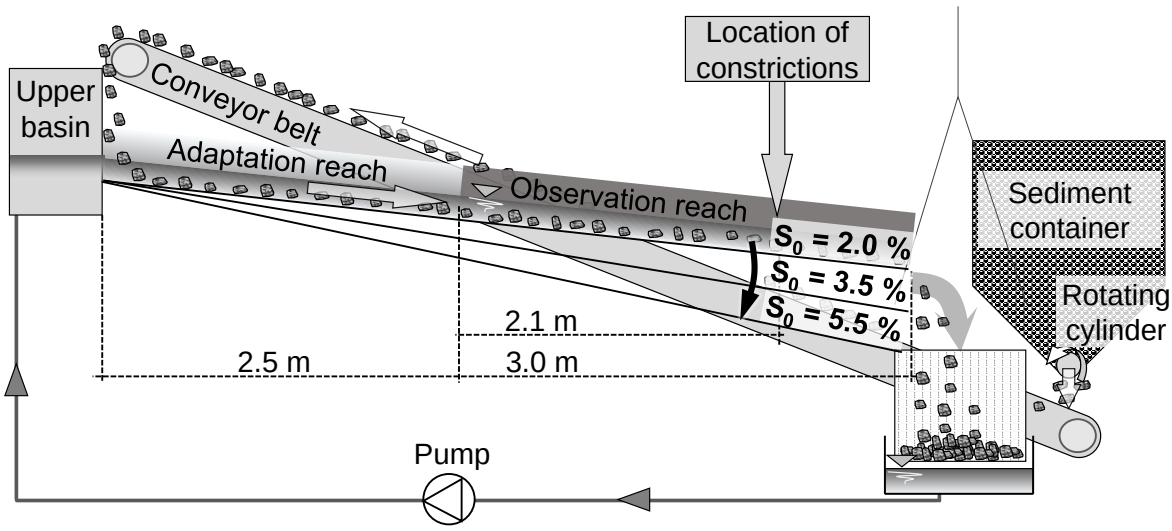

Figure 5.2 – *Schematic illustration of the model adjustments in terms of the variation of the channel slope S_0 by 2.0 %, 3.5 % and 5.5 %.*

The analysis in this chapter refers to the following measurements (cf. Chpt. 3.2.5, page 45 ff.):

- Flow depth (ultrasonic sensors);
- Flow rate (electromagnetic flow meter);
- Sediment outflow (scales); and
- Geometric channel and constriction dimensions (laser and caliper);

A total of 925 experimental runs with flow constriction and 202 reference tests in the non-constricted channel were conducted with and without a supply of bed load corresponding to transport capacity conditions, as listed in Tab. 5.1.

Table 5.1 – *Number of experimental runs in the non-constricted channel as reference and in the constricted channel with and without sediment supply at bed load transport capacity Q_b.*

Flow condition	**Non-constricted**		**Free surface**		**Pressurized**		**Total**
Sediment supply	–	Q_b	–	Q_b	–	Q_b	
Experiments with S_0 = 2.0 %	63	34	74	32	82	83	368
Experiments with S_0 = 3.5 %	31	24	58	58	116	124	411
Experiments with S_0 = 5.5 %	25	25	61	59	85	93	348
Total	119	83	193	149	283	300	1 127

The slope-dependent solution to the discharge capacity requires the separate consideration of the free surface and pressurized flow at the constriction.

5.2.2 Free surface flow

The relation between the discharge and the flow depth upstream of lateral flow constrictions has been analyzed in the previous chapter, based on the expressions from Kindsvater et al. (Eq. 4.6,

page 55) and Armanini and Larcher (Eq. 4.3, page 54). The equation from Kindsvater et al. leads to consistent results consideration the coefficient of discharge c_K as a function of the upstream Froude number (cf. Fig. 4.9, page 63). However, Eq. 4.6 refers to the flow characteristics from upstream and downstream of the constriction. This makes the application of Eq. 4.6complex and computational error-prone. The equation from Armanini and Larcher is based on the upstream flow conditions only and the theoretic critical flow depth in the constriction. But the uncertainties in the computation, e.g., related to the position of the critical flow section in the constriction or the length of the drawdown of the backwater curve, result in ambiguous evaluation trends. Moreover, the former equations (Kindsvater et al., 1953; Armanini and Larcher, 2001) do not imply the channel slope directly and under- or overestimate the discharge capacity (Piton and Recking, 2016a; Schwindt et al., 2017c).

The approaches from Kindsvater et al. (1953) and Armanini and Larcher (2001) are combined here, considering the outflow section of the constriction as a control section and also accounting for the channel slope. It is assumed that the position of the control section can be related to the channel slope S_0 and the drawdown length L_w of the maximum backwater depth, as indicated by the qualitative backwater curve shown in Fig. 5.3. Thus, L_w describes the distance between the location where the backwater depth is maximum and the control section. The position, where the maximum backwater depth was measured by the ultrasonic sensor, could not be varied along the channel axis in the tests. Hence, this position did not correspond exactly to the varying beginning of the drawdown curve.

The assessment of the drawdown length related to the discharge capacity Q_c requires a complex iterative solution with the three unknown variables of Q_c, h_0 and L_w. Therefore, a simplified solution is investigated here by assuming that the drawdown length is a slope-dependent multiple f_c of the constriction thickness, which is 0.03 m, i.e., $L_w = f_c \cdot 0.03$ m. The factor f_c is an empirically driven, dimensionless constant that is evaluated here in terms of the slope-sensitive drawdown length.

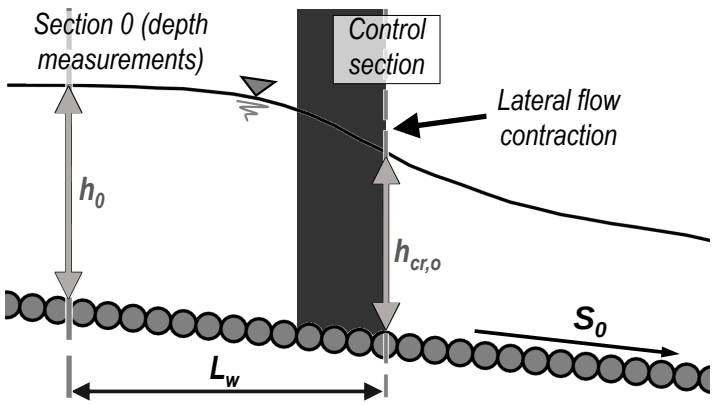

Figure 5.3 – *Qualitative sketch of the water surface at lateral constrictions, indicating the drawdown length L_w, the flow depths at the upstream section 0 and the control section, and the channel slope S_0.*

Introducing f_c into a combination of the equations from Kindsvater et al. (1953) and Armanini and Larcher (2001) results in the following equation for the discharge capacity (in $m^3\ s^{-1}$) of sharp-edged

lateral flow constrictions with regard to varying channel slopes:

$$Q_c = c'_{KQ} \cdot A_0 \cdot \sqrt{2\,g \cdot \left(\frac{3}{2} h_{cr,o} - h_0 - f_c \cdot S_0 \cdot L_w\right)} \tag{5.1}$$

Here, $h_{cr,o}$ denotes the critical flow depth at the outflow section of the lateral constriction (in m). Energy losses originate from several factors, such as flow constriction or the constriction edge shape. Further calculation errors are due to the averaging over the flow cross section. The resulting inaccuracy is taken into account by Kindsvater et al. (1953) in terms of the previously tested coefficient of discharge c_K (dimensionless). In Eq. 5.1, a modification is introduced in terms of the slope-corrected coefficient of discharge c'_{KQ} (dimensionless).
Moreover, the widely used Eq. 5.2 is evaluated in terms of the discharge coefficient μ_f (dimensionless), where H_0 (in m) denotes the head upstream of the constriction (Leys, 1976; Zollinger, 1983; Piton and Recking, 2016a).

$$Q_c = \mu_f \cdot b \cdot \sqrt{2\,g} \cdot H_0^{\frac{3}{2}} \tag{5.2}$$

With respect to the former findings (cf. Fig. 4.12, page 68), b is substituted by the mean width of the trapezoidal flow cross section. Eq. 5.2 implies the integration of the flow velocity under pressurized flow conditions. However, this hypothesis is problematic at the free water surface in the absence of any hydrostatic pressure (cf. Chpt. 4.5.3). The additional inaccuracy due to this assumption is evaluated in this chapter with respect to varying channel slope.

5.2.3 Pressurized flow

Vena contracta effects occur in the case of pressurized flow through the constriction. The discharge capacity is determined by integrating vertically over the constriction and considering the total head H_0. The simplified formula for rectangular shapes is subsequently also applied for trapezoidal cross sections, where b can be replaced by the mean width of a trapezoid (cf. Fig. 4.12, page 68):

$$Q_c = \frac{2}{3} \mu_p \cdot b \cdot \sqrt{2\,g} \left[H_0^{\frac{3}{2}} - (H_0 - a)^{\frac{3}{2}}\right] \tag{5.3}$$

The discharge coefficient μ_p was the focus of earlier studies; however, it still represents a factor of uncertainty in steep channels in the presence of bed load transport. Therefore, μ_p is evaluated in the following with regard to the effects of changing channel slopes.

5.2.4 Bed load transport

The bed load transport capacity Q_b related to the discharge is determined through the sediment outflow measurements as the maximum bed load transport rate that does not cause sediment deposition in the observation reach (Fig. 5.2). Its effect on the flow depth is considered by adding the volumetric bed load transport to the water discharge. Thus, bed load increases the flow depth, and therefore, represents an additional energy sink in the flow.
The measured bed load transport capacity in the non-constricted channel is compared to the

results of the bed load transport equations from (1) Smart and Jaeggi (1983) / Smart (1984) and (2) Rickenmann (1991). Both expressions were experimentally derived on steep channels with a mobile bed and boundaries that confine the channel slope. Many other equations for the assessing bed load transport can be found in the literature (cf. Chpt. 2.3.2); however, such equations often have restrictions such as limited sediment supply due to bed armoring and effects of non-linearity or limitations in terms of the channel slope.

5.2.5 Dimensional considerations

The hydraulics and the slope-dependent effect of flow constrictions on the bed load transport capacity are described by the following set of parameters:

$$\Lambda = f\left(a, b, g, h, S_0, m, Q, Q_b, z, \nu, \rho_f, \rho_s\right) \tag{5.4}$$

The previous analysis (Chpt. 4) has shown that both the upstream flow depth and the Froude number are relevant to the description of the hydraulics of flow constrictions. Based on these findings, the theoretic critical flow depth h_{cr} of the non-constricted channel is used in this chapter. h_{cr} is evaluated by the solution to Eq. 2.9 (page 14), provided that the Froude number is unity. Thus, h_{cr} depends only on the discharge, and therefore, it is independent from all other measurements. With respect to these considerations, a dimensional matrix, consisting of the three independent variables of g, ρ_f and h_{cr}, is applied to the dimensional analysis according to Chpt. 3.1 (page 37). For the evaluation of the results, the following dimensionless variables are retained:

- Relative transcritical constriction height $a_{*cr} = a \,/\, h_{cr}$;
- Relative transcritical constriction width $b_{*cr} = b \,/\, h_{cr}$;
- Relative transcritical upstream flow depth $h_{*cr} = (h_0 \,/\, h_{cr})^{-1}$;
- Channel slope S_0;
- Density ratio $s = \rho_s \,/\, \rho_f$; and
- Dimensionless bed load transport capacity referring to the non-constricted critical flow depth $Q_{b*cr} = \frac{Q_b}{A_{cr}\sqrt{g\, h_{cr}\, (s-1)\, \rho_f}}$.

The inverse of the normalization of the upstream flow depth is used here to obtain an analogy to the Froude number; i.e., for subcritical flow, the relative upstream flow depth h_{*cr} is smaller than unity, and for supercritical flow, it is larger than unity.
With the introduction of lateral or vertical flow constrictions, the bed load transport capacity of the channel decreases. This reduction is measured here by the ratio of the bed load transport capacity of the constricted and non-constricted channels:

$$\theta = \frac{Q_{b*cr}(\text{constricted})}{Q_{b*cr}(\text{non-constricted})} \tag{5.5}$$

5.2.6 Case study for validation

The results obtained from the experiments are validated by stage-discharge measurements from a 1:42 scaled physical Froude model. This model served for optimizing an instream open check

dam at the Dranse River upstream from the town of Martigny (Switzerland). This check dam has an opening with a height of 2.5 m and a width of 4 m, as well as two spillways with a width of 10 m each and a 4 m wide central column (Fig. 5.4). The upstream river section is characterized by a trapezoidal cross section, with a base width of approximately 12 m, a bank slope of 1:1 and a channel slope of 2.4 %. For model discharges up to approximately 2.9 l/s (corresponding to 33 m^3/s in prototype), the opening represents a lateral flow constriction with a theoretical discharge capacity according to Eq. 5.1. The opening is under pressure for higher discharges, where Eq. 5.3 applies. The spillways are activated when the discharge exceeds 5 l/s, i.e., 57 m^3/s in the prototype (Schwindt et al., 2016a). The performance of Eqs. 5.1 and 5.3 is evaluated by comparing the computed discharge (Eqs. 5.1 and 5.3) with the measured discharge of the site-specific physical model. The discharge of the spillways is evaluated considering the approach described by Khatsuria (2005).

Figure 5.4 – *Scaled model (1:42) of the in-stream check dam at the Dranse, Martigny (Switzerland), with opening, central pile and spillways; view from upstream.*

5.3 Results

The establishment of some relationship between the constriction geometry and its effect on the upstream hydraulics serves as the basis for further analyses. Therefore, the evolution of the relative upstream flow depth h_{*cr}, which is measured directly upstream of the constriction, is analyzed as a function of the relative constriction height a_{*cr} (Fig. 5.5 a), which also shows the regression curve. This regression curve follows the above-mentioned power law with the coefficients $p1$, $p2$ and $p3$ according to Tab. 5.2:

$$Y_{data} = p1 \cdot X_{data}^{p2} + p3 \tag{5.6}$$

For composed pressurized constrictions with a trapezoidal bottom and an upper rectangular part, the relative upstream flow depth h_{*cr} is a function of the relative constriction height a_{*cr} multiplied by the relative constriction width b_{*cr}, as shown in Fig. 5.5 b). The regression curve follows the power law (Eq. 5.6) with coefficients according to Tab. 5.2.
For lateral flow constrictions, the relative upstream flow depth h_{*cr} is plotted in Fig. 5.6 a) as a function of the relative constriction width b_{*cr}, resulting in three different trendlines for the three tested channel slopes. A general relationship between the relative constriction width and h_{*cr} is obtained by multiplying b_{*cr} by the channel slope S_0. The relative upstream flow depth h_{*cr} as a function of this slope-corrected relative constriction width $b_{*cr} \cdot S_0$ is shown in Fig. 5.6 b), in which the regression curve (Eq. 5.6) is indicated.

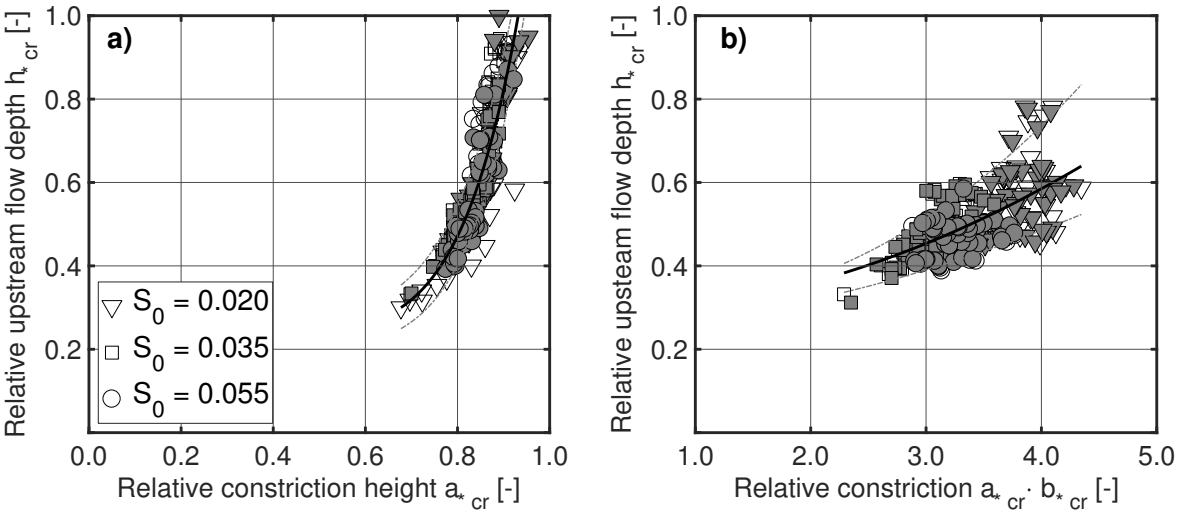

Figure 5.5 – *The relative upstream flow depth h_{*cr} as a function of a) the relative contraction height a_{*cr} for only vertically constricted flow and b) the relative constriction dimensions $a_{*cr} \cdot b_{*cr}$ for vertically and laterally constricted flow, related to the non-constricted critical flow depth and for three different channel slopes S_0. The regression curve is shown with indication of the 68 % confidence interval. The filled symbols indicate measurements with bed load.*

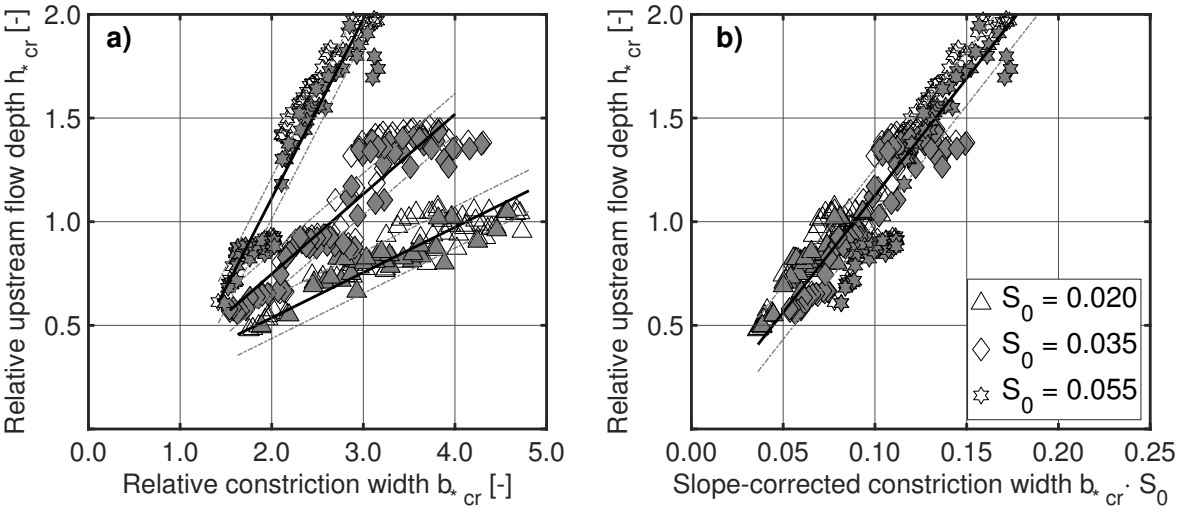

Figure 5.6 – *The relative upstream flow depth h_{*cr} as a function of a)the relative constriction width b_{*cr} and b) its slope correction $b_{*cr} \cdot S_0$ (free surface flow), related to the non-constricted critical flow depth and for three different channel slopes S_0. The regression curve is shown, and the 68 % confidence interval is indicated. The filled symbols indicate measurements with bed load.*

When $b_{*cr} \cdot S_0$ exceeds a value of approximately 0.08, the relative upstream flow depth exceeds unity ($h_{*cr} \geq 1$). These measurements result from experiments in which a flow-structure interaction is observed, even if no hydraulic jump occurs upstream of the constriction (Chow, 1959). The linear regression curves in Fig. 5.6 can be expressed by a simplification of the power law ($p2 = 1$) according to the coefficients listed in Tab. 5.2.

The local head loss coefficient ζ_c is evaluated using the cross-section-averaged energy balance (cf. Eq. 4.7, page 56) upstream and downstream of the constriction. In Fig. 5.7 a), the local head loss coefficient is shown for both types of flow constrictions, i.e., free surface flow and pressurized flow, and the regression curve is shown (Eq. 5.6 and Tab. 5.2).
When the relative upstream flow depth approaches unity, i.e., critical flow conditions, the head losses vanish and ζ_c converges toward zero. This behavior is similar to non-constricted uniform flow, where energy losses are minimum for critical flow conditions (Chow, 1959). Supercritical flow conditions were only observed with lateral constriction, as vertical flow constriction always caused a hydraulic jump when applied in the experiments. Therefore, the head loss coefficient ζ_c is also evaluated for supercritical upstream flow conditions, but only for lateral constriction. The evaluation is based on the slope-corrected relative constriction width $b_{*cr} \cdot S_0$ to directly account for the effects of the channel slope (Fig. 5.7 b). The linear regression curve can be derived from the power law (Eq. 5.6) with the coefficients shown in Tab. 5.2.

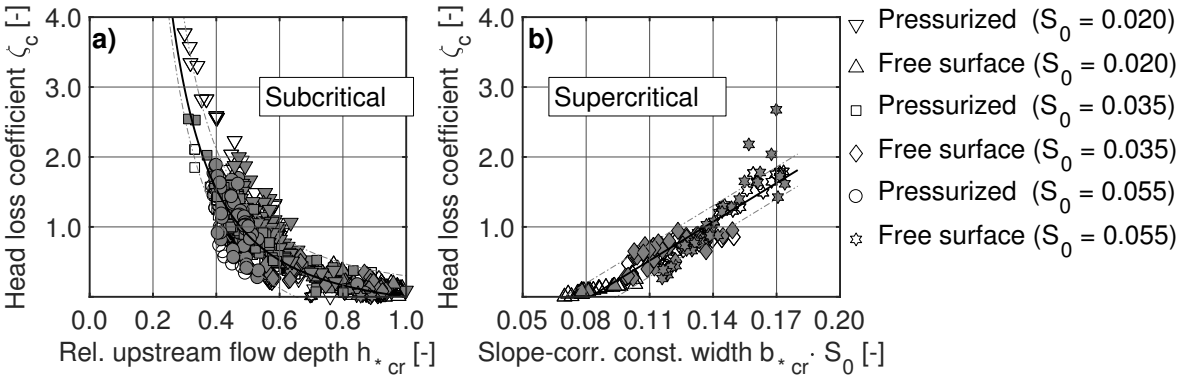

Figure 5.7 – *The local head losses ζ_c of constrictions with pressurized and free surface flow conditions as a function of a) the relative upstream flow depth h_{*cr} for subcritical upstream flow conditions and b) the slope-corrected relative constriction width $b_{*cr} \cdot S_0$ for supercritical upstream flow conditions. The data refer to the non-constricted critical flow depth and the three different channel slopes S_0. The regression curves are shown, and the 68 % confidence intervals are indicated. The filled symbols indicate measurements with bed load.*

The adapted coefficient of discharge c_{KQ} is evaluated in Fig. 5.8 a) based on the ratio between the measured and computed discharges Q / Q_c, where the latter is derived using Eq. 5.1 independently for every channel slope configuration. Based on this evaluation of c_{KQ}, the correction factor f_c for the drawdown length is evaluated through an empirical best-fit analysis of the computed and measured discharges. This analysis results in f_c = -100. Then, the slope-corrected discharge coefficient is analyzed as a function of the channel slope, with the target of unifying the three graphs

shown in Fig. 5.8 a) into one single graph (Fig. 5.8 b). This requires that some ratio of the channel slope S_0 and the discharge coefficient c_{KQ} is applied with respect to a best-fit analysis. Thus, the following empirical relationship was found:

$$c'_{KQ} = 1.25 \cdot \frac{0.25\ S_0 - c_{KQ}}{S_0 - 1} \tag{5.7}$$

The application of this slope-corrected discharge coefficient c'_{KQ} is shown in Fig. 5.8 b). With respect to the optimization of the empirically driven factor for the drawdown length of the backwater and for the channel slope, Eq. 5.1 becomes the following:

$$Q_c = 1.25 \cdot \frac{0.25\ S_0 - c_{KQ}}{S_0 - 1} \cdot A_0 \cdot \sqrt{2\ g \cdot \left(\frac{3}{2} h_{cr,o} - h_0 + 10^2 \cdot\ S_0 \cdot L_w\right)} \tag{5.8}$$

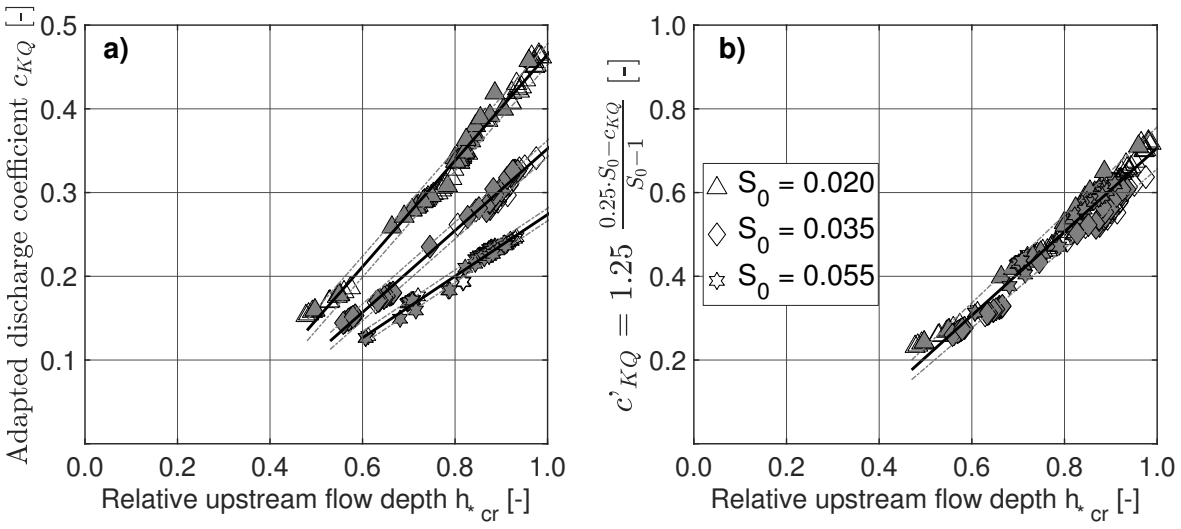

Figure 5.8 – *Evaluation of a) the discharge coefficient c_{KQ} (Kindsvater et al., 1953) as a function of the relative upstream flow depth h_{*cr} , related to the non-constricted critical flow depth; and b) the slope-corrected discharge coefficient c'_{KQ}. The regression curves are shown, and the 68 % confidence interval are indicated. The filled symbols indicate measurements with bed load.*

The alternative application of Eq. 5.2 is evaluated in terms of the discharge coefficient μ_f (Fig. 5.9). The evaluation as a function of the relative upstream flow depth h_{*cr} reveals an important scattering between the three different channel slopes with increasing h_{*cr} (Fig. 5.9 a). A significant trend can be identified by multiplying h_{*cr} by the channel slope S_0 (Fig. 5.9 b). The coefficients of the regression curve according to Eq. 5.6 are listed in Tab. 5.2.
For pressurized flow conditions, the discharge coefficient μ_p as introduced in Eq. 5.3 is shown in Fig. 5.10. The regression curves are also based on the power law (Eq. 5.6) with the respective coefficients listed in Tab. 5.2. The supplementary evaluation of both discharge coefficients μ_f (free surface) and μ_p (pressurized) as a function of the upstream Froude number (used in Chpt. 4) is included in Appendix A.3.4 (page X.19).

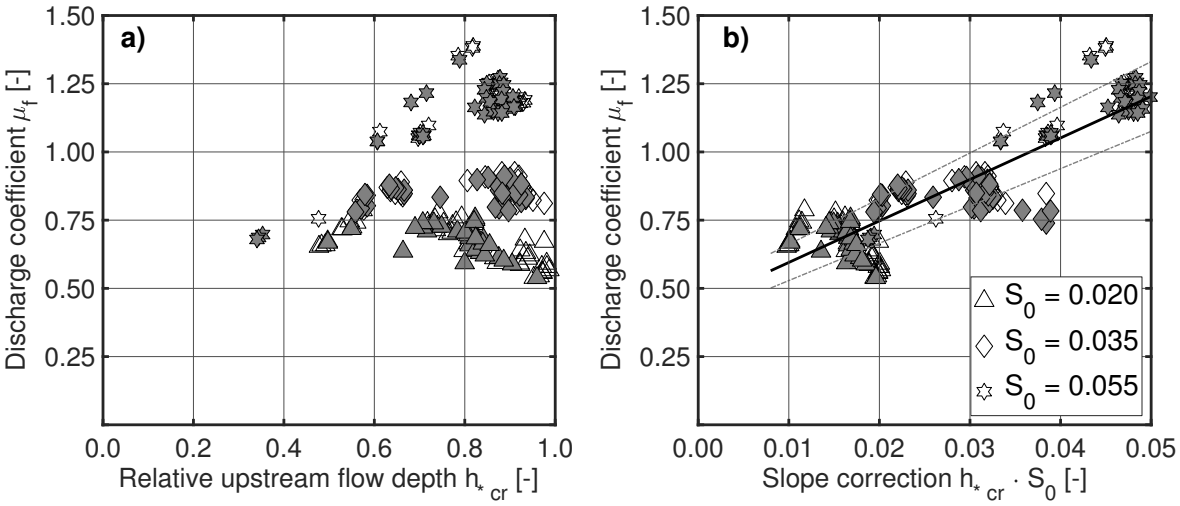

Figure 5.9 – *Evaluation of the discharge coefficient μ_f (Eq. 5.2) for free surface flow conditions, related to the non-constricted critical flow depth, a) as a function of h_{*cr} and b) as a function of the slope-corrected upstream flow depth $h_{*cr} \cdot S_0$, along with the regression curve and the 68 % confidence interval. The filled symbols mark measurements with bed load.*

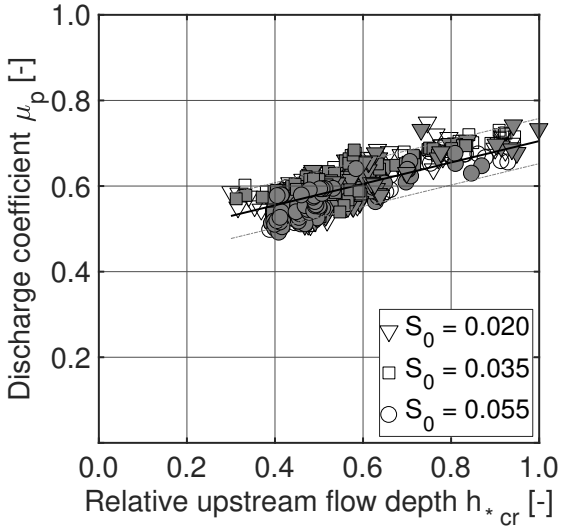

Figure 5.10 – *The discharge coefficient μ_p (pressurized flow, Eq. 5.3) as a function of the relative upstream flow depth h_{*cr}, related to the non-constricted critical flow depth and for three different channel slopes S_0. The regression curve is shown, and the 68 % confidence interval is indicated. The filled symbols indicate measurements with bed load.*

The decrease in the bed load transport capacity θ (Eq. 5.5), as shown in Fig. 5.11, is total when the relative upstream flow depth is less than approximately 0.5. A reduction induced by lateral flow constriction can already be observed when the flow is still supercritical ($h_{*cr} > 1$). No effect on the bed load transport can be observed for values of $h_{*cr} > 1.5$.

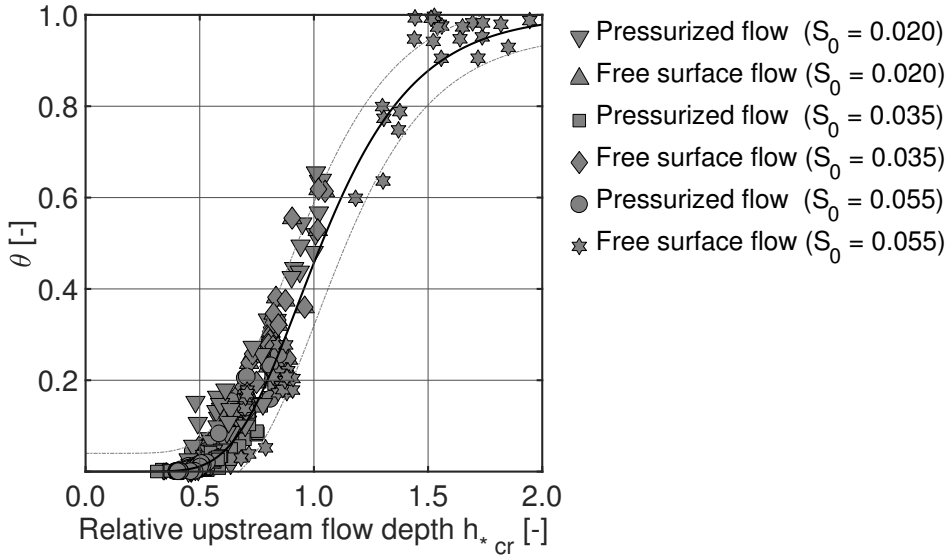

Figure 5.11 – *The reduction in the bed load transport capacity θ due to constrictions with pressurized and free surface flow conditions as a function of the relative upstream flow depth h_{*cr}, related to the non-constricted critical flow depth and for three different channel slopes S_0. The regression curve is shown, and the 68 % confidence interval is indicated.*

The regression curve shown in Fig. 5.11 corresponds to the following sigmoid function ($R^2 = 0.96$):

$$\theta(h_{*cr}) = \frac{1}{\left[1 + exp(-3.6 \cdot h_{*cr})\right]^{29}} \tag{5.9}$$

The data shown in Figs. 5.5 to 5.11 are listed numerically in Appendix A.4.1 (page X.20 ff.).

Table 5.2 – *Empirical coefficients $p1$, $p2$ and $p3$ for regression curves based on the power law (Eq. 5.6) as indicated in Figs. 5.5 to 5.10 for pressurized and free surface flows in the constriction.*

Flow condition	$Y(X)$	$p1$	$p2$	$p3$	R^2
Relative upstream flow depth h_{*cr} (Figs. 5.5 and 5.6)					
Free surface	$h_{*cr}(a_{*cr})$	1.32	7.70	0.23	0.98
Pressurized[a)]	$h_{*cr}(b_{*cr} \cdot S_0)$	11.3	1.00	-0.002	0.84
Pressurized[b)]	$h_{*cr}(a_{*cr} \cdot b_{*cr})$	0.02	2.00	0.28	0.55
Head loss coefficient ζ_c (Fig. 5.7)					
All	$\zeta(h_{*cr} < 1.0)$	0.30	-2.00	-0.30	0.83
Free surface	$\zeta(b_{*cr} \cdot S_0, h_{*cr} > 1.0)$	18.5	1.00	-1.51	0.85
Discharge coefficients (Fig. 5.8 a) and c'_{KQ} (Fig. 5.8 b) where f_c = -10[2]					
Free surface	$c_{KQ}(h_{*cr}, S_0 = 2.0\ \%)$	0.63	1.00	-0.17	0.98
Free surface	$c_{KQ}(h_{*cr}, S_0 = 3.5\ \%)$	0.49	1.00	-0.13	0.99
Free surface	$c_{KQ}(h_{*cr}, S_0 = 5.5\ \%)$	0.37	1.00	-0.09	0.97
Free surface	$c'_{KQ}(h_{*cr})$	1.00	1.00	-0.29	0.95
Discharge coefficient μ_f (Fig. 5.9 b)					
Free surface	$\mu_f(h_{*cr} \cdot S_0)$	15.2	1.00	0.44	0.81
Discharge coefficient μ_p (Fig. 5.10)					
Pressurized[a),b)]	$\mu_p(h_{*cr})$	0.25	1.00	0.46	0.65

[a)] Purely trapezoidal cross section

[b)] Composed cross section, i.e. rectangular and trapezoidal part

5.4 Discussion

5.4.1 Pressurized flow conditions

Vertical submerged flow constrictions cause a rapid increase in the upstream flow depth with the formation of a hydraulic jump. The water surface upstream of the constriction has the shape of an S1 backwater curve and appears to be independent of the channel slope, as shown in Fig. 5.5. The water surface downstream of the constriction is of the S2 type and has no influence on the upstream flow conditions. Therefore, the relation between the discharge capacity of the constriction and the upstream flow depth can be derived independently from the slope (Eq. 5.3) and with the discharge coefficient μ_p for pressurized flow conditions (cf. Fig. 5.10). The relative upstream flow depth (Fig. 5.5 b) shows that the results are less significant when the flow is additionally subjected to lateral flow constriction. The spurious data are primarily caused by measurements where the relative width ratio b_{*cr} is less than 2.5 (very narrow). Ignoring these measurements (approximately 20 % of the points) leads to a better correlation, without changing the coefficients shown in Tab. 5.2. The channel slope has no significant influence on the hydraulic effects of the flow constriction when the flow is pressurized.

5.4.2 Free surface flow conditions

For free surface flow in lateral constrictions the backwater surface is only far upstream similar to the case of pressurized flow in the constriction. The upstream flow approaching a lateral constriction starts to draw down earlier, still upstream of the constriction. Fig. 5.6 a) shows that this drawdown can be described by a function of the relative backwater depth h_{*cr}, taking the channel slope and the relative constriction ratio into account. The derivation of the boundary conditions for the computation of backwater curves is possible by applying the discharge capacity according to Eq. 5.8. The product of the channel slope and the drawdown length in Eq. 5.8 essentially represents the difference in the bottom channel elevation between the location where the backwater drawdown begins and the outflow section of the flow constriction.
The factor f_c is an empirically evaluated multiplier of the constriction length (here: 0.03 m) based on a best-fit analysis. This allows for a simplified evaluation of the drawdown length. This hypothesis implies that the drawdown length primarily depends on the channel slope and that the influence of the geometry of the lateral constriction is small. f_c is negative with respect to the positive x-axis in the flow direction and indicates an important length of the drawdown, which is consistent with examples in the literature (National Hydraulic Team, 1961). Check dams are considered here as a punctual constriction of the flow, and therefore, the influence of the constriction thickness is neglected.
Uncertainties may emerge due to flow turbulence, local roughness or the hypothesis of 1D flow, which can only be evaluated using sensitive or intrusive measuring devices that are inconvenient for experiments with the presence of bed load in comparatively shallow flumes. For this reason, the empirical best-fit analysis of the factor f_c and the slope-corrected discharge coefficient c'_{KQ} was used in this analysis.
The resulting slope-corrected discharge coefficient c'_{KQ} can either be derived based on Eq. 5.7 and the explanations from Kindsvater et al. (1953) or directly by $c'_{KQ} = h_{*cr}$ - 0.29 (Eq. 5.6 and Tab. 5.2).

Moreover, the application of Eq. 5.2 requires the consideration of the channel slope because the discharge is overestimated for lower channel slopes ($\mu_f < 1$) and overestimated for the highest slope ($\mu_f > 1$). Fig. 5.9 also indicates that μ_f tends to be constant for values of $h_{*cr} > 0.5$ in the case of lower slopes, but increases linearly for the highest slope. According to Fig. 5.9 b), μ_f can be derived as a linear function of the slope-corrected upstream flow depth ($h_{*cr} \cdot S_0$). The derivation of μ_f as some function of $b_{*cr} \cdot S_0$, analogous to Fig. 5.6 b), is not significant.

5.4.3 Validation of discharge capacity

The discharge capacity for lateral flow constrictions through Eq. 5.8 considering the channel slope and the variation of the discharge coefficient μ_p for pressurized flow as a function of the relative upstream flow depth are new elements introduced in this chapter. The proof of the application is attempted by comparing the results with those from the above-introduced study at the Dranse river.

The comparison of the computed discharge according to Eqs. 5.3 and 5.8 plus spillway discharge according to Khatsuria (2005) with the discharge measured at the site-specific model is shown in Fig. 5.12. Of special interest is the comparison of discharges less than 5 l/s, as there is no additional bias due to spillway discharge and only Eqs. 5.3 and 5.8 apply. The comparison in Fig. 5.12 indicates that both Eqs. 5.3 and 5.8 slightly underestimate the discharge capacity, particularly with increasing discharge. The relative error of the estimates of both equations is less than 10 %. The error percentiles shown in Fig. 5.12 indicate that the uncertainties incorporated in Eq. 5.8, which are related to the measurement instrumentation, are considerable. The point density in the region of particular interest ($Q < 5$ l/s) is rather scarce, as the primary focus of the experiments at the Dranse river was to prove the use of theoretical equations for deriving a stage-discharge relation. Thus, the comparison essentially proves the applicability of the adaptations proposed in this chapter, but it also shows that further validation is needed.

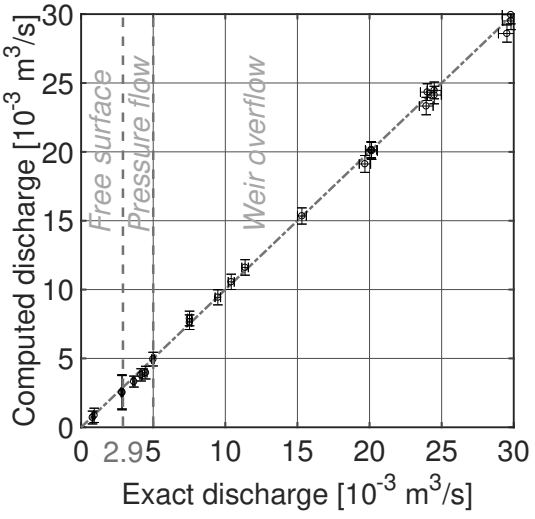

Figure 5.12 – *Validation of Eq. 5.1 for $Q < 2.9$ l/s and of Eq. 5.3 for $Q > 2.9$ l/s, in terms of measured and computed discharge on the scaled model of the Dranse River, with consideration of spillway discharge for discharges $Q > 5$ l/s, along with the measurement-induced error bars based on a 68 % confidence interval.*

5.4.4 Energy losses

The energy losses at the constriction primarily depend on the relative upstream flow depth and vanish when the upstream flow depth approaches critical flow conditions. An exponential increase in the head loss coefficient ζ_c is observed when the relative upstream flow depth decreases to values below 0.75. For subcritical upstream flow conditions, the influence of the channel slope is incorporated in the value of the relative upstream flow depth for free surface flow conditions. The energy head losses in terms of ζ_c differ from the discharge coefficients applied for the discharge capacity (Eqs. 5.1 and 5.3) because ζ_c is based not only on flow depth measurements upstream of the constriction but also on measurements downstream of the constriction.
In the case of supercritical upstream flow conditions, the flow constriction interferes only with the adjacent flow but does not cause backwater (Chow, 1959). The application of the relative upstream flow depth for the derivation of head losses in the case of supercritical flow incorporates a slope-dependent shift of the data sets. Therefore, the linear increase of head losses as a function of the slope-corrected relative constriction width is shown in Fig. 5.7 b). This increase in the head losses is consistent with an increase in the Froude number at the constriction, which is proportional to the upstream relative flow depth.

5.4.5 Bed load

The bed load transport capacity of the non-constricted channel can be reproduced by the empirical formulae from Smart and Jaeggi (1983) / Smart (1984) and Rickenmann (1991), as shown in Fig. 5.13 (cf. Eqs. 2.18 and 2.19 on page 17). The applicability of both formulae has been proven in former studies (e.g., Chiari et al., 2010). The computation of Q_b with both formulae is based on a dimensionless bed load transport rate with a different set of repeating variables for the dimensional analysis (D_{84}, g and ρ_f). The comparison of the empirical formulae with the measurements from this study is shown here with dimensions, which are introduced by multiplying the dimensionless transport rate by $w \cdot \rho_f \cdot \sqrt{(s-1)\, g\, D_{84}}$ (e.g., Einstein, 1950; Heller, 2011). The results of both empirical formulae are similar, as they are partially based on the same experimental data from a mobile-bed channel. The formula from Rickenmann (1991) underestimates Q_b for small slopes, but it provides a better estimate than the Smart and Jaeggi (1983) formula for steeper slopes. This result is also reflected by the statistical goodness of both formulae in terms of the coefficient of determination R^2 (Tab. 5.3).
A fixed-bed channel was used here, which causes differences with respect to the empirical formulae. This fixed bed corresponds to non-alluvial or colluvial paved mountain torrents, which are characterized by an external bed load supply as long as no breaking of the bed armor occurs. Thus, there is no or little exchange between the channel bed and the bed load transport in non-alluvial or colluvial channels according to the concept of “traveling bed load” (Yu et al., 2009; Piton and Recking, 2017).

Based on the assumption of important sediment supply from external sources, such as debris flow, bed load is analyzed in this chapter in terms of the transport capacity. This discharge-related bed load transport capacity of the non-constricted channel depends on the channel slope (Fig. 5.13). However, the reduction in the bed load transport capacity for constricted flow as a function of the

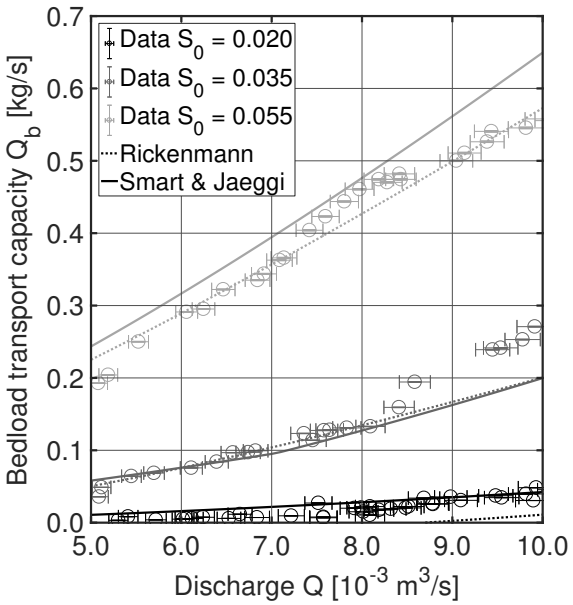

Figure 5.13 – *Comparison of the measured bed load transport capacity in the non-constricted channel with the expressions from Smart and Jaeggi (1983) / Smart (1984) and Rickenmann (1991); the measurement-induced error bars are based on a 68 % confidence interval.*

Table 5.3 – *Coefficient of determination R^2 for the bed load transport formulae from Smart and Jaeggi (1983) / Smart (1984) and Rickenmann (1991) compared with the new measurements.*

Formula	R^2 ($S_0 = 0.020$)	R^2 ($S_0 = 0.035$)	R^2 ($S_0 = 0.055$)
Rickenmann (1991)	0.59	0.95	0.96
Smart and Jaeggi (1983)	0.72	0.95	0.91

dimensionless relative upstream flow depth h_{*cr} is not sensitive to the channel slope (Fig. 5.11). The effect of the slope is already incorporated in h_{*cr}, which is only sensitive for lateral flow constriction. Some sigmoid function (Eq. 5.9) provides a channel slope-independent and reliable estimate for this constriction-induced reduction in the bed load transport capacity.

The inflection point of the sigmoid curve is at the position $h_{*cr} \approx 1.0$ and $\theta(h_{*cr}) \approx 0.5$. This characteristic indicates that θ is the most sensitive when the flow conditions directly upstream of the constriction are critical. With decreasing h_{*cr}, i.e., decreasing Froude number, the bed load transport capacity of a channel with a constriction significantly decreases. When h_{*cr} decreases below a value of approximately 0.5, only some grains may be mobilized. However, this observation is only valid for grains that are larger than the minimum grain size of the used grain mixture. Considering this minimum grain size by the D_{16}, the lower application limit of the results is D_{16} / $h_{cr} \geq 0.11$. The grain mobility can be considerably higher in the case where the ratio between the finest grains and the critical discharge related flow depth is less than 0.11. The risk of the increased grain mobility is that unwanted self-emptying of the sediment trap occurs (Zollinger, 1983).

5.5 Conclusions

Instream open check dams can be considered as local flow constrictions that confine the flow laterally (free surface flow) or vertically (pressurized flow). Both types of constrictions cause backwater, which can be characterized by the relative transcritical upstream flow depth, defined as the ratio of the critical flow depth and the flow depth upstream of the constriction. Previous studies relate the formation of backwater to the constriction width without considering the channel slope. This analysis shows that the formation of backwater in terms of the relative transcritical flow depth upstream of lateral flow constrictions is also linearly dependent on the channel slope.
The related local energy losses and the reduction in the bed load transport capacity can be derived directly, and thus, they are slope-independent from the relative transcritical upstream flow depth. Critical flow conditions upstream of the constriction are of particular interest because only a slight variation of the discharge causes important changes in the local head losses and the reduction in the bed load transport capacity.
Furthermore, it could be demonstrated that the bed load transport capacity of the non-constricted fixed-bed channel is accurately reproduced by the application-typical formulae from Smart and Jaeggi (1983), and Rickenmann (1991).
For free surface flow, the discharge capacity has to be computed as a function of the constriction width and the channel slope. For pressurized flow in the opening, the discharge capacity can be computed utilizing a backwater-dependent discharge coefficient. A validation based on a real case study shows that the revised equations for free surface flow and pressurized openings tend to slightly underestimate the discharge capacity.
These findings contribute to the evaluation of hydraulically induced bed load retention in mountain rivers.

6 Analysis of mechanical-hydraulic bed load deposition control measures [1]

Abstract

During floods, the bed load transport of steep headwaters can exceed the hydraulic transport capacity of milder downstream reaches where settlements are often situated. Therefore, sediment retention barriers are typically installed upstream of such sensitive areas. These barriers trigger bed load trapping via two control mechanisms, either hydraulic or mechanical. Both deposition controls, pertaining instream sediment trapping structures, are analyzed experimentally in this study. Bed load trapping by hydraulically controlled barriers is prone to sediment flushing, i.e., the re-mobilization of formerly deposited sediment, in particular when the barrier is simultaneously under- and overflown. In this case, the re-mobilization rate is close to the bed load transport capacity of the non-constricted channel. Mechanical deposition control by screens is in turn sensitive to the grain size. Thus, both deposition control concepts may fail, and bed load may be transported downstream at a rate corresponding to the transport capacity of headwaters, thereby endangering urban areas. This study shows that the combination of both deposition control concepts is suitable for improving the control of bed load retention. With this combination, undesired sediment flushing of the upstream channel due to insufficient hydraulic control is prevented. Furthermore, the uncertainty related to the estimation of the representative grain size in the design of mechanical control barriers is reduced.

[1] This chapter is based on the research paper draft "Analysis of mechanical-hydraulic deposition control measures" by S. Schwindt, M.J. Franca, G. De Cesare and A.J. Schleiss (Schwindt et al., 2017a). The experiments and analyses hereafter are original and were developed by the author. The measurement data are included in the Appendix (A.4.2).

6.1 Introduction

A major flood in August 2005 caused in the Swiss locality of Bristen sediment deposits in the village center with severe structural damage and many similar cases have been reported for the same flood event (Bezzola and Hegg, 2007; Bezzola, 2008). Such undesired deposits can be prevented by instream-sediment traps, which are typically constituted by a torrential barrier with an opening (open check dam) to limit the downstream bed load transport in the case of floods (Leys, 1976; Zollinger, 1983; Piton and Recking, 2016a).
Such flow barriers may suffer failures for structural or functional reasons in the case of floods. Structural failure occurs when the barrier stability is compromised, e.g., due to insufficient foundation (Suda and Rudolf-Miklau, 2008). This can be prevented by paving the opening bottom and by a proper static assessment of the structure (Bezzola, 2008; Suda et al., 2009; Piton and Recking, 2016a). Functional failure occurs when the barrier does not work as desired (Hübl et al., 2005), e.g., when the sediment retention is insufficient or when previously deposited material is re-mobilized in undesired quantities during floods. Such undesirable sediment re-mobilization is subsequently referred as unwanted sediment flushing. The functional failure depends on the sediment deposition control provided by the permeable barrier, as introduced above (Chpt. 2.7.2). The two deposition control principles are recalled here:

- *Hydraulic control*, i.e., the bed load transport capacity of the channel reduces due to backwater of the permeable barrier (Chpt. 2.7.3).
- *Mechanical control*, i.e., the size of the transported objects in the shape of sediment or driftwood exceeds the clearance dimensions of the opening(s) of the barrier (Chpt. 2.7.4).

Hydraulic control is usually achieved by barriers with slits or slots. Slits are lateral flow constrictions with free surface flow, and slots are vertical flow constrictions with pressure flow conditions. The hydraulic control has been found in the previous chapters (Chpts. 4 and 5) to depend on the flow conditions in the backwater of constriction-like barriers, and on the channel slope.
The reliable application of hydraulic control barriers can be achieved through adjustable opening sizes, e.g., by weirs, such as that at the Schächen torrent in Switzerland or the Schnannerbach torrent in Austria (Kanton Uri, 2016; die.wildbach, 2016). However, the installation of mobile measures requires vulnerable mechanical equipment, triggering devices for hydraulic controls and permanent stand-by duty which are cost-intensive in remote alpine regions. The decision making for triggering weir adjustments requires the definition of threshold values in terms of the river discharge. To the authors' best knowledge, guidelines for weir adjustments are not part of any legal framework. Thus, the answer to the question concerning the responsibility for damages downstream of adjustable measures is a contentious issue. Because of the high costs and the legal implications of adjustable weir openings, alternative, passively working solutions are preferable.
Mechanical control is induced by barriers with multiple openings or screens, where the narrower opening clearance dimension is decisive in clogging (Piton and Recking, 2016a). The geometric design criteria that lead to mechanically induced bed load retention have been analyzed in previous studies. The probability of clogging is high when the clearance height or width of opening(s) is smaller than the characteristic dimensions of the transported objects, e.g., the representative grain diameter of the sediment. For clearance dimensions of twice this diameter or more, the clogging probability is low (according to Tab. 2.5 on page 29 and Watanabe et al., 1980; Zollinger, 1983;

Ikeya, 1989; Uchiogi et al., 1996; Frey and Tannou, 2000; Bezzola et al., 2004; Wallerstein et al., 2013; Takahashi, 2014; Piton and Recking, 2016a). The complete mechanical obstruction of a barrier is not prone to unwanted sediment flushing (self-emptying), but malfunction remains possible when the sediment size is smaller than expected (Hübl et al., 2006). Decreasing the effective flow clearance of the opening(s) enhances the safety against unwanted sediment flushing. But, undersized clearances may involve regular sediment deposits upstream of sediment check dams. This deposited sediment has to be frequently dredged and it is missing in downstream reaches, with negative effects on the river morphology (Kondolf, 1997b; Brandt, 2000; Schleiss et al., 2014).

Thus, hydraulic and mechanical control measures have certain disadvantages. Both types and their combination are considered in this chapter to overcome negative consequences due to uncertainties related to insufficient or excessive sediment retention. In practice, the implementation of both control mechanisms is sometimes applied for the combined retention of driftwood and sediment, where a mechanical control barrier in the shape of a screen is designed based on the expected size of driftwood (Hübl et al., 2003). Some study cases for the combination of hydraulic and mechanical retention of bed load exclusively can be found (Piton and Recking, 2016b; Schwindt et al., 2016a), but the systematic experimental study as made herein is novel.

The main objective in this chapter is to investigate the sediment transfer at barriers designed for hydraulic or mechanical control and of barriers that combine both types of controls. Sediment transfer is exclusively considered in terms of bed load. Thus, the mitigation of debris flow and woody debris–related hazards, which requires structures upstream of the herein considered barriers, are not addressed.

The particular interest of this chapter is the conception of barriers to enable fluvial bed load transport until some threshold discharge is exceeded. For higher discharges, bed load should be retained without the possibility of being re-mobilized, i.e., to prevent unwanted sediment flushing. The results from the previous chapters (Chpts. 4 and 5) are considered for the reference bed load transport in the channel without barriers and without sediment deposits, as well as for the design of the hydraulic control barrier. In contrast and complementary to the previous chapters, the formation of deposits upstream and overflow of the barrier are investigated.

6.2 Methodology

6.2.1 Adjustment of the experimental set-up

The experiments were performed in the previously used rough trapezoidal channel with constant longitudinal slope S_0 = 5.5 %, bank inclination $m \approx 2.25$ and bottom width $w \approx 0.11$ m. Accordingly, the sediment mixture was used as previously (cf. characteristics in Tab. 3.1, page 42). The discharge Q varied between 3.0 and 10.0 l/s. The configuration of the experimental set-up is qualitatively recalled in Fig. 6.1.

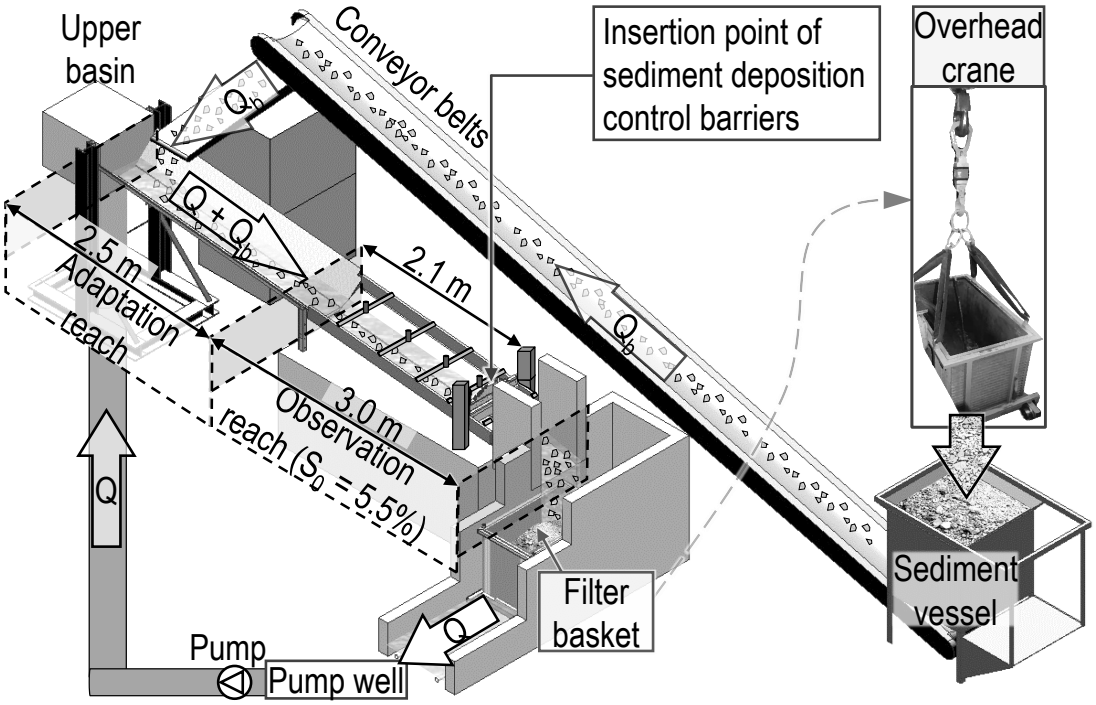

Figure 6.1 – *Recall of the model conception, with the sediment supply system consisting of the sediment vessel and conveyor belts; the upstream adaptation reach for mixing of sediment and water; and the observation reach. The flow control barriers were introduced in the lower third of the observation reach. The outflowing sediment was collected and transferred in the filter basket, back to the sediment vessel.*

The following measurement instrumentation applies in this chapter (cf. Chpt. 3.2.5, page 45 ff.):

- Ultrasonic sensors for the flow depth;
- Electromagnetic flow meter for pump discharges;
- Scales for weighing the sediment outflow; and
- Laser and caliper for geometric dimensions.

6.2.2 Bed load control

The occurrence of sediment deposition imposed by flow barriers is subsequently related to the occurrence of ordinary and exceptional flood events (Lenzi et al., 1999). With respect to morpho-

logical river continuity, deposition control barriers should not affect the bed load transport for ordinary floods (cf. 2.1 and Schleiss et al., 2014). These ordinary floods vary from case to case and can be referred to as a morphologically effective discharge (cf. Chpt. 2.5 Wolman and Leopold, 1957a,b; Wolman and Miller, 1960), which is essential for the channel bed morphology. Discharges that are subsequently labeled as exceptional refer to floods that endanger urban areas over the river banks. For the present experiments, the differentiation between ordinary (smaller) and exceptional (higher) discharges is abstracted in terms of some dimensionless parameters. The essential point for the experiments is that there are certain small discharges at which sediment transfer is possible and ordinary discharges at which sediment is retained.

Hydraulic control barriers were analyzed in terms of vertical and lateral flow constrictions in the shape of mobile PVC elements imposing a flow constriction, with height a and width b (dark gray elements in Fig. 6.2). The description of the upstream hydraulics requires the differentiation between pressure (vertical constriction) and free surface (lateral constriction) flow conditions in the constriction (Chpt. 5). For hydraulic control, experiments were conducted without and with overflow of the barrier crest.

The conception of mechanical control devices was related to the grain size of the transported sediment, according to traveling bed load in nature (Piton and Recking, 2016a). This type of bed load transport refers to the grain size of sediment deposits from former floods at the banks of the upstream channel.

An inclined bar screen with cylindrical, vertically inclined bars (inclination of 2:1, light gray elements in Fig. 6.2) was applied for mechanical control. The inclined bars favor the sliding and passage of potentially occurring driftwood over the structure, when it is overflown. Thus, the risk of unwanted driftwood accumulations and the obstruction of the screen are reduced. In practice, additional structures for the downstream driftwood retention should be considered (Bezzola et al., 2004; Lange and Bezzola, 2006; Piton and Recking, 2016b). The design of the mechanical control barrier in this chapter was based on the size of the transported sediment, not in direct dependence on the discharge, according to literature findings (Ono et al., 2004; Piton and Recking, 2016a; Shima et al., 2016). Based on these previous findings, the clearance height between the channel bottom and the lower end of the vertical bars was determined as a multiple f_m of the representative grain size D_{84} (Fig. 6.2 and Tab. 2.5 on page 29). Small clearance heights ($f_m < 1.5$) were expected to cause sediment deposition as soon as sediment was supplied to the flume. However, for not interrupting the continuity of sediment transport, which is eco-morphologically preferable (e.g., Piton and Recking, 2016c; Simoni et al., 2017), the retention of small bed load transport rates is not appropriate. Therefore, small clearance heights of $f_m < 1.5$ are subsequently not considered. But the clogging of the screen is advantageous to ensure complete mechanical sealing in the case of intense bed load transport and thereby to avoid unwanted sediment flushing.

In this chapter, f_m was tested incrementally, starting from $f_m \approx 1.5$, to assess the optimum clearance height, which is defined as the maximum height $f_{m,opt} \cdot D_{84}$ that can cause sediment retention. This optimum clearance is related to the possibility of sediment transfer for ordinary (smaller) discharges and the safe occurrence of mechanical barrier clogging for exceptional (higher) discharges. The herein considered principle of mechanical clogging focuses on the trapping of bed load occurring with exceptional floods, where the active bed load layer is thicker than during smaller, ordinary discharges (Du Boys, 1879; Church and Haschenburger, 2017). The entangled grains cause an additional resistance to the flow, which causes the further retention of grains.

Therefore, the maximum bed load transport that can pass through the mechanical barrier (bar screen), without the entanglement of grains between the bars, was tested for several pairs of constant discharge and incrementally increasing sediment supply. In this process, for a fixed discharge, the sediment supply was increased step-wise until the screen was mechanically clogged. The highest supply rate that did not lead to the clogging of the screen was then taken as the maximum bed load transport corresponding to the fixed discharge and to a barrier configuration. The bed load transport was measured as explained above. This procedure was repeated three times and the average value of the maximum bed load transport was taken. The barrier clogs instantaneously for solid discharges that are higher than the maximum bed load transport capacity. This analysis served for the identification of an optimum value for the clearance in terms of $f_{m,opt}$, which is high enough to not interfere with bed load transport for small discharges but low enough to enable mechanical clogging for higher discharges. The steady discharge refers to different flood stages, where in practice instantaneous *quasi*-steady flow conditions for the triggering of bed load retention may be admitted.

The horizontal bar interspace is taken to be equal to D_{84} to ensure clogging for higher discharges (Uchiogi et al., 1996; Wallerstein et al., 2013; Piton and Recking, 2016a,b, according to Tab. 2.5, page 29). An additional bearing beam was installed for the support for the vertical bars. No considerable influence of this structural element on the functioning of the barrier was observed.

Preliminary tests showed that the overlapping part of the vertical bars, beneath the bearing beam (Fig. 6.2), was essential for enabling the mechanical clogging. The jumping grains of the bed load became entangled between these free ends of the vertical bars. This entangling required a minimum overlapping length according to the D_{84}.

The sediment retention due to hydraulic control by the flow constriction and mechanical control by the bar screen was tested individually and in combination. Fig. 6.2 illustrates schematically the transversal and longitudinal sections. The tests related to purely hydraulic control were conducted twice: (i) with a quasi-infinite barrier height (no possibility of overflow) and (ii) with a limited barrier height of 0.11 m, which corresponded to $8 \times D_{84}$. The height of the screen was not considered as a factor for mechanical clogging and was maintained as constant at 0.11 m. The overflow section was 0.23 m wide. The location of flow depth measurements are also qualitatively indicated in Fig. 6.2.

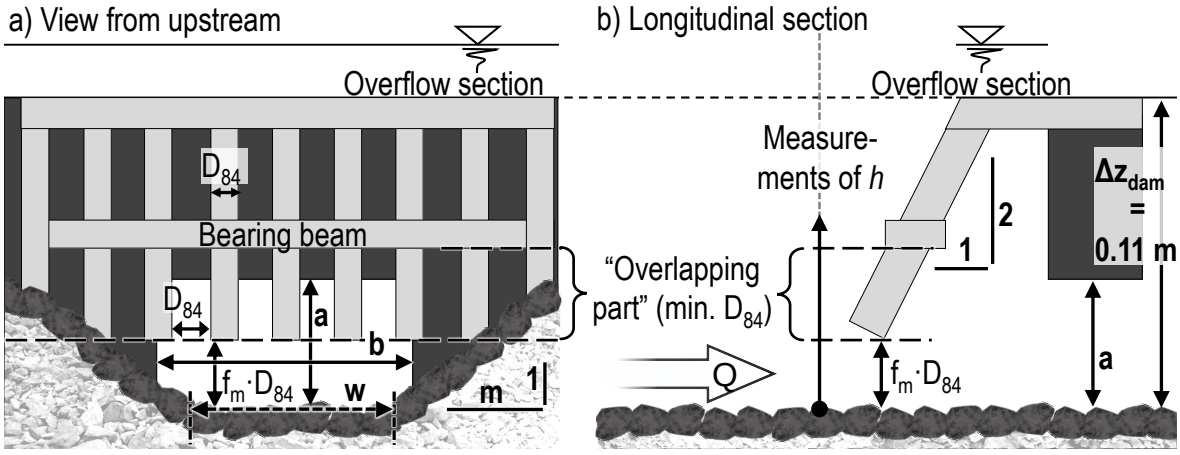

Figure 6.2 – *Qualitative illustration of the combination of bed load retention control measures based on hydraulic control by flow constrictions, with height a and width b, and mechanical control by a bar screen; the illustration shows a) the cross sectional view from upstream and b) the longitudinal channel section. The barrier height Δz_{dam} was limited to 0.11 m in experiments with overflow. The elements constituting the hydraulic control are represented in dark gray, whereas the elements in light gray correspond to mechanical control.*

6.2.3 Parameters and dimensional analysis

The phenomena considered in this chapter may be described by the following set of parameters:

$$\Lambda = f\left(a, b, D_{84}, f_m, g, h, S_0, m, Q, Q_b, \nu, \rho_f, \rho_s\right) \tag{6.1}$$

As the focus of this study is on bed load transport, the dimensionally independent variables of D_{84}, g and ρ_f are used for the derivation of the following dimensionless parameters (cf. Chpt. 3.1, page 37 ff. and Einstein, 1950; Yalin, 1977):

- Grain-related opening height of vertical flow constrictions $a_{*D} = a \,/\, D_{84}$;
- Grain-related opening width of lateral flow constrictions $b_{*D} = b \,/\, D_{84}$;
- Factor of D_{84} for the clearance height under the bar screen f_m;
- Relative flow depth upstream of the hydraulic control barrier $h_{*D} = h \,/\, D_{84}$;
- Grain-related flow velocity $F_* = Q \,/\, (A \cdot \sqrt{g\, D_{84}})$;
- Density ratio $s = \rho_s \,/\, \rho_f$;
- Bed load transport intensity corresponding to transport capacity conditions $\Phi = Q_b \,/\, (w_m \cdot \rho_f \cdot \sqrt{(s-1)\, g\, D_{84}^3})$.

In this context, it is recalled that $A = h \cdot w_m$ denotes the flow cross section, where $w_m = w + h \cdot m$ is the mean width of the trapezoidal channel (cf. Fig. 6.2). The hydraulic effects of the deposition control barriers on the upstream grain-related flow velocity F_* are evaluated by relating the constriction height to the flow depth upstream of the barrier. The previous chapters have shown that the constriction height a is the governing geometric dimension for pressurized flow through hydraulic barriers. In the case of exclusively lateral constriction, the constriction width b governs the upstream

flow conditions (Chpts. 4 and 5). Therefore, the relative submergence is considered by a_{*D} / h_{*D} and b_{*D} / h_{*D} for vertical and lateral constriction by hydraulic control barriers, respectively. The relation f_m / h_{*D}, which is equivalent to $f_m \cdot D_{84}$/ h, is applied for the assessment of the flow conditions upstream of the bar screen for mechanical control only.

6.2.4 Experiment design

The bed load transport capacity is evaluated for three cases, with respect to the deposition control types, as illustrated in Fig. 6.3:

Case 1: Sediment deposits upstream of the hydraulic control barriers
Hy-no – Infinite barrier height (no overflow is possible), imposing flow constrictions with varying height a and varying width b;
Hy-o – Limited barrier height (with overflow), imposing flow constrictions with varying height a and constant width b;
Case 2: ***Mec*** – Mechanical control barriers by a bar screen; and
Case 3: ***HyMec*** – Combination of hydraulic and mechanical controls.

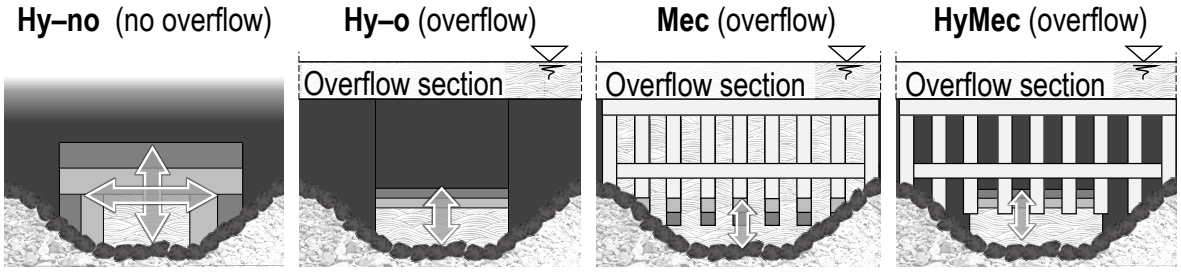

Figure 6.3 – *Conceptual sketch of the barriers analyzed in this study: (Hy-no) infinitely high hydraulic barriers, with varying constriction width and height; (Hy-o) simultaneously over- and under-flown hydraulic barriers, with varying constriction height (hydraulic control only); (Mec) bar screens only, for the optimization of the clearance height under the screen (mechanical control only); and (HyMec) combination of the bar screen superposed to the hydraulic barrier, with varying constriction height. The hatched areas indicate effective flow sections of the barrier.*

In addition, this chapter refers to data from the previous chapter (Chpt. 5), where infinitely high barriers without upstream sediment deposits were analyzed (Chpt. 5). The flow was generally supercritical in the steep rough laboratory channel (the Froude number varied between 1.4 and 1.9), similar to natural mountain rivers. Thus, barriers cause backwater, and a hydraulic jump occurs in the upstream (Chpt. 2.7.2, page 26). According to the literature (Armanini and Larcher, 2001; Campisano et al., 2014; Piton and Recking, 2016a), the hydraulically controlled formation of sediment deposits upstream of the barrier is initiated immediately downstream of this hydraulic jump. The additional volume of this sediment deposit provokes an increase in the length of the backwater and, in turn, causes a shift of the hydraulic jump in the upstream direction. Accordingly, for constant discharge, the location where bed load deposits is also shifted in the upstream direction, as it is illustrated in Fig. 6.4. This formation of an elongated deposit evolving in the upstream direction occurs in the case *Hy-no*, for constant sediment supply and discharge, and infinitely high barriers. In the case *Hy-no*, sediment was supplied until the deposit reached the upstream boundary of the

observation reach (cf. Fig. 6.1). Multiple combinations of constriction heights a and widths b were tested (Tab. 6.1).

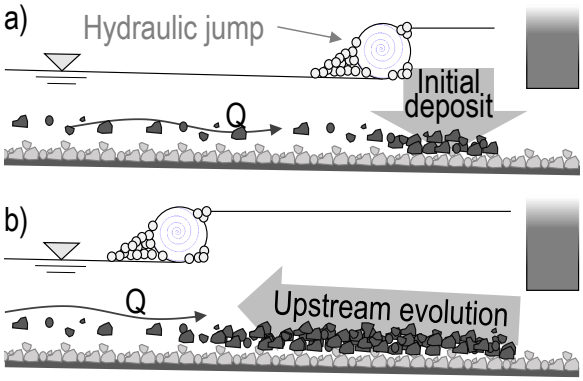

Figure 6.4 – *Qualitative illustration of the evolution of an elongated sediment deposit upstream of an infinitely high barrier (case Hy-o) with steady discharge and sediment supply: a) at the beginning of an experiment, the sediment deposit occurs immediately downstream of the hydraulic jump, upstream of the barrier; and later b) an upstream shift of the hydraulic jump is caused by the deposited sediment; progressively, the sediment deposit edge and the hydraulic jump move upstream.*

The limitation of the barrier height prevents the upstream evolution of the backwater, which causes the deposit to evolve in the downstream direction. When the deposit front reaches the barrier, the formation of a secondary deposit layer can be expected on top of the previous deposit. Thus, the deposit evolves in a succession of *quasi*-equilibrium states until it reaches the barrier height (Armanini and Larcher, 2001; Jordan et al., 2003; Campisano et al., 2014; Piton and Recking, 2016a). Such hydraulically controlled sediment deposition patterns upstream of permeable barriers occur in the case *Hy-o*, also with a constant sediment supply and discharge but for overflown barriers. For the case *Hy-o*, the barrier height Δz_{dam} was limited to 0.11 m, according to the above statements (Fig. 6.2), with variable constriction height a, but with constant width b (Tab. 6.1).
In the cases *Hy-no* and *Hy-o*, the maximum sediment outflow rate, related to each of the tested constant discharges, was retained. These values refer to sediment flushing phases that occurred at the end or during the tests. Thus, the maximum sediment outflow rates represent peak values for bed load transport downstream of the tested barriers.
The second test series (*Mec*) served for the optimization of the bar screen. A particularity of the bar screen is a free space between the screen bottom and the channel bed. This bottom clearance height below the bar screen, defined as $f_m \cdot D_{84}$, was analyzed experimentally. An optimum value of $f_{m,opt} \cdot D_{84}$ was investigated to allow for sediment transfer for ordinary (smaller) discharges and sediment retention for higher discharges. This optimum clearance height was retained for the following experiments.
The upstream flow conditions and the bed load transport through the combination of hydraulic (flow constriction) and mechanical (bar screen) control constitute the test cases *HyMec*. For this combined control, the same constriction geometries were applied as for the hydraulic barrier only, with limited height (*Hy-o*).
The experimental test cases considered in this chapter, with the corresponding parameter combinations and types of sediment retention control, are summarized in Tab. 6.1.

Table 6.1 – *List of experiments for the determination of the maximum bed load transport of instream barriers for hydraulic, mechanical and combined control.*

Case	Number of	Mechanical control		Hydraulic control				Barrier height	Discharge	
	tests [−]	$f_{m,min}$ [−]	$f_{m,max}$ [−]	a_{min} [m]	a_{max} [m]	b_{min} [m]	b_{max} [m]	Δz_{dam} [m]	Q_{min} [l/s]	Q_{max} [l/s]
Hy-no	89	*none*		0.047	inf.	0.10	0.14	inf.	5.0	10.0
Hy-o	25	*none*		0.040	0.047	0.15		0.11	6.0	10.0
Mec	87	1.54	1.90	*none*		*none*		0.11	3.1	8.8
HyMec	85	$f_{m,opt}$		0.040	0.047	0.15		0.11	3.2	8.6
	$\sum$ 286									

6.3 Results and Analysis

6.3.1 Bed load transport without deposition control

The evaluation of the so-called non-constricted flow, i.e., channel without barrier, was performed previously in Chpts. 4 and 5, where the presence of sediment deposits was not considered. However, these previous experiments indicate that the sediment transport through the barrier might increase when the sediment deposits are present upstream of the constriction. In this chapter, the maximum bed load transport intensity Φ is represented in Fig. 6.5 as a function of the grain-related flow velocity F_* instead of the discharge, as previously reported. The bed load transport intensity without sediment deposition control measures can be reproduced by the semi-empiric formula from Smart and Jaeggi (1983), using Eq. 2.18 (page 17) with the measured flow depth. Similar application cases for this formula can be found in previous studies (Sindelar et al., 2016). The flow in the non-constricted channel was generally supercritical (Chpt. 5).

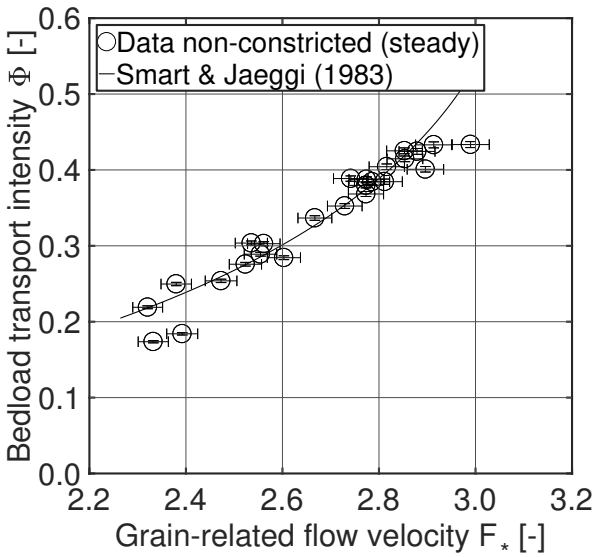

Figure 6.5 – *Comparison of the measured bed load transport intensity in the non-constricted channel, presented in Chpt. 5, with the results obtained with the formula from Smart and Jaeggi (1983).*

The formula of Smart and Jaeggi (1983) refers to a mobile channel bed, where the bed load transport complies with the maximum transfer rate, corresponding to the hydraulic conditions in terms of

the roughness, channel geometry, slope and discharge. The formula is subsequently considered for the evaluation of the bed load transport capacity of the barrier-free flow.

6.3.2 Hydraulic control (*Hy-no* and *Hy-o*)

The observed evolution of sediment deposits in the backwater of infinitely high barriers (*Hy-no*, no overflow) is in good agreement with the descriptions from the literature (Armanini and Larcher, 2001; Campisano et al., 2014; Piton and Recking, 2016a). The sediment deposits caused an increase in the backwater upstream of the barrier. With increasing backwater, the hydraulic jump, and therefore also the tail of the deposit, moved in the upstream direction without further evolution of the deposit front. This observation corresponds to the literature observations (cf. Fig. 6.4) of elongated sparse deposits, as illustrated in the underwater pictures shown in Fig. 6.6. When the backwater tail reached the upstream model limit (corresponding to a limitation of the set-up in terms of the observational length), the experiments were stopped. This procedure is similar to earlier experiments on sediment traps (Zollinger, 1984).

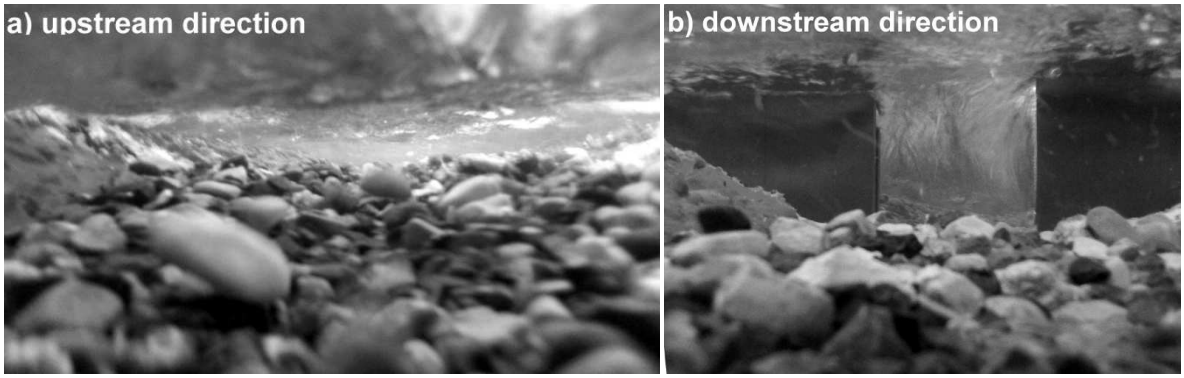

Figure 6.6 – *Flat and elongated sediment deposits upstream of the infinitely high hydraulic barrier (Hy-no) at the end of an experimental run; view in the a) upstream direction and b) downstream direction, toward the barrier.*

The typical evolution of the sediment deposit in the study case *Hy-o*, i.e., overflow of a hydraulic barrier with a limited height of Δz_{dam} = 0.11 m, is illustrated in Fig. 6.7 through top-view pictures. First, the supplied sediment started to deposit upstream of the hydraulic barrier (Fig. 6.7 a). Similar to the previous experiments without barrier overflow, the deposit evolved in the upstream direction. However, when the tail of the deposit reached the end of the backwater reach of the barrier (Fig. 6.7 b), a new deposit layer developed on top of the previous layer, as described in the literature (Fig. 6.7 c) (Campisano et al., 2014). This process repeated until the height of the deposit reached approximately the same height as the barrier crest (Δz_{dam} = 0.11 m, Fig. 6.7 d). Then, the sediment supply was stopped, while the discharge was kept constant. Thus, the ratio between solid and water discharge was reduced, i.e., the discharge was no longer saturated with sediment. This leads to an excess of the bed load transport capacity which potentially provokes sediment flushing (Zollinger, 1983). Preliminary experiments had shown that supplying subsequently more sediment was not a reasonable option, as this would entail an evolution of the sediment deposit similar to the situation of non-overflown barriers. The sediment flushing began at the tip of the deposit (Fig. 6.7 d and e)

until the total emptying of the upstream channel. The discharge was constant throughout every experimental run.

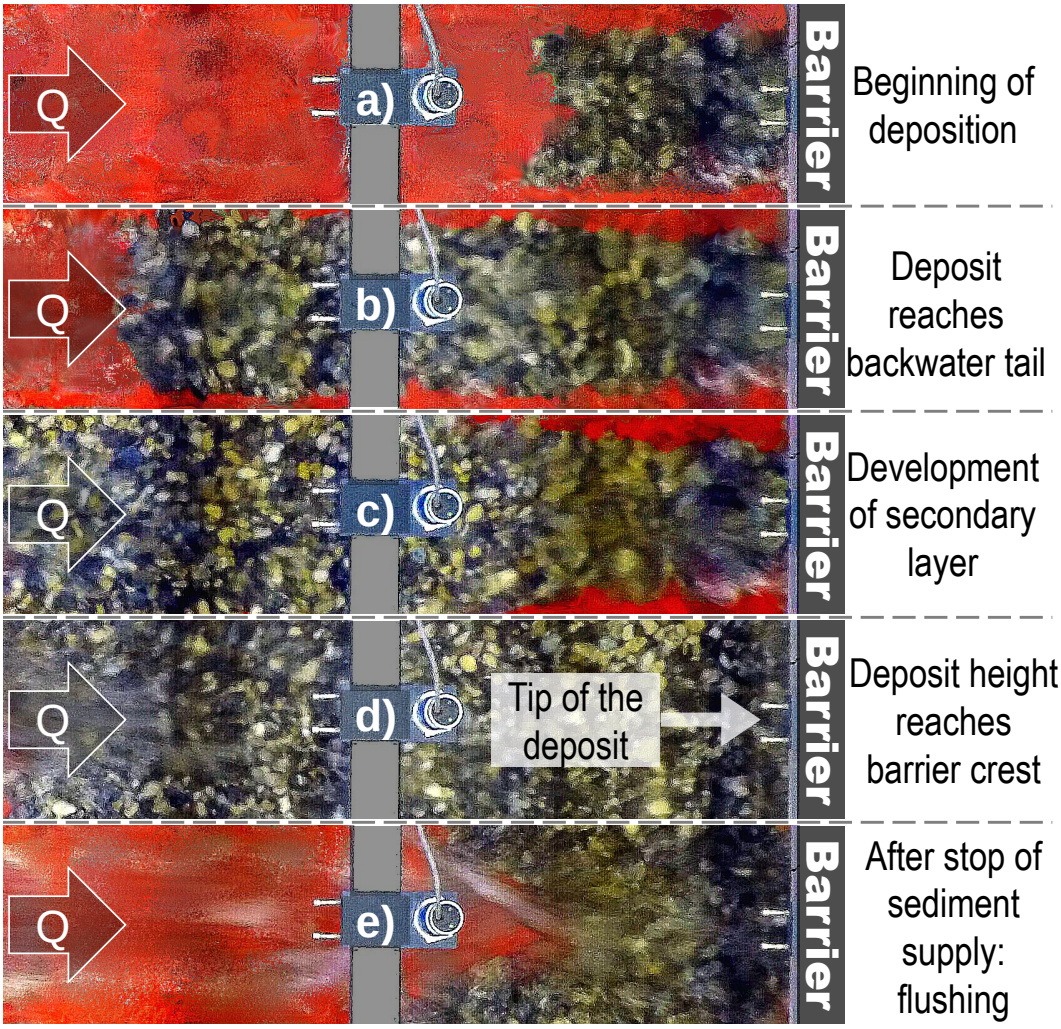

Figure 6.7 – *Top view showing the temporal evolution of sediment deposits over the channel bottom (in red), upstream of hydraulically controlled barriers, with structure overflow (Hy-o): (a) first deposit; (b) beginning of the secondary deposit layer; (c) evolution of the secondary layer from upstream toward the barrier; (d) maximum deposit size, immediately before flushing occurs; and (e) flushing. In the middle of each picture, one ultrasonic sensor with support structure is visible. The barrier is hidden by another ultrasonic sensor.*

Fig. 6.8 a) illustrates the dimensionless bed load transport intensity Φ as a function of F_*, without sediment deposits upstream of the hydraulic barriers, obtained previously (Chpt. 5). These data correspond to the highest value of bed load transport that did not cause sediment deposition upstream of the hydraulic barrier when it was not overflown. In Fig. 6.8 b), Φ is evaluated based on the experiments with sediment deposits upstream of infinitely high (*Hy-no*, no overflow) and height-limited, overflown (*Hy-o*) barriers. For the case *Hy-no*, both vertical flow constrictions, with pressurized flow conditions, imposed by the constriction height a and lateral flow constrictions with free surface flow conditions, imposed by the constriction width b, are represented. Φ refers

to the maximum sediment outflow rates that were measured downstream of the barrier during the flushing phases (Fig. 6.7). The maxima of Φ, with barrier overflow (*Hy-o*), are one order of magnitude higher than in the case of infinitely high barriers without overflow (*Hy-no*). However, the bed load transport intensity observed during the flushing episodes never exceeded the values observed without deposits (cf. Fig. 6.5).
The comparison of Fig. 6.8 a) and b) shows that the maximum bed load transport intensity downstream of a hydraulic barrier without the occurrence of overflow is similar considering or not the existence of upstream sediment deposits.

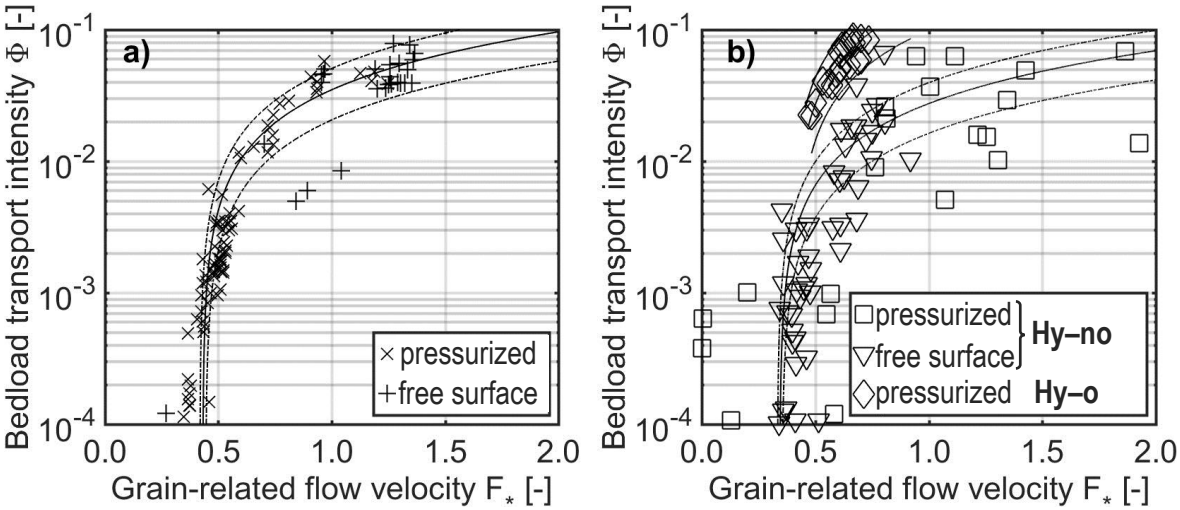

Figure 6.8 – *The bed load transport intensity* Φ *as a function of the grain-related flow velocity* F_* *(a) without (Chpt. 5) and with (b) sediment deposits upstream of the hydraulic control barriers with infinite height (Hy-no, no overflow) and with limited height (Hy-o, with overflow). Regression curves (continuous lines) are indicated with 68 % confidence intervals (dashed lines).*

The grain-related flow velocity, defined as $F_* = Q \,/\, (A \cdot \sqrt{g\, D_{84}})$, is used in Fig. 6.8 for the description of Φ. The relation between them can be interpolated by regression curves (continuous lines) according to the following expressions.

- No deposit (Fig. 6.8 a)
  → Infinite barrier height (Chpt. 5) $\Phi = 0.061 \cdot F_* - 0.027$ ($R^2 = 0.88$);
- With deposit (Fig. 6.8 b)
  → Infinite barrier height (*Hy-no*) $\Phi = 0.042 \cdot F_* - 0.014$ ($R^2 = 0.68$);
  → Limited barrier height (*Hy-o*) $\Phi = 0.028 \cdot F_* - 0.114$ ($R^2 = 0.79$).

The regression curves indicate that the bed load transport in terms of Φ becomes larger than zero when F_* exceeds the absolute value of the constant term, i.e., $F_* \geq 0.33$ in case *Hy-no* and $F_* \geq 0.25$ in case *Hy-o*. Therefore, the constant term may be considered as a critical value of F_*, where sediment deposition occurs when F_* is smaller than this critical value. These observations refer to subcritical flow conditions (Froude numbers smaller than unity, namely approximately 0.2 to 0.3). In theory, the grain mobility in the backwater of hydraulic barriers can be assessed using the grain-related dimensionless bed shear stress τ_*. Grain deposition is likely to occur when $\tau_* < \tau_{*cr}$, where

τ_{*cr} denotes a critical value of τ_* (Shields, 1936; Einstein, 1950). The value of τ_{*cr} increases with the channel slope and can be assessed for gravel bed rivers by $\tau_{*cr} = 0.15\ S_0^{0.25}$ according to (Lamb et al., 2008). Recking (2013b) proposes an alternative expression which also implies the representative grain size D_{84}: $\tau_{*cr}(D_{84}) = (1.32\ S_0 + 0.037)\ (D_{84}/D_{50})^{-0.93}$. For this study, the expressions from Lamb et al. (2008) and Recking (2013b) result in τ_{*cr} values of 0.73 and 0.67, respectively. For steady and uniform flow, the dimensionless bed shear stress can be computed by $\tau_* = h \cdot S_0 \ /\ (s\text{-}1)\ D_{84}$ (Von Karmàn, 1930; Kramer, 1932). Thus, the measurements in the non-constricted channel, according to the onset of sediment deposition, correspond to values of $\tau_{*cr} = 0.061 \pm 0.005$. This value of τ_{*cr} refers to the threshold for grain deposition, which was found to be smaller than τ_{*cr} for grain mobilization (Ancey et al., 2002). Hence, the smaller measurement values of τ_{*cr} can be considered to be consistent with the literature and observations in natural streams. However, the flow in the backwater of the flow constrictions is not uniform, and the channel slope S_0 needs to be substituted by the energy slope. This evaluation, based on the friction law (Chézy, 1776), results in values of $\tau_{*cr} \approx 0.04 \pm 0.005$ in the backwater of the hydraulic barriers (cf. Chpt. 4).
The relationship between F_* and the relative submergence of the orifice is assessed in Fig. 6.9. A clear and unique trend cannot be identified for pressurized orifice flow (Fig. 6.9 a), in particular for case *Hy-o* where overflow occurs. For free surface flow (lateral constrictions), clear linear trends between the relative submergence, assessed in terms of $b_{*D}\ /\ h_{*D}$, and the grain-related flow velocity F_* are identified (Fig. 6.9 b):

- No deposit (Chpt. 5) → $F_* = 0.855 \cdot b_{*D}\ /\ h_{*D}$ - 0.047 ($R^2 = 0.90$);
- With deposit (case *Hy-no*) → $F_* = 0.37 \cdot b_{*D}\ /\ h_{*D} + 0.049$ ($R^2 = 0.86$).

A clear and unique trend between the grain-related flow velocity F_* upstream of the hydraulic barriers and the relative orifice submergence (a_{*D}/h_{*D} and b_{*D}/h_{*D}) can only be identified in the case of solely laterally constricted, free surface flow (Fig. 6.9 b). The relationship between F_* and the relative submergence $a_{*D}\ /\ h_{*D}$ of vertical constrictions can be grouped by deposit allowances (literature data, as well as data of cases *Hy-no* and *Hy-o*; Fig. 6.9 a). Some sub-grouping can also be observed within the cases *Hy-no* and *Hy-o*, but the author could not parametrize these sub-groups based on the present data.

6.3.3 Mechanical control (*Mec*)

The effects of the bar screen on the upstream flow depth are evaluated in terms of the grain-related flow velocity F_* as a function of the ratio $f_m\ /\ h_{*D}$ (Fig. 6.10). The clearance height $f_m \cdot D_{84}$ under the screen was incrementally increased in millimeters. The normalized parameter $f_m\ /\ h_{*D}$ is used to relate the submergence of the barrier to the discharge, which is incorporated in the grain-related flow velocity F_*. No clear trend between $f_m\ /\ h_{*D}$ and F_* can be observed in Fig. 6.10. However, Fig. 6.10 allows one to estimate the flow resistance effects of the bars, which increases with decreasing clearance under the bars, i.e., decreasing f_m. The hydraulic effects of screens are commonly quantified by a local head loss coefficient as a function of the flow effective screen clearance, bar shape and inclination (Hager, 2010; Di Stefano and Ferro, 2013, 2014).
The corresponding maximum bed load transport intensity Φ that could still pass the bar screen is shown in Fig. 6.11, related to the grain-related flow velocity F_*. These values were measured

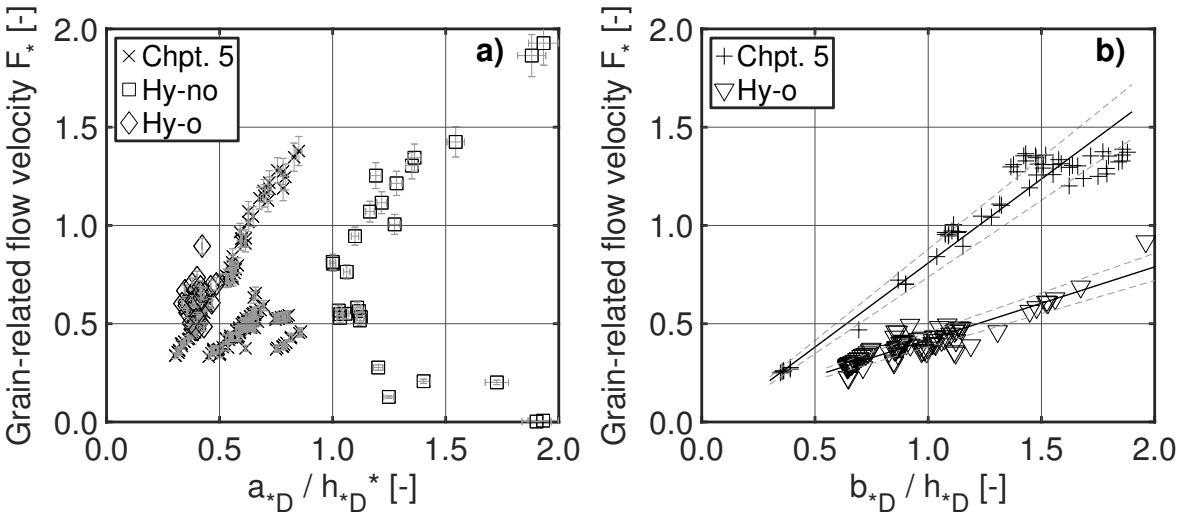

Figure 6.9 – *Evaluation of the grain-related flow velocity F_* as a function of the relative submergence of hydraulic barriers with (a) vertical, pressurized a_{*D} / h_{*D} and (b) lateral, free surface flow constrictions. The data from Chpt. 5 correspond to experiments with neither upstream sediment deposits nor structure overflow; the new experiments correspond to case Hy-no with upstream deposit but without structure overflow; and case Hy-o corresponds to upstream deposit and structure overflow. Regression curves (continuous lines) are indicated with 68 % confidence intervals (dashed lines).*

downstream of the bar screen, which clogged instantaneously under higher transport intensities compared to the intensities shown in Fig. 6.11.

The values shown in Fig. 6.11 are grouped by f_m. The bar screen clogged quickly (lower values of Φ) when $f_m < 1.7$. For $f_m \approx 1.83$, clogging was only sometimes observed, and important bed load rates could pass the barrier under the higher discharges ($F_* > 1.5$). The bar screen was nearby ineffective (clogging was very rarely observed) when f_m was further increased ($f_m \approx 1.90$). For $f_m \approx 1.75$, clogging was very probable for higher discharges ($F_* > 1.5$), whereas the bed load transport was not interrupted for ordinary (smaller) discharges ($F_* < 1.3$). Thus, the desired bed load retention function of the mechanical barrier in terms of the bar screen was achieved at a value of $f_m \approx 1.75$. This value was retained for the subsequent experiments, where combined hydraulic and mechanical control was investigated.

6.3.4 Combined mechanical-hydraulic control (*HyMec*)

The same experimental procedure was used for the combination of the hydraulic and mechanical control barrier as for the hydraulic control only. Thus, the barrier height, defining the level over which overflow occurs, was kept at Δz_{dam} = 0.11 m (both hydraulic and mechanical, cf. Figs. 6.2 and 6.3). Regarding the hydraulic control structure, a varying constriction height a and a constant width b were applied (*Hy-o*, Fig. 6.3). The bar screen was placed with the optimum bottom clearance of 1.75·D_{84} according to the previous experiments (*Mec*). By definition, the hydraulic control barrier governs the hydraulics upstream of the barrier in terms of the constriction dimensions. Therefore, F_* is shown in Fig. 6.12 as a function of the relative submergence of the hydraulic control a_{*D} / h_{*D}. This relationship can be interpolated by F_* = 1.35·a_{*D}/h_{*D} - 0.11 (R^2 = 0.89).

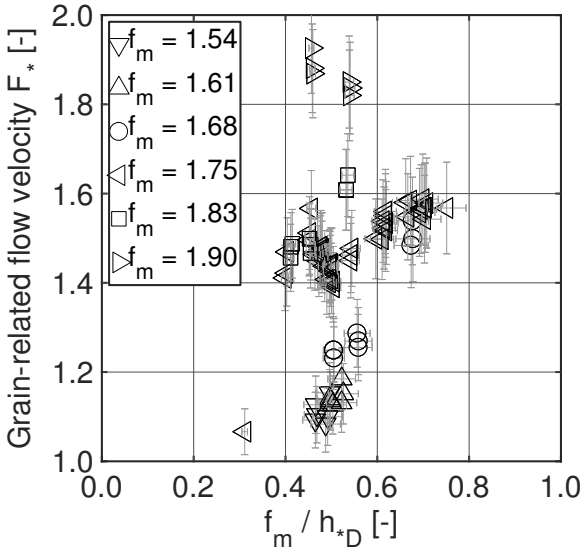

Figure 6.10 – *Evaluation of the grain-related flow velocity F_* as a function of the relative submergence of mechanical barriers in terms of the bar screen, defined as $f_m/h_{*D} = f_m \cdot D_{84}/h_{*D}$ (Mec, Fig. 6.3).*

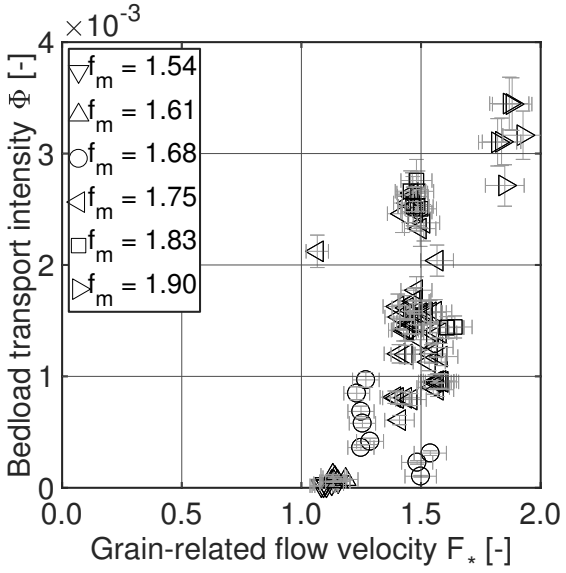

Figure 6.11 – *The bed load transport intensity Φ as a function of the grain-related flow velocity F_*, with varying bottom clearance height $f_m \cdot D_{84}$ for mechanical barriers in terms of the bar screen (Mec, Fig. 6.3).*

The bed load transport intensity Φ through the combined control barrier is shown in Fig. 6.13 as a function of the grain-related flow velocity F_*. The figure shows that the maximum values of Φ increase with increasing F_* and with increasing relative constriction height a_*.
Once a deposit developed during the tests, the barrier was obstructed such that sediment flushing could not occur, as illustrated in Fig. 6.14.

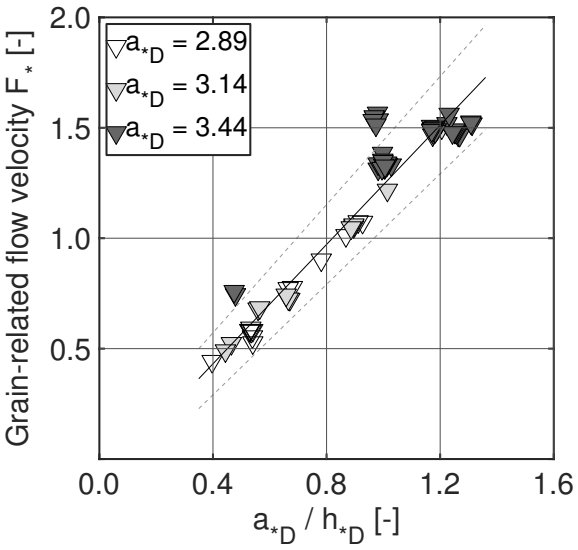

Figure 6.12 – *Evaluation of the grain-related flow velocity F_* as a function of the relative submergence a_{*D} / h_{*D} for combined (hydraulic and mechanical) control barriers (HyMec, Fig. 6.3), for a constant value of $f_{m,opt}$ = 1.75, with varying constriction height a and constant constriction width b.*

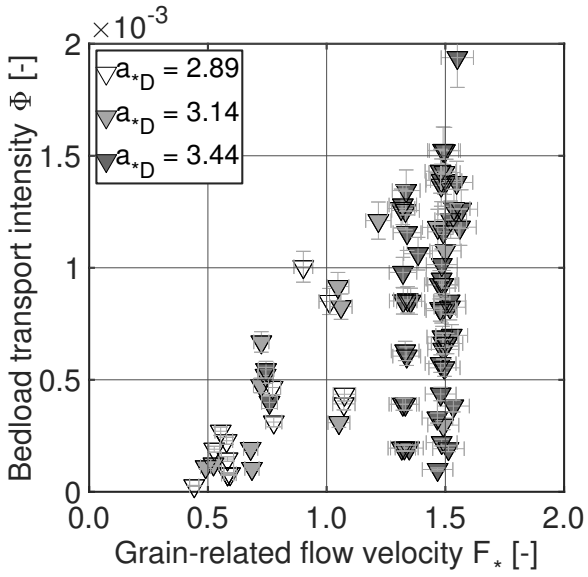

Figure 6.13 – *The bed load transport intensity Φ as a function of the grain-related flow velocity F_* for combined (hydraulic and mechanical) control barriers (HyMec, Fig. 6.3), for a constant value of $f_{m,opt}$ = 1.75, with varying constriction height a and constant constriction width b.*

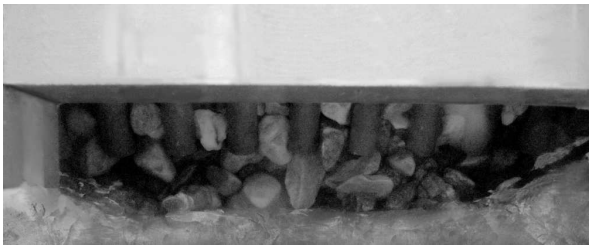

Figure 6.14 – *Entangled grains at the combined (hydraulic and mechanical) control barrier (HyMec, Fig. 6.3); cross sectional view from downstream.*

6.4 Discussion

The grains used in the present experimental work were rather coarse (w / D_{84} ≈ 8.0). However, finer sediment is also expected to deposit with the reduction in the flow transport capacity which reduces in the backwater of the hydraulic barrier.
Related to the hydraulic control, the description of the upstream flow conditions is based on flow depth measurements made in the vicinity of the barriers. This is possible because the sediment deposit never interacted directly with the barrier, i.e., the measured flow depth always refers to the clear water depth over the channel bottom.
The flushing of sediment deposited upstream of the barrier was not possible once the bar screen was clogged. However, sediment transfer without barrier clogging is desirable for ordinary (smaller) discharges (Surian and Rinaldi, 2003; Simoni et al., 2017). The optimum value of $f_{m,opt} \cdot D_{84} = 1.75 \cdot D_{84}$ for the bottom clearance of the screen (Fig. 6.2) is sensitive to the sediment grain size, and other studies report slightly different values of f_m for the occurrence of clogging (Zollinger, 1983; Uchiogi et al., 1996; Lien, 2003; Ono et al., 2004; Mizuyama, 2008; Canelas et al., 2015; Piton and Recking, 2016a, and Tab. 2.5 on page 29). With respect to the measurement inaccuracy (cf. Tab. 3.2, page 47), the error of measurement in f_m is approximately ±0.07, i.e., $f_m = 1.75 \pm 0.07$, within a 68 % confidence interval. This overlaps with the values of f_m that correspond to experimental observations of more prompt ($f_m = 1.68$) or rare ($f_m = 1.83$) clogging. Therefore, the design of barriers for mechanical control requires special attention in practice, as there are often uncertainties regarding the sediment size, and also driftwood, which is not considered by this study, may also occur.
Unwanted flushing of sediment deposits upstream of hydraulic control barriers represents a major problem in practice. Herein, three practical cases of sediment control structures are discussed vis-à-vis the experimental results. The flushing of sediment deposits is of particular interest in these practical cases, which are the following:

- The previous barrier of *Stiglisbrücke* at the Schächen torrent (Canton of Uri, Switzerland), which consists of a slit check dam (open-crested torrential barrier with narrow vertical orifice, i.e., lateral flow constriction) with horizontal beams in the orifice (Bezzola, 2008);
- The slot check dam (close-crested torrential barrier with wide and low openings) at the headwaters of the Schnannerbach torrent in the Tyrol (Austria, Fig. 6.15);
- The filter check dam at the Dranse torrent (close-crested sill with one opening in Canton of Valais, Switzerland), as previously introduced in Chpt. 5.2.6(page 78), was also tested with an upstream superposed bar screen (Schwindt et al., 2016a), which is of particular interest in the context of this chapter.

In the case of the Schächen torrent, the Stiglisbrücke barrier was filled up and flushed out several times during a major flood in August 2005 (Püntener, 2006). The main cause for the unwanted sediment flushing of Stiglisbrücke was temporary scour of the unpaved bottom outlet and the downstream stilling basin. But, the observed flushing processes at Stiglisbrücke were similar to the phenomena described in the present analysis, corresponding to Fig. 6.7, for overflown hydraulic control barriers. Although Stiglisbrücke was primarily designed for mechanical control, the process analysis of the 2005 flood event indicates that the barrier did not clog mechanically and therefore acted similar to an insufficient hydraulic control measure (Bezzola, 2008). This underlines the necessity of the consideration of the hydraulic control of such slit check dams. The Stiglisbrücke

barrier was remodeled using a robust mobile weir that currently serves for adjusting the height of one opening in the now close-crested barrier (Kanton Uri, 2016). This constitutes an adjustable hydraulic control measure. However, this is a cost-intensive solution that requires regular maintenance works and stand-by duty on site in the case of floods. As mentioned in the introduction, the legal framework and responsibility of triggering weir adjustments cause further implications. Therefore, it is advantageous to substitute such adjustable technical solutions with passive measures such as the presently studied combination of hydraulic and mechanical control.
During the same flood event in August 2005, the barrier at the Schnannerbach was also subjected to unwanted sediment flushing. This barrier is a massive concrete structure with multiple slots (Fig. 6.15). At the beginning of the flood, the barrier acted as desired and caused upstream sediment deposition. But at some unknown instant, sediment flushing occurred and caused important damage in downstream urban reaches. The sediment transport processes were described as fluvial bed load transport, without the occurrence of debris flow and woody debris (Hübl et al., 2006). In Fig. 6.15, it can be observed that the sediment size is significantly smaller than the opening size. Therefore, it is likely that the barrier acted exclusively as a hydraulic control measure.

Figure 6.15 – *Picture of the slot barrier at the Schnannerbach torrent (Austria) after the flood event in August 2005; view from downstream. © Michael Sturm, Uni Innsbruck, with permission.*

These observations raise the question of whether an upstream superposed mechanical control barrier, as applied in the experiments in this study, can prevent unwanted sediment flushing even if the representative grain size is smaller than expected. Such a case was studied through physical experiments at the Dranse torrent (Switzerland) using a physical Froude model of scale 1:42. One of the objectives of this study was the verification of the working principle of a filter check dam composed of an upstream superposed bar screen for mechanical control and a downstream slot for hydraulic control (Schwindt et al., 2016a, according to Fig. 6.16 a). This mechanical barrier was composed of vertical bars with an inclination of 2:1 and horizontal interspace corresponding to the D_{84} of the supplied sediment. The bottom clearance height of the screen was set to $2.6 \cdot D_{84}$, but the vertical bars used in the Dranse model did not overlap the bearing beam as in this chapter (cf. Fig. 6.2). The experiments with the Dranse model were conducted with constant water discharge and sediment supply for investigating hydraulic sediment retention and the obstruction of the barrier.
The formation of sediment deposits was observed in the backwater of the barrier. These deposits evolved slowly in the downstream direction toward the barrier. When the deposit front reached the barrier, the superposed screen was obstructed as shown in Fig. 6.16 c. This obstruction was not

observed for higher values of f_m or without a mechanical control device, as shown in Fig. 6.16 d (Schwindt et al., 2016a). This shows that the sensitivity of clogging of mechanical barriers in terms of the grain size decreases in the backwater of hydraulic barriers because clogging is still possible for f_m = 2.6. Without the backwater of the hydraulic barriers, clogging is not possible for $f_m > 2$, as shown in this chapter and according to literature findings (Zollinger, 1983; Uchiogi et al., 1996; Lien, 2003; Mizuyama, 2008; Piton and Recking, 2016a; Shima et al., 2016, and Tab. 2.5 on page 29). In addition, the weak point of the hydraulic barrier, i.e., unwanted sediment flushing, was prevented by the upstream bar screen.

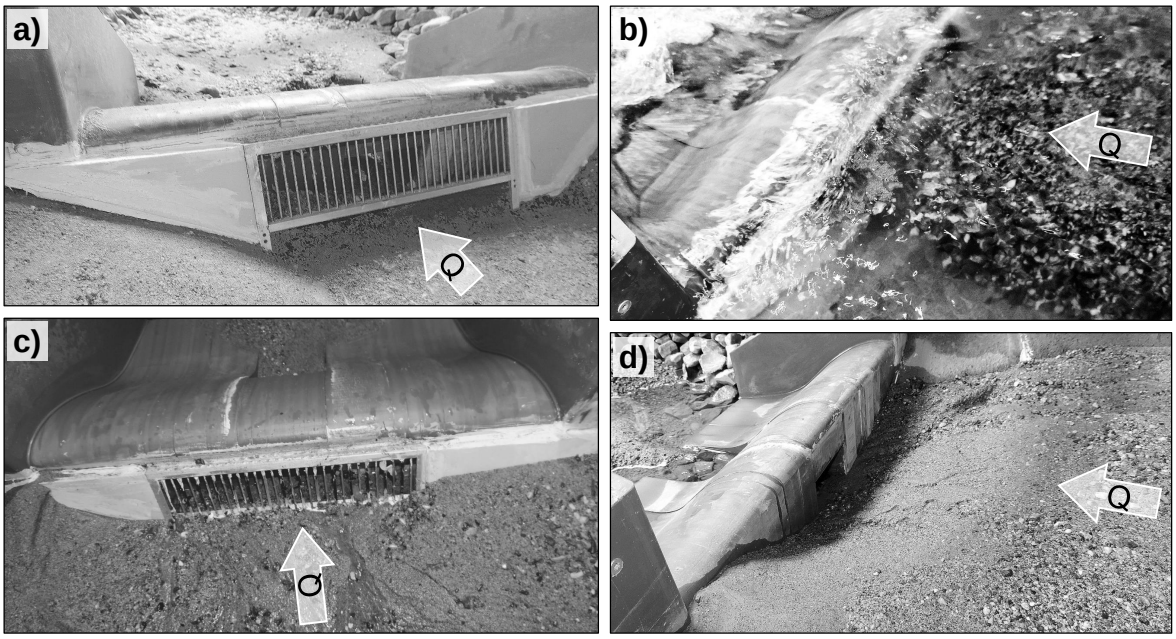

Figure 6.16 – *Model of the check dam at the Dranse torrent (Schwindt et al., 2016a); a) the barrier composed of an inclined bar screen (mechanical control) upstream of a massive structure with a slot for hydraulic control, b) the sediment front arriving at the barrier, c) mechanical obstruction of the upstream screen after the arrival of the sediment front, and d) aspiration cone in the sediment deposit upstream of the barrier without the screen. © Sebastian Schwindt.*

The comparison of Figs. 6.8 b and 6.13 shows that the maximum bed load transport intensity Φ of overflown hydraulic barriers is approximately two orders of magnitude higher than in the case of overflown barriers with an upstream screen for mechanical control connected to a downstream hydraulic barrier. This analysis is based on the grain-related flow velocity F_*, which is, for overflown structures, a linear function of the ratio of the relative constriction height and upstream flow depth (Fig. 6.12).

The establishment of discharge rating curves upstream of deposition control measures is in practice often impossible during floods due to morphological changes, i.e., channel adjustments caused by temporal sediment deposition and re-mobilization (Piton, 2016). Thus, it might be useful to relate bed load retention exclusively to the discharge, without the necessity of a discharge rating curve. For the present data, the Smart and Jaeggi (1983) formula is used (cf. Fig. 6.5 and Eq. 2.18 on page 17) as reference for the bed load transport capacity of the channel without barrier (Fig. 6.17). The Smart and Jaeggi (1983) formula overestimates the bed load transport of steep headwaters

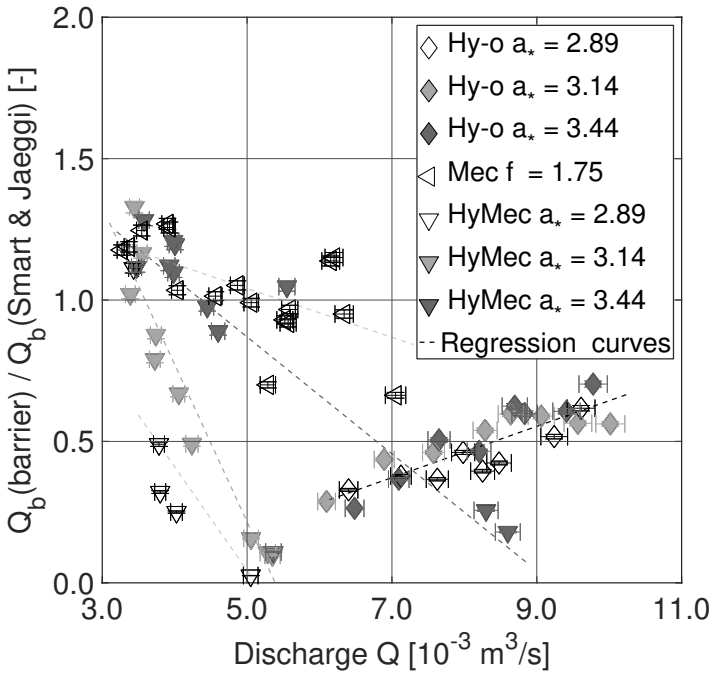

Figure 6.17 – *Comparison of the ratio between bed load passing the barrier and bed load according to the Smart and Jaeggi (1983) formula as a function of the discharge Q for overflown hydraulic, mechanical and combined barriers. The dashed lines indicate regression curves (Tab. 6.2), and the error bars refer to the inaccuracy of the measuring equipment.*

with limited sediment supply by approximately two orders of magnitude (Rickenmann, 2001). However, sediment deposits upstream of hydraulic barriers may represent an important sediment source in the case of sediment flushing. This may cause artificial debris flow, as observed, e.g., at Slovenian mountain rivers (Sodnik et al., 2015). According to the present study, such intense sediment transport may occur when hydraulic barriers transform typically supply-limited channels into channels with locally unlimited sediment supply (Recking, 2012) This difference in bed load transport between the Smart and Jaeggi (1983) formula and naturally supply-limited channels may represent a hazard to urban downstream river reaches, where the transport capacity can be reduced at bottlenecks such as bridges. The ratio of the bed load transport capacity with hydraulic, mechanical or combined (mechanical plus hydraulic) barriers Q_b (barrier) determined in this chapter and by the Smart and Jaeggi (1983) formula Q_b (Smart&Jaeggi) is shown in Fig. 6.17 as a function of the discharge. When this ratio is unity, the bed load transported through the barrier corresponds to the bed load transport given by the Smart and Jaeggi (1983) formula. The coefficients of the linear regression curves (dashed lines) of the shape $p1 \cdot Q + p2$ in Fig. 6.17 are listed in Tab. 6.2.

Table 6.2 – *Parameters of the linear regression curves in Fig. 6.17 with indication of the coefficients of determination R^2.*

Case	(Graph)	$p1$	$p2$	R^2
Hy-o	(all)	90.6	-0.26	0.72
Mec	(f_m = 1.75)	-86.39	1.47	0.42
HyMec	(a_{*D} = 2.89)	-366.7	1.88	0.64
HyMec	(a_{*D} = 3.14)	-556.7	3.00	0.92
HyMec	(a_{*D} = 3.44)	-206.7	1.90	0.70

For hydraulic control, a single linear regression curve indicates that the bed load transport capacity increases with discharge. According to the regression coefficients (Tab. 6.2), the bed load transport of the overflown hydraulic barrier is equivalent to the bed load transport estimated with the Smart and Jaeggi (1983) formula when the discharge is $Q \approx 14$ l/s. An additional test run with approximately $Q = 12.3$ l/s, which is not shown here, confirmed this trend. Higher discharges were not possible due to the model limitations.
In the presence of a mechanical control barrier (bar screen), the regression curves indicate a decay of the transport capacity with discharge. Considering the findings of this chapter and the physical model study of the Dranse, the combination of hydraulic and mechanical control barriers improves the control of sediment retention when a flood threshold discharge is exceeded. Simultaneously, the safety against unwanted sediment flushing is increased.
As demonstrated in this chapter, the bottom clearance height of the bar screen should be determined independently from the hydraulic barrier. This results in some multiple $f_m < 2$ of the expected sediment size in terms of D_{84}. A bar screen that is designed in such a manner, combined with a hydraulic barrier, will also clog in the case whereby the transported grains are smaller than the expected D_{84}. As per the Dranse study, such a bar screen upstream superposed to a hydraulic barrier clogs even up to $2.6 \cdot D_{84}$. The height of the constriction imposed by a hydraulic barrier can be used to adjust the triggering of sediment deposition, as shown in Figs. 6.13 and 6.17. The width of the constriction in the overflown hydraulic barrier (*Hy-o* and *HyMec*) was slightly larger than the bottom channel width. This aims at avoiding effects on the flow due to the barrier up to the occurrence of small floods, to promote the longitudinal river continuity.
The typical approach for the design of structural mitigation measures considers barriers with slots or slits for water and sediment retention in terms of sediment dosing or sorting (cf. Chpt. 2.6.2, page 22 ff.). In this context, it is recalled that dosing is the temporary, partial retention of sediment, and sorting is the filtering of coarse material. Sectional and lattice barriers are used to target partial sediment retention in terms of dosing or sorting (cf. Tab. 2.4, page 23). Sectional barriers consist of vertical bars; lattice barriers consist of screens with vertical bars and horizontal beams, similar to the application in the present systematic experiments (Hübl et al., 2003, 2005, according to Fig. 2.5, page 24).
According to the present analysis, slot or slit barriers should be used for hydraulic control only (sediment dosing). Inclined lattice barriers, such as the bar screen superposed upstream of a hydraulic barrier applied in this study, are conceivable for sediment sorting and for preventing unwanted sediment flushing during floods. The size of the sorted (retained) sediment is determined as a function the clearance of the screen, as discussed in the study in terms of the multiplier f_m.

6.5 Conclusions

This chapter analyzes the retention of bed load due to hydraulic control based on discharge and its combination with a mechanical control device. The hydraulic control is prone to the unwanted flushing of formerly deposited sediment. Backfilled, overflown hydraulic barriers may release bed load that can reach more than 50 % of the bed load transport capacity corresponding to the Smart and Jaeggi (1983) formula.
The retention of bed load by mechanical control is analyzed based on the height of the bottom clearance in terms of some factor of the characteristic grain size. With regard to morphological river continuity, the optimum bottom clearance is the maximum height that still allows for mechanically controlled bed load deposition. This value is found here as $1.75 \cdot D_{84}$ of the sediment supply. If finer bed load is transported, the grains cannot entangle in the mechanical control barrier, which is then ineffective.
The combination of hydraulic and mechanical control barriers enables sediment retention, with a lower sensitivity to the representative grain size and with a lower risk of unwanted sediment flushing. In practice, barriers with flexible opening sizes are sometimes installed to overcome the uncertainties related to each control mechanism. The flexible opening height is linked with legal implications and requires robust hydro-mechanical equipment, as well as stand-by duty service. Therefore, the combination of hydraulic and mechanical control barriers, as analyzed in this chapter, represents a cost-effective and passively working alternative.

7 Experimental study on permeable sediment traps with guiding channel [1]

Abstract

Sediment traps created by partially open torrential barriers are crucial elements for flood protection in alpine regions. The trapping of sediment is necessary when intense sediment transport occurs during floods which may endanger urban areas at downstream river reaches. In turn, the unwanted permanent trapping of sediment during small, non-hazardous floods can result in the ecological and morphological depletion of downstream reaches. This study analyzes experimentally a new concept for permeable sediment traps. For ensuring the sediment transfer up to small floods, a guiding channel implemented in the deposition area of the sediment trap was studied systematically. The bank-full discharge of the guiding channel refers to a dominant morphological discharge. At the downstream end of the guiding channel, a permeable barrier triggers sediment retention and deposition. The permeable barrier consists of a bar screen for mechanical deposition control, installed in front of a flow constriction for the hydraulic control. The fail-safe clogging of the barrier and the sediment deposition upstream can be ensured for discharges that are higher than the bank-full discharge of the guiding channel.

[1] This chapter is based on the scientific paper draft "Experimental study of sediment traps permeable for frequent floods" by S. Schwindt, M.J. Franca, A. Reffo and A.J. Schleiss. The experiments and analyses hereafter are original and were developed by the author. The data shown in the figures are listed in the Appendix (A.4.3).

7.1 Introduction

The sediment supply of mountain rivers is a substantial source for the dynamics of river ecosystems. Artificial barriers, such as dams, can affect the natural flow regime variability with direct impacts on the eco-morphological state of rivers (Allan and Castillo, 2007; Sponseller et al., 2013). Maintaining the natural conditions of rivers is a multidisciplinary concern and artificial interventions require the consideration of ecological and morphological site evaluations (cf. Chpt. 2.5 Bain et al., 1999). The morphological processes in mountain rivers depend and interact with the transport of sediment (e.g., Buffington and Montgomery, 1999; Hassan et al., 2005; Recking et al., 2016). In this context, the sediment supplied by the headwaters is essential for the ecologic diversity of downstream river reaches (Milhous, 1998; Gomi et al., 2002; Denic and Geist, 2015). Accordingly, the sediment transport and morphological pattern have to be considered for the assessment of the state of a river in terms of the quality of aquatic habitats and biodiversity (Modde et al., 1991; Jensen and Bourgeron, 2012; Church and Ferguson, 2015). Therefore, sediment transport-related criteria can also be designated as "eco-morphological" river characteristics (Moyle and Mount, 2007). These characteristics can often be attributed to a certain discharge which alters and rearranges the channel bed morphology. This discharge may be assessed by the dominant, morphologically effective discharge (cf. Chpt. 2.5 and Wolman and Leopold, 1957a,b; Wolman and Miller, 1960). However, the artificially forced retention of sediment, especially bed load, may be required for exceptional floods which endanger potentially downstream riparian urban areas using sediment traps. A concept for permeable sediment traps, which enables the passage of non-hazardous bed load transport and the safe retention of bed load when it is transported in hazardous amounts during floods, is introduced and analyzed in this chapter.

7.2 Design approach for permeable sediment traps

The typical concept of sediment traps is recalled in Fig. 7.1, with the following elements: ① a barrier with opening (open check dam) with an open or close crest and ② downstream abutments with counter dam for scour protection; ③ a retention basin, i.e., deposition area; ④ lateral dykes for limiting the deposition area; ⑤ a maintenance access; and ⑥ an inlet structure with scour protection (Wang, 1903; Hampel, 1968; Kronfellner-Krauss, 1972; Hübl et al., 2005; Mizuyama, 2008; Piton and Recking, 2016a). The river discharge should pass the deposition area and the barrier opening(s) without interaction, unless intense bed load transport occurs. The triggering of bed load retention can be a result of hydraulic control since a certain flood discharge is exceeded or mechanical control due to entangled coarse sediment or wood (cf. Chpt. 2.7.2).
In this context, inlet structures (Fig. 7.1) in the form of sills are, besides the barrier itself, an additional obstacle regarding the longitudinal river connectivity. Such sills can cause downstream scour or dead storage volume (Zollinger, 1983). Therefore, inlet structures are avoided when possible in practice (Piton and Recking, 2016a) and they are subsequently not considered.
According to the analyses in Chpts. 4 and 5, the retention of bed load is hydraulically initiated, when the barrier causes a hydraulic jump upstream underlying generally supercritical flow conditions. Then the opening in the barrier acts like a vertical or lateral flow constriction that causes backwater in the deposition area during floods. Therefore, the free surface flow capacity of the barrier

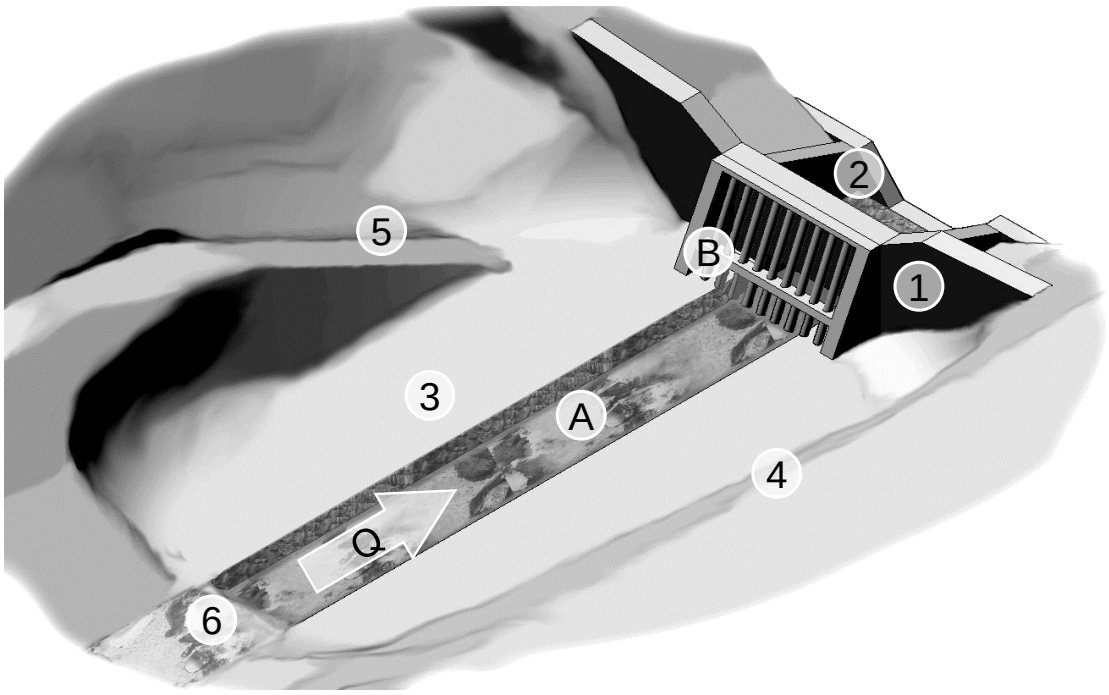

Figure 7.1 – *Concept of a permeable sediment trap consisting of ① an open barrier (open check dam) with overflow crest for flood release, followed by ② downstream abutments with counter dam (sill); ③ a reservoir or deposition area, limited by ④ lateral dykes; ⑤ a maintenance access; and ⑥ an inlet structure with scour protection (adapted from Zollinger, 1983; Piton and Recking, 2016a). For permeable sediment traps, the novel element of Ⓐ a guiding channel is introduced with Ⓑ a barrier consisting of a bar screen for mechanical control and a barrier with an opening for the hydraulic control of bed load retention (cf. Chpt. 6).*

opening(s) without backwater should be smaller than to the sediment-laden flood discharge which potentially endangers urbanized downstream regions.
The combination of both hydraulic and mechanical control was obtained in Chpt. 6 by installing a bar screen in front of an opening of a barrier (open check dam). This combination has been shown to be advantageous to avoid the unwanted flushing of formerly deposited sediment in the deposition area. Based on the previous findings (Chpt. 6), the implementation of a bar screen for the mechanical control and a flow constriction for the hydraulic control (Ⓑ in Fig. 7.1) is considered in this chapter with a widened upstream deposition area. A guiding channel (Ⓐ in Fig. 7.1) in the deposition area is introduced as a novel element with the purpose to improve the sediment transfer through the sediment trap up to small, non-hazardous floods. This sediment trap concept has the purpose to ensure the sediment transfer up to the bank-full discharge of the guiding channel and the safe sediment retention for higher discharges. In practice, the bank-full discharge of the guiding channel should correspond at least to small floods referring to the dominant, morphologically effective discharge (Wolman and Leopold, 1957a,b; Wolman and Miller, 1960), whereas the highest possible permeability of a sediment traps is preferable regarding downstream morphodynamics. A sediment trap which is permeable up to a maximum, site-related and morphologically relevant discharge is developed in the following with the guiding channel as central element. However, it is important that such a sediment trap also enables the safe retention of bed load when it was hazardous to downstream urbanized river reaches. Therefore, a so-called permeable sediment trap is suggested and experimentally tested with a standardized hydrograph, corresponding to typical hydrological characteristics of mountain rivers. Special attention is drawn in supplementary experimental runs on the possibility of self-flushing of sediments.

7.3 Methodology

7.3.1 Adjustment of the experimental set-up

General

The experimental set-up, as previously described (Chpt. 3.2), is recalled in Fig. 7.2. For the present analyses the minimum and maximum pump discharges were 5.5 l/s and 12.5 l/s, respectively. The barriers in terms of a bar screen and mobile PVC elements were introduced in the lower third of the observation reach, approximately 0.9 m upstream of the model outlet. The model adaptations in terms of a widened deposition area with guiding channel are introduced in the following sections.
This analysis refers to the records of the pump discharges Q and minute-wise measurements outflowing sediments (bed load outflow $Q_{b,o}$), according to Chpt. 3.2.5. The volumes and patterns of the sediment deposits were recorded using the motion sensing camera (Microsoft Kinect V2) at the end of every test. This application has been shown promising, but the results were still affected by some uncertainties (Lachat et al., 2015). For this reason, complementary and redundant reference measurements were made using the laser. Thus, a redundant bathymetric record was produced by centimeter-wise measurements along 16 cross sections with an interspace of 0.10 m (according to the gridlines indicated in Fig. 7.3), which corresponds to approximately 650 point measurements. The accuracy of both measurement techniques was evaluated using the total weight and the packed density ρ'_s of the sediment (gravel with ρ'_s = 1 550 kg/m^3, supplier information). The

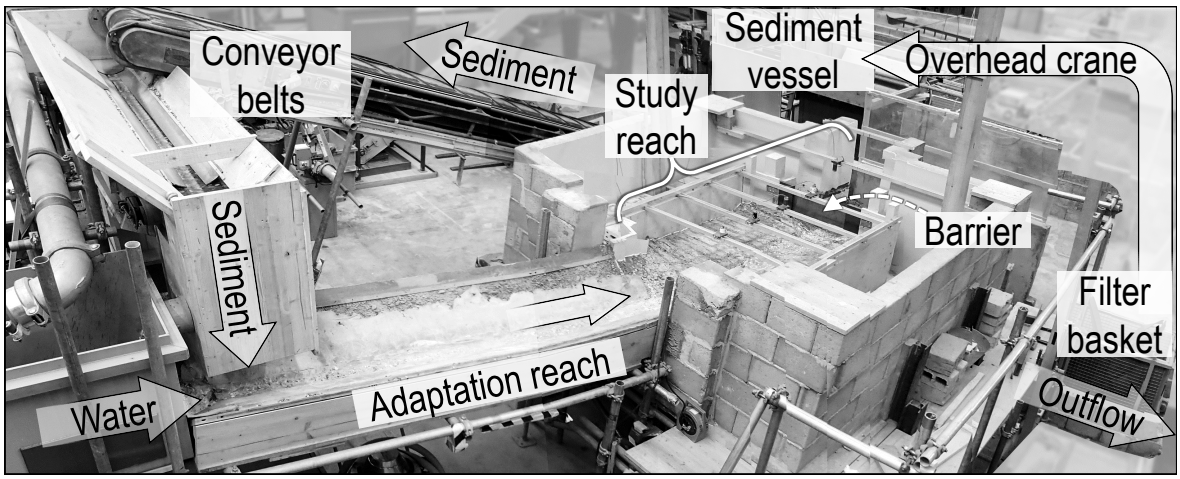

Figure 7.2 – *Picture of the experimental set-up with sediment supply system, consisting of a sediment vessel and conveyor belts; with indication of the water supply by the laboratory pump system, and the adaptation reach that leads the discharges to the observation reach. The barriers were placed at the downstream end of the observation reach. The outflowing sediment and water were separated by a filter basket at the downstream model end.*

evolution of the deposit pattern during the hydrograph experiments was observed by the GoPro Hero4 Silver (2016) camera taking top-view time-lapse pictures (every 10 s).

Deposition area with guiding channel

The observation reach was extended by a wide deposition area with guiding channel according to the sediment trap concept shown in Fig. 7.1. The geometry of the deposition area refers to the desirable optimum between sediment retention and flushing: the trapping efficiency of reservoirs (Brown, 1943), as well as the sediment flushing potential, which increases with increasing length and decreasing width of the deposition area (Zollinger, 1983, 1984; Piton and Recking, 2016a). However, the unwanted flushing of sediment traps represents a high risk at urban downstream reaches and should be avoided (Morris et al., 2008; Sodnik et al., 2015). For a high trapping efficiency and simultaneously a limited risk of unwanted sediment flushing, a rectangular deposition area with a width to length ratio of 3:4 was used for the experiments, as previously proven for being suitable for an optimum functionality of the sediment trap (Zollinger, 1983). The opening angle of the deposition area was set to 30°, which is oriented at the opening angle of natural alluvial deposition cones formed by continuous sediment supply (Parker et al., 1998).
According to the above-mentioned criteria and the model limitations, the deposition area (Fig. 7.3 a) had a length of 1.60 m, a width of 1.20 m, a longitudinal slope S_0 of 5.5 % (as previously in Chpt. 6) and an opening angle of 30°. For the description of the sediment deposits, a model coordinate system was defined with the origin at the location of the barrier. Thus, the positive x-axis points in the upstream direction and $x = 0$ corresponds to the insertion point of the barrier; the positive y-axis points toward the right bank and $y = 0$ corresponds to the flume center; the positive z-axis points upward and $z = 0$ corresponds to the flume bottom at the barrier.
The bottom of the deposition area consisted of gravel from the supply mixture. For ensuring the

same initial conditions for every experimental run, cement grout was poured over the shaped, loose foundation gravel (cf. Fig. 7.3 b and c).

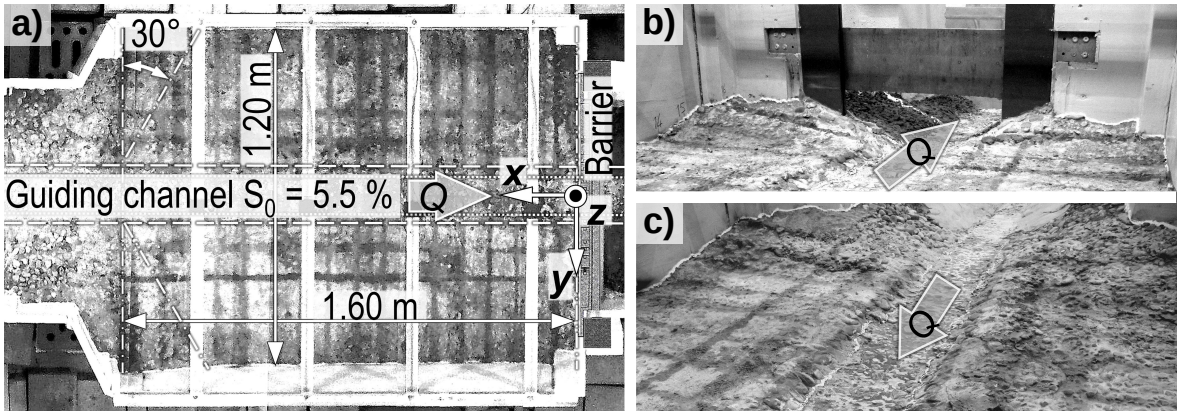

Figure 7.3 – *Details of the observation reach consisting of the deposition area (reservoir) with guiding channel. The marked grid lines on the bottom were used for qualitative purposes and have an interspace of approximately 0.1 m: a) top-view with indication of the reservoir length (1.60 m), width (1.20 m), opening angle (30°) and longitudinal slope (5.5 %), as well as the model coordinate system (x, y, z axis), used for the evaluation of sediment deposits; b) location of barriers, view in the downstream direction; and c) deposition area (reservoir), view in the upstream direction.*

The guiding channel (Ⓐ in Fig. 7.3) enables not only the sediment transfer during low flows, but it also maintains the desired hydraulic functioning of the barrier according to the analyses in Chpts. 4 and 5, as it represents a morphological fixation of the deposition area up to its bank-full discharge. This is important because the dimensions of the hydraulic barrier are a function of the discharge and the upstream channel geometry. Therefore, the hydraulic control works only as desired when the morphology of the upstream channel does not vary.

In the model, the hydraulic design and bank-full discharge of the guiding channel correspond to "small" discharges which are equivalent to the dominant, morphologically effective discharge referring to pristine downstream river reaches (cf. Chpt. 2.5) in practice. A flood hydrograph with higher discharges than the bank-full discharge of the guiding channel was simulated. Due to the model limitations, the guiding channel had a bank-full discharge of Q_{bf} = 5.5 l/s. In practice, the bank-full discharge should refer to approximately 1.1 times the effective discharge to enable the eco-morphological flow continuum through the sediment trap.

The guiding channel had a trapezoidal cross section, as shown in Fig. 7.4, with a bank inclination of m = 2.25 (dimensionless) and a bottom channel width of w = 0.11 m. According to the previous analyses, the discharge-dependent roughness of the guiding channel corresponds to a Mannings' n of $n \approx (1.3{\cdot}10^{-5} \cdot Q^{-2.5}{+}56.6)^{-1}$, i.e., n (Q_{bf} = 5.5 l/s) ≈ 0.02 $\mathrm{m}^{-1/3}$ s. The roughness was constituted by grains larger than the D_{84} of the sediment supply mixture. With respect to the Gauckler–Manning–Strickler formula, the bank-full discharge of 5.5 l/s corresponds to a flow depth of 0.032 m. The shape of the guiding channel was fixed by pouring cement grout in the spaces between the loose grains.

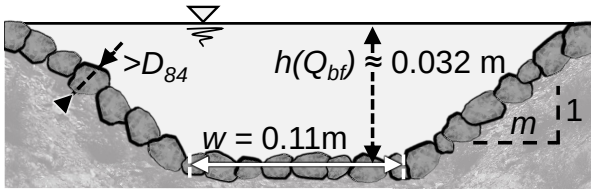

Figure 7.4 – *The cross section of the trapezoidal guiding channel, lined with fixed grains larger than the D_{84} of the sediment supply mixture and designed for bank overtopping for discharges higher than 5.5 l/s.*

Tested deposition control modes of the barrier

The torrential barrier consisting of a flow constriction for the hydraulic control and a bar screen for the mechanical control of bed load retention was introduced at the downstream end of the deposition area. Similar to Chpt. 6, the following three cases of deposition control types are considered:

Case 1 – hydraulic deposition control only, where two situations are considered:
Hy-no **–** a non-overflown, infinitely high barrier with constant opening dimensions (Fig. 7.5 a);
Hy-o **–** an overflown barrier with limited height and constant opening height (Fig. 7.5 b);
Case 2 – *Mec* mechanical deposition control by a bar screen with constant spacing (Fig. 7.5 c);
Case 3 – *HyMec* combined deposition control, i.e., a bar screen upstream of an overflown hydraulic control barrier with variable opening height (Fig. 7.5 d).

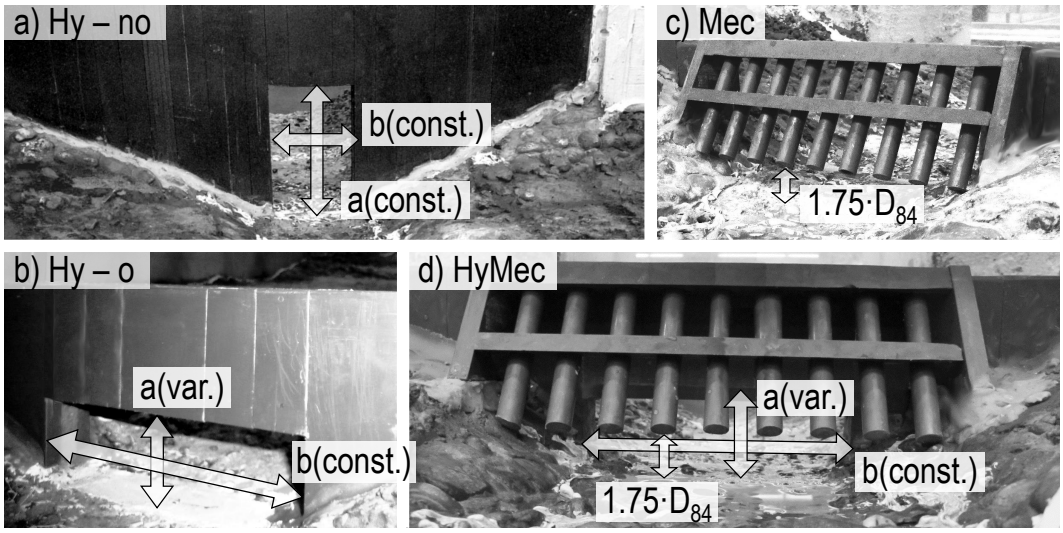

Figure 7.5 – *Tested barrier types: Hydraulic deposition control with constriction height a and width b; a) case Hy-no without the possibility of structure overflow and b) case Hy-o, with limited barrier height (0.11 m); mechanical deposition control by c) a bar screen (case Mec) with a height of 0.11 m; and d) the combination of hydraulic and mechanical deposition control (case HyMec), with the bar screen superposed to the flow constriction with variable constriction height a and constant width b.*

For the hydraulic control only, two types of flow situations were considered: case *Hy-no*, with infinite barrier height, where barrier overflow was not possible and case *Hy-o*, with overflown barrier, where the barrier height was limited to 0.11 m. In case *Hy-no*, the constriction height a was constantly 0.152 m and the constriction width b was constantly 0.076 m. The opening height

of 0.152 m corresponds to the technical maximum possible constriction height due to the model limitations; the width of 0.076 m is determined according to Chpt. 5 for hydraulically triggering sediment retention when the bank-full guiding channel discharge of 5.5 l/s is exceeded. Smaller widths were not considerable with respect to the flow and sediment continuity in practice.
The unwanted flushing of sediment was observed in previous studies when barriers were overflown (e.g., Zeller, 1973, and Chpt. 6), as considered by the cases *Hy-o*, *Mec* and *HyMec* with limited the barrier height. However, the creation of a sediment deposit that can be flushed requires the initial impounding without barrier overflow. Thus, the barrier height was determined in a manner that the opening is pressurized for discharges higher than 5.5 l/s and so that the barrier could not be overflown for discharges up to 7.0 l/s corresponding to the first incremental increase of the hydrograph. The barrier overflow for discharges which are smaller than 7.0 l/s can be achieved when the cross-section-averaged energy head of the flow is not higher than the barrier (Piton and Recking, 2016a). In the model, the head upstream of the barrier and corresponding to a discharge of 7.0 l/s was approximately 0.11 m, which was decisive for limiting also the barrier height to 0.11 m.
The width of the opening in the overflown hydraulic control barrier (cases *Hy-o* and *HyMec*) was 0.15 m, which is slightly larger than the bottom width of the guiding channel. This choice was made to minimize the effects of the barrier on the flow when the guiding channel is not overtopped. The corresponding opening height for the hydraulically controlled retention of sediment was 0.040 m for a discharge of 5.5 l/s, according to the previous analyses (Chpts. 4, 5, and 6).
For the combined control barrier, also higher opening heights were analyzed to study the effect of the hydraulic opening height on the deposition control by combined barriers. Thus, the opening heights tested by the case *HyMec* were 0.040 m, 0.043 m and 0.047 m, where the constriction width was constantly 0.15 m.
Pure mechanical deposition control (case *Mec*) was tested by a bar screen with a height of 0.11 m and a bar width, as well as an interspace between the bars corresponding to the D_{84} of the sediment supply mixture. Due to the findings from the analysis in Chpt. 6, the clearance between the guiding channel bottom and the lower end of the bars was $1.75 \cdot D_{84}$. Also the bar screen inclination of 2:1 to favor the passage of driftwood over the barrier (Bezzola et al., 2004; Lange and Bezzola, 2006; Piton and Recking, 2016b) was adopted, but driftwood was not introduced in the experiments.
As the combination of hydraulic and mechanical controls has been shown to be promising in view of reducing risks due to individual uncertainties related to the unwanted sediment flushing and sediment size, respectively (Schwindt et al., 2016c, and Chpt. 6), this combined control type is also here considered by the case *HyMec*. This barrier type was constituted by the superposition of the bar screen to the hydraulic barrier with variable constriction height a and constant width b, according to the test case *Hy-o*.

7.3.2 Generic hydrograph and flushing attempts

Each barrier set-up was tested two times (α and β tests) with the same generic hydrograph which was established based on the following criteria:

- The duration of the falling limb t_- (in s) is 1.7 times as long as the rising limb t_+ (in s), which is typical for floods of mountain rivers (D'Agostino and Lenzi, 1996; Rickenmann et al., 1998; Armanini and Larcher, 2001; Kaitna et al., 2011; Piton and Recking, 2016a);

- The initial discharge of 5.5 l/s corresponds to the bank-full discharge of the guiding channel and the peak discharge of 12.5 l/s is imposed by the model limitations;
- The ratio between the sediment supply rate (bed load inflow $Q_{b,i}$) and the pump discharge Q is 0.5 % (weight-specific), according to the analyses of bed load transport (Chpt. 5);
- The total supply volume V_Σ (in m^3) is higher than the plain storage volume (0.127 m^3) of the deposition area (reservoir) considering a barrier height of 0.11 m.

The plain storage volume in the deposition area corresponds to the horizontal filling of the deposition area with a deposition slope $S_{dep} = 0$. Values of $S_{dep} > 0$ would suggest an extra storage volume that might not be available in practice. For this reason, the safer choice of $S_{dep} = 0$ was made here. The criteria above lead to a hydrograph with a rising limb duration of $t_+ = 1\,129$ s (≈ 19 min) and a falling limb duration of $t_- = 1\,920$ s (≈ 32 min). The water and solid discharge supply were adapted in steps of four minutes. The resulting total volume of the sediment supply of the generic flood hydrograph was $V_\Sigma = 0.137$ m^3. The time variation curve of the hydrograph with sediment supply is shown in Fig. 7.6 with respect to the subsequently introduced dimensionless parameters.
After the hydrograph, the possibility of sediment flushing was examined by empirical variations of the discharge, i.e., different sudden increases and decreases in the discharge were tested with the goal of observing sediment flushing. The flushing attempts were only meaningful for the cases with hydraulic barriers, as the flushing of clogged mechanical barriers is not possible (cf. Chpt. 6).

7.3.3 Parameters and dimensional considerations

This study focuses on the deposition pattern and volume due to the generic hydrograph, considering the occasional subsequent sediment flushing, and the corresponding transfer of bed load. These phenomena may be described by the following set of parameters:

$$\Lambda = f\left(a, b, D_{84}, g, h, Q, Q_{b,i}, Q_{b,o}, S_0, t, t_+, t_-, V_{dep}, V_\Sigma, \nu, \rho_f, \rho_s, \rho'_s\right) \tag{7.1}$$

where a and b are the height (in m) and width (in m) of the hydraulic flow constrictions, respectively; D_{84} is the representative grain size; g denotes the gravitational acceleration (9.81 m/s^2); h is the flow depth; Q is the pump discharge (in l/s); $Q_{b,i}$ and $Q_{b,o}$ denote the sediment supply and outflow rates (in kg/s), respectively; S_0 is the longitudinal slope of the guiding channel (5.5 %); t is the experiment duration (in s); t_+ and t_- are the duration of the rising and falling limb (in s) of the hydrograph, respectively; V_{dep} is the volume of sediment deposits (in m^3); ν is the kinematic viscosity of water (10^{-6} m^2/s); ρ_f and ρ_s are the water density (1 000 kg/m^3) and the sediment grain density (2 680 kg/m^3), respectively; and ρ'_s (1 550 kg/m^3) is the density of sediment deposits, according to the supplier's data.
With respect to the analysis of bed load transport-related phenomena, the dimensional analysis was based on the independent variables of D_{84}, g and ρ_f (according to Chpt. 3.1 and Einstein, 1950; Yalin, 1977). The discharge Q is subsequently considered relative to the bank-full discharge of the guiding channel ($Q_{bf} = 5.5$ l/s) corresponding to the discharge for triggering sediment retention. In addition, the time t is considered relative to the duration of the rising limb of the hydrograph; and the volume of sediment deposits V_{dep} is considered relative to the cumulative volume of the hydrograph sediment supply ($V_\Sigma = 0.137$ m^3). This leads to the following set of

relevant dimensionless parameters:

- $a_{*D} = a \,/\, D_{84}$, grain related opening height of vertical flow constrictions;
- $b_{*D} = b \,/\, D_{84}$, grain related opening width of lateral flow constrictions;
- $Q_* = Q \,/\, Q_{bf}$, relative discharge;
- $s = \rho_s \,/\, \rho_f$, density ratio;
- $t_* = t \,/\, t_+$, relative duration;
- $V_* = V_{dep} \,/\, V_\Sigma \cdot 100$, percentaged relative deposit volume;
- X_*, Y_* and Z_* correspond to x/D_{84}, y/D_{84} and z/D_{84}, respectively;
- $\Phi_i = Q_{b,i} \,/\, (w \cdot \rho_f \cdot \sqrt{(s-1)\, g\, D_{84}^3})$, intensity of bed load supply;
- $\Phi_o = Q_{b,o} \,/\, (w \cdot \rho_f \cdot \sqrt{(s-1)\, g\, D_{84}^3})$, intensity of outflowing bed load.

Flow depth related parameters are not considered since the measurement of the flow depth was not possible by non-intrusive techniques in the shallow flow over the rapidly changing morphology of the sediment deposits.
The flushing phases were simulated according to the occurrence of a successive flood with empirically varying discharges, with and without sediment supply. The duration of the flushing depended on the observation of the morphological activity in terms of sediment displacements in the deposition area and the outflowing bed load.

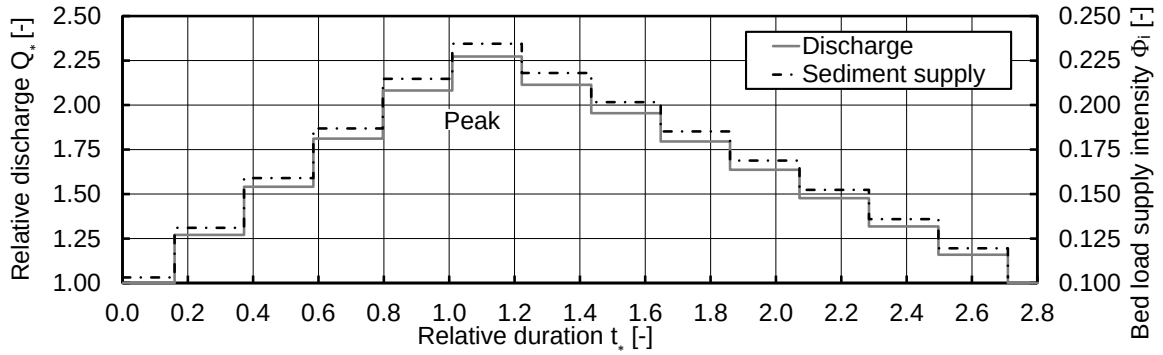

Figure 7.6 – *The generic hydrograph used for the experiments, based on the dimensionless expressions of relative discharge $Q_* = Q \,/\, Q_{bf}$, bed load supply intensity Φ_i and the relative time $t_* = t \,/\, t_+$.*

7.3.4 Summary of experimental procedures

The experimental plan according to the above definitions and dimensionless numbers is listed in Tab. 7.1. The hydrograph was applied two times (α and β tests) for every barrier configuration, except for the overflown hydraulic barrier (case *Hy-o*), as this adjustment has shown to be not suitable due to unwanted sediment flushing in the first hydrograph test.

Table 7.1 – *Denomination and characterization of test runs with hydrograph and flushing episodes.*

Case	Type	Rel. barrier height [-] $0.11/D_{84}$	Relative constriction height [-] a/D_{84}	Relative constriction width [-] b/D_{84}	Bar screen placed	Hydro-graph tests	Flush-ing
Hy-no	Hydraulic	inf	11.1	5.6	No	2	Yes
Hy-o	Hydraulic	8.0	a_1=2.89	11.0	No	1	No
Mec	Mechanical	8.0	–	–	Yes	2	No
HyMec.a_1	Combined	8.0	a_1=2.89	11.0	Yes	2	No
HyMec.a_2	Combined	8.0	a_2=3.14	11.0	Yes	2	Yes
HyMec.a_3	Combined	8.0	a_3=3.44	11.0	Yes	2	No

7.4 Results and Analysis

7.4.1 Evolution bed load transfer through the barrier

The outflowing sediment rates in terms of the bed load transport intensity Φ_o are shown in Fig. 7.7 for the cases *Hy*, *Mec* and *Hy-Mec*, as a function of the relative hydrograph duration t_* and for the two repetitive runs α and β. In addition, the shape of the deposits at the peak of the hydrograph are shown in the top-view pictures. These pictures show the representative α–tests, as no major differences between the pattern of the two repetitive tests (α and β) were observed.
In case ***Hy-no*** (Fig. 7.7 a), the outflowing bed load intensity Φ_o dropped in both tests (α and β) after a duration of approximately t_* = 0.5. This drop in Φ_o corresponds to the hydraulic clogging of the barrier. In parallel, the backwater of the infinitely high barrier increased with increasing discharge (t_* <1) and resulted in a regressive evolution of the sediment deposit in the upstream direction (according to Fig. 6.4). The corresponding longitudinal evolution of the deposit is reflected in the top-view picture of the deposition area (Fig. 7.7 a) at the flood peak. Due to the influence of the deposit, the hydraulic jump could not migrate back in the downstream direction during the falling limb of the hydrograph (t_* >1, Fig. 7.7 a). In consequence, the sediment flux through the barrier ceased with the flood peak (Φ_o = 0) an the deposit spread toward the banks of the deposition area at the end of the hydrograph.
In case ***Hy-o***, the relative constriction height a_{*D} was significantly smaller than previously (2.89 against 11.1 in case *Hy-no*). Therefore, nearby all of the supplied sediment was retained in the first half of the rising limb (t_* <0.5, Fig. 7.7 a). Accordingly, the outflowing bed load intensity Φ_o decreased rapidly to zero, but Φ_o restarted to increase with the second increase of the discharge. The raise in the discharge (cf. Fig. 7.6) at t_* = 0.37 corresponds to an increase from Q = 7 l/s to Q = 8.5 l/s, i.e., the desired threshold value for initiating the barrier overflow. Thus, the sediment flushing started already before the flood peak ($t_* < 1$), as it can be observed in the top-view picture (lower top-view picture on Fig. 7.7 a). After the flood peak ($t_* \geq 1$), the flushing of nearby all the previously deposited sediment occurred. The observed maximum of Φ_o = 0.32 during the flushing corresponds to approximately 1.4 times the maximum supply rate of Φ_i = 0.23 at the flood peak. A repetitive run of this configuration was discarded due to the unwanted sediment flushing observed before the flood peak. In practice, every barrier can be overflown when the discharge is high enough. However, the comparison of the cases *Hy-no* and *Hy-o* shows that barriers for hydraulic control only need to be sufficiently high to avoid such unwanted sediment flushing. Even though decreasing the dimensions of the opening in the barrier could increase the safety against self-flushing, smaller constriction heights or widths were not tested to avoid sediment retention before the bank-full discharge of the guiding channel (5.5 l/s) is reached.
In case ***Mec*** (Fig. 7.7 b), the temporal evolution of the outflowing bed load intensity Φ_o was similar to the supply intensity Φ_i (cf. Fig. 7.6) until the flood peak occurred (t_* = 1). Hence, only marginal sediment deposits close to the barrier can be observed in the top-view picture of the deposition area at the flood peak. At a relative flood duration of approximately t_* <1.25, the bar screen was mechanically clogged, and consequently, the outflowing bed load intensity Φ_o decreased in both tests (α and β) to zero by stages. An elongated deposit in the deposition area was observed at the end of the hydrograph, according to the descriptions from Campisano et al. (2014); Piton and Recking (2016a).

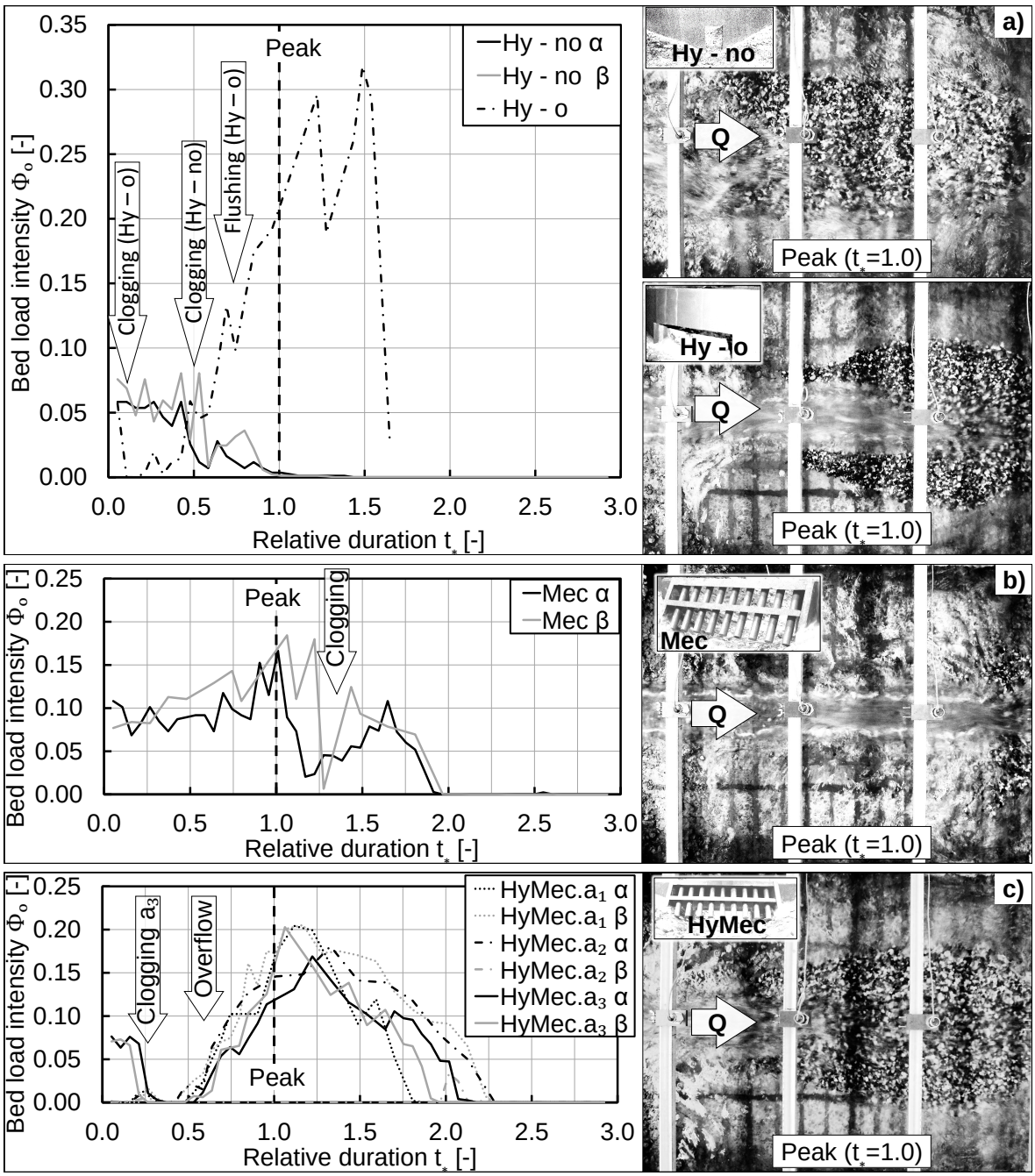

Figure 7.7 – *The outflowing bed load transport intensity Φ_o as a of function the relative time t_* and for the two repetitive tests α and β. a) for hydraulic control without barrier overflow (Hy-no) and with barrier overflow (Hy-o); b) for mechanical control by the bar screen (Mec); and c) for combined deposition controls (HyMec), i.e., the combination of hydraulic barrier with varying opening heights $a_{1,2,3}$ and upstream superposed bar screen. The top-view pictures at the right show the sediment deposits at the flood peak of the α–tests.*

In case ***HyMec*** (Fig. 7.7 c), the outflowing bed load intensity Φ_o decreased rapidly to zero for the smaller opening heights a_1 and a_2. With the largest opening height a_3, Φ_o was similar to the supply intensity Φ_i at the beginning. Only with the second increment of the discharge and sediment supply at $t_* = 0.37$, the barrier clogged. After the barrier clogging, an elongated deposit developed layer-wise until it reached the barrier height at $t_* \approx 0.6$ for the three considered constriction heights. In consequence, the supplied sediment was transported over the barrier, which is reflected in the evolution of the outflowing bed load intensity Φ_o which corresponds to the supply intensity Φ_i (cf. Fig. 7.6). However, Φ_o is slightly smaller than Φ_i, as the deposit enlarged after $t_* = 0.6$. This enlarged deposit shape can be observed in the according top-view picture of the deposition area (Fig. 7.7 c). The repetitive tests (α and β) resulted in similar outflow rates for the three opening heights.
A major difference in Φ_o can be observed in the test $3.a_2\ \beta$, where a constant discharge of 5.5 l/s with sediment supply was applied prior to the hydrograph, for a duration corresponding to t_+, i.e., $t_* \approx 1$. This combination of low discharge and sediment supply led to the decelerated clogging of the combined barrier. The consequence was an early evolution of the backwater in upstream direction, beyond the upper limit of the observation reach, and the subsequent almost total retention of the sediment supply.

7.4.2 Sediment deposits in the deposition area

Volumes

The volumes of sediment deposits were measured by three redundant tools, namely the laser, the motion sensing camera (Kinect) and the total weight of the deposited sediment measured with the industrial scale. This redundant evaluation was necessary because the scale gives only information about the sediment weight and the bathymetric data from the motion sensing camera and laser are subjected to individual measurement errors (Lachat et al., 2015). The motion sensing camera provides a high-resolution bathymetric image of the deposit, but the image required a correction due to distortion and the surface texture. The laser measurements are exact but the point density is low, which leads to averaging errors in the surface interpolation. For the determination of the deposit volume with both approaches, the bathymetric surface data of the empty deposition area were subtracted from the surface data of the sediment deposits. Technical descriptions of the motion sensing camera-application are included in Appendix A.3.3 (page X.17). An example application of the bathymetric recording of the deposit with the motion sensing camera after the test *HyMec.*$a_1\ \alpha$ is shown in Fig. 7.8. The bathymetric deposit volume V_{dep}(Bathymetric) according to both the camera and the laser was then determined using CAD software.

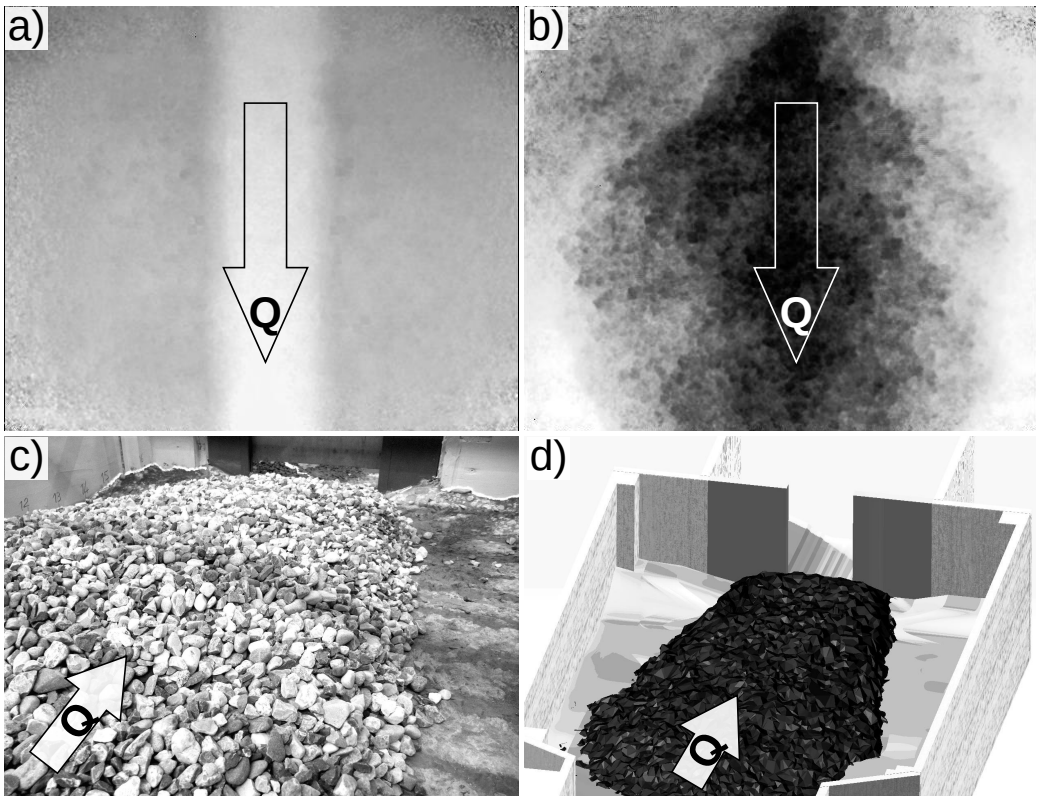

Figure 7.8 – *Example of the recording of the deposition area bathymetry with the motion sensing camera: (a) a gray-scale picture of the empty deposition area (top-view) and (b) a gray-scale picture of the deposition area with sediment (top-view). A picture from a standard camera of the deposit at the end of the HyMec.a_1 α–test is shown in (c), with its numerical representation derived from the motion sensing camera (d).*

After every hydrograph test, the deposited sediments were flushed (without any barrier) in the filter basket which was weighed with the industrial scale. This weight was divided by the deposit density ρ'_s of 1 550 kg/m^3 to obtain the according deposit volume V_{dep}(Scale). The comparison of V_{dep}(Scale) and V_{dep}(Bathymetric) was used to evaluate the percentaged error ϵ_V of the bathymetric tools (except for the case *Hy–no*, where sediment flushing was examined after the hydrograph).

$$\epsilon_V = \frac{V_{dep}\left(\text{Bathymetic}\right) - V_{dep}\left(\text{Scale}\right)}{V_{dep}\left(\text{Scale}\right)} \cdot 100 \tag{7.2}$$

The error ϵ_V is shown in Fig. 7.9 for the cases *Mec* and *HyMec*, where the bar screen was applied. The graphs show that both bathymetric techniques tend to underestimate the deposit, but this effect is significantly less pronounced for the camera data (in average, ϵ_V = 2.7%) than for the laser data (in average, ϵ_V = 14.8%).
The complex application of the centimeter-wise laser measurements was restricted to 16 profiles (approximately 650 points), and therefore, it is less precise than the camera data (mm-wise, $1.92{\cdot}10^6$ points). Hence, the motion sensing camera is subsequently used for the analysis of the deposit pattern.

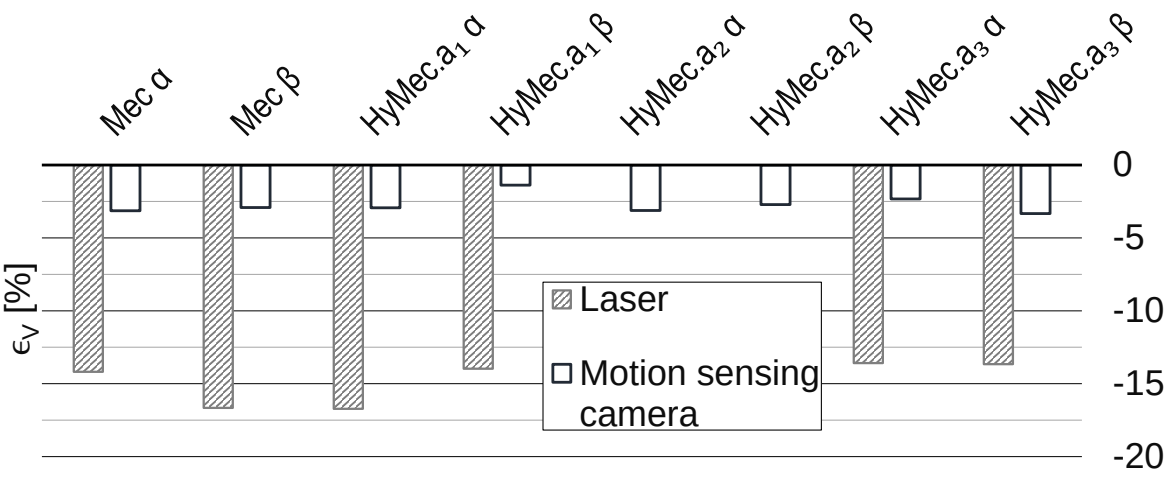

Figure 7.9 – *The percentaged error ϵ_V of the sediment volume derived from weight measurements (assuming ρ'_s = 1 550 kg/m^3) and the deposit volume measurements based on the bathymetric scans using the laser and the motion sensing camera; the bathymetric records were made after the repetitive α and β tests with the bar screen only (Mec) and the combination of the bar screen with the open hydraulic barrier HyMec, with varying opening heights $a_{1,2,3}$.*

The relative deposit volumes V_*, i.e., the ratio of the deposit volumes V_{dep} and the supply volumes V_Σ, are shown in Fig. 7.10 based on the scale measurements as a function of the test cases. As expected from the results regarding the sediment outflow rates (cf. Fig. 7.7), the total deposit volume is very small in the case *Hy-o*, while it is high in the test *HyMec.*$a_2\beta$. The case *Hy-no* is not evaluated because sediment flushing with additional sediment supply was tested after the hydrograph. However, the graphs of the bed load intensity Φ_o (Fig. 7.7 a) indicate that V_* is close to 100 % in the case *Hy-no*. The relative deposit volume V_* varied in the cases *Mec* and *HyMec* between approximately 40 and 55 %, invariant of the presence of the bar screen. In these cases (*Mec* and *HyMec*), V_* refers to the backwater-driven storage space upstream of the clogged barrier without the occupation of the entire width of the deposition area. This indicates that the barrier height is essential for the amounts of retained sediment, independent from the control type (mechanical and/or hydraulic). However, the moment of the barrier clogging, as a function of t_*, is important for the attenuation of sediment peak flows, as the comparison between Fig. 7.7 b) and Fig. 7.7 c) shows.

Deposition patterns

The final shapes of the sediment deposits were recorded at the end of every hydrograph test. According to the evolution of the sediment outflow (cf. Fig. 7.7), the deposition patterns of the repetitive α and β–tests were almost similar. Therefore, the deposition patterns obtained by the motion sensing camera are compared in Fig. 7.11 with top-view pictures, only for the α–tests. Moreover, only one representative graph (test *HyMec.*a_3 α) of the relative deposit height Z_* is shown for the three constriction heights applied in the case *HyMec*, as the constriction height variation had no measurable effect on the sediment deposit.

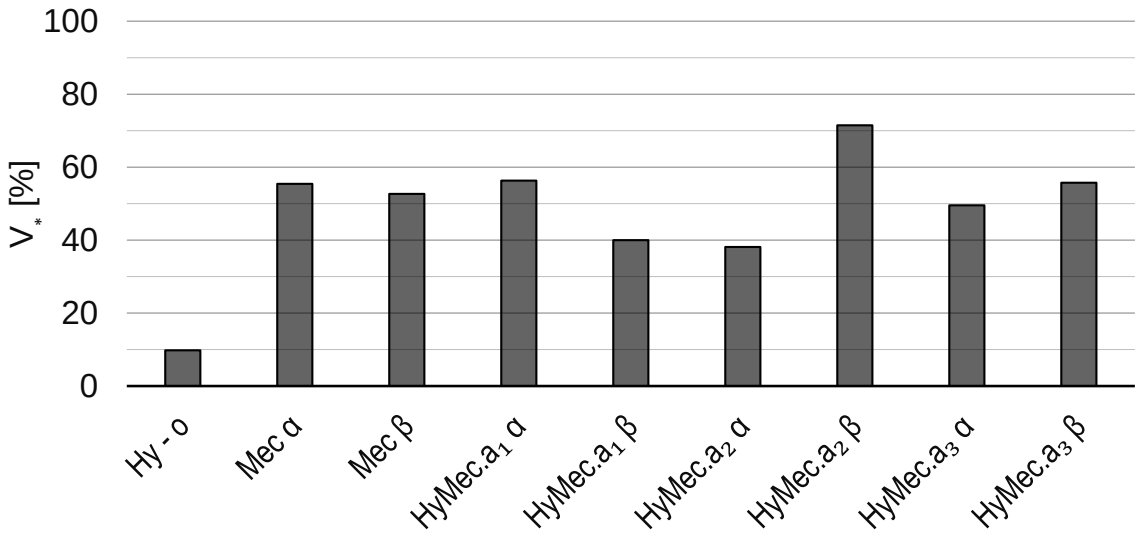

Figure 7.10 – *The ratio V_* (in %) of the deposit volume V_{dep} and the supply volume V_Σ after the repetitive hydrograph tests α and β for the cases of the non-overflown flow constriction (Hy-no), overflown bar screen (Mec) and the combination of overflown bar screen superposed to the flow constriction (HyMec), with varying opening heights $a_{1,2,3}$.*

Similar to the sediment outflow rates (cf. Fig. 7.7) and relative deposit volumes (cf. Fig. 7.10), it can be observed that the deposit is wide and deep in the case *Hy-no*. The deposition patterns of the cases *Mec* (mechanical barrier only) and *HyMec* (combined barrier) differ only marginally.
According to the relative retention volumes V_* (cf. Fig. 7.10), the volume and deposition pattern differences between the tests *HyMec.*a_1 α and *HyMec.*a_3 β are small. Both tests correspond to the minimum and maximum constriction heights a_1 and a_3, respectively. In addition, the deposit height was slightly lower in the tests *HyMec.*a_1 β, *HyMec.*a_2 α and *HyMec.*a_3 α. These observations indicate that there is no evident effect of the (relative) constriction height on the deposition patterns within the tested range of a_{*D}(min) = 2.89 and a_{*D}(max) = 3.44. Also this observation is in agreement with the sediment outflow rates (cf. Fig. 7.7 c), where the time variation curves of Φ_o are very close to each other.
The deposition pattern after the *Hy-o*–test was not recorded, as there were only small sediment remains in overbank areas, as shown in Fig. 7.12.

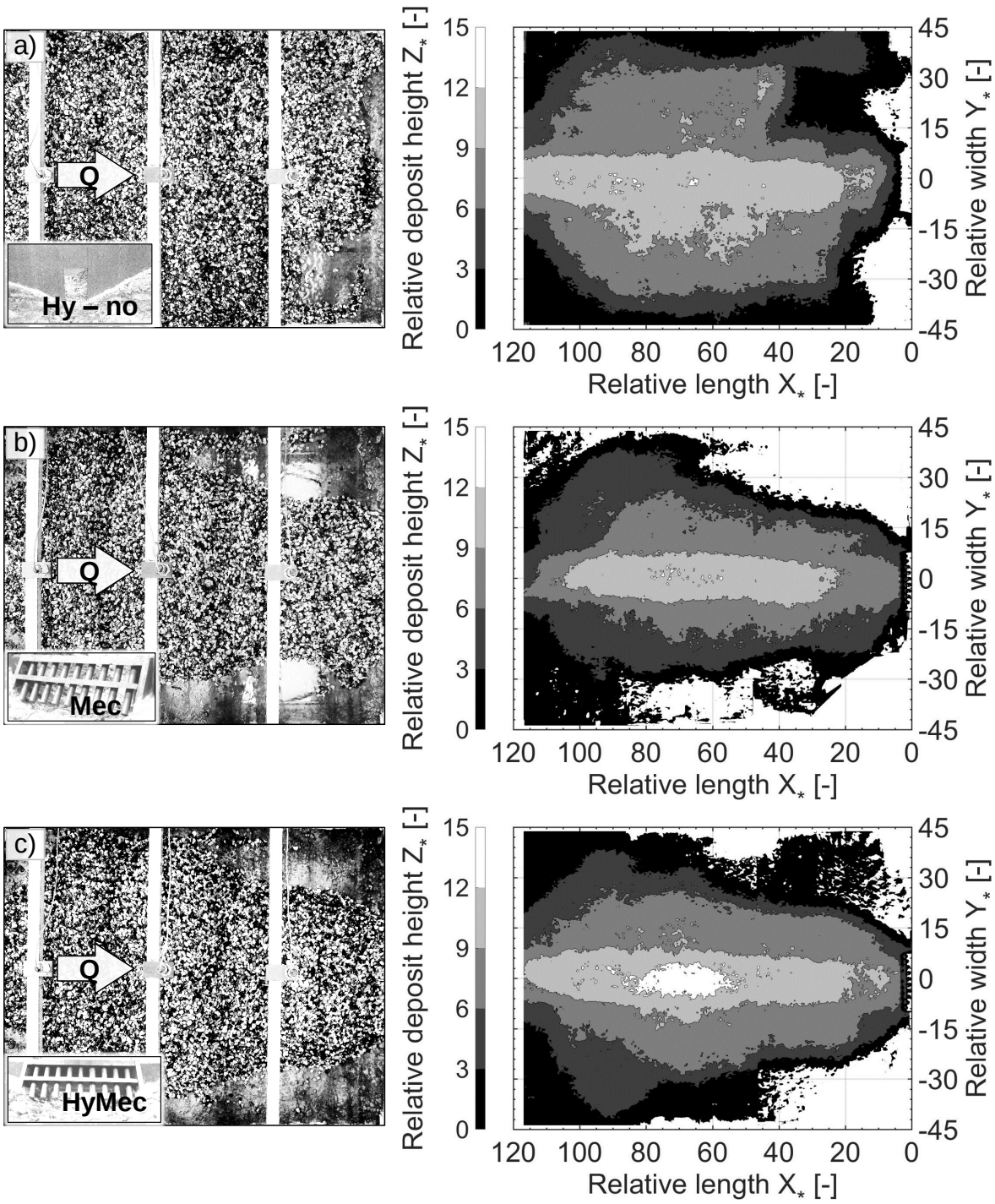

Figure 7.11 – *Deposition patterns at the end of the hydrograph tests; left column: top-view pictures; right column: bathymetric records, a) in case* Hy-no *(α–test), with non-overflown hydraulic barrier; b) in case* Mec *(α–test), with bar screen for mechanical control only; and c) case* HyMec *(test* $a_3\alpha$*), with combined hydraulic barrier and upstream superposed bar screen.*

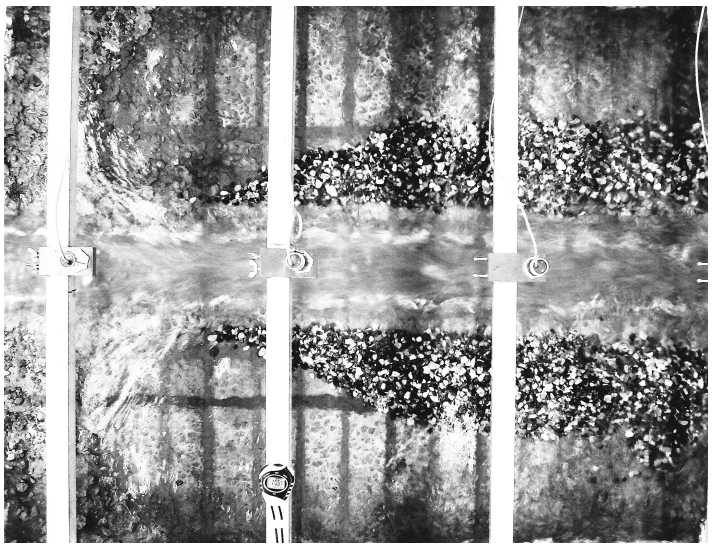

Figure 7.12 – *The remaining sediment deposits at the end of the hydrograph test Hy-o.*

7.4.3 Sediment flushing

Fig. 7.13 shows the time variation curves of the outflowing bed load intensity Φ_o for the flushing in the case *Hy-no* (non-overflown flow constriction) after the hydrograph tests α and β, as a function of the multiple duration t_+ of the hydrograph rising limb. Although, similar tests were run for the case *HyMec.a*$_2$ (combined barrier), these results are not shown here because it was impossible to remobilise sediments from the deposit (Φ_o is a horizontal zero-line).

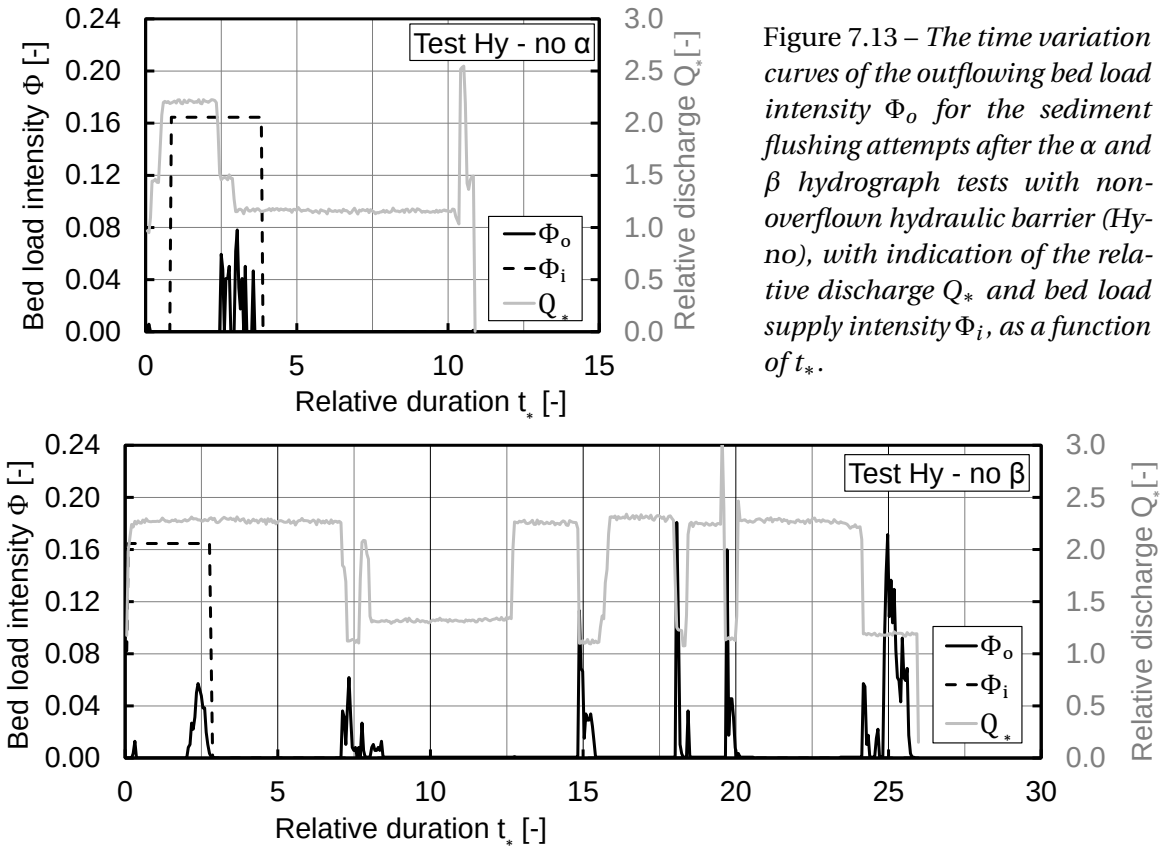

Figure 7.13 – *The time variation curves of the outflowing bed load intensity Φ_o for the sediment flushing attempts after the α and β hydrograph tests with non-overflown hydraulic barrier (Hy-no), with indication of the relative discharge Q_* and bed load supply intensity Φ_i, as a function of t_*.*

The technical maximum possible sediment volume (model limits) was supplied at the beginning, followed by a phase of clear water flow for both flushing attempts (α and β). The flushing of test *Hy-no* α showed some sheet-wise grain mobilizations from the deposit between t_* = 2.5 and t_* = 3.5 when the discharge was decreased (Fig. 7.13, *Hy-no* α). Only minor morphological activity was observed after the discharge decrease. Also a sudden, arbitrary increase in the discharge with subsequent decrease toward the end of the experiment did not remobilise the grains. The flushing of test *Hy-no* α was stopped after a duration of more than 12 times the rising limb of the hydrograph, as no further morphological activity was observed.

The flushing of the test *Hy-no* β continued for 26 times the duration of the rising limb of the hydrograph, with several empirical discharge variations. Similar to the α–test, the maximum possible sediment volume was supplied at the beginning. After every decrease in the discharge, the sheet-wise flushing of sediment from the tip of the deposit was observed. The maximum of these flushings reached an outflow intensity Φ_o corresponding to the supply peak of the hydrograph

(Fig. 7.13, *Hy-no* β and Fig. 7.6). These flushings occurred particularly when the discharge conditions in the flow constriction changed from pressurized to free surface flow.
Toward the end of the β–test, from $t_* \approx 22$ to $t_* \approx 23$, an attempt was made to induce the flushing of the guiding channel. This was achieved by the empirical, successive removal of the upper layer of the deposit along the axis of guiding channel. The empirically created depression had a depth of approximately $2 \cdot D_{84}$ and a width of approximately 0.1 m, corresponding to the bottom width of the guiding channel. This empirical depression was created stepwise, beginning at the tip of the deposit (downstream end), then continuing the excavation in the upstream direction. However, only marginal morphological activity was observed, unless the tail of the deposit (upstream end), i.e., the hydraulic jump, was directly connected with the opening through the depression. Small meanderings were observed at the beginning of the flushing through the empirical depression (Fig. 7.14 a–c). In the following, the depression incised from the upstream toward the downstream direction (Fig. 7.14 d–e), until the guiding channel was completely cleared (Fig. 7.14 f). The relative discharge during the flushing of the guiding channel was $Q_* = 1.2$, i.e., $Q = 1.2 \cdot Q_{bf}$. A comparison of the maximum sediment outflow intensity Φ_o with the Smart and Jaeggi (1983) formula applied to the geometry of the guiding channel, showed good agreement between Φ_o and the formula, as it has already been proven in the previous analyses (Chpts. 5 and 6).

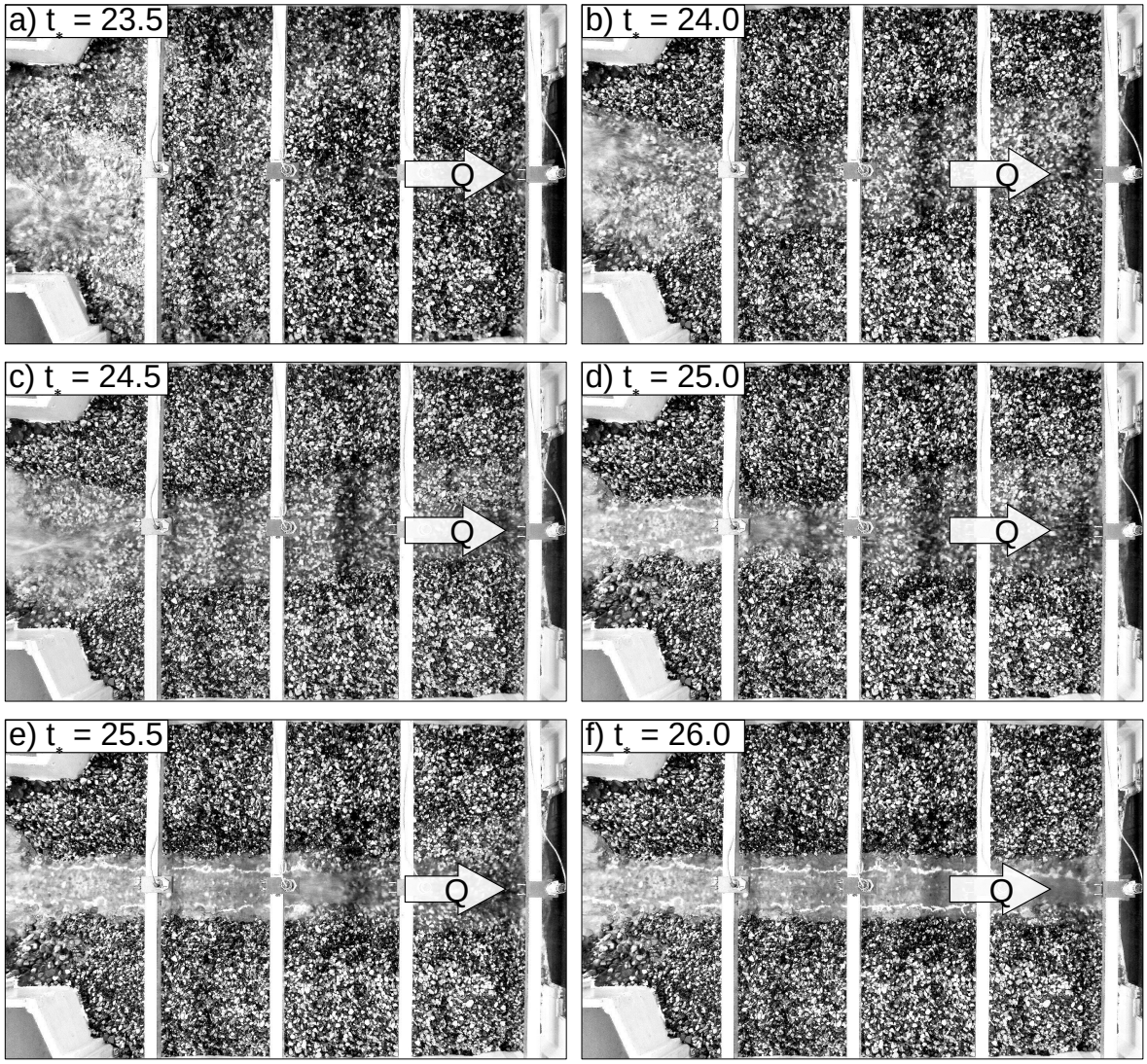

Figure 7.14 – *Controlled flushing of the guiding channel after the hydrograph test Hy-no β, in time lapses of 0.5·t_*, starting from t_* = 23.5, after creating gradually an artificial depression above the guiding channel, until t_* = 26.0, where the guiding channel was completely cleared.*

7.5 Discussion

7.5.1 Sediment deposition

The elongated deposits at the end of the hydrograph tests were characteristic for the overflown barrier (cf. Fig. 7.11 b and c), where the deposition control functioned as desired without unwanted flushing (*Mec* and *HyMec*). The high, non-overflown barrier (*Hy-no*) caused a wider and longer spread of the deposit (cf. Fig. 7.11 a), which is in agreement with the observations from Zollinger (1983). The storage volume upstream of overflown barriers may increase when the deposition slope S_{dep} is additionally considered. According to the literature, S_{dep} can be estimated as a function of the channel slope S_0 and it is typically in the range of $1/2 \cdot S_0$ for small floods and $2/3 \cdot S_0$ for large floods with high sediment concentration (D'Agostino, 2013; Osti and Egashira, 2013; Piton and Recking, 2016a). The deposition slopes observed in the present study can be obtained by the relative deposit height Z_* at the longitudinal section at the axis of the guiding channel ($Y_* = 0$). Linear regression curves have been established in Fig. 7.15 to estimate Z_* as a function of X_* in the empirically determined aggradation zone upstream of the barriers. Thus, the slope of the regression curves corresponds to the deposition slope S_{dep} in the considered aggradation zones. This evaluation results in S_{dep}(*Hy-no*) = 6.5 %, S_{dep}(*Mec*) = 12 % and S_{dep}(*HyMec*) = 9.5 %. Compared with the bottom slope S_0 of the guiding channel, these values correspond to S_{dep}(*Hy-no*) = [1–2]$\cdot S_0$, which is significantly higher than the literature values.
The deposition slope can also be approached using the equilibrium slope, assuming that the sediment supply and erosion are balanced on a reach scale. Zollinger (1983) proposed to solve the Smart and Jaeggi (1983) formula with respect to zero-transport conditions ($\Phi = 0$). This approach could not be applied for the experiments, as the clear water depth was highly variable and not measurable due to the shallow flow over the changing sediment deposits. As an alternative, the following relationship for the equilibrium slope was applied, as proposed by Johnson (2016):

$$S_{\text{(Johnson, 2016)}} = \frac{C \cdot w}{Q} \cdot D_{84}^{3/2} \cdot (s-1) \cdot \left[\left(\frac{\Phi_o}{3.97} \right)^{2/3} + \tau_{*cr} \right]^{3/2} \tag{7.3}$$

Eq. 7.3 was evaluated by using the peak discharge of the hydrograph and the bed load transport intensity over the barrier (*HyMec*). The width w was substituted by the barrier spill width of 0.234 m and a value of 0.05 was considered for the dimensionless bed shear stress τ_{*cr}. This results in equilibrium slopes between 12 and 15 % for the *HyMec*-tests. Applying Eq. 7.3 at the instant when the sediment transport across the barrier ceased, results in very small values of S_{dep} <1 %. Thus, Eq. 7.3 is not appropriate for estimating the deposition slope. In practice, it is safer to assume small values of the deposition slope for estimating the maximum storage upstream of the barrier. Such a safe estimate can be made by the relationship $S_{dep} = 1/2 \cdot S_0$.
The deposit shape, independent of the barrier height and type, is in practice often confined by the terrain morphology. Thus, the deposition area of such confined sediment traps corresponds to the river bed and its overbanks. Such elongated, natural deposition areas are more exposed to sediment flushing because of the higher concentration of the stream power over the width of the deposition area (e.g., Leys, 1976; Zollinger, 1983).

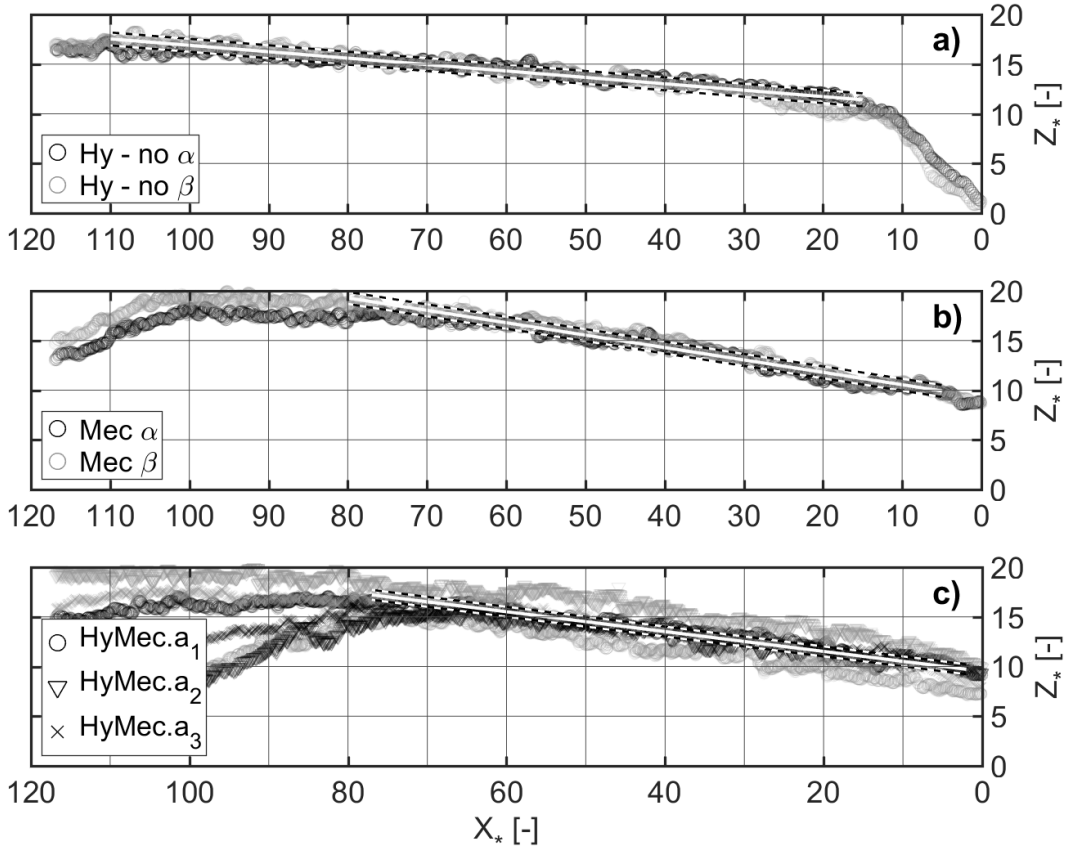

Figure 7.15 – *Relative deposit height Z_* at the longitudinal axis of the guiding channel ($Y_* = 0$) after the repetitive α and β hydrograph tests; upstream of a) the non-overflown hydraulic barrier (Hy-no); b) the mechanical barrier only (Mec); and c) the combined barrier (HyMec) with varying opening heights $a_{1,2,3}$. The linear regression curves of the aggradation zones are shown (close white lines), with indication of the corresponding 68 % confidence intervals (dashed lines).*

7.5.2 Morphological characteristics

At the end of the hydrograph runs, grain segregation and sorting effects could be observed, as shown in Fig. 7.16, where some smaller grains can only be identified at the upstream tail of the deposit. However, the surface of the main deposit was primarily constituted by grains that were larger than approximately 0.01 m ($> D_{50}$).

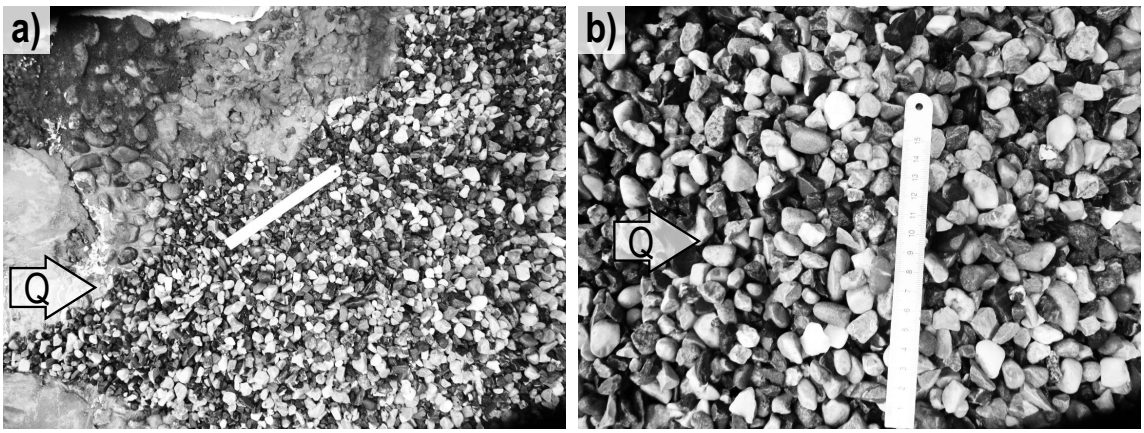

Figure 7.16 – *Pictures of the deposit indicating grain segregation and sorting: a) tail of the deposit where some small grains (< 0.01 m) can be observed; b) detailed picture of the deposit near the barrier. The pictures were made after a hydrograph test with the overflown mechanical-hydraulic barrier (case HyMec). A 0.15-m-long metallic ruler enables the qualitative identification of grain sizes.*

According to Fig. 7.7, the sediment transport ceased during the experiments with the overflown mechanical-hydraulic barrier (*HyMec*) at $t_* \approx 2.0$. Based on the observation, the deposit morphology varied merely after the cession of the sediment transport over the barrier. Therefore, the Smart and Jaeggi (1983) equation can be solved for zero-transport conditions ($\tau_* = \tau_{*cr}$, according to Eq. 2.18) to identify the dimensionless critical bed shear stress for grain mobility:

$$\tau_{*cr} = \frac{h \cdot S_{dep}}{(s-1) \cdot D_{84}} \tag{7.4}$$

The flow depth h can be derived from the measurements of the ultrasonic sensor directly upstream of the barrier assuming that the deposit height corresponding to the barrier height (0.11 m) needs to be subtracted. Then, the evaluation of Eq. 7.4 results in $\tau_{*cr} \approx 0.0124$, which refers to sediment deposition. According to Eq. 2.14, the critical value for sediment mobilization for a slope of $S_{dep} = S_0 = 0.095$ is $\tau_{*cr} \approx 0.0117$, which is slightly smaller than for sediment deposition.
This observation can be attributed to armoring of the deposit through segregation and sorting effects. It is important to account for the armoring of the deposit when controlled sediment flushing, i.e., the partial re-mobilization of the deposit, is targeted in practice to reduce necessary dredging works after a major flood event.

7.5.3 Sediment flushing

The flushing of the non-overflown barrier (*Hy-no*) was not possible without artificial intervention due to the development of the armoring layer in the deposition area. However, the overflown hydraulic barrier (*Hy-o*) is prone to unwanted flushing, as it was observed during the hydrograph. The safety against unwanted flushing through such overflown permeable barriers may also be increased by reducing the dimensions of the opening, but smaller constriction dimensions are not convenient with respect to the eco-morphological river continuity. Thus, the application of permeable barriers with very limited height for solely the hydraulic control of bed load retention is not recommendable for the practice.
The height of the overflown permeable barrier in the case *Hy-o* corresponded to the theoretic cross-section-averaged energetic head (clear water flow) in the guiding channel with respect to the target discharge for the initiation of overspill of the barrier. Naturally, these observations show that the maximum possible backwater depth caused by flow barriers, as analyzed in Chpts. 4 and 5 with an infinite hight, is a decisive factor for the reduction of the energy slope upstream of the barrier. The previous chapters have shown that the dimensions of the opening in the barrier are important to the formation of backwater. This chapter highlights that also the barrier height needs to be considered, as it plays an essential role in sediment flushing. This affirmation results from the comparison of the herein considered barriers with infinite and limited heights. Accordingly, in future works the influence of the barrier height on sediment flushing through hydraulic control openings needs to be systematically considered.
The sediment flushing through the mechanically clogged bar screen was impossible, as shown by the attempts after the *HyMec.*a_2 hydrograph-tests. The flushing attempts through the non-overflown hydraulic barrier (*Hy-no*) have shown that the tip of the deposit repetitively collapses, when the flow conditions in the opening of the barrier pass from pressurized to free surface flow. Such observations were already made in earlier studies (e.g., Zeller, 1973).
Other studies documented the flushing processes of sediment traps as being a succession of the discharge-driven reshaping of a network of sub-channels in the deposition area. The continuous reshaping led to the gradual incision of the deposit along the longitudinal axis of the initial river bed (Zollinger, 1983; Armanini and Larcher, 2001; Busnelli et al., 2001; Piton and Recking, 2016a). This observation was not made in the present study, as grain apparent imbrication caused the armoring of the surface layer of the deposit. Only the empirical, artificial breaking of the armoring layer along the longitudinal axis of the guiding channel enabled sediment flushing. The subsequent morphological activity caused further incision of the initiated channel, with only little meandering. Once the guiding channel was cleared, no further lateral or vertical erosion was possible. Thus, the guiding channel represents not only a tool for directing sediment-laden flows through the sediment trap up to small flood discharges for which no sediment retention is required. The guiding channel also allows the controlled, desired flushing of previously retained sediments through a hydraulic control barrier. The triggering of such desired sediment flushing requires the prior removable of mechanical log jams. The remaining deposits need to be excavated and may be replenished downstream at suitable locations for improving sediment transport dynamics (Battisacco et al., 2016).

7.5.4 Eco-morphological aspects

The guiding channel enables the undisturbed conveyance of sediment-laden (flood) discharges until its bank-full discharge is reached. Therefore, the opening in the hydraulic barrier should not affect the flow before the bank-full discharge of the guiding channel is reached. The previously established relationships for estimating the discharge capacity of the opening (flow constriction) in the hydraulic barrier can be used to determine the extent of backwater due to the barrier (cf. Chpts. 4 and 5). These formulae refer to the upstream flow conditions, i.e., the flow conditions in the guiding channel, and can be used to design the opening in a way that it does not cause backwater until the bank-full discharge of the guiding channel is reached. In this context, the opening width should at least correspond to the bottom width of the guiding channel.
The guiding channel should be designed based on the dominant, morphologically effective discharge in view of the dynamic evolution of downstream reaches. Moreover, the guiding channel should provide appropriate hydraulic conditions for fish migration, in terms of the required flow depth and maximum velocity (e.g., Baigún et al., 2012; Tamagni, 2013; DWA, 2014; Gisen et al., 2017). This can be achieved through a nature-oriented trapezoidal cross section geometry, with a rough channel bottom, characterized by coarse, fixed blocks, and a sufficient channel width.
For the eco-morphological abundance of downstream reaches, also driftwood is important (Gilvear et al., 2013). However, the retention of driftwood is sometimes necessary when trunks or rootstocks cannot pass downstream bottlenecks at urbanized river reaches (Lassettre and Kondolf, 2012; Mazzorana et al., 2012). Driftwood was not analyzed in the present study, but appropriate measures for its retention were proposed, e.g., by Lange and Bezzola (2006), Comiti et al. (2012) or Schmocker and Weitbrecht (2013).

7.5.5 Application limits

In strongly armored mountain rivers or channels confined by bedrock outcrops, the dominant discharge can be very high (Hassan et al., 2014). In such rivers it may be preferable to forgo the permeability of sediment traps, as the transport of sediment is related to exceptional floods. In these cases, the installation of barriers combining mechanical and hydraulic controls, as discussed here, is also advantageous to ensure the fail-safe sediment retention. Then the design of the barrier should refer to the sediment characteristics of the catchment area and the flood discharge which potentially endangers urban downstream reaches.

7.6 Conclusions

The concept of typical sediment traps, consisting of a widened deposition area with downstream deposition control barrier, is enriched by a guiding channel and tested with different partially open barrier types.
The guiding channel ensures that sediments are transported through the deposition area, without any deposition, up to its bank-full discharge. Moreover, the guiding channel serves for the flow control in the deposition area, which is important to ensure the desired functioning of the permeable barrier.
The open barrier needs to be designed for bed load retention once the bank-full discharge of

the guiding channel is exceeded. The bed load retention due to the barrier is differentiated here between hydraulic and mechanical controls, as well as the combination of both.
This experimental study of the guiding channel combined with the barrier for hydraulic and/or mechanical controls, based on a generic hydrograph with occasional, subsequent flushing shows that:

- The guiding channel fulfills its purpose of promoting the river continuity until its bank-full discharge is exceeded;
- Overflown barriers with hydraulic control only are susceptible to unwanted sediment flushing during floods;
- The fail-safe obstruction of open barriers can be achieved by combining the hydraulic and mechanical controls to compensate individual risks related to unwanted sediment flushing and the grain size;
- Partial, desired sediment flushing through hydraulic control barriers after a flood can be artificially enabled.

8 Practical recommendations: Concept for sediment traps permeable for non-hazardous floods

8.1 Requirements

Sediment traps aim at the retention of fluvial bed load transport during hazardous floods only and should not disturb the river runoff otherwise. The design of sediment traps is faced to two requirements in view of a lower and an upper limit for triggering the retention of sediment (cf. Chpt. 2):

Retention	vs.	**Continuity**
Sediment needs to be retained sufficiently and fail-safe for ensuring the safety of urban downstream regions.		Sediment transfer is preferable up to smaller, non-hazardous floods.

The existing concepts for sediment traps are not suitable to satisfy both requirements at the same time, as they either tend to unwanted sediment flushing during hazardous floods or retain continuously sediment, even when the discharge is not hazardous to urban downstream regions.
The experimental study in the previous chapter (Chpt. 7) shows, that it is possible to enable the sediment transfer for small discharges related to frequent floods by implementing a guiding channel in a sediment trap. At the same time, the fail-safe retention of sediment is achieved during hazardous floods by torrential barriers combining the principles of hydraulically and mechanically controlled bed load retention (Chpt. 6).
This concept of a permeable sediment trap is shown in Fig. 8.1, including the following typical and new elements (according to Chpt. 7 and Zollinger, 1983; Piton and Recking, 2016a):

① Inlet structure with scour protection;
② Deposition area (reservoir) with shape-defining lateral confinements;
③ The new guiding channel to transfer sediment and water discharge up to potentially hazardous floods;
④ Maintenance access;
⑤ Permeable barrier consisting of an inclined bar screen upstream of a barrier with opening;
⑥ Downstream scour protection consisting of lateral abutments with concrete-reinforced riprap in the channel and downstream counter dam.

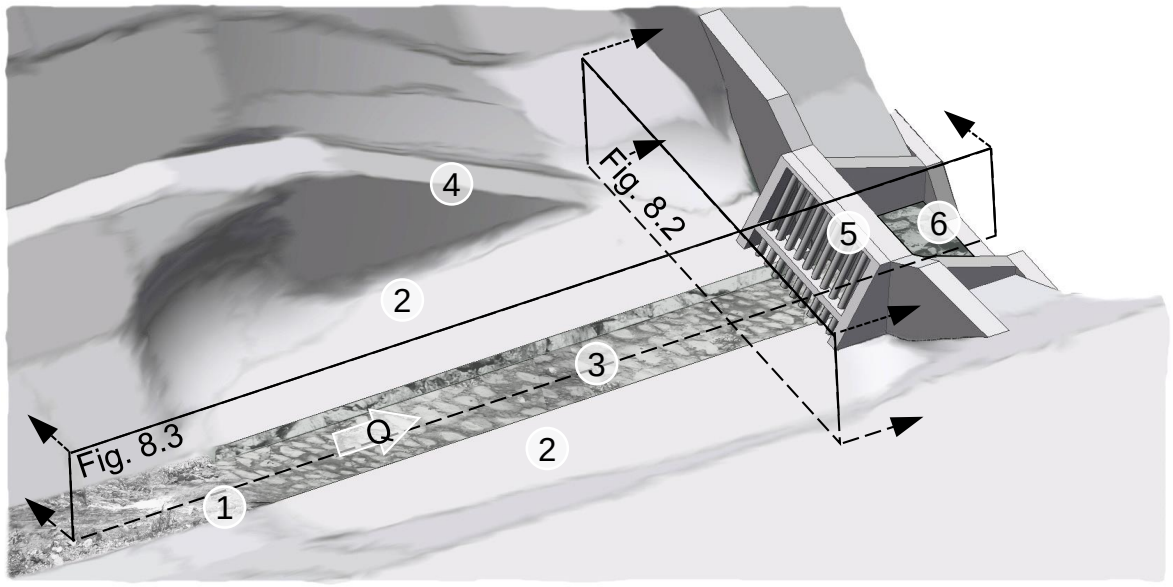

Figure 8.1 – *Illustration of the of a sediment trap that is permeable for non-hazardous, frequent floods, including the typical and new elements of: ① an inlet structure; ② a retention reservoir with lateral confinements; ③ a guiding channel; ④ a maintenance access; ⑤ a permeable barrier consisting of an inclined bar screen for mechanical control upstream of a torrential barrier with an opening for hydraulic control; and ⑥ scour protection. The cross sectional (Fig. 8.2) and longitudinal views (Fig. 8.3) are also indicated.*

The implementation of the guiding channel ③ with the combined barrier ⑤ for mechanical and hydraulic controls of bed load retention have been experimentally proven for enabling the possibility of sediment transfer during low flows. Simultaneously, this concept increases the safety against unwanted sediment flushing (self-emptying) during higher discharges of hazardous floods (cf. Chpts. 6 and 7).

Prior to the design of a sediment trap, an assessment of site-specific, relevant hazard processes (cf. Chpt. 2.6) is necessary to determine the required retention volume (expected amount of sediments during a hazardous flood), the structure location and the potential need for complementary structures, e.g., debris flow breakers or equipment for driftwood-handling (Romang, 2004).

Although, a sediment trap serves for retaining sediment exclusively, the definition of a target flood discharge is required for triggering the retention passively. Higher discharges are potentially hazardous to downstream urban regions. Thus, the target discharge corresponds to the runoff which can still be safely transferred through downstream reaches with low slopes or at bottlenecks such as bridges.

The bed load transport capacity of the guiding channel can be estimated using the Smart and Jaeggi (1983) formula with respect to the target discharge. The application of the Smart and Jaeggi (1983) formula should refer to the channel characteristics at urban downstream regions and the grain size distribution of sediment accumulations that were deposited by previous flood events over the banks of the upstream channel, according to the concept of “traveling bed load” (Piton and Recking, 2017). Moreover, the discharge-driven transport of blocks or boulders, which can lead to the mechanical obstruction of bridges, needs to be considered with respect to the block diameter.

The design of the elements ① to ⑥ is described in detail in the following sections, from a hydraulic and a functional point of view.

8.2 Detailed functional design

8.2.1 Inlet structure

The inlet structure ① in the shape of a sill is only sometimes required in steep terrains to overcome height differences that occur when the longitudinal slope of the retention reservoir is flatter than the natural channel slope. Such sills may cause scour in the absence of sediment transport or dead storage volume in the case of burdening due to continuous, moderate sediment transport (Zollinger, 1983). In addition, sills represent obstacles for the longitudinal river connectivity, e.g., for fish migration. Therefore, inlet structures in terms of sills should be avoided or substituted by stable block ramps, as proposed by Tamagni (2013) or Weitbrecht et al. (2016).

8.2.2 Deposition area

The available space for the widening that constitutes the deposition area ② (retention reservoir) is often confined by the terrain topography. Otherwise, the shape of the reservoir can be artificially adapted by lateral dykes. For the optimization of the shape of the deposition area, the trapping efficiency, defined as the ratio of the potential sediment storage volume and active storage volume, can be used. The trapping efficiency decreases with increasing reservoir width and vice versa (Zollinger, 1983). However, wide reservoirs are less susceptible to the unwanted flushing of previously retained sediments during hazardous floods. A preferable length to width ratio of 4:3 for an acceptable trapping efficiency and a reduced risk of unwanted sediment flushing is recommended, according to (Zollinger, 1983).

8.2.3 Guiding channel

The guiding channel ③ serves for the morphological fixation and flow control in the deposition area, up to the occurrence of the target discharge for bed load retention, i.e., hazardous flood (Chpt. 7). Corresponding to connatural flow conditions in mountain rivers, the guiding channel should have a trapezoidal cross section, with a bank slope m of approximately 1:2.25, and a rough, paved bed constituted by blocks larger than the D_{84} of the upstream channel bed (Fig. 8.2). The channel roughness can be assessed by a skin friction-type parameter such as the Strickler coefficient (in $m^{1/3}\ s^{-1}$): $k_{st} = 26/(1.25 \cdot D_{84})^{1/6}$ (e.g., Meyer-Peter and Müller, 1948; Smart and Jaeggi, 1983; Rickenmann and Recking, 2011). The guiding channel axis should be straight or oriented at the initial river bed. The bottom slope S_0 of the guiding channel should correspond to the channel slope at urban downstream reaches that are intended to be protected by the sediment trap.
The discharge capacity Q of the guiding channel results from the relationship $Q = u \cdot A$, as a function of the flow velocity u and the flow cross section surface is $A = h \cdot (w + h \cdot m)$, where h denotes the flow depth and w is the channel bottom width (Fig. 8.2).
The flow velocity can be evaluated based on the hypothesis of *quasi* uniform flow conditions

in the guiding channel and the presence of skin friction only, i.e., in terms of k_{st}. Thus, the Gauckler–Manning–Strickler formula can be applied to assess stage-discharge relations for the guiding channel and to ensure that the bank-full discharge corresponds to the target discharge for triggering bed load retention.

Moreover, stage discharge-relations can be used to derive the flow velocity in the guiding channel for discharges, which are important to the ecological river connectivity in terms of fish migration. The relevant discharges for fish migration are typically in a range between Q_{30} (discharge that is not exceeded over 30 days per year) and Q_{330} (discharge that is not exceeded over 330 days per year); according to DWA (2009) and Tamagni (2013). Within this range of discharges, the migration of fish is additionally bound to upper limits of the flow velocity and lower limits of the flow depth. The upper limit for the admissible cross-section-averaged flow velocity (in m s^{-1}) can be estimated as follows: $u_{max} \leq 5 \cdot L_{fish}$ per second. L_{fish} denotes the length (in m) of indigenous, adult fish (Bainbridge, 1958; DWA, 2005; Tamagni, 2013). In general, the maximum flow velocity for weak fish, e.g., bullhead, is approximately 0.3 m s^{-1}, and for strong fish, e.g., salmon or trout, the maximum admissible flow velocity is approximately 1.0 m s^{-1}. The mean flow depth is required to be at least 0.3 m to 0.4 m to enable the migration of salmon or trout, respectively (DWA, 2009; Tamagni, 2013). At the same time, the bed load transport capacity of the guiding channel should not be smaller than the bed load transport of the morphologically effective, dominant discharge (Wolman and Miller, 1960), and not larger than the bed load transport capacity at the downstream reaches that require protection. In line with the previous statements, the Smart and Jaeggi (1983) equation provides a reliable estimate for the evaluation of the bed load transport capacity (Chpts. 5 and 6).

An iterative design approach is required to meet the hydraulic criteria in terms of fish migration and the bed load transport capacity. In addition, concrete reinforcement of the guiding channel bottom is important in the vicinity and downstream of the barrier to avoid erosion.

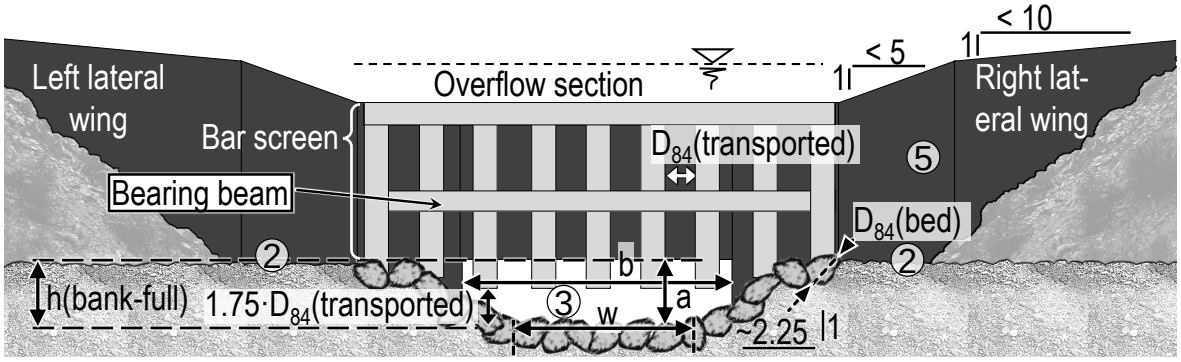

Figure 8.2 – *The cross section of the permeable sediment trap shown in Fig. 8.1, with guiding channel and combined barrier in the background. The guiding channel bottom width w, the hydraulic opening height a and width b, and the bank-full flow depth h(bank-full) of the guiding channel are indicated. D_{84} (transported) and D_{84} (bed) denote the characteristic grain size of traveling bed load and the upstream channel bed, respectively.*

8.2.4 Maintenance access

The sediment trap needs to be accessible for construction vehicles. Therefore, the maintenance access (4) should have a width of 3.2 m, a driveway slope smaller than 10 % and a maximum talus inclination of 2:3.

8.2.5 Permeable barrier

The permeable barrier (5) is a two-way sediment deposition control measure (cf. Chpt. 6). An inclined bar screen superposed to a concrete barrier (open check dam) with one opening serve for the mechanical and hydraulic controls of bed load retention, respectively.
The mechanical control occurs when the grains entangle between the vertical, rounded bars of the screen. This is achieved by a horizontal bar interspace corresponding to the D_{84} of the transported (traveling) bed load (Fig. 8.2). The clearance height below the bar screen should be $1.75 \cdot D_{84}$ (transported) to enable the sediment transfer for discharges that are smaller than the target discharge for triggering bed load retention (Chpt. 6). A horizontal bearing beam should be considered to increase the stability of the screen. The diameter of the bars results from a stability assessment depending on the construction material. The bar screen inclination of 2:1 favors the transfer of driftwood (D'Agostino et al., 2000; Bergmeister et al., 2009; Piton and Recking, 2016b). Structures simultaneously aiming at the combined sediment and driftwood retention are not recommended due to conflicting characteristic length scales of sediment and driftwood.
The hydraulic deposition control is imposed by the backwater of a flow constriction, due to a reduction in the bed shear stress upstream of the barrier. The flow constriction can be obtained through an opening in a concrete barrier (open check dam). The constriction height a corresponds to the bank-full flow depth h(bank-full) of the guiding channel. The constriction width b should be equal to the mean flow width of the guiding channel at bank-full discharge, i.e., $b \approx w + h$(bank-full)$\cdot m$.
Multiple or compound opening geometries are not suitable regarding the difficulties in estimating the complex effects of such multiple constrictions on the flow and bed load transport. The discharge capacity of a singular, pressurized opening with a (partially) trapezoidal shape can be computed as a function of the upstream head $H = h + u^2/(2g)$; where h and u refer to the flow depth and cross-section-averaged flow velocity upstream of the constriction without sediment deposit (Chpt. 4):

$$Q_c = \mu_p \sqrt{2\,g}\,\frac{2}{3}\,\frac{b+w}{2}\left[H^{\frac{3}{2}} - (H-a)^{\frac{3}{2}}\right] \tag{8.1}$$

where g is the gravity acceleration, taken as 9.81 m s^{-2}. The discharge coefficient μ_p depends on the magnitude of the backwater caused by the barrier. Thus, μ_p is approximately 0.7 for small backwater extents, i.e., $u/\sqrt{h \cdot g} > 0.5$ and decreases linearly to values of approximately 0.5 for pronounced backwater, i.e., $u/\sqrt{h \cdot g}$ is close to zero (cf. Chpts. 4 and 5).
The barrier height has to be determined as a function of the sediment volume that needs to be retained, and the size of the deposition area (2). Piton and Recking (2016a) propose an iterative determination of the barrier height and the geometry of the deposition area, corresponding to the required retention volume. However, the extent of the deposition area is often limited by external

factors such as the terrain topography or roads. Then the barrier height is the only variable for adjusting the retention volume. In view of unwanted sediment flushing, it is preferable to use high barriers. The retention volume can be derived from the integration of the deposition area cross section (Fig. 8.2) along the longitudinal channel axis regarding the height of the overflow crest of the barrier (open check dam). Supplementary storage volume can be obtained when the deposition slope S_{dep} is additionally considered (Fig. 8.3). The deposition slope can be estimated by $S_{dep} = 1/2 \cdot S_0$ (cf. Chpt. 7).
The barrier crest is horizontal in the overflow section (Fig. 8.2), but the crest of the lateral wings needs to be beveled toward the channel axis to center the flow in the case of barrier overflow. The overflow section should correspond to design standards and referring to an extreme flood event (e.g., USACE, 1992; Khatsuria, 2005). The bevelling of the lateral wings should be at least 1:10, but it must be steeper than the natural upstream channel slope (Fig. 8.2), and serves for centering the flow at the overflow section of the barrier in the case of hazardous floods. The centering of the flow is essential to avoid lateral erosion beyond the wings of the barrier. In addition, the anchoring of the lateral wings in the terrain is important to avoid such lateral erosion.

8.2.6 Downstream abutments and scour protection

The design of the downstream abutments and scour protection with counter dam, i.e., a ground sill, (Fig. 8.3) has to be adapted to stability assessments, based on an extreme flood event. Complete, freely distributed calculation guides are available (e.g., Khatsuria, 2005).

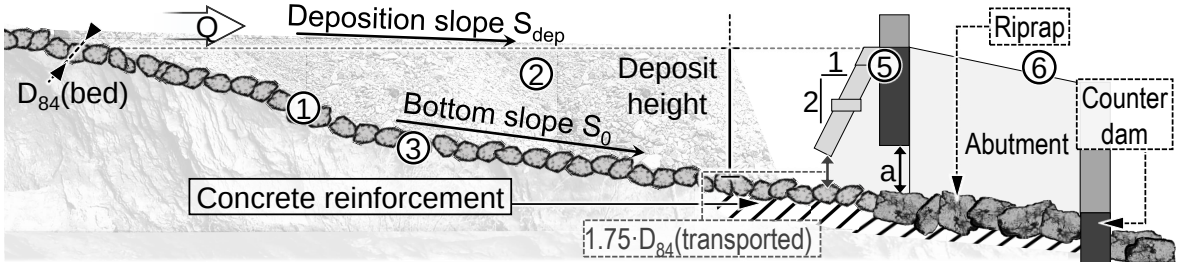

Figure 8.3 – *The longitudinal section of the (filled) permeable sediment trap shown in Fig. 8.1, with guiding channel and combined barrier equipped with an opening of the height a. The filling is indicated by a sediment deposit upstream of the permeable barrier ⑤. D_{84} (transported) and D_{84} (bed) denote the characteristic grain size of traveling bed load and the upstream channel bed, respectively.*

8.3 Concluding remarks

The design of the bar screen (upstream part of the permeable barrier (5)) refers to the characteristic size of sediment. This is in contrast to the existing design approach for such screens, which often refers primarily to the characteristic diameter or length of driftwood. The newly proposed concept for permeable sediment traps is based on the assumption that driftwood is mainly mobilized by exceptional floods overflowing vegetated river banks. The smaller, non-hazardous floods, that should not be affected by permeable sediment traps, are assumed not to overflow vegetated river banks. Therefore, the amounts of driftwood transported by non-hazardous floods are expected to be small. If driftwood occurs nevertheless, it clogs the bar screen and triggers bed load retention earlier than desired. Such early clogging is disadvantageous in view of sediment continuity, but it even increases the safety of urban downstream reaches. For improving the passage of driftwood, screens with multiple inclinations (shallow at the bottom, steep toward the crest) may be considered (Bergmeister et al., 2009).
The controlled, wanted flushing of a permeable sediment trap after a hazardous flood with sediment deposition is only possible when the mechanical log jam is manually removed.
For the proper functioning of the permeable barrier, regular controls should ensure that the bar screen is free from minor log jams, e.g., due to occasionally transported wood.

9 Conclusions and future research

9.1 Conclusions

9.1.1 Main contributions

Sediment traps are designed for the retention of heavy bed load during fluvial floods that exceed the transport capacity of downstream river reaches. Such hazardous floods may endanger riverine urban areas and infrastructures. Therefore, sediment traps are necessary upstream of potentially endangered urban downstream reaches. The main elements of a typical sediment trap are a deposition area with a downstream torrential control barrier with opening(s) for controlling the retention of bed load. Many existing sediment traps retain sediment already during small, frequent floods which are not yet hazardous. The resulting interruption of the sediment transport leads to the eco-morphological depletion of downstream river reaches. In turn, some sediment traps are prone to the unwanted flushing of sediments stored in the deposition area during hazardous floods. New design aspects for permeable sediment traps are developed to improve the sediment transfer during small, non-hazardous floods and to reduce the risk related to unwanted sediment flushing. The analysis of torrential control barriers at the downstream end of a sediment trap is differentiated between two working principles for triggering bed load retention: (1) the previously rarely analyzed hydraulic control and (2) the well-understood mechanical control.
The hydraulic control type is experimentally analyzed and then applied to a concept of permeable sediment traps. The permeability was achieved by introducing the novel element of a guiding channel across the deposition area in conjunction with barriers combining the hydraulic and mechanical controls of bed load retention. The main contributions of this research are:

- Approaches and parameters which enable the assessment of the flow and bed load transport through constrictions, as they occur at open torrential barriers, considering different channel slopes and with a particular focus on:
  - The formation of backwater and related head loss;
  - The discharge and associated bed load transport capacity; and
  - The process of bed load deposition in the backwater upstream.

- Demonstration that a guiding channel across the deposition area can ensure the bed load trans-

fer through a permeable barrier up to small, non-hazardous floods without creating backwater and deposition.

- A barrier concept combining an inclined sediment bar screen for the mechanical initiation of bed load retention upstream of a hydraulic barrier with an adequate opening for the hydraulic control of the onset of backwater and bed load retention. The experiments show that the combined mechanical-hydraulic control reduces risks, which are due to the estimated grain size and unwanted sediment flushing in the cases of only mechanical or hydraulic control, respectively.

The findings can be applied to the design of new, as well as existing sediment traps to reduce the need for maintenance works and to ensure the safe retention of bed load during hazardous floods.

9.1.2 Hydraulic control barriers

The analysis of barriers aiming at the hydraulic control of bed load retention highlights the following aspects:

- The hydraulic control of bed load retention can be achieved by barriers equipped with a trapezoidal- or rectangular-shaped opening acting like a flow constriction, which can be characterized as follows:
  - Openings that confine the flow vertically (orifices or slots) represent pressurized flow constrictions.
  - Openings that confine the flow from the sides only (slits) are lateral flow constrictions representing a control section with open-channel flow under critical conditions.
- The flow conditions upstream of such constrictions can be predicted by the upstream Froude number Fr_0, which is a function of the upstream flow depth, channel geometry and discharge.
- The slope of the upstream channel has to bed considered for assessing the effects of constrictions on the flow.
- The discharge capacity Q_c of constriction-like openings can be estimated as follows:
  - For openings with pressurized flow (orifices), modified existing formulae with an adapted discharge coefficient μ_p are applicable (Eqs. 5.3 or 8.1 for parameter descriptions):
    $Q_c = \frac{2}{3}\mu_p \cdot b \cdot \sqrt{2\,g}\,\left[H_0^{\frac{3}{2}} - (H_0 - a)^{\frac{3}{2}}\right]$
    - → μ_p takes values of 0.70±0.04 for upstream Froude numbers Fr_0 larger than 0.5;
    - → μ_p decreases as a linear function of the upstream Froude number when Fr_0 is smaller than 0.5;
    - → μ_p takes a value of $\mu_p \approx 0.5$ when the upstream Froude number Fr_0 is close to zero.
  - For openings with free surface flow (slits), the discharge capacity can be derived as a function of the channel slope and using the cross-section-averaged energy balance between a section in upstream vicinity of the opening and the cross section in the opening (Eq. 5.8 for parameter descriptions):
    $Q_c = 1.25 \cdot \frac{0.25\ S_0 - c_{KQ}}{S_0 - 1} \cdot A_0 \cdot \sqrt{2\ g \cdot \left(\frac{3}{2} h_{cr,o} - h_0 + 10^2 \cdot\ S_0 \cdot L_w\right)}$
- The head loss caused by a flow constriction can be estimated using the loss coefficient ζ_c, which

is an exponentially-decreasing function of the upstream flow conditions in terms of Fr_0 (Eq. 5.6 and Tab. 5.2 for parameter descriptions):
$\zeta_c = 0.3 \cdot h_{*cr}^{-2} + 0.3$

- The bed load transport capacity decreases with rising backwater, i.e., decreasing upstream Froude number.
- The bed load transport capacity strongly reduces when the upstream flow conditions are close-to-critical ($Fr_0 = 1$) and becomes infinitesimally small with further increase of the backwater.
- The reduction θ in the bed load transport capacity due to a flow constriction can be estimated with the following relationship (Eq. 5.9 for parameter descriptions):
$\theta = \left[1 + exp\left(-3.6 \cdot h_{*cr}\right)\right]^{-29}$

9.1.3 New concept of permeable sediment traps with guiding channel

The previous findings on the hydraulic flow and bed load retention controls are implemented in the design of permeable sediment traps. A new concept for permeable sediment traps with a guiding channel is proposed and systematically studied on an experimental basis. The experimental study also considers the risk of unwanted sediment flushing and possibilities to avoid this risk. The main findings are:

- The unwanted flushing of previously deposited sediments in the deposition area can occur during hazardous floods at flow constrictions only aiming at the hydraulic control of bed load retention, in particular:
  - When free surface flow conditions prevail in the constriction. Such a situation can occur during the falling limb of a flood.
  - Through pressurized constrictions when the barrier height is very limited. Such a situation can be associated with the rising limb of a flood and with the flood peak.
- The bed load transport through an inclined bar screen aiming at the mechanically controlled bed load retention can be enabled up to small (flood) discharges, when:
  - The vertical clearance between the bottom of the bars and the channel is approximately 1.75 times the characteristic grain size D_{84} of the transported bed load. For higher discharges, the bar screen is mechanically clogged by coarse particles that entangle between the bars.
  - The horizontal clearance between the bars corresponds to D_{84} of the transported bed load.
- The combination of an inclined bar screen for the mechanical control and a barrier with an opening (orifice) for the hydraulic control favors the safe and robust functioning of a sediment trap as follows:
  - The bar screen prevents unwanted sediment flushing through the pressurized opening (orifice) for the hydraulic control.
  - The backwater upstream of the hydraulic control enhances the mechanical clogging of the bar screen, even though the transported grains are smaller than the estimated characteristic grain size D_{84}. Thus, clogging still occurs when the size of D_{84} is underestimated by 50 %.
- A guiding channel in the deposition area of a sediment trap serves for the local morphological fixation of the flow upstream of a combined permeable barrier (bar screen superposed to an

open check dam with a slot) and ensures the desired functioning of the barrier.
- The discharge capacity of the guiding channel and of downstream reaches should be slightly higher than the morphologically effective, dominant discharge. This criterion is necessary to enhance the eco-morphologically important sediment transfer toward downstream reaches.
- Permeable sediment traps can be achieved by integrating a guiding channel in conjunction with a barrier combining the mechanical (bar screen) and hydraulic (open check dam with a slot) controls.

The amounts of driftwood that can be expected during small, frequent floods are considered to be low, and therefore, driftwood was not tested herein. If driftwood is present, it can be expected that mechanical clogging occurs already for smaller discharges.

9.2 Future research

This research experimentally investigates the sediment transfer through permeable barriers (open check dams) with infinite and strongly limited height. Varying opening dimensions, as well as three different channel slopes and the supplementary application of a bar screen aiming at the mechanical control of bed load retention under steady and *quasi*-unsteady flow conditions are considered. For future research, replication of the experiments is needed to systematically analyze the interplay between the barrier height and the sediment transfer, under unsteady flow conditions, and with varying sediment supply intensity. It is also conceivable to extent the analysis to steeper channel slopes.
The present study refers to a scaled skin-friction-type of roughness based on the average of a set of field data. Even though the roughness can be controlled by adjusting the guiding channel, variations of the roughness may occur in practice. Additional experiments can serve for analyzing the obstruction of flow control barriers regarding roughness variations.
The concept for combined control barriers was successfully tested on a physical model of a case study. In a next step, it is desirable to test the newly developed concept for permeable sediment traps on more structures in practice.
The evaluation of eco-morphological aspects is achieved in the present research based on the capability of sediment traps to convey the dominant, morphologically effective discharge. For future research, particular ecological parameters, which are relevant to the design and functioning of permeable sediment traps, should be investigated.
This research provides an experimental evaluation of the cross-section-averaged head loss due to flow barriers with an opening in rough turbulent flows with bed load. The application of the relationship identified here between the sediment-laden discharge through such openings and the head loss may also serve for improving numerical models. Thus, the testing and verification of such numerical models based on experimental data from this study is an important task for future research.

Bibliography

Aberle, J. and Smart, G. M. (2003). The influence of roughness structure on flow resistance on steep slopes. *Journal of Hydraulic Research*, 41(3):259–269.

Abrahams, A. D., Li, G., and Atkinson, J. F. (1995). Step-pool streams: adjustment to maximum flow resistance. *Water Resources Research*, 31(10):2593–2602.

Allan, D. J. and Castillo, M. M. (2007). *Stream Ecology - Structure and Function of Running Waters*. Springer, Dordrecht, The Netherlands, Second edition.

Ancey, C., Bigillon, F. m. c., Frey, P., Lanier, J., and Ducret, R. (2002). Saltating motion of a bead in a rapid water stream. *Physical Review E*, 66(3):036306.

Andrews, E. D. (1980). Effective and bankfull discharges of streams in the Yampa River basin, Colorado and Wyoming. *Journal of Hydrology*, 46(3-4):311–330.

Armanini, A., Dalri, C., and Larcher, M. (2006). Slit-Check Dams for Controlling Debris Flow and Mudflow. In *International Symposium Disaster Mitigation of Debris Flows, Slope Failures and Landslides*, pages 141–148, Niigata, Japan. Universal Academy Press, Inc.

Armanini, A., Dellagiacoma, F., and Ferrari, L. (1991). From the check dam to the development of functional check dams. In *Fluvial Hydraulics of Mountain Regions*, volume 37 of *Lecture Notes on Earth Sciences*, pages 331–344. Springer-Verlag, Berlin, Heidelberg, Gemany.

Armanini, A. and Larcher, M. (2001). Rational criterion for designing opening of slit-check dam. *Journal of Hydraulic Engineering*, 127(2):94–104.

Arnaud-Fassetta, G., Astrade, L., Bardou, E., Corbonnois, J., Delahaye, D., Fort, M., Gautier, E., Jacob, N., Peiry, J.-L., Piégay, H., and Penven, M.-J. (2009). Fluvial geomorphology and flood-risk management. *Géomporphologie. Relief, Processus, Environnement*, 15(2):109–128.

ASTM D2487-11 (2011). *Standard Practice for Classification of Soils for Engineering Purposes (Unified Soil Classification System)*. ASTM International, West Conshohocken, PA.

Auble, G. T., Friedman, J. M., and Scott, M. L. (1994). Relating Riparian Vegetation to Present and Future Streamflows. *Ecological Applications*, 4(3):544–554.

Bacchi, V., Recking, A., Eckert, N., Frey, P., Piton, G., and Naaim, M. (2014). The effects of kinetic sorting on sediment mobility on steep slopes. *Earth Surface Processes and Landforms*, 39(8):1075–1086.

Bagnold, R. A. (1980). An empirical correlation of bedload transport rates in flume and natural rivers. *Proceedings of the Royal Society of London*, A(372):453–473.

Baigún, C. R. M., Nestler, J. M., Minotti, P., and Oldani, N. (2012). Fish passage system in an irrigation dam (Pilcomayo River basin): When engineering designs do not match ecohydraulic criteria. *Neotropical Ichthyology*, 10(4):741–750.

Bain, M. B., Hughes, T. C., and Arend, K. K. (1999). Trends in Methods for Assessing Freshwater Habitats. *Fisheries*, 24(4):16–21.

Bainbridge, R. (1958). The Speed of Swimming of Fish as Related to Size and to the Frequency and Amplitude of the Tail Beat. *Journal of Experimental Biology*, 35(1):109–133.

Barenblatt, G. I. (1987). *Dimensional Analysis*. Gordon and Breach Science Publishers, New York.

Barenblatt, G. I. (1996). *Scaling, self-similarity and intermediate asymptotics. Dimensional Analysis and Intermediate Asymptotics*. Cambridge University Press.

Barry, J. J., Buffington, J. M., and King, J. G. (2004). A general power equation for predicting bed load transport rates in gravel bed rivers. *Water Resources Research*, 40(W10401):1–22.

Barry, J. J., Buffington, J. M., and King, J. G. (2005). Reply to comment by Claude Michel on "A general power equation for predicting bed load transport rates in gravel bed rivers". *Water Resources Research*, 41(W07016):1–2.

Battisacco, E., Franca, M. J., and Schleiss, A. J. (2016). Sediment replenishment: Influence of the geometrical configuration on the morphological evolution of channel-bed. *Water Resources Research*, 52(11):8879–8894.

Baumer (2010). *Ultrasonic distance measuring sensors UNAM 30*.

Beamish, F. W. (1978). Swimming Capacity. In Hoar, W. S. and Randall, D. J., editors, *Locomotion*, chapter 2, pages 101–187. Academic Press, Inc., New York, USA.

Benda, L. (1990). The influence of debris flows on channels and valley floors in the Oregon coast range, U.S.A. *Earth Surface Processes and Landforms*, 15(5):457–466.

Benson, M. A. and Thomas, D. M. (1966). A definition of dominant discharge. *Bulletin of the International Association of Hydrological Sciences*, 11:76–80.

Bergmeister, K., Suda, J., Hübl, J., and Rudolf-Miklau, F. (2009). *Schutzbauwerke gegen Wildbachgefahren: Grundlagen, Entwurf und Bemessung, Beispiele [Alpine flood protection: Planning basics, Design and Dimensioning, Examples]*. Ernst & Sohn, Berlin, Germany.

Bernhardt, E. S., Palmer, M., Allan, J., Alexander, G., Barnas, K., Brooks, S., Carr, J., Clayton, S., Dahm, C., Follstad-Shah, J., et al. (2005). Synthesizing U.S. river restoration efforts. *Science*, 308:636–637.

Beschta, R. L. (1979). Debris removal and its effects on sedimentation in an Oregon Coast Range stream. *Northwest Science*, 53(1):71–77.

Beschta, R. L. and Jackson, W. L. (1979). The Intrusion of Fine Sediments into a Stable Gravel Bed. *Journal of the Fisheries Research Board of Canada*, 36(2):204–210.

Bezzola, G. R. (2008). Unerwartete Prozesse in einem Geschiebesammler [Unexpected processes in a sediment retention basin]. In *Proceedings of INTERPRAEVENT: Sediment / erosion control and avalanche prevention in the European Alpine region*, pages 271–282, Dornbirn, Austria. International Research Society Interpraevent.

Bezzola, G. R., Gantenbein, S., Hollenstein, R., and Minor, H. (2002). *Verklausung von Brückenquerschnitten [Log-jams at bridges]*. Minor, H.-E, ed.: Mitteilung Nr. 175 der Versuchsanstalt für Wasserbau, Hydrologie und Glaziologie (VAW) an der Eidgenössischen Technischen Hochschule Zürich, Zürich, Switzerland.

Bezzola, G. R. and Hegg, C., editors (2007). *Ereignisanalyse Hochwasser 2005, Teil 1 - Prozesse, Schäden und erste Einordnung [Event analyses of the 2005 flood, part 1 - Processes, damages and preliminary classification]*. Swiss Federal Office for the Environment FOEN / Eidgenössische Forschungsanstalt WSL, Bern / Birmensdorf.

Bezzola, G. R., Sigg, H., and Lange, D. (2004). Schwemmholzrückhalt in der Schweiz [Driftwood retention in Switzerland]. In *Proceedings of INTERPRAEVENT*, pages 29–40, Klagenfurt, Austria. International Research Society Interpraevent.

Biedenharn, D. S., Thorne, C. R., Soar, P. J., Hey, R. D., and Watson, C. (2000). *Effective Discharge Calculation: A Practical Guide*, volume ERDC/CHLTR-00-15. U.S. Army Corps of Engineers, Washington, DC.

Bisson, P. A., Montgomery, D. R., and Buffington, J. M. (2007). Valley, Segments, Stream Reaches and Channel Units. In Hauer, F. and Lamberti, G., editors, *Methods in Stream Ecology*, chapter 2, pages 23–49. Elsevier Science Publishers.

Blom, A. and Parker, G. (2004). Vertical sorting and the morphodynamics of bed form-dominated rivers: A modeling framework. *Journal of Geophysical Research: Earth Surface*, 109(F2):F02007.

Blom, A., Parker, G., Ribberink, J. S., and de Vriend, H. J. (2006). Vertical sorting and the morphodynamics of bed-form-dominated rivers: An equilibrium sorting model. *Journal of Geophysical Research: Earth Surface*, 111(F1):F01006.

Böll, A., Kienholz, H., and Romanh, H. (2008). *Beurteilung der Wirkung von Schutzmassnahmen gegen Naturgefahren als Grundlage für ihre Berücksichtigung in der Raumplanung, Teil E: Wildbäche [Assessment of the effect of protection measures against natural hazards as basis for their consideration in spatial planning, Part E: Mountain Rivers]*. Swiss Confederation: National Platform for Natural Hazards (PlaNat), v1.02d edition.

Box, G. E. P., Hunter, S. J., and Hunter, W. G. (2005). *Statistics for Experimenters: Design, Innovation, and Discovery*. John Wiley & Sons, Hoboken, New Jersey, 2nd edition.

Brandt, S. A. (2000). Classification of geomorphological effects downstream of dams. *CATENA*, 40:375–401.

Braudrick, C. A. and Grant, G. E. (2000). When do logs move in rivers? *Water Resources Research*, 36(2):571–583.

Bridgwater, J., W, S. N., and C, S. D. (1969). Particle mixing by percolation. *Transactions of the Institute of Chemical Engineers*, 47:T114–T119.

Brooke Benjamin, T. (1955). On the flow in channels when rigid obstacles are placed in the stream. *Journal of Fluid Mechanics*, 1(2):227–248.

Brown, C. B. (1939). Silting of reservoirs. In *Technical Bulletin No. 524*. U.S. Department of Agriculture.

Brown, C. B. (1943). Discussion of 'Sedimentation in reservoirs' by B. J. Witzig. *Proceedings of the American Society of Civil Engineers*, 69(6):793–815.

Brune, G. M. (1953). Trap efficiency of reservoirs. *Eos, Transactions American Geophysical Union*, 34(3):407–418.

Buckingham, E. (1915). Model experiments and the forms of empirical equations. *Transactions of the American Society of Mechanical Engineers*, 37:263–296.

Buffington, J. M., Lisle, T. E., Woodsmith, R. D., and Hilton, S. (2002). Controls on the size and occurrence of pools in coarse-grained forest rivers. *River Research and Applications*, 18:507–531.

Buffington, J. M. and Montgomery, D. R. (1999). Effects of supply on surface textures of gravel-bed rivers. *Water Resources Research*, 35(11):3523–3530.

Buffington, J. M., Woodsmith, R. D., Booth, D. B., and Montgomery, D. R. (2003). Fluvial Processes in Puget Sound Rivers and the Pacific Northwest. In Montgomery, D. R., Bolton, S., Booth, D., and Wall, L., editors, *Restoration of Puget Sound Rivers*, chapter 3, pages 46–78. University of Washington Press, Seattle, WA.

Bull, W. B. (1977). The alluvial-fan environment. *Progress in Physical Geography*, 1(2):222–270.

Busnelli, M. M., Stelling, G. S., and Larcher, M. (2001). Numerical Morphological Modeling of Open-Check Dams. *Journal of Hydraulic Engineering*, 127(2):105–114.

Campisano, A., Cutore, P., and Modica, C. (2014). Improving the Evaluation of Slit-Check Dam Trapping Efficiency by Using a 1D Unsteady Flow Numerical Model. *Journal of Hydraulic Engineering*, 140(7):04014024, 1–11.

Canelas, R. B., Domínguez, J. M., Crespo, A. C., Silva, M., and Ferreira, R. M. L. (2015). Debris flow modelling with high-performance meshless methods. In *Congresso de Métodos Numéricos em Engenharia*, pages 1–14, Lisbon.

Carson, M. A. and Griffiths, G. A. (1987). Influence of channel width on bed load transport capacity. *Journal of Hydraulic Engineering*, 113(12):1489–1508.

Castillo, C., Pérez, R., and Gómez, J. A. (2014). A conceptual model of check dam hydraulics for gully control: efficiency, optimal spacing and relation with step-pools. *Hydrology and Earth System Science*, 18:1705–1721.

Catford, J. A. and Jansson, R. (2014). Drowned, buried and carried away: effects of plant traits on the distribution of native and alien species in riparian ecosystems. *New Phytologist*, 204(1):19–36.

Chapra, S. C. and Canale, R. P. (2010). *Numerical Methods for Engineers*. Mc Graw Hill, New York, 6th edition.

Chézy, A. d. (1776). Formula to find the uniform velocity that the water will have in a ditch or in a canal of which the slope is known. In *Collection of Manuscripts in the Library of the Ecole des Ponts et Chaussées*, volume 61 (No. 847) of *Ms.1915*, pages 165–269. École des Ponts et Chaussées, Paris, France.

Chiari, M., Friedl, K., and Rickenmann, D. (2010). A one-dimensional bedload transport model for steep slopes. *Journal of Hydraulic Research*, 48(2):152–160.

Chow, V. T. (1959). *Open-Channel Hydraulics*. Civil Engineering. McGraw-Hill, Tokyo, Japan.

Church, M. (1977). Palaeohydrological Reconstructions From a Holocene Valley Fill. *Fluvial Sedimentology*, Memoir 5:743–772.

Church, M. and Ferguson, R. I. (2015). Morphodynamics: Rivers beyond steady state. *Water Resources Research*, 51:1883–1897.

Church, M. and Haschenburger, J. K. (2017). What is the "active layer"? *Water Resources Research*, 53:5–10.

Church, M. and Zimmermann, A. (2007). Form and stability of step-pool channels: Research progress. *Water Resources Research*, 43(3):W03415.

Comiti, F., Cadol, D., and Wohl, E. (2009). Flow regimes, bed morphology, and flow resistance in self-formed step-pool channels. *Water Resources Research*, 45(4):W04424.

Comiti, F., D'Agostino, V., Moser, M., Lenzi, M. A., Bettella, F., Dell'Agnese, A., E., R., Gius, S., and Mazzorana, B. (2012). Preventing wood-related hazards in mountain basins: from wood load estimation to designing retention structures. In *Proceedings of INTERPRAEVENT*, pages 651–662, Grenoble, France. International Research Society Interpraevent.

Comiti, F., Mao, L., Wilcox, A., Wohl, E., and Lenzi, M. (2007). Field-derived relationships for flow velocity and resistance in high-gradient streams. *Journal of Hydrology*, 340(1-2):48–62.

Conesa Garcia, C. and Lenzi, M. A., editors (2011). *Check Dams, Morphological Adjustments and Erosion Control in Torrential Streams*. Environmental Science, Engineering and Technology. Nova Science Publishers, Inc., Hauppauge, NY.

Copeland, R. R., McComas, D. N., Thorne, C. R., Soar, P. J., Jonas, M. M., and Fripp, J. B. (2001). *Hydraulic Design of Stream Restoration Projects*. US Army Corps of Engineers.

Crowder, D. W. and Knapp, V. H. (2005). Effective discharge recurrence intervals of Illinois streams. *Geomorphology*, 64(3-4):167–184.

Cummins, K. W. (1962). An Evaluation of Some Techniques for the Collection and Analysis of Benthic Samples with Special Emphasis on Lotic Waters. *The American Midland Naturalist*, 67(2):477–504.

D'Agostino, V. (2013). Filtering-retention check dam design in mountain torrents. In Garcia, C. and Lenzi, M. A., editors, *Check dams, morphological adjustments and erosion control in torrential streams*, chapter 9, pages 185–210. Nova Science.

D'Agostino, V., Degetto, M., and Righetti, M. (2000). Experimental investigation on open check dam for coarse woody debris control. *Dynamics of water and sediments in mountain basins, Quaderni di Idronomia Montana*, 20:201–212. BIOS, Cosenza, Italy.

D'Agostino, V. and Lenzi, M. A. (1996). La valutazione del trasporto solido di fondo nel bacino attrezzato del Rio Cordon [The validation of bed-load transport in the Rio Cordon catchment]. *L'Acqua*, 4:23–40.

Darcy, H. (1857). *Recherches Experimentales Relatives au Mouvement de L'Eau dans les Tuyaux [Experimental Researches Relating to the Movement of Water in Pipes]*. 2 volumes. Mallet-Bachelier, Paris, France.

De Vries, M. (1993). River Engineering. In *Lecture notes*, number 250 in f10. Delft University of Technology, Faculty of Civil Engineering.

Deigaard, R. and Fredsøe, J. (1978). Longitudinal Grain Sorting by Current in Alluvial Streams. *Hydrology Research*, 9(1):7–16.

Demars, B. O., Wiegleb, G., Harper, D. M., Bröring, U., Brux, H., and Herr, W. (2014). Aquatic Plant Dynamics in Lowland River Networks: Connectivity, Management and Climate Change. *Water*, 6(4):868–911.

Denic, M. and Geist, J. (2015). Linking Stream Sediment Deposition and Aquatic Habitat Quality in Pearl Mussel Streams: Implications for Conservation. *River Research and Applications*, 31(8):943–952.

Dey, S. (2014). Fluvial Processes: Meandering and Braiding. In *Fluvial Hydrodynamics*, GeoPlanet: Earth and Planetary Sciences, pages 529–562. Springer-Verlag, Berlin Heidelberg.

Di Stefano, C. and Ferro, V. (2013). Experimental Study of the Stage-Discharge Relationship for an Upstream Inclined Grid with Longitudinal Bars. *Journal of Irrigation and Drainage Engineering*, 139:691–695.

Di Stefano, C. and Ferro, V. (2014). Closure to "Experimental Study of the Stage-Discharge Relationship for an Upstream Inclined Grid with Longitudinal Bars". *Journal of Irrigation and Drainage Engineering*, 07014028:1.

Dietrich, W. E., Dunne, T., Neil, F. H., and Reid, L. M. (1982). Construction of sediment budgets for drainage basins. In Swanson, F. J., Janada, R. J., Dunne, T., and Swanson, D. N., editors, *Sediment budgets and routing in forested drainage basins: Portland, Oregon, Pacific North-west Forest and Range Experiment Station*, pages 5–23. U.S. Department of Agriculture.

Dietrich, W. E., Kirchner, J. W., Ikeda, H., and Iseya, F. (1989). Sediment supply and the development of the coarse surface layer in gravel-bedded rivers. *Nature*, 340:215–217.

die.wildbach (2016). Hightech am Schnannerbach: Bundesminister Rupprechter gratuliert zur modernen Schutzanlage [Hightech at the Schnannerbach: The federal minister Rupprechter congratulates to the modern protection system]. Wildbach- und Lawinenverbauung (Abteilung III/5).

DIN 1319-3 (1996). *Grundlagen der Messtechnik [Basics of measurement technology]*. Deutsches Institut für Normung e. V.

DIN 18127 (2012). *Soil, investigation and testing - Proctor test*. Deutsches Institut für Normung e. V.

DIN 19663-1985:6) (1985). *Wildbachverbauung; Begriffe, Planung und Bau [Torrent Control - Terms, Planning and Construction]*. Deutsches Institut für Normung e. V.

Doyle, M. W., Stanley, E. H., Strayer, D. L., Jacobson, R. B., and Schmidt, J. C. (2005). Effective discharge analysis of ecological processes in streams. *Water Resources Research*, 41(11):W11411.

Du Boys, P. (1879). Etudes du régime du Rhône et l 'action exercée par les eaux sur un lit à fond de graviers indéfiniment affouillable [Studies of the flow of the Rhone and the forces exerted by the waters on an indefinitely erodible gravel bed]. *Annales des Ponts et Chaussées*, 5(18):141–195.

Dudill, A., Frey, P., and Church, M. (2016). Infiltration of fine sediment into a coarse mobile bed: a phenomenological study. *Earth Surface Processes and Landforms*, ESP-16-0043.R2:1–15.

Dust, D. and Wohl, E. (2012). Characterization of the hydraulics at natural step crests in step-pool streams via weir flow concepts. *Water Resources Research*, 48(9):W09542.

DWA (2005). *WW-8.1. Fischschutz- und Fischabstiegsanlagen - Bemessung, Gestaltung, Funktionskontrolle [Fish protection and fish passage facilities - Design, configuration, performance check]*. 2. Korrigierte Auflage. (Deutsche Vereinigung für Wasserwirtschaft, Abwasser und Abfall e.V.), Hennef, Germany.

DWA (2009). *WW-1.2. Naturnahe Sohlgleiten [Natural block ramps]*. (Deutsche Vereinigung für Wasserwirtschaft, Abwasser und Abfall e.V.), Hennef, Germany.

DWA (2014). *Merkblatt DWA-M 509. Fischaufstiegsanlagen und fischpassierbare Bauwerke [Technical bulletin for fishways]*. (Deutsche Vereinigung für Wasserwirtschaft, Abwasser und Abfall e.V.), Hennef, Germany.

Einstein, H. A. (1942). Formulas for the Transportation of Bed Load. *Transactions of the American Society of Civil Engineers*, 107(1):561–577.

Einstein, H. A. (1950). The Bed-Load Function for Sediment Transport in Open Channel Flows. *Technical Bulletin of the USDA Soil Conservation Service*, 1026:71.

Ensign, S., Siporin, K., Piehler, M., Doyle, M. W., and Leonard, L. (2013). Hydrologic Versus Biogeochemical Controls of Denitrification in Tidal Freshwater Wetlands. *Estuaries and Costs*, 36(3):519–532.

Everett, R. A. and Ruiz, G. M. (1993). Coarse woody debris as a refuge from predation in aquatic communities. *Oecologia*, 93(4):475–486.

Exner, F. M. (1925). Über die Wechselwirkung zwischen Wasser und Geschiebe in Flüssen [About the Interdependency of Water and Bed load in Rivers]. *Akademie der Wissenschaften in Wien, math.-naturw. Klasse, Sitzungsberichte, Abt. IIa*, 134:165–203.

FAO and DVWK, editors (2002). *Fish passes - Design, dimensions and monitoring*. Food and Agriculture Organization of the United Nations in arrangement with Deutscher Verband für Wasserwirtschaft und Kulturbau e.V., Rome, Italy.

Ferguson, R. (2007). Flow resistance equations for gravel- and boulder-bed streams. *Water Resources Research*, 43:W05427.

Ferguson, R. (2010). Time to abandon the Manning equation? *Earth Surface Processes and Landforms*, 35:1873–1876.

Ferguson, R. I. (2012). River channel slope, flow resistance, and gravel entrainment thresholds. *Water Resources Research*, 48:1–13.

Frey, P. (2014). Particle velocity and concentration profiles in bedload experiments on a steep slope. *Earth Surface Processes and Landforms*, 39(5):646–655.

Frey, P. and Tannou, S. (2000). Experimental study on bed load control in torrents by open slit dams. In *Joint Conference on Water Resources Engineering and Water Resources Planning and Management*, page 10, Minneapolis.

Frey, P., Tannou, S., Tacnet, J., Richard, D., and Koulinski, V. (1999). Interactions Ecoulements torrentiels - Ouvrages terminaux de plages de dépôt [Interactions between torrential flows and open check dams]. In *Pôle grenoblois d'Etudes et de Recherche pour la prévention des risques naturels*, Grenoble, France.

Geitner, V. and Drewes, U. (1990). Entwicklung eines neuartigen pfahlfischpasses [development of a novel pale fish passage]. *Wasser & Boden*, 42:604–607.

Ghilardi, T. (2014). *Sediment Transport and Flow Conditions in Steep Rivers with Large Immobile Boulders, Thèse No. 5979*. PhD thesis, École Polytechnique fédérale de Lausanne. Directors: Schleiss, A.J. and Franca, M. J.

Ghilardi, T., Franca, M. J., and Schleiss, A. J. (2014). Bed load fluctuations in a steep channel. *Water Resources Research*, 50(8):6557–6576.

Gibson, S., Abraham, D., Heath, R., and Schoellhamer, D. (2009). Vertical gradational variability of fines deposited in a gravel framework. *Sedimentology*, 56(3):661–676.

Gibson, S., Abraham, D., Heath, R., and Schoellhamer, D. (2010). Bridging Process Threshold for Sediment Infiltrating into a Coarse Substrate. *Journal of Geotechnical and Geoenvironmental Engineering*, 136(2):402–406.

Gilvear, D. J., Spray, C. J., and Casas-Mulet, R. (2013). River rehabilitation for the delivery of multiple ecosystem services at the river network scale. *Environmental Management*, 126:30–43.

Gisen, D. C., Weichert, R. B., and Nestler, J. M. (2017). Optimizing attraction flow for upstream fish passage at a hydropower dam employing 3D Detached-Eddy Simulation. *Ecological Engineering*, 100:344–353.

Goñi, M. A., Hatten, J. A., Wheatcroft, R. A., and Borgeld, J. C. (2013). Particulate organic matter export by two contrasting small mountainous rivers from the Pacific Northwest, U.S.A. *Journal of Geophysical Research: Biogeosciences*, 118(1):112–134.

Gomi, T., Sidle, R. C., and Richardson, J. S. (2002). Understanding processes and downstream linkages of headwater systems. *BioScience*, 52(10):905–916.

GoPro Hero4 Silver (2016). *GoPro User Manual*.

Goris, A. and Schneider, K., editors (2012). *Schneider Bautabellen für Ingenieure mit Berechnungshinweisen und Beispielen [Abacuses for engineers with calculation notes and examples]*. 20. Auflage. Werner Verlag, Cologne, Germany.

Gostner, W., Alp, M., Schleiss, A. J., and Robinson, C. C. (2013). The hydro-morphological index of diversity: a tool for describing habitat heterogeneity in river engineering projects. *Hydrobiologia*, 712(1):43–60.

Graf, W. and Altinakar, M. (2011). *Hydraulique fluviale*, volume 16 of *Traité de Génie Civil*. Presses polytechniques et universitaires romandes, Lausanne, Switzerland.

Gregoretti, C. (2008). Inception Sediment Transport Relationships at High Slopes. *Journal of Hydraulic Engineering*, 134(11):1620–1629.

Guo, J. (2002). Hunter Rouse and Shields diagram. In *Advances in hydraulics and water engineering*, volume 2 of *13th IAHR-APD Congress, World Scientific*, Singapore.

Haden, G. A., Blinn, D. W., Shannon, J., and Wilson, K. P. (1999). Driftwood: an alternative habitat for macroinvertebrates in a large desert river. *Hydrobiologia*, 397(0):179–186.

Hager, W. H. (2010). *Wastewater Hydraulics, Theory and Practice, Second Edition*. Springer-Verlag, Berlin, Heidelberg.

Hager, W. H. and Schleiss, A. J. (2009). *Constructions hydrauliques [Hydraulic structures]*, volume 15. Presses polytechniques et universitaires romandes.

Hamilton, K. (1984). *Methods to estimate aquatic habitat variables*. Colorado Cooperative Fishery Research Unit, Colorado State University, Fort Collins, CO.

Hampel, R. (1968). Geschiebeablagerung in Wildbächen dargestellt in Modellversuchen [Bed load deposition in mountain rivers illustrated in physical experiments]. *Wildbach- und Lawinenverbauung*, 1,2:100.

Hampel, R. (1974). Die Wirkungsweise von Wildbachsperren [The effects of torrential barriers]. *Wildbach- und Lawinenverbau and Österreichische Wasserwirtschaft*, 38/26:2–79/265–273.

Hankin, D. G. and Reeves, G. H. (1988). Estimation total fish abundance and total habitat area in small streams based on visual estimation methods. *Canadian Journal of Fisheries and Aquatic Sciences*, 45(5):834–844.

Hartlieb, A. and Bezzola, G. R. (2000). Ein Überblick zur Schwemmholzproblematik. *Wasser Energie Luft*, 92(1/2):1–5.

Hartung, J., Elpelt, B., and Klösener, K. (2005). *Statistik: Lehr- und Handbuch der angewandten Statistik [Statistics: Text- and Handbook of applied Statistics]*. Oldenbourg Verlag, Munich, Germany, 14 edition.

Harvey, A. M. (1969). Channel capacity and the adjustment of streams to hydrologic regime. *Journal of Hydrology*, 8(1):82–98.

Hassan, M., Brayshaw, D., Alila, Y., and Andrews, E. (2014). Effective discharge in small formerly glaciated mountain streams of British Columbia: Limitations and implications. *Water Resources Research*, 50(5):4440–4458.

Hassan, M. A. (2005). Characteristics of gravel bars in ephemeral streams. *Journal of Sedimentary Research*, 75(1):29–42.

Hassan, M. A., Church, M., Lisle, T. E., Brardinoni, F., Benda, L., and Grant, G. E. (2005). Sediment transport and channel morphology of small, forested streams. *Journal of the American Water Resources Association*, 41(4):853–876.

Hassan, M. A., Smith, B. J., Hogan Dan, L., Luzi David, S., Zimmermann, A. E., and Eaton, B. C. (2008). *Chpt. 18: Sediment storage and transport in coarse bed streams: scale considerations*, chapter 18, pages 473–496. Gravel-Bed Rivers VI: From Process Understanding to River Restoration. Elsevier.

Hassan, M. A. and Woodsmith, R. D. (2004). Bed load transport in an obstruction-formed pool in a forest, gravelbed stream. *Geomorphology*, 58(1-4):203–221.

Hassan, M. A. and Zimmermann, A. E. (2012). *Gravel-bed Rivers: Processes, Tools Environments: Channel Response and Recovery to Changes in Sediment Supply*, chapter 33, pages 464–473. John Whiley & Sons.

Hauenstein, W. (2003). Entsorgungspflicht versus Nutzen von Totholz im Gewässer - ein Interessenkonflikt für die Wasserkraft [Disposal obligation versus use of deadwood in the aquatic environment - a conflict of interests for hydropower]. *Wasser Energie Luft*, 95(11/12):363–366.

Heller, V. (2011). Scale effects in physical hydraulic engineering models. *Journal of Hydraulic Research*, 49(3):293–306.

Henderson, F. M. (1966). *Open Channel Flow*. The Macmillan Company, New York.

Hersberger, D. S. (2002). *Wall Roughness Effect on Flow and Scouring in curved channels with Gravel Bed, Thèse No. 2632*. PhD thesis, École Polytechnique fédérale de Lausanne. Director: Schleiss, A.J.

Hogan, D. L., Bird, S. A., and Hassan, M. A. (1998). Spatial and temporal evolution of small coastal gravel-bed streams: Influence of forest management on channel morphology and fish habitat. In Klingeman, P. C., Beschta, R. L., Komar, P. D., and B, B. J., editors, *Gravel-bed Rivers in the Environment*, pages 365–392. Water Resources Publication Highlands Ranch, Colorado.

Hostmann, M. (2005). *Decision Support for River Rehabilitation*. PhD thesis, Eidgenössische Technische Hochschule Zürich (ETHZ).

Howard, A. D. (1980). Threshold in river regimes. *Thresholds in geomorphology*, 11:227–258.

Hübl, J. (2006). Vorläufige Erkenntnisse aus 1:1 Murenversuchen: Prozessverständnis und Belastungsannahmen [Preliminary findings from 1:1 debris flow experiments: Process understanding and load cases]. In *Geotechnik und Naturgefahren: Balanceakt zwischen Kostendruck und Notwendigkeit (VÖBU)*. FFIG, Reiser, G., Vienna, Austria.

Hübl, J., Ganahl, E., Bacher, M., Chiari, M., Holub, M., Kaitna, R., Prokop, A., Dunwoody, G., Forster, A., and Schneiderbauer, S. (2006). *Dokumentation der Wildbachereignisse vom 22./23. August 2005 in Tirol, Detaillierte Aufnahme (unveröffentlicht) [Documentation of the torrential floods from 22./23. August 2005 in Tyrol, Detailed inventory (unpublished)]*, volume IAN Report 109 Band 2. University of Natural Resources and Life Sciences, Vienna, Austria.

Hübl, J., Holub, M., and Suda, J. (2005). Structural mitigation measures. In Bergmeister, K., Rickenmann, D., Strauss, A., Wieshofer, S., Curbach, M., and Proske, D., editors, *3rd Probabilistic Workshop: Technical Systems + Natural Hazards*, Schriftenreihe des Departments Nr.7, pages 115–126. Universität für Bodenkultur, Department für Bautechnik und Naturgefahren, Vienna, Austria.

Hübl, J., Holzinger, G., and Wehrmann, H. (2003). Entwicklung von Grundlagen zur Dimensionierung kronenoffener Bauwerke für die Geschiebebewirtschaftung in Wildbächen: Klassifikation von Wildbachsperren [Development of design basics for open-gap crested structures for the management of bed load in mountain rivers: Classification of torrenital barriers]. In *WLS Report 50 - Band 2*, page 85. BMLFUW.

Hunziker, R. P. and Jaeggi, M. N. R. (2002). Grain Sorting Processes. *Journal of Hydraulic Engineering*, 128(12):1060–1068.

Hunzinger, L., Hunziker, R., and Zarn, B. (1995). Der Geschiebehaushalt in lokalen Aufweitungen [Bed load budget in local widenings]. *Wasser Energie Luft*, 87(9):195–200.

Hunzinger, L. and Zarn, B. (1996). Geschiebetransport und Ablagerungsprozesse in Wildbachschalen [Sediment Transport and Aggradation Processes in Rigid Torrent Channels]. In *Proceedings of INTERPRAEVENT*, volume 4, pages 221–230, Garmisch-Partenkirchen, Germany. International Research Society Interpraevent.

Ikeda, S., Parker, G., and Kimura, Y. (1988). Stable width and depth of straight gravel rivers with heterogeneous bed materials. *Water Resources Research*, 24(5):713–722.

Ikeya, H. (1989). Debris flow and its countermeasures in Japan. *Bulletin of the International Association of Engineering Geology*, 40(1):15–33.

Indlekofer, H. (2004). Zur hydraulischen Wirkung von flexiblem Bewuchs [About the hydraulic effect of flexible vegetation]. *Wasser und Abfall*, 6(4):20–23.

Iverson, R. M. (2005). Debris flow mechanics. In Jakob, M. and Hungr, O., editors, *Debris-flow Hazards and Related phenomena*, chapter 6, pages 105–134. Springer, Berlin Heidelberg.

Jaeggi, M. N. R. (1992). Effect of Engineering Solutions on Sediment Transport. In Billi, R., Hey, R., Thorne, C., and Tacconi, P., editors, *Dynamics of Gravel-Bed Rivers*, pages 593–605. John Wiley & Sons Ltd, Chichester, UK.

Jansen, P., Van Bendegom, L., Van den Berg, J., De Vries, M., and Zanen, A. (1994). Scale models. In *Principles of river engineering: The non-tidal alluvial river*, Institutional Repository, pages 305–321. Delftse Uitgevers Maatschappij, Delft, The Netherlands.

Jarrett, R. D. (1992). Hydraulics of mountain rivers. In Yen, B. C., editor, *Channel flow resistance: centennial of Manning's formula*, pages 287–298. Water Resource Publications, Littleton CO.

Järvelä, J. (2002). Flow resistance of flexible and stiff vegetation: a flume study with natural plants. *Journal of Hydrology*, 269(1-2):44–54.

Jensen, A. J. and Aass, P. (1995). Migration of a fast-growing population of brown trout (Salmo trutta L.) through a fish ladder in relation to water flow and water temperature. *Regulated Rivers Research & Management*, 10(2-4):217–228.

Jensen, M. E. and Bourgeron, P. S., editors (2012). *A Guidebook for Integrated Ecological Assessments*. Springer Science+Business Media, New York, NY.

Ji, U., Velleux, M., Julien, P. Y., and Hwang, M. (2014). Risk assessment of watershed erosion at Naesung Stream, South Korea. *Environmental Management*, 136:16–26.

Johnson, J. P. L. (2016). Gravel threshold of motion: a state function of sediment transport disequilibrium? *Earth Surface Dynamics*, 4:685–703.

Johnson, S. L., Rodgers, J. D., Solazzi, M. F., and Nickelson, T. E. (2005). Effects of an increase in large wood on abundance and survival of juvenile salmonids (Oncorhynchus spp.) in an Oregon coastal stream. *Canadian Journal of Fisheries and Aquatic Sciences*, 62(2):412–424.

Jordan, F., Jaeggi, M. N., and Nigg, U. (2003). Modélisation physique d'un piège à graviers, le cas du Baltschiederbach. *Wasser Energie Luft*, 9(10):283–290.

Kaitna, R., Chiari, M., Kerschbaumer, M., Kapeller, H., Zlatic-Jugovic1, J., Hengl, M., and Hübl, J. (2011). Physical and numerical modelling of a bedload deposition area for an alpine torrent. *Natural Hazards and Earth System Sciences*, 11(6):1589–1597.

Kaitna, R. and Hübl, J. (2013). Silent witnesses for torrential processes. In Schneuwly-Bollschweiler, M., Stoffel, M., and Rudolf-Miklau, F., editors, *Dating torrential processes on fans and cones*, volume 47, pages 111–130. Springer, Dordrecht Heidelberg New York London.

Kanton Uri (2016). Gesamtschau Schutzwasserbau Urner Talboden. In *KOHS-Tagung*, pages 1–39, Olten, Switzerland.

Kettl, W. (1973). Sortierbauwerke im Pongau: Theorien, Erfahrungen [Sorting dams in the Pongau: theories, experiences]. *Wildbach- und Lawinenverbau*, 2:15–23.

Keulegan, G. H. (1938). *Laws of turbulent flow in open channels*, volume 21. U.S. National Bureau of Standards.

Khatsuria, R. (2005). Hydraulics of Spillways and Energy Dissipators. In Meyer, M. D., editor, *Civil and Environmental Engineering*, chapter 4, pages 41–62. Marcel Dekker, New York, USA.

Kindsvater, C. E., Carter, R. W., and Tracy, H. J. (1953). Computation of peak discharge at contractions. *Geological Survey Circular*, 284:1–35.

Klonsky, L. and Vogel, R. M. (2008). Effective Measures of "Effective Discharge". In *World Environmental and Water Resources Congress 2008*, pages 1–10. American Society of Civil Engineers, Ahupua'A.

Knighton, A. D. (1980). Longitudinal changes in size and sorting of stream-bed material in four English rivers. *Geological Society of America Bulletin*, 91(00110):55–62.

Kobus, H. and Abraham, G. (1978). *Wasserbauliches Versuchswesen*, volume 4. Deutscher Verband fur Wasserwirtschaft (DVWW).

Kondo, H. and Sakai, A. (2015). Micro-landform Structure and Tree Distribution in Subalpine Riparian Area of V-shaped Valley, Minami Alps, Central Japan. *Geographical review of Japan series B*, 88(1):23–37.

Kondolf, G. M. (1995). Geomorphological stream channel classification in aquatic habitat restoration: Uses and limitations. *Aquatic Conservation: Marine and Freshwater Ecosystems*, 5(2):127–141.

Kondolf, G. M. (1997a). Application of the pebble count: Notes on purpose, method and variants. *Journal of the American Water Resources Association*, 33(1):78–87.

Kondolf, G. M. (1997b). Hungry Water: Effects of Dams and Gravel Mining on River Channels. *Environmental Management*, 21:533–551.

Kramer, H. (1932). *Modellgeschiebe und Schleppkraft [Modelling bed load and drag force]*, volume 9. Preußische Versuchsanstalt für Wasserbau und Schiffbau.

Kronfellner-Krauss, G. (1972). Neue Bauweisen in der Wildbach- und Lawinenverbauung in internationaler Sicht [New construction methods of torrent and avalanche control from an international point of view]. *Centralblatt für das gesamte Forstwesen*, 1(159):33–57.

Kuglerová, L., Jansson, R., Sponseller, R. A., Laudon, H., and Malm-Renöfält, B. (2015). Local and regional processes determine plant species richness in a river-network metacommunity. *Ecology*, 96(2):381–391.

Kundu, P. and Cohen, I. (2008). *Fluid Mechanics*. Elsevier Inc., San Diego, California, 4th edition.

Lachat, E., Macher, H., Mittet, M., Landes, T., and Grussenmeyer, P. (2015). First experiences with Kinect V2 sensor for close range 3D modelling. *The International Archives of the Photogrammetry, Remote Sensing and Spatial Information Sciences*, XL-5/W4:93–100.

Lamb, M. P., Dietrich, W. E., and Venditti, J. G. (2008). Is the critical Shields stress for incipient sediment motion dependent on channel-bed slope? *Journal of Geophysical Research*, 113(F2):F02008.

Lane, E. W. (1955). The importance of fluvial geomorphology in hydraulic engineering. *Proceedings of the American Society of Civil Engineering*, 81:1–17.

Lane, S. N., Bakker, M., Balin, D., Lovis, B., and Regamey, B. (2014). Climate and human forcing of Alpine River flow. In Schleiss, A. J., De Cesare, G., Franca, M. J., and M, P., editors, *River Flow 2014*, pages 7–15, Lausanne, Switzerland. Taylor & Francis Group.

Lane, S. N. and Richards, K. S. (1997). Linking River Channel Form and Process: Time, Space and Causality Revisited. *Earth Surface Processes and Landforms*, 22(3):249–260.

Lange, D. and Bezzola, G. R. (2006). *Schwemmholz Probleme und Lösungansätze [Driftwood problems and approaches for solutions]*. Minor, H.-E, ed.: Mitteilung Nr. 188 der Versuchsanstalt für Wasserbau, Hydrologie und Glaziologie an der Eidgenössischen Technischen Hochschule Zürich, Zürich, Switzerland.

Lassettre, N. S. and Kondolf, G. M. (2012). Large Woody Debris in Urban Stream Channel: Redefining the Problem. *River Research and Applications*, 28:1477–1487.

Leite Ribeiro, M., Blanckaert, K., and Schleiss, A. J. (2016). Local tributary widening for river rehabilitation. *Ecohydrology*, 9(2):204–217.

Lenzi, M. A., D'Agostino, V., and Billi, P. (1999). Bedload transport in the instrumented catchment of the Rio Cordon Part I: Analysis of bedload records, conditions and threshold of bedload entrainment. *Catena*, 36:171–190.

Leopold, L. B. and Maddock, T. J. (1953). The Hydraulic Geometry of Stream Channels and Some Physiographic Implications. *Geological Survey Professional Paper*, 252:64.

Leopold, L. B. and Wolman, M. G. (1957). River Channel patterns: Braided meandering and straight. *USGS professional paper*, 282-B:45–62.

Leopold, L. B., Wolman, M. G., and Miller, J. P. (2012). *Fluvial processes in geomorphology*. Courier Corporation.

Leys, E. (1973). Vorschlag für die Systemeinteilung der Quer- und Längsbauten in der Wildbachverbauung [Proposal for the system classification of transverse and longitudinal torrential barriers]. *Wildbach- und Lawinenverbau*, 37(1):43–60.

Leys, E. (1976). *Die technischen und wirtschaftlichen Grundlagen in der Wildbachverbauung der großdoligen und der kronenoffenen Bauweise [Technical and economical basics of hydraulic constructions in mountain rivers in terms of large openings and open crested architecture]*. PhD thesis, Universität für Bodenkultur, Vienna.

Lien, H.-P. (2003). Design of slit dams for controlling stony debris flows. *International Journal of Sediment Research*, 18(1):74–87.

Lisle, T. E. (1982). Effects of Aggradation and Degradation on Riffle-Pool Morphology in Natural Gravel Channels, Northwestern California. *Water Resources Research*, 18(6):1643–1651.

Lisle, T. E. (1986). Stabilization of a gravel channel by large streamside obstructions and bedrock bends, Jacoby Creek, northwestern California. *Geological Society of America Bulletin*, 97(8):999–1011.

Luchnikov, V. A., Medvedev, N. N., Oger, L., and Troadec, J. P. (1999). Voronoi-delaunay analysis of voids in systems of nonspherical particles. *Physical Review*, 59(6):7205–7212.

Manning, R. (1891). *Transactions of the Institution of Civil Engineers of Ireland*, volume 20, chapter *On the flow of water in open channels and pipes*, pages 161–207. Civil Engineers of Ireland.

Maynard, T., Smith, N., and Vincenti, A., editors (2012). *Geomorphology and changing flood risk in the UK*. LLOYD'S, London, UK.

Mazzorana, B., Comiti, F., Scherer, C., and Fuchs, S. (2012). Developing consistent scenarios to assess flood hazards in mountain streams. *Environmental Management*, 94(1):112–124.

McEnroe, B. M. (2009). Hydrologic Design of Bridges and Culverts: A Historical Review. In *World Environmental and Water Resources Congress*, Great Rivers History, pages 83–90.

Meitzen, K. M., Doyle, M. W., Thoms, M. C., and Burns, C. E. (2013). Geomorphology within the interdisciplinary science of environmental flows. *Geomorphology*, 200:143–154. The Field Tradition in Geomorphology 43rd Annual Binghamton Geomorphology Symposium, held 21-23 September 2012 in Jackson, Wyoming USA.

Mejean, S., Piton, G., and Recking, A. (2015). Caractérisation des conditions hydrauliques du piégeage de la charge sédimentaire grossière des torrents [Characterization of hydraulic conditions for the trapping of the coarse sediment load of torrents]. In *Erosion torrentielle neige et avalanche Grenoble*, page 90. IRSTEA.

Meyer-Peter, E. and Müller, R. (1948). Formulas for Bed-Load transport. *IAHSR, appendix 2*, 2nd meeting:39–65.

Milhous, R. T. (1998). Modelling of instream flow needs: the link between sediment and aquatic habitat. *Regulated Rivers: Research & Management*, 14(1):79–94.

Mizuyama, T. (1993). Structural and Non-Structural Debris-Flow Countermeasures. In Shen, H. W., Su, S. T., and Wen, F., editors, *Hydraulic engineering '93*, pages 1914–1919. American Society of Civil Engineers, New York.

Mizuyama, T. (2008). Structural Countermeasures for Debris Flow Disasters. *International Journal of Erosion Control Engineering*, 1(1):38–43.

Modde, T., Ford, R. C., and Parsons, M. G. (1991). Use of a habitat-based stream classification system for categorizing trout biomass. *North American Journal of Fisheries Management*, 11(3):305–311.

Molnar, P., Densmore, A. L., McArdell, B. W., Turowski, J. M., and Burlando, P. (2010). Analysis of changes in the step-pool morphology and channel profile of a steep mountain stream following a large flood. *Geomorphology*, 124(2010):85–94.

Montgomery, D. R. (1999). Process domains and the river continuum. *Journal of the American Water Resources Association*, 35(2):397–410.

Montgomery, D. R., Abbe, T. B., Buffington, J. M., Peterson, N. P., Schmidt, K. M., and Stock, J. D. (1996). Distribution of bedrock and alluvial channels in forested mountain drainage basins. *Nature*, 381:587–589.

Montgomery, D. R. and Buffington, J. (1997). Channel-reach morphology in mountain drainage basins. *Geological Society of America Bulletin*, 105(5):596–611.

Montgomery, D. R. and Piégay, H. (2003). Wood in rivers: interactions with channel morphology and processes. *Geomorphology*, 51(1-3):1–5.

Morris, G. L., Annandale, G., and Hotchkiss, R. (2008). Reservoir sedimentation. In García, M. H., editor, *Sedimentation Engineering*, number 110 in ASCE Manuals and Reports on Engineering Practice, chapter 12, pages 579–612. American Society of Civil Engineers, Reston, VA.

Moyle, P. B. and Mount, J. F. (2007). Homogenous rivers, homogenous faunas. *Proceedings of the National Academy of Sciences of the United States of America*, 104(14):5711–5712.

National Hydraulic Team (1961). *Design Charts for Open-Channel Flow*. U.S. Department of Transportation - Federal Highway Administration.

Nazari-Giglou, A., Jabbari-Sahebari, A., Shakibaeinia, A., and Borghei, S. M. (2016). An Experimental Study of Sediment Transport in Channel Confluences. *International Journal of Sediment Research*, 31(1):87–96.

Nikora, V., Goring, D., McEwan, I., and Griffiths, G. (2001). Spatially Averaged Open-Channel Flow over Rough Bed. *Journal of Hydraulic Engineering*, 127(2):123–133.

Nikora, V., McEwan, I., McLean, S., Coleman, S., Dubravka, P., and Walters, R. (2007). Double-Averaging Concept for Rough-Bed Open-Channel and Overland Flows: Theoretical Background. *Journal of Hydraulic Engineering*, 133(8):873–883.

Nitsche, M., Rickenmann, D., Kirchner, J. W., Turowski, J. M., and Badoux, A. (2012). Macroroughness and variations in reach-averaged flow resistance in steep mountain streams. *Water Resources Research*, 48(12):W12518.

Norman, L. M. and Niraula, R. (2016). Model analysis of check dam impacts on long-term sediment and water budgets in Southeast Arizona, USA. *Ecohydrology & Hydrobiology*, 16(3):125–137.

Novák, P. and Cabelka, J. (1981). *Models in Hydraulic Engineering: Physical Principles and Design Applications*. Pitman Publication, London.

Ono, G.-i., Mizuyama, T., and Matsumura, K. (2004). Current practices in the design and evaluation of steel sabo facilities in Japan. In *Proceedings of INTERPRAEVENT*, pages 253–264, Riva, Trient, Italy. International Research Society Interpraevent.

ONR 24800 (2014). Schutzbauwerke der Wildbachverbauung - Begriffsbestimmungen und Klassifizierungen. In Austrian Standards Institute, editor, *Normensammlung Schutz vor Naturgefahren*, Umwelt. Austrian Standards Plus Publishing, Vienna, Austria.

Osanai, N., Mizuno, H., and Mizuyama, T. (2010). Design Standard of Control Structures Against Debris Flow in Japan. *Journal of Disaster Research*, 5(3):307–314.

Osti, R. and Egashira, S. (2013). Sediment transportation from bed-load to debris-flow and its control by check dams in torrential streams. In Garcia, C. and Lenzi, M. A., editors, *Check dams, morphological adjustments and erosion control in torrential streams*, chapter 8, pages 151–184. Nova Science.

Pagliara, S. and Chiavaccini, P. (2006). Flow Resistance of Rock Chutes with Protruding Boulders. *Journal of Hydraulic Engineering*, 132(6):545–552.

Pagliara, S. and Palermo, M. (2008). Scour Control Downstream of Block Ramps. *Journal of Hydraulic Engineering*, 134(9):1376–1382.

Parker, G. (1990). Surface-based bedload transport relation for gravel rivers. *Journal of Hydraulic Research*, 28(4):417–436.

Parker, G., Klingemann, P. C., and McLean, D. G. (1982). Bedload and Size Distribution in Paved Gravel-Bed Streams. *Journal of the Hydraulics Division of the American Society of Civil Engineers*, 108(4):544–571.

Parker, G., Paola, C., Whipple, K. X., and Mohrig, D. (1998). Alluvial Fans formed by channelized fluvial and sheet flow. I: Theory. *Journal of Hydraulic Engineering*, 124(10):985–995.

Pavlov, D. S. (1989). Structures assisting the migrations of non-salmonid fish: USSR. In *FAO Fisheries Technical Paper No. 308*. Food and Agriculture Organization of the United Nations, Rome, Italy.

Peakall, J., Ashworth, P., and Best, J. (1996). Physical Modelling in Fluvial Geomorphology: Principles, Applications and Unresolved Issues. In Rhoads, B. L. and Thorn, C. E., editors, *The Scientific Nature of Geomorphology: Proceedings of the 27th Binghamton Symposium in Geomorphology held 27-29 September 1996*. John Wiley & Sons Ltd., Binghamton, N.Y.

Peakall, J. and Warburton, J. (1996). Surface tension in small hydraulic river models - the significance of the Weber number. *Journal of Hydrology (New Zealand)*, 35(2):199–212.

Pickup, G. and Warner, R. F. (1976). Effects of hydrologic regime on magnitude and frequency of dominant discharge. *Journal of Hydrology*, 29(1-2):51–75.

Pierson, T. C. (2005). Hyperconcentrated flow - transitional process between water flow and debris flow. In Jakob, M. and Hungr, O., editors, *Debris-flow Hazards and Related phenomena*, chapter 8, pages 159–202. Springer-Verlag, Berlin, Heidelberg, Germany.

Pitlick, J., Mueller, E. R., Segura, C., Cress, R., and Torizzo, M. (2008). Relation between flow, surface-layer armoring and sediment transport in gravel-bed rivers. *Earth Surface Processes and Landforms*, 8(33):1192–1209.

Pitlick, J. and Van Steeter, M. M. (1998). Geomorphology and endangered fish habitats of the upper colorado river. 2. linking sediment transport to habitat maintenance. *Water Resources Research*, 34(2):303–316.

Piton, G. (2016). *Sediment control by check dams and open check dams in Alpine torrents*. PhD thesis, Irstea Grenoble - Equipe ETNA: Erosion Torrentielle, Neige et Avalanches. Director: Recking, A.

Piton, G., Carladous, S., Recking, A., Tacnet, J. M., Liébault, F., Kuss, D., Quefféléan, Y., and Marco, O. (2016). Why do we build check dams in Alpine streams? An historical perspective from the French experience. *Earth Surface Processes and Landforms*, page 23.

Piton, G. and Recking, A. (2016a). Design of Sediment Traps with Open Check Dams. I: Hydraulic and Deposition Processes. *Journal of Hydraulic Engineering*, 142(2):04015045.

Piton, G. and Recking, A. (2016b). Design of Sediment Traps with Open Check Dams. II: Woody Debris. *Journal of Hydraulic Engineering*, 142(2):04015046.

Piton, G. and Recking, A. (2016c). Effects of check dams on bed-load transport and steep-slope stream morphodynamics. *Geomorphology*, in press:05533–12.

Piton, G. and Recking, A. (2017). The concept of travelling bedload and its consequences for bedload computation in mountain streams. *Earth Surface Processes and Landforms*, (*in press*):52. note: ESP-16-0103.R2.

Powell, D. M. (1998). Patterns and processes of sediment sorting in gravel-bed rivers. *Progress in Physical Geography*, 22:1–32.

Powell, M. D. (2014). Flow resistance in gravel-bed rivers: Progress in research. *Earth-Science Reviews*, 136(2014):301–338.

Prancevic, J. P., Lamb, M. P., and Fuller, B. M. (2014). Incipient sediment motion across the river to debris-flow transition. *Geology*, 42(3):191–194.

Pretty, J. L.and Harrison, S. S. C., Shepherd, D. J., Smith, C., Hildrew, A. G., and Hey, R. D. (2003). River rehabilitation and fish populations: assessing the benefit of instream structures. *Journal of Applied Ecology*, 40(2):251–265.

Püntener, P. (2006). *Hochwasser vom 22./23. August 2005 - Schlussbericht zu den Bereichen Wasserbau und Strassen [Flood from 22/23. August 2005 - Final report on the areas of hydraulic structures and roads]*. Amt für Tiefbau des Kantons Uri, Altdorf, CH.

Raudkivi, A. J. (1976). *Loose boundary hydraulics, 2nd Edition.* Pergamon, Oxford, UK.

Recking, A. (2009). Theoretical development on the effects of changing flow hydraulics on incipient bed load motion. *Water Resources Research*, 45(4):W04401.

Recking, A. (2012). Influence of sediment supply on mountain streams bedload transport. *Geomorphology*, 175-176(2012):139–150.

Recking, A. (2013a). An analysis of nonlinearity effects on bed load transport prediction. *Journal of Geophysical Research and Earth Surface*, 118(3):1264–1281.

Recking, A. (2013b). Simple method for calculating reach-averaged bed-load transport. *Journal of Hydraulic Engineering*, 139:70–75.

Recking, A., Frey, P., Paquier, A., Belleudy, P., and Champagne, J. Y. (2008a). Bed-Load Transport Flume Experiments on Steep Slopes. *Journal of Hydraulic Engineering*, 134:1302–1310.

Recking, A., Frey, P., Paquier, A., Belleudy, P., and Champagne, J. Y. (2008b). Feedback between bed load transport and flow resistance in gravel and cobble bed rivers. *Water Resources Research*, 44(5):W05412.

Recking, A., Piton, G., Vazquez-Tarrio, D., and Parker, G. (2016). Quantifying the morphological print of bedload transport. *Earth Surface Processes and Landforms*, 41(6):809–822.

Rickenmann, D. (1991). Hyperconcentrated flow and sediment transport at steep slopes. *Journal of Hydraulic Engineering*, 117(11):1419–1439.

Rickenmann, D. (1997). Schwemmholz und Hochwasser [Driftwood and floods]. *Wasser Energie Luft*, 89(5/6):115–119.

Rickenmann, D. (2001). Comparison of bed load transport in torrents and gravel bed streams. *Water Resources Research*, 37(12):3295–3305.

Rickenmann, D., D'Agostino, V., Dalla Fontana, G., and Lenzi, M. A. (1998). New results from sediment transport measurements in two alpine torrents. *Hydrology, Water Resources and Ecology in Headwaters (Proceedings of the HeadWater Conference)*, 248:283–289.

Rickenmann, D. and Recking, A. (2011). Evaluation of flow resistance in gravel-bed rivers through a large field data set. *Water Resources Research*, 47:W07538.

Rimböck, A. (2003). *Schwemmholzrückhalt in Wildbächen [Driftwood retention in mountain rivers]*. PhD thesis, Technischen Universität München, Munich, Germany.

Rohde, S., Schütz, M., Kienast, F., and Englmaier, P. (2005). River widening: an approach to restoring riparian habitats and plant species. *River Research and Applications*, 21(10):1075–1094.

Romang, H. (2004). *Wirksamkeit und Kosten von Wildbach-Schutzmassnahmen [Effectiveness and Costs of Torrential Protection Measures]*, volume G 73. Geographica Bernensia, Universität Bern, Bern, Switzerland.

Rosgen, D. L. (1994). A classification of natural rivers. *Catena*, 22:169–199.

Ruiz-Villanueva, V., Bodoque, J. M., Díez-Herrero, A., Eguibar, M. A., and Pardo-Igúzquiza, E. (2013). Reconstruction of a flash flood with large wood transport and its influence on hazard patterns in an ungauged mountain basin. *Hydrological Processes*, 27(24):3424–3437.

Ruiz-Villanueva, V., Piégay, H., Gurnell, A. M., Marston, R. A., and Stoffel, M. (2016). Recent advances quantifying the large wood dynamics in river basins: New methods and remaining challenges. *Review of Geophysics*, 54:611–652.

SABO Division, editor (2000). *Guideline for driftwood countermeasures. Part II: Design.* Japanese Ministry of Construction, Tokyo, Japan.

Sawada, T., Ashida, K., and Takahashi, T. (1983). Relationship between channel pattern and sediment transport in a steep gravel bed river. *Zeitschrift für Geomorphologie, Supplementband*, 46:55–66.

Schleiss, A. J., Boes, R., Doering, M., Franca, M., Nadyeina, O., Pfister, M., Robinson, C., Scheidegger, C., Vetsch, D., Weber, C., Weitbrecht, V., and Werth, S. (2014). Geschiebe- und Habitatsdynamik - Forschungsprogramm *Wasserbau und Ökologie* [The research program *Sediment and Habitat Dynamics*]. *Wasser Energie Luft*, 106:117–122.

Schleiss, A. J., Peter, A., Fäh, R., and Scheidegger, C. (2008). Dynamische Lebensräume und Hochwasserschutz - Forschungsprojekt « Integrales Flussgebietsmanagement ». *Wasser Energie Luft*, 100(3):187–194.

Schmocker, L. and Hager, W. H. (2013). Scale Modeling of Wooden Debris Accumulation at a Debris Rack. *Journal of Hydraulic Engineering*, 139(8):827–836.

Schmocker, L. and Weitbrecht, V. (2013). Driftwood: Risk analysis and engineering measures. *Journal of Hydraulic Engineering*, 139(7):683–695.

Schwindt, S., De Cesare, G., Boillat, J.-L., and Schleiss, A. J. (2016a). Physical modelling optimization of a filter check dam in Switzerland. In Koboltschnig, G., editor, *Proceedings of INTERPRAEVENT: Hazard and risk mitigation*, volume 13, pages 828–836, Lucerne, Switzerland. International Research Society Interpraevent.

Schwindt, S., Franca, M. J., De Cesare, G., and Schleiss, A. J. (2017a). Analysis of mechanical-hydraulic deposition control measures. *Geomorphology*, [under revision]:33.

Schwindt, S., Franca, M. J., and Schleiss, A. J. (2016b). The influence of the opening width of check dams on bedload continuity of mountain rivers. In Constantinescu, G., Garcia, M., and Hanes, D., editors, *River Flow 2016*, pages 1156–1160, St. Louis, MO, USA.

Schwindt, S., Franca, M. J., and Schleiss, A. J. (2017b). Bottom slope influence on flow and bedload transfer through contractions. *Journal of Hydraulic Research*, [under revision]:20.

Schwindt, S., Franca, M. J., and Schleiss, A. J. (2017c). Effects of lateral and vertical constrictions on flow in rough steep channels with bedload. *Journal of Hydraulic Engineering*, [accepted]:44 p.

Schwindt, S., Piton, G., De Cesare, G., Recking, A., and Schleiss, A. J. (2016c). Study of the effects of a distanced retention basin combined with an open check dam on a physical model. In Koboltschnig, G., editor, *Proceedings of INTERPRAEVENT: Hazard and risk mitigation, Extended Abstracts*, volume 13, pages 322–323, Lucerne, Switzerland. International Research Society Interpraevent.

Shields, A. (1936). *Anwendung der Ähnlichkeitsmechanik und der Turbulenzforschung auf die Geschiebebewegung [Application of the similarity in mechanics and turbulence research on the mobility of bed load]*, volume 26. Preußische Versuchsanstalt für Wasserbau und Schiffbau, Berlin edition.

Shima, J., Moriyama, H., Kokuryo, H., Ishikawa, N., and Mizuyama, T. (2016). Prevention and Mitigation of Debris Flow Hazards by Using Steel Open-Type Sabo Dams. *International Journal of Erosion Control Engineering*, 9(3):135–144.

Simoni, S., Vignoli, G., and Mazzorana, B. (2017). Enhancing sediment flux control and natural hazard risk mitigation through a structured conceptual planning approach. *Geomorphology*, [in press]:05903–15.

Sindelar, C., Schobesberger, J., and Habersack, H. (2016). Effects of weir height and reservoir widening on sediment continuity at run-of-river hydropower plants in gravel bed rivers. *Geomorphology*, [in press]:05679–10.

Slattery, M. C. and Phillips, J. D. (2011). Risk assessment of watershed erosion at Naesung Stream, South Korea. *Environmental Management*, 92(2):284–289. Rorke Bryan Special Issue.

Smart, G. M. (1984). Sediment Transport Formula for Steep Channels. *Journal of Hydraulic Engineering*, 110(3):267–276.

Smart, G. M., Duncan, M. J., and Walsh, J. M. (2002). Relatively Rough Flow Resistance Equations. *Journal of Hydraulic Engineering*, 128(6):568–578.

Smart, G. M. and Jaeggi, M. N. R. (1983). *Sedimenttransport in steilen Gerinnen [Sediment Transport on Steep Slopes]*. Mitteilung Nr. 64 der Versuchsanstalt für Wasserbau, Hydrologie und Glaziologie an der Eidgenössischen Technischen Hochschule Zürich, Zürich.

Sodnik, J., Martinčič, M., Mikoš, M., and Kryžanowski, A. (2015). Are Torrent Check-Dams Potential Debris-Flow Sources? In Lollino, G., Giordan, D., Crosta, G. B., Corominas, J., Azzam, R., Wasowski, J., and Sciarra, N., editors, *Engineering Geology for Society and Territory - Volume 2: Landslide Processes*, chapter 79, pages 485–488. Springer International Publishing.

Sponseller, R. A., Heffernan, J. B., and Fisher, S. G. (2013). On the multiple ecological roles of water in river networks. *Ecosphere*, 4(2):1–14.

Strickler, A. (1923). Beiträge zur Frage der Geschwindigkeitsformel und der Rauhigkeitszahlen für Ströme, Kanäle und geschlossene Leitungen [Contributions to the question of the velocity formula and the roughness figures for streams, channels and closed pipes]. *Mitteilungen des Amtes für Wasserwirtschaft*, 16:357.

Suda, J. and Rudolf-Miklau, F. (2008). Schadmechanismen an Wildbachsperren aus Konstruktionsbeton. *Wasser Energie Luft*, 100(1):59–68.

Suda, J., Strauss, A., Rudolf-Miklau, F., and Hübl, J. (2009). Safety assessment of barrier structures. *Structure and Infrastructure Engineering*, 5(4):311–324.

Surian, N. and Rinaldi, M. (2003). Morphological response to river engineering and management in alluvial channels in Italy. *Geomorphology*, 50:307–326.

Sutherland, D. G., Hansler Ball, M., Hilton, S., and Lisle, T. E. (2002). Evolution of a landslide-induced sediment wave in the Navarro River, California. *Geological Society of America Bulletin*, 114(8):1036–1048.

Swiss Confederation (1991). *Federal Act on the Protection of Waters*. 814.20. The Federal Assembly of the Swiss Confederation, Bern.

Takahashi, T. (2014). *Debris flow: Mechanics, Prediction and Countermeasures*. CRC Press, London, UK, 2nd edition.

Tamagni, S. (2013). *Unstructured block ramps*. Mitteilung Nr. 223 der Versuchsanstalt für Wasserbau, Hydrologie und Glaziologie der Eidgenössische Technische Hochschule Zürich, Zürich, Switzerland.

Troadec, J. and Dodds, J. (1993). Global geometrical description of homogeneous hard sphere. In Bideau, D. and Hansen, A., editors, *Disorder and Granular Media*, pages 133–163. Elsevier Science Publishers, Amsterdam.

Üblagger, G. (1973). Retendieren, Dosieren und Sortieren [Retention, Dosing and Sorting]. *Mitteilungen der Forstlichen Bundesversuchsanstalt Wien*, 102:335–372.

Uchiogi, T., Shima, J., Tajima, H., and Ishikawa, Y. (1996). Design methods for wood-debris entrapment. In *Proceedings of INTERPRAEVENT*, volume 5, pages 279–288, Klagenfurt, Austria. International Research Society Interpraevent.

U.S. Army Corps of Engineeers (2016). Hydrologic Engineering Centers River Analysis System (HEC-RAS).

USACE (1992). Hydraulic Design of Spillways. In *Engineering and Design*, number EM 1110-2-1603 in Engineer Manual. U.S. Army Corps of Engineers.

USACE (1997). *Channel stability assessment for flood control projects*. Technical engineering and design guides. Issue 20. American Society of Civil Engineers, New York.

Vanoni, V. A., editor (1975). *Sediment engineering*. Number 54 in ASCE manuals and reports on engineering practice. American Society of Civil Engineers, New York.

VAW (2017). Laboratory of Hydraulics, Hydrology and Glaciology (VAW) of the Swiss Federal Institute of Technology Zurich (ETHZ): BASEMENT v2.7.

Von Karmàn, T. (1930). Mechanische Ähnlichkeit und Turbulenz [Mechanical similarity and turbulence]. In *Third International Congress for Applied Mechanics*, volume 1, pages 79–93. Stockholm.

Von Mises, R. (1917). Berechnung von Ausfluss- und Ueberfallzahlen [Computation of discharge coefficients]. *Zeitschrift des Vereins deutscher Ingenieure*, 61(22):447–452,469–474,493–498.

Wagner, W. and Kretzschmar, H. (2008). *International Steam Tables - Properties of Water and Steam based on the Industrial Formulation IAPWS-IF97*. Springer, second edition.

Wallerstein, N., Scott, A., and Blanc, J. (2013). *Culvert design and operation guide supplementary technical note on understanding blockage risks*. Publication C720. CIRIA, London.

Wang, F. (1901). *Grundriss der Wildbachverbauung*. Erster Theil. Verlag von S. Hirzel, Leipzig, Germany.

Wang, F. (1903). *Grundriss der Wildbachverbauung*. Zweiter Theil. Verlag von S. Hirzel, Leipzig, Germany.

Watanabe, M., Mizuyama, T., and Uehara, S. (1980). Review of debris flow countermeasure facilities. *Journal of the Japan Erosion Control Engineering Society*, 115:40–48.

Wehrmann, H., Hübl, J., and Holzinger, G. (2006). Classification of Dams in Torrential Watersheds. In *Proceedings of INTERPRAEVENT*, pages 829–838, Tokyo, Japan. International Research Society Interpraevent.

Weisbach, J. L. (1845). *Lehrbuch der Ingenieur- und Maschinen-Mechanik [Textbook of engineering and machine mechanics]*, volume 1-3. Friedrich Vieweg und Sohn, Braunschweig, Germany.

Weitbrecht, V., Tamagni, S., and Boes, R. (2016). Stability of Unstructured Block Ramps. *Journal of Hydraulic Engineering*, 0(0):04016095–1–9.

Werner, W. (1963). Ableitung einer kinematischen Beziehung zur Berechnung des Durchflusses unter Planschützen nach der Theorie freier Stromlinien [Derivation of a kinematic relation for the computation of the discharge under sluice gates according to the theory of free streamlines]. *Wissenschaftliche Zeitschrift der Technischen Universität Dresden*, 12(6):1693–1699.

White, J. R., Carreiro, M. M., and Zipperer, W. C. (2014). Woody plant communities along urban, suburban, and rural streams in Louisville, Kentucky, USA. *Urban Ecosystems*, 17(4):1061–1094.

Whittaker, J. and Jaeggi, M. N. R. (1982). Origin of step-pool systems in mountain streams. *Journal of the Hydraulics Division: Proceedings of the American Society of Civil Engineers*, 108:99–104.

Whittaker, J. G. and Jaeggi, M. G. (1986). *Blockschwellen [Sills]*. Mitteilung Nr. 91 der Versuchsanstalt für Wasserbau, Hydrologie und Glaziologie an der Eidgenössischen Technischen Hochschule Zürich, Zürich, Switzerland.

Wilcock, P. (1993). Critical shear stress of natural sediments. *Journal of Hydraulic Engineering*, 119:491–505.

Wilcock, P. (2008). *Sediment Transport Primer (Estimating Bed-Material Transport in Gravel-bedded Rivers)*. USDA Forest Service.

Wilcox, A. C., Nelson, J. M., and Wohl, E. E. (2006). Flow resistance dynamics in step-pool channels: 2. Partitioning between grain, spill, and woody debris resistance. *Water Resources Research*, 42(5):W05419.

Williams, G. P. (1978). Bank-Full Discharge of Rivers. *Water Resources Research*, 14(6):1141–1154.

Williams, G. P. and Wolman, M. G. (1984). Downstream Effects of Dams on Alluvial Rivers. In *Geological Survey Professional*, page Paper 1286. U.S. Government, Washington, DC.

Wohl, E. E. (2000). *Mountain rivers*, volume 14. American Geophysical Union, Washington, DC.

Wolman, M. G. and Leopold, L. B. (1957a). River Channel Patterns: Braided, Meandering and Straight. *Physiographic and hydraulic studies of rivers. Geological Survey Professional Paper*, 282-B:1–85.

Wolman, M. G. and Leopold, L. B. (1957b). River flood plains some observations on their formation. *Physiographic and hydraulic studies of rivers. Geological Survey Professional Paper*, 282-C:1–107.

Wolman, M. G. and Miller, J. P. (1960). Magnitude and frequency of forces in geomorphic processes. *The Journal of Geology*, 68(1):54–74.

Wong, M. and Parker, G. (2006). Reanalysis and Correction of Bed-Load Relation of Meyer-Peter and Müller Using Their Own Database. *Journal of Hydraulic Engineering*, 132(11):1159–1168.

Woolsey, S., Capelli, F., Gonser, T., Hoehn, E., Hostmann, M., Junker, B., Paetzold, A., Roulier, C., Schweizer, S., Tiegs, S. D., Tockner, K., Weber, C., and Peter, A. (2007). A strategy to assess river restoration success. *Freshwater Biology,*, 52(4):752–769.

Yalin, M. S. (1971). *Theory of hydraulic models*, volume 266 of *Civil Engineering Hydraulics*. Macmillan, London.

Yalin, M. S. (1977). *Mechanics of sediment transport*, volume 2. Pergamon press Oxford, Oxford and New York.

Yamada, S. (1999). The role of soil creep and slope failure in the landscape evolution of a head water basin: field measurements in a zero order basin of northern Japan. *Geomorphology*, 28(3-4):329–344.

Yu, G., Wang, Z., Zhang, K., Chang, T., and Liu, H. (2009). Effect of incoming sediment on the transport rate of bed load in mountain streams. *International Journal of Sediment Research*, 24(3):260–273.

Zeller, J. (1973). Die Entleerung verlandeter Geschieberückhalteräume, Diskussionsbeitrag [The flushing of up-silted sediment retention basins, discussion]. *Mitteilung der Forstlichen Bundesversuchsanstalt Wien*, 102:389–397.

Zimmermann, A. (2010). Flow resistance in steep streams: An experimental study. *Water Resources Research*, 46:W09536.

Zollinger, F. (1983). *Die Vorgänge in einem Geschiebeablagerungsplatz: ihre Morphologie und ihre Möglichkeiten einer Steuerung [The processes in sediment traps: their morphology and their possibilities of control]*. No. 7419, ETH Zürich, Zürich, Switzerland. Directors: Grubinger, H. and Vischer, D.

Zollinger, F. (1984). Die verschiedenen Funktionen von Geschieberückhaltebauwerken [The different functions of debris retention dams]. In *Proceedings of INTERPRAEVENT*, pages 147–160, Klagenfurt, Austria. International Research Society Interpraevent.

Appendices

A.1 River inventory

The following 132 datasets from field observations were considered to respect length ratios, such as D_{pq} / w, and to review relevant channel S_0 and bank slopes m. The following country codes are used in the table:

- **AT** - Austria
- **CH** - Switzerland
- **CN** - China
- **FR** - France
- **IT** - Italy
- **JP** - Japan
- **NZ** - New Zealand
- **US** - United States of America

Blank fields are due to missing or ambiguous information.

Country	Mountain range	River Name	Source	Bed grain sizes [m]				Discharges [m³/s]									Base width	Slope	Bank Slope	Check dam
Code	***Mountain Range***	***River Name***	***Database***	***D 30***	***D 50***	***D 84***	***D 90***	***Q bf***	***Q m***	***Q 2.33***	***Q 5***	***Q 10***	***Q 30***	***Q 50***	***Q 100***	***Q 300***	***w [m]***	***S_0 [-]***	***m [-]***	***[-]***
CH	Alps	Grosse Bachtale	BAfU	0.0100	0.0200		0.0700								12.0		6.90	0.3111		
CN	Tian Shan	Urumqi river	Guerit		0.0265				7.5									0.0200		
CH	Pre-Alpes	Avancon	Ghilardi	0.0120	0.0340		0.2000		3.9				60.0		79.0	96.0		0.0470		
US	Rocky Mountains	Blackmare Creek	AWAE		0.1490		0.2100		0.7								5.18	0.0299		
US	Rocky Mountains	Dollar Creek	AWAE		0.1000		0.1640		0.7								8.38	0.0146		
US	Rocky Mountains	Eggers Creek	AWAE		0.0228		0.1640		0.0									0.0747		
US	Rocky Mountains	Fourth of July Creek	AWAE		0.0510		0.1370		0.4								6.55	0.0202		
US	Rocky Mountains	HawleyCreek	AWAE		0.0400		0.1400		0.5								6.10	0.0233		
US	Rocky Mountains	Johns Creek	AWAE		0.2070		1.0080		4.5								0.61	0.0207		
US	Rocky Mountains	Jarbidge River	AWAE		0.0950		0.2230		1.0								10.00	0.0160		
US	Rocky Mountains	Little Buckhorn Creek	AWAE		0.1190		0.1910		0.1								3.35	0.0509		
US	Rocky Mountains	Little Slate Creek	AWAE		0.2070		0.4500		3.1								12.50	0.0268		
US	Rocky Mountains	South Fork Red River	AWAE		0.0860		0.1650		1.4								7.90	0.0146		
US	Rocky Mountains	Squaw Creek	AWAE		0.0270		0.0740		0.1								2.30	0.0240		
US	Rocky Mountains	Thompson Creek	AWAE		0.0660		0.1300		0.4								5.33	0.0153		
US	Rocky Mountains	Trapper Creek	AWAE		0.0670		0.1360		0.4								5.20	0.0414		
US	Rocky Mountains	West Fork Buckhorn Creek	AWAE		0.1800		0.7500		0.7								7.60	0.0320		
US	Rocky Mountains	Deadhorse Creek	AWAE	0.0120	0.0500		0.0900	0.2									1.80	0.0290		
US	Rocky Mountains	St Louis Creek	AWAE	0.0260	0.0500		0.0200		1.0								2.94	0.0500		
US	Rocky Mountains	Halfmoon Creek	AWAE	0.0450	0.0610		0.1300		1.1								8.60	0.0150		
FR	Alpes	Rivieres des Pluies	Pouget	0.0160	0.0850		0.4000					370.0	760.0		1000.0			0.0220		
JP		Unonogawa	Nakaya	0.0090	0.0491												40.00	0.0238		
US	Rocky Mountains	Abraham creek	USGS		0.1200				2.2								21.03	0.0170		
US	Rocky Mountains	Patterson Creek	USGS		0.0470				6.6								13.35	0.2050		
US		Gantz	ODNR		0.0580	0.2300				8.3		20.8					4.69	0.0150		
US		Meadowlands	ODNR		0.0810	0.1400				0.1		0.3					1.62	0.0220		
US		ODOT 37	ODNR		0.0540	0.0300				3.8		9.8					4.27	0.0400		
US		Woodiebrook	ODNR		0.0180	0.1300				0.7		1.6					3.02	0.0140		
US		Fall Creek	Leopold Wolman	0.1300	0.2100	0.3800	0.5120		1.0								7.47	0.0360		
US		West Pork' Rock Creek	Leopold Wolman		0.2680	0.7300			2.4								10.06	0.0350		
US		Rock Creek	Leopold Wolman	0.1280	0.2040	0.5880			4.7								8.69	0.2100		
US		Clear Creek	Leopold Wolman		0.1770	0.6550			2.0								12.80	0.0240		
US		North Fork'Clcar Creek	Leopold Wolman		0.1430	0.3050			0.5								7.01	0.0280		
US		LS	Gomi and Sidle		0.0350				2.7								1.20	0.4000		
US		YA	Gomi and Sidle		0.0345				5.5								1.10	0.3700		
US		CC	Gomi and Sidle		0.0300				5.1								0.90	0.3600		
US		OG	Gomi and Sidle		0.0335				8.2								1.20	0.2700		
CH	Alps	Grosse Bachtale	BAfU	0.0100	0.0200		0.0700								12.0		6.90	0.3111	3.25	1
CH	Alps	Eistlenbach	BAfU	0.0100	0.0200		0.0550		9.0						30.0		15.30	0.1778	2.37	1
CH	Alps	Innerer Blindlauigraben	BAfU	0.0200	0.0300		0.0500		0.5						3.0		1.90	0.3111	1.55	1
CH	Alps	Val Gronda	BAfU	0.0100	0.0200		0.0600								20.0		3.20	0.2667	2.10	1
CH	Alps	Val Parghera	BAfU	0.0100	0.0250		0.0650								13.0		3.00	0.2000		1

Code	Mountain Range	River Name	Database	D 30	D 50	D 84	D 90	Q bf	Q m	Q 2.33	Q 5	Q 10	Q 30	Q 50	Q 100	Q 300	w [m]	S_0 [-]	m [-]	[-]
CH	Alps	Humligenbach	BAfU	0.0200	0.0250		0.0700								11.5		5.00	0.5100		1
CH	Alps	Steinibach (Dallenwil)	BAfU	0.0200	0.0350		0.1250		25.0				40.0		65.0	85.0	6.00	0.2444	2.28	1
CH	Alps	Bitzighoferbach	BAfU	0.0100	0.0150		0.0500		5.0						21.0		5.00	0.1778	1.96	1
CH	Alps	Edisriedbach	BAfU	0.0100	0.0200		0.0650		7.0						30.0		6.00	0.2444	1.82	1
CH	Alps	Grosse Schliere	BAfU	0.0150	0.0350		0.1300		27.5				90.0		150.0		12.00	0.0667	2.50	1
CH	Alps	Melbach	BAfU	0.0200	0.0300		0.1100								17.0		2.00	0.1778	2.26	1
CH	Alps	Erlenbach	Rickenmann/BAfU	0.0483	0.1272		0.4609		0.5					10.0	13.2		3.80	0.1900	1.43	
CH	Alps	Melera / Poschiavo	Rickenmann	0.0120	0.0150		0.3000		0.5	1.6	2.6	3.2	4.1	4.5	5.0	5.9	5.40	0.1700	1.43	
IT	Alps	Rio Cordon	Rickenmann		0.0667		0.1933		2.0								5.00	0.1300		
CH	Alps	Rappengraben 2	Rickenmann	0.0200	0.0250		0.0700		0.3					2.5			3.50	0.1100		
CH	Alps	Sperbelgraben	Rickenmann	0.0200	0.0250		0.0700		0.0	0.6	0.9	1.1	1.5	1.8	2.1	2.7	0.50	0.1163		
CH	Alps	Pitzbach	Rickenmann		0.0220		0.1200		2.0								8.00	0.0800		
CH	Alps	Bas Arolla	Rickenmann		0.0200		0.0450		2.4								6.40	0.0700		
CH	Alps	Bridge Creek	Rickenmann		0.0175		0.0500										2.30	0.0670		
CH	Alps	Rappengraben 1	Rickenmann		0.0250		0.0700		0.4				2.1				4.20	0.0600		
CH	Alps	Schwändlibach	Rickenmann		0.0800		0.2550		1.5					8.7			5.50	0.0550		
CH	Alps	Rotenbach	Rickenmann		0.0650		0.2250		2.5					19.0			3.50	0.0500		
US	Rocky Mountains	Sagehen Creek	Rickenmann		0.0390		0.0900										5.00	0.0100		
AT	Alps	Vorderbergerbach	Auth. AT		0.0220		0.0700		0.5		17.0		77.0		120.0		1.85	0.0400		1
CH	Alps	Baltschiederbach	LCH	0.0315	0.0875		0.3850		0.2					50.0	95.0		5.00	0.0670		1
CH	Alps	Baye de Clarens	LCH	0.0310	0.0880		0.2850				30.0		53.0		65.0	74.0	7.00	0.0300		
CH	Alps	Engelberger Aa	BAfU / LCH	0.0348	0.0495		0.1733		11.7	72.0	95.0	111.0	138.0	152.0	171.0	205.0	19.00	0.0070		
CH	Alps	Kelchbach	LCH		0.0250				0.5						69.0		8.00	0.0500		
CH	Alps	Drance	LCH	0.0290	0.0528	0.3471	0.4353	30.0	10.0	86.0	105.0	119.0	130.0	175.0	230.0	280.0	12.00	0.0240	2.70	(1)
CH	Alps	Sandbach	BAfU	0.0100	0.0500		0.6000								10.5		4.50	0.2800		
CH	Alps	Rietholzbach	BAfU						0.1	3.5	5.5	7.2	10.4	12.1	14.8	19.9	1.50	0.0467		
CH	Alps	Lütschine (Gsteig)	BAfU		0.2280		0.7970		18.8	123.0	149.0	167.0	196.0	210.0	229.0	263.0	21.00	0.0056		
CH	Alps	Massa (Blatten)	BAfU						13.4	86.0	101.0	111.0	125.0	132.0	140.0	154.0	15.00	0.0525		
CH	Alps	Dischmabach	BAfU						1.7	11.0	14.0	16.0	18.0	19.0	20.0	22.0	8.00	0.0320		
CH	Alps	Lonza (Blatten)	BAfU						4.7	35.0	44.0	52.0	65.0	71.0	81.0	98.0	9.50	0.0413		
CH	Alps	Poschiavino - La Rösa	BAfU						0.6	6.0	9.0	11.0	14.0	15.0	16.0	20.0	4.50	0.1200		
CH	Alps	Allenbach - Adelboden	BAfU	0.0020	0.0570		0.1980		1.2	21.0	36.0	49.0	74.0	87.0	108.0	147.0	5.00	0.0375		
CH	Alps	Rom - Müstair		0.0200	0.0470		0.1450		2.6	12.0	15.0	17.0	20.0	21.0	23.0		8.00	0.0200		
CH	Alps	Grossbach - Einsiedeln							0.3	13.0	21.0	30.0	48.0	59.0	77.0		4.00	0.0333		
CH	Alps	Forestay - Chexbres	VD						0.3	7.3	9.1	10.6		13.8	15.2	17.3	5.00	0.0755		
CH	Alps	Necker - Mogelsberg							3.3	85.0	142.0	192.0	290.0	346.0	433.0	607.0	7.00	0.0113		
CH	Alps	Croisette	BAFU	0.0050	0.0100		0.0300		7.0						19.7		5.00	0.4160	1.90	1
CH	Alps	La Tiniere	BAFU	0.0050	0.0100		0.0300		15.0						61.2		7.00	0.1950	2.50	1
CH	Alps	Morges - Patinoire	VD						0.4	12.8	16.1	18.8		24.8	27.3	31.3	5.00	0.0150		
CH	Alps	Wyna	AG						0.9	16.0					44.0		5.00	0.0075		
CH	Alps	Rhein - Bad Ragaz	GR	0.0080	0.0120		0.1010		154.9								90.00	0.0030		
CH	Alps	Steinenbach (Kaltbrunn)	SG, BAfU	0.0203	0.0239		0.0713		1.0	29.0	33.0	39.0		46.0	49.0		9.00	0.0150		
CH	Alps	Ahornweidbach	BAfU	0.0260	0.0388		0.1765								5.7		8.00	0.2500		

Code	Mountain Range	River Name	Database	D 30	D 50	D 84	D 90	Q bf	Q m	Q 2.33	Q 5	Q 10	Q 30	Q 50	Q 100	Q 300	w [m]	S_0 [-]	m [-]	[-]
CH	Alps	Riale Grande	BAfU	0.0238	0.0536		0.2545								30.0		6.00	0.0870		
CH	Alps	Fossé de Talons	BAfU	0.0193	0.0223		0.0538								30.0		5.00	0.0140		
IT	Alps	Passer 1	Patscheider/Gostner	0.0070	0.0217		0.0820		7.6	161.6	229.5	266.8	321.5	345.2	377.1		50.00	0.0130		
IT	Alps	Passer 2	Patscheider/Gostner	0.0082	0.0240		0.1040		8.4	179.4	254.9	296.2	357.1	383.4	418.7		35.00	0.0220		
IT	Alps	Passer 3	Patscheider/Gostner	0.0100	0.0280		0.1019		9.9	210.7	299.3	347.8	419.3	450.2	491.7		90.00	0.0180		
IT	Alps	Passer 4	Patscheider/Gostner	0.0060	0.0152		0.0600		10.1	214.9	305.3	354.9	427.7	459.2	501.6		30.00	0.0040		
IT	Alps	Suldenbach Channel	Patscheider/Gostner	0.0110	0.0263		0.1029		6.4	57.8		95.9	123.7	136.9	155.7	187.7	7.00	0.0120		
IT	Alps	Suldenbach Pradersand	Patscheider/Gostner	0.0046	0.0134		0.0423		6.4	57.8		95.9	123.7	136.9	155.7	187.7	150.00	0.0060		
NZ		Porter 1	Wohl, et al		0.0380	0.2350		1.3									2.20	0.0800		
NZ		Porter 2	Wohl, et al		0.0650	0.1400		1.0									3.60	0.0500		
NZ		Porter 3	Wohl, et al		0.1200	0.2140		1.9									2.60	0.0460		
NZ		Porter 4	Wohl, et al		0.1420	0.2350		1.8									2.70	0.0200		
NZ		Porter 5	Wohl, et al		0.1120	0.3150		2.5									3.60	0.0400		
NZ		Porter 6	Wohl, et al		0.1550	0.4100		2.6									5.60	0.0470		
NZ		Porter 7	Wohl, et al		0.1980	0.2220		3.0									5.80	0.0500		
NZ		Porter 8	Wohl, et al		0.1090	0.2450		2.7									9.30	0.0430		
NZ		Porter 9	Wohl, et al		0.0600	0.2070		2.0									8.10	0.0340		
NZ		Porter 10	Wohl, et al		0.1280	0.2580		8.0									4.80	0.0220		
NZ		Porter 11	Wohl, et al		0.1500	0.1640		7.8									7.20	0.0160		
NZ		Porter 12	Wohl, et al		0.0960	0.5350		15.9									13.00	0.0200		
NZ		Kowai 1	Wohl, et al		0.2400	0.5350		7.1									10.30	0.1700		
NZ		Kowai 2	Wohl, et al		0.2750	0.6950		22.4									11.40	0.1500		
NZ		Kowai 3	Wohl, et al		0.1700	0.3300		19.6									5.00	0.0600		
NZ		Kowai 4	Wohl, et al		0.2000	0.6100		21.1									7.40	0.0700		
NZ		Kowai 5	Wohl, et al		0.2100	0.6800		43.2									14.70	0.0500		
NZ		Kowai 6	Wohl, et al		0.2100	0.5200		47.5									23.50	0.0450		
NZ		Kowai 7	Wohl, et al		0.1700	0.4350		27.4									7.80	0.0540		
NZ		Kowai 8	Wohl, et al		0.0600	0.1800		54.7									16.50	0.0260		
NZ		Kowai 9	Wohl, et al		0.0950	0.1550		62.2									12.90	0.0260		
NZ		Camp 1	Wohl, et al		0.2800	0.5900		3.2									3.50	0.1900		
NZ		Camp 2	Wohl, et al		0.3000	1.0000		14.6									11.80	0.1400		
NZ		Camp 3	Wohl, et al		0.5500	1.1200		43.3									18.50	0.2400		
NZ		Camp 4	Wohl, et al		0.6500	1.2600		47.7									26.30	0.1700		
NZ		Camp 5	Wohl, et al		0.4500	1.3500		47.9									16.70	0.2000		
NZ		Camp 6	Wohl, et al		0.6400	1.1900		48.5									23.00	0.1700		
NZ		Camp 7	Wohl, et al		0.4300	0.9100		49.4									13.00	0.2000		
NZ		Camp 8	Wohl, et al		0.1900	0.5800		50.6									11.50	0.1500		
NZ		Crooked 1	Wohl, et al		0.4900	1.0200		178.5									38.00	0.0290		
NZ		Brown 1	Wohl, et al		0.2700	0.6800		32.3									14.40	0.0500		
NZ		Slaty 1	Wohl, et al		0.2500	0.5300		18.8									8.80	0.0360		
NZ		Sneeze 1	Wohl, et al		0.1380	0.3000		4.8									7.00	0.0700		
US	Rocky Mountains	Barlow Creek	AWAE	0.0226	0.0640		0.3700	2.8									6.80	0.0240		
US	Rocky Mountains	Coon creek	AWAE	0.0540	0.0830		0.2520	2.8									5.90	0.0310		

Code	Mountain Range	River Name	Database	D 30	D 50	D 84	D 90	Q bf	Q m	Q 2.33	Q 5	Q 10	Q 30	Q 50	Q 100	Q 300	w [m]	S_0 [-]	m [-]	[-]
US	Rocky Mountains	East St Louis	AWAE	0.0280	0.0500		0.2050	0.8									2.94	0.0500		
US	Rocky Mountains	East fork encampment	AWAE	0.0330	0.0500		0.2100	1.5									6.20	0.0380		
US	Rocky Mountains	Florida River	AWAE	0.0900	0.2000		0.7500	14.5									12.00	0.0130		
US	Rocky Mountains	Fool Creek	AWAE	0.0200	0.0380		0.1250	0.3									1.97	0.0440		

A.2 Theory of scaled models

The prediction of the physical behavior of fluids in nature can be enabled by small-scale model observations. This requires the dynamic similarity of dimensionless quantities of the model and the prototype application. Such dimensionless expressions can be derived either based on a dimensional analysis of relevant variables or directly from the governing (differential) equations (Kundu and Cohen, 2008). The dimensional analysis of quantities, as applied in this study, is shown subsequently in Appendix A.2.1. The simplified mathematical description is illustrated in Appendix A.2.2, in terms of the one-dimensional Navier-Stokes equation for incompressible fluids. On this basis, the similitude concepts of open channel flow and sediment transport are commented in Appendix A.2.3.

A.2.1 Vaschy–Buckingham Π theorem

In relativistic mechanics, any quantity ξ_i can be expressed by units of length L (in m), time T (in s) and mass M (in kg) (Yalin, 1971; Barenblatt, 1987):

$$[\xi_i] = L^{\alpha} \cdot T^{\beta} \cdot M^{\gamma} \tag{A.1}$$

where	$\alpha \neq 0$	$\beta = 0$	$\gamma = 0$	denotes geometric quantities;
		$\beta \neq 0$	$\gamma = 0$	denotes kinematic quantities; and
			$\gamma \neq 0$	denotes dynamic quantities.

In the context of this research, temperature is not considered as being relevant to the experimental analysis. The quantities that are relevant to to the analysis can be reduced to a set Λ of independent and quantitative parameters ξ_i. Thus, the quantitative properties of the observed phenomena in terms of Λ can be expressed as a function of the quantities ξ_i:

$$\Lambda = f_{\Lambda}(\xi_1, \xi_2, \xi_i, \ldots, \xi_n) \tag{A.2}$$

Three basic quantities (ξ_I, ξ_{II} and ξ_{III}) from the set Λ can be used to derive dimensionless expressions of the remaining n - 1 quantities. The three basic quantities need to be dimensionally independent and invariable. Based on the three basic quantities, the dimensionless expression Π_{Λ} of a phenomenon can be derived by:

$$\Pi_{\Lambda} = \xi_I^{x_{\Lambda}} \cdot \xi_{II}^{y_{\Lambda}} \cdot \xi_{III}^{z_{\Lambda}} \cdot \Lambda \tag{A.3}$$

where x_{Λ}, y_{Λ} and z_{Λ} denote exponents that are obtained based on the requirement that Π_{Λ} is dimensionless. For instance, the dimensionless expression of ξ_1 is:

$$\Pi_1 = \xi_I^{x_{\Lambda}} \cdot \xi_{II}^{y_{\Lambda}} \cdot \xi_{III}^{z_{\Lambda}} \cdot \xi_1 \tag{A.4}$$

Assuming that ξ_1 is a length variable, the exponents for its dimensionless expression Π_1 are calcu-

lated on the basis of the three fundamental dimensions M, L and T:

$$M^0\ L^0\ T^0\ = (M\ L\ T)^{x_\Lambda} \cdot (M\ L\ T)^{y_\Lambda} \cdot (M\ L\ T)^{z_\Lambda} \cdot L^1 \tag{A.5}$$

An example application of this theory is illustrated here, with respect to relevant parameters from this study. It should be stressed here that the phenomena considered in Chpts. 4 and 5 (primarily hydraulic flow properties) differ from those considered in Chpts. 6 and 7 (primarily bed load transport). This calls for the necessity of differentiated scaling considerations for applying the experimental results in practice. The subsequent example shows the dimensional analysis of the phenomenon of "sediment transport" in a rectangular and straight channel reach with the length $\Delta\ x$, similar to Chpts. 6 and 7. In this example, the Buckingham Π theorem is applied, assuming steady and uniform flow conditions ($S_e = S_0$). In this case, the decomposition the forces acting on a particle need to be considered by the following set of $N = 12$ quantitative parameters (Barenblatt, 1987; Kundu and Cohen, 2008):

$$\Lambda = f_\Lambda \left(D, F_d, g, h, S_0, Q, Q_b, w, \Delta\ x, \nu, \rho_f, \rho_s\right). \tag{A.6}$$

F_d denotes the drag force (in kg m s^{-2}). With these parameters, the dimensional matrix is:

Λ	D	F_d	g	h	S_0	Q	Q_b	w	$\Delta\ x$	ν	ρ_f	ρ_s
M	0	1	0	0	0	0	1	0	0	0	1	1
L	1	1	1	1	0	3	0	1	1	2	-3	-3
T	0	-2	-2	0	0	-1	-1	0	0	-1	0	0

The rank $\Re$ of the dimensional matrix is defined by the maximum number of variables that have linearly independent dimensions. Then, the set of quantitative parameters Λ can be combined to N - $\Re$ independent non-dimensional variables, the so-called Π numbers. This requires the selection of $\Re$ repeating parameters with linearly independent dimensions. In the case of sediment transport, the fluid density ρ_f (= ξ_I), the particle diameter D (= ξ_{II}) and the gravity constant g (= ξ_{III}) are preferable (Einstein, 1950; Yalin, 1971, 1977). Their independence is verified by the determinant of the dimensions matrix (Barenblatt, 1987; Kundu and Cohen, 2008):

$$\det \begin{array}{c} \\ M: \\ L: \\ T: \end{array} \begin{array}{c} \begin{array}{ccc} \rho_f & D & g \end{array} \\ \begin{pmatrix} 1 & 0 & 0 \\ -3 & 1 & 1 \\ 0 & 0 & -2 \end{pmatrix} \end{array} = 1$$

The drag force F_d can be expressed as some function of the other quantities: $F_d = \Delta\ x\ h\ g\ S_0\ \rho_f$. Thus, the number of relevant parameters reduces to $N = 11$. The remaining 11 - 3 = 8 Π numbers

are:

$$
\begin{array}{lllll}
\Pi_1: & s & = & \rho_s/\rho_f & \text{relative sediment density} \\
\Pi_2: & h_* & = & h/D & \text{relative flow depth} \\
\Pi_3: & S_0 & & & \text{channel slope} \\
\Pi_4: & F_* & = & \dfrac{Q}{h\, w \cdot \sqrt{D\, g}} & \text{some characteristic flow number} \\
\Pi_5: & \Phi & = & \dfrac{Q_b}{w\, \rho_f\, \sqrt{(s-1)\, g\, D}} & \text{bed load transport intensity} \\
\Pi_6: & w_* & = & w/D & \text{relative flow width} \\
\Pi_7: & \Delta x_* & = & \Delta x/D & \text{relative reach length} \\
\Pi_8: & R_* & = & \dfrac{\nu}{D^{3/2}\, g^{1/2}} & \text{some grain related friction factor}
\end{array}
$$

Some of these parameters can be combined to deduce the grain related Reynolds Re_* and Froude Fr_* numbers (Yalin, 1971, 1977):

$$
\begin{aligned}
Re_* &= \frac{\sqrt{g\, R_h\, S_0}\, D}{\nu} \\
Fr_* &= \frac{R_h\, S_0}{(s-1)\, D}
\end{aligned}
$$

This illustration can be directly applied to Chpts. 6 and 7. In Chpts. 4 and 5, the set of repeating variables is constituted by h, g and ρ_f.

A.2.2 Mathematical model description

The flow in mountain rivers can be expressed by a simplified expression of the one-dimensional Navier-Stokes equation for incompressible fluids, assuming hydrostatic pressure distribution (Kundu and Cohen, 2008; Graf and Altinakar, 2011)). This results in the Saint-Venant shallow water equations as used in some hydraulic computer models, e.g., HEC-RAS or BASEMENT 1D (U.S. Army Corps of Engineeers, 2016; VAW, 2017). This shallow water equation consists of five terms (Jansen et al., 1994):

$$
\overbrace{\frac{1}{g}\frac{\partial u}{\partial t}}^{I} + \overbrace{\frac{u}{g}\frac{\partial u}{\partial x}}^{II} + \overbrace{\frac{\partial h}{\partial x}}^{III} + \overbrace{\frac{\partial z}{\partial x}}^{IV} = \overbrace{-\frac{u|u|}{C^2 h}}^{V=J_e} \tag{A.7}
$$

The five terms can be related separately to each other for the derivation of scale factors λ. Thus,

equating the scales of the terms I and II results in (De Vries, 1993):

$$\frac{\lambda_u}{\lambda_t} = \frac{\lambda_u^2}{\lambda_l} \Longrightarrow \lambda_l = \lambda_u \cdot \lambda_t \tag{A.8}$$

where λ_u ≡ velocity scale
λ_t ≡ time scale.

Postulating that the gravity scale λ_g is unity, the comparison of the scales of terms II and V results in:

$$\frac{\lambda_u^2}{\lambda_l} = \frac{\lambda_u^2}{\lambda_C^2 \cdot \lambda_h} \Longrightarrow \lambda_C^2 = \sqrt{\frac{\lambda_l}{\lambda_h}} \tag{A.9}$$

where λ_C ≡ Chézy roughness scale.

A.2.3 Similitude concepts

The similarity of the Froude number in a scaled model and a prototype is achieved based on the Froude condition, which results from equating the scales of terms II and III of Eq. A.7 (De Vries, 1993):

$$\frac{\lambda_u^2}{\lambda_l} = \frac{\lambda_h}{\lambda_l} \Longrightarrow \lambda_u = \sqrt{\lambda_h}. \tag{A.10}$$

The similarity of sediment transport is of particular interest in this study and requires that the scales of the dimensionless bed shear stress τ_* (Eq. 2.11 on page 14) and of the bed load transport intensity Φ (page 17) are unity; i.e., $\lambda_{\tau_*} = 1$ and $\lambda_\Phi = 1$ (De Vries, 1993).
With respect to the shear velocity $u_* = \sqrt{\tau/\rho_f} = \sqrt{\tau_* \, (s-1) \, g \, D}$ and the requirement of $\lambda_{\tau_*} = 1$, the similarity of sediment transport is given when (Jansen et al., 1994):

$$\lambda_u^2 \approx \lambda_s \cdot \lambda_D \tag{A.11}$$

where λ_s ≡ scale of relative sediment density
λ_D ≡ scale of grain diameter.

The similarity of unitary sediment transport, i.e., per unit width, can be verified based on the scale λ_{q_b}, which is derived from the Exner equation (Exner, 1925):

$$\frac{\partial z}{\partial t} = -\frac{1}{1-\zeta} \cdot \frac{\partial q_s}{\partial x} \tag{A.12}$$

With respect to the scale considerations above, λ_{q_b} is derived as:

$$\frac{\lambda_l}{\lambda_t} = \frac{\lambda_{q_b}}{\lambda_l} \Rightarrow \lambda_{q_b} = \frac{\lambda_l^2}{\lambda_t} = \lambda_l^{3/2} \tag{A.13}$$

λ_{q_b} refers to volumetric fluxes. The scale of the mass flow rate $\lambda_{\dot{q}_b}$ can be computed by multiplying Eq. A.12 by the sediment density ρ_s. Postulating the density scale of $\lambda_s = 1$, the mass flow rate scale is also $\lambda_{\dot{q}_b} = \lambda_l^{3/2}$.
The boundary conditions imposed by the feasibility of the laboratory experiments entail that the densities of the sediment in nature and in the model are similar, i.e., $\lambda_s = 1$. Thus, the Froude similarity ($\lambda_u = \sqrt{\lambda_h}$) and the similarity of sediment transport ($\lambda_u = \sqrt{\lambda_D}$) require that $\lambda_D = \lambda_h$; i.e., the same geometric scales apply to the grain diameter as well as to the flow depth (Jansen et al., 1994). This condition can be considered as fulfilled in this study, as of coarse sediments in the shape of gravel are used for the experiments.

A.3 Complementary information on the experimental set-up

A.3.1 Pictures

Fig. A.1 shows the a) top-view and b) panoramic view of the experimental set-up, with the indication of the following elements: ① sediment container; ② system of conveyor belts; ③ upstream adaptation reach; ④ observation reach, consisting of a trapezoidal flume for the experiments in Chpts. 4 to 6, and a retention reservoir with guiding channel for the experiments in Chpt. 7; ⑤ insertion point of the flow constrictions and barriers; and ⑥ filter basket for the separation of outflowing sediments and water. In addition, the sediment and water cycles are represented.

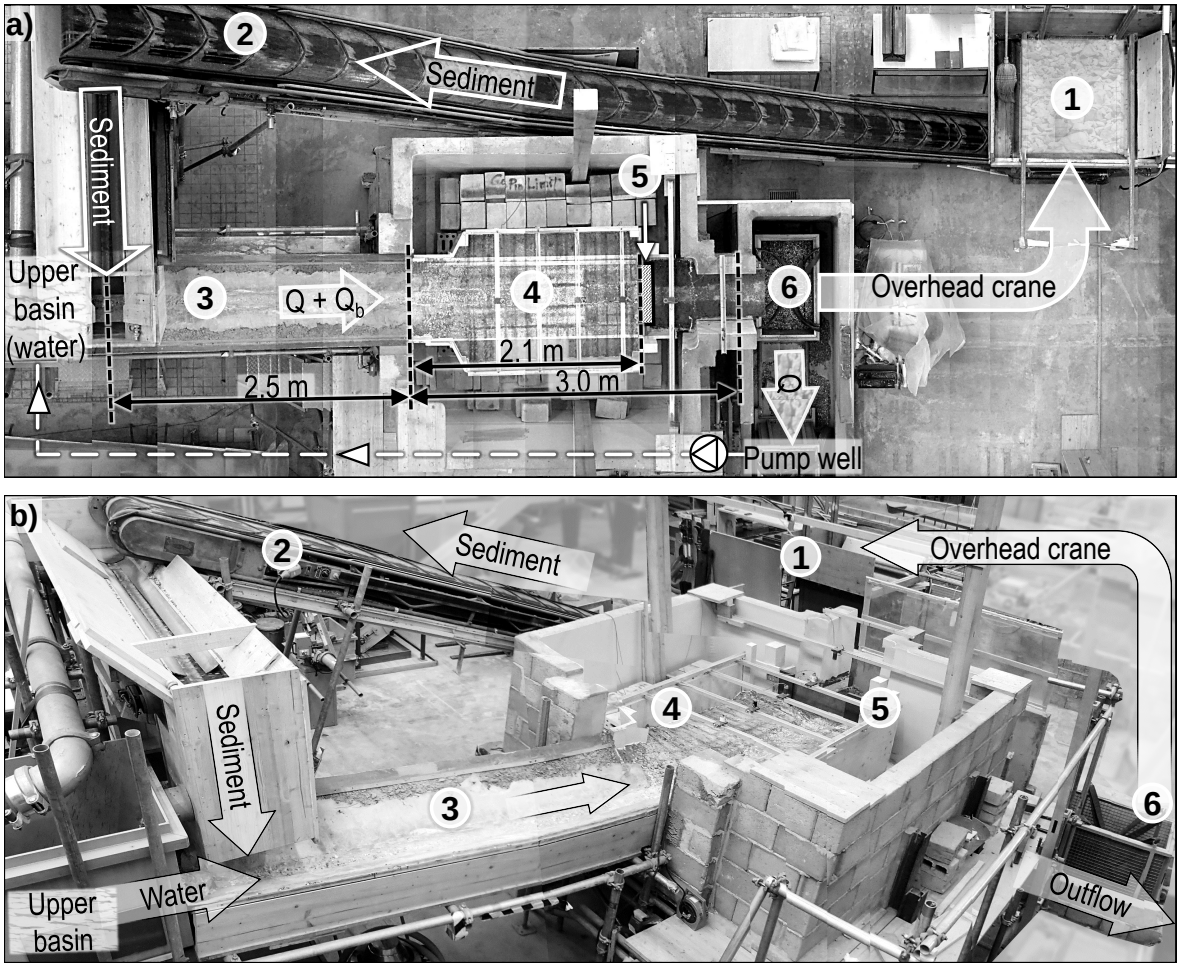

Figure A.1 – *Composed (a) top-view and (b) panoramic pictures of the experimental set-up, with indication of the sediment and water cycles. The circled numbers indicate the ① sediment container, ② system of conveyor belts, ③ upstream adaptation reach, ④ observation reach consisting of a trapezoidal flume (Chpts. 4 - 6) or a retention reservoir with guiding channel (Chpt. 7), ⑤ insertion point of the flow constrictions and barriers, and ⑥ filter basket (adopted from Schwindt et al., 2017b).*

Fig. A.2 shows the outflow section of the model with the filter basket attached to the industrial scale (cf. Chpt. 3.2.5, page 45) and the overhead crane; and Fig. A.3 illustrates the construction of the channel with the hydraulic barriers.

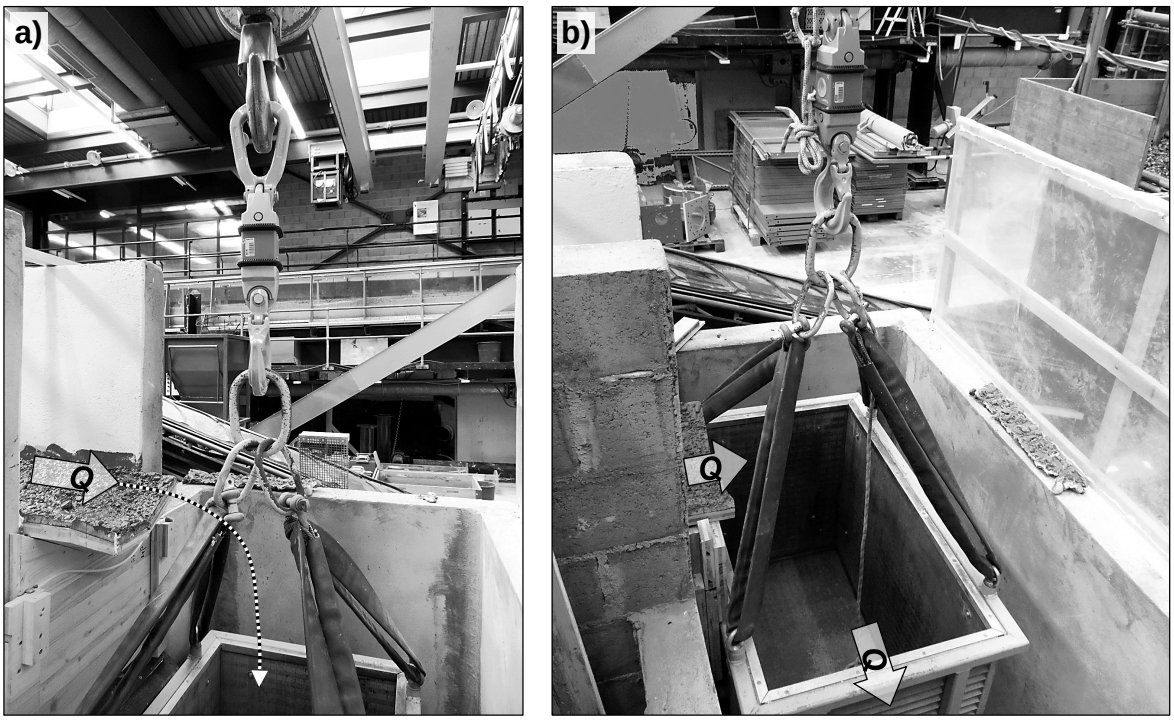

Figure A.2 – *The outflow section of the model from two perspectives (a and b), with the filter basket attached to the industrial scale and overhead crane.*

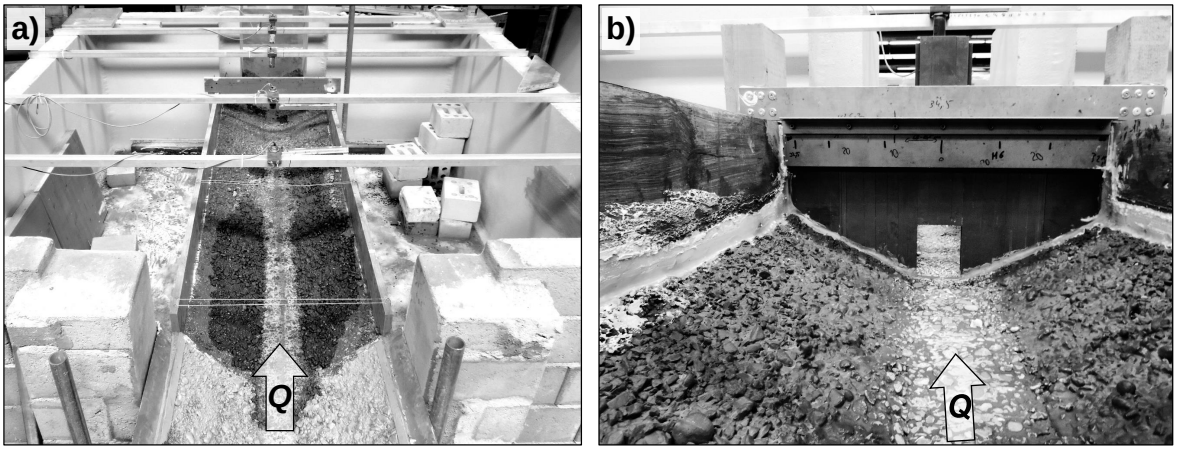

Figure A.3 – *Pictures of the a) channel construction (Chpts. 4 to 6) and b) the installation of the flow constriction (Chpts. 4 and 5) in terms of the mobile PVC elements.*

Figs. A.4 a) and b) show pictures of the model from different perspectives and Fig. A.4 c) illustrates the reservoir used for the analysis in Chpt. 7. Fig. A.5 shows the sediments container with its control unit and the pump with the principal basin (pump well).

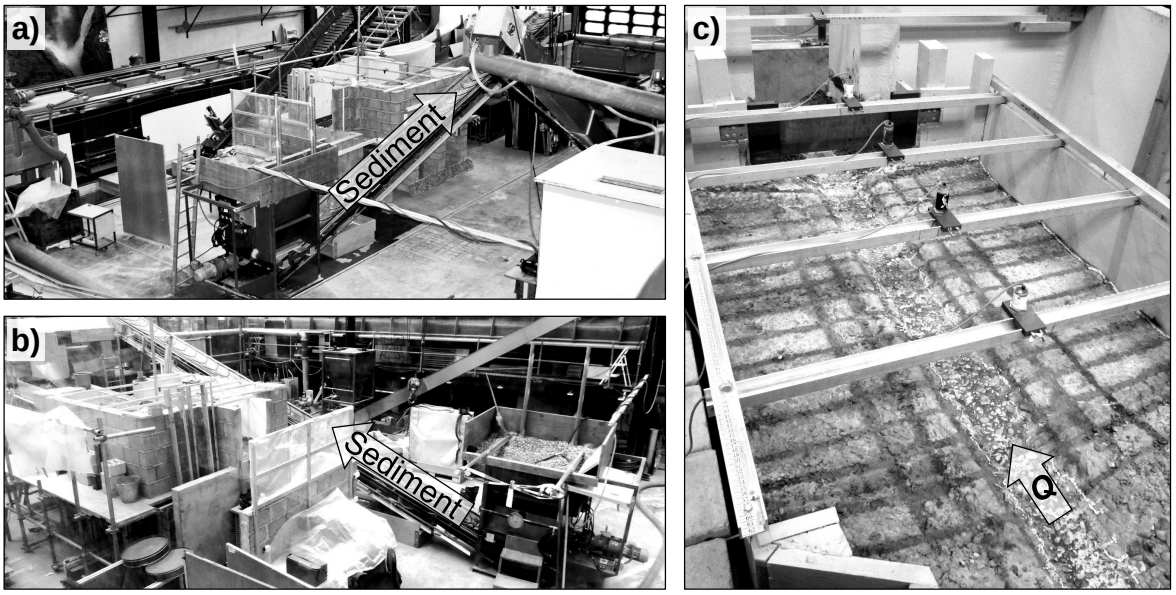

Figure A.4 – *Pictures of the model in the laboratory, from two different positions (a and b), and c) picture of the reservoir used for the analysis in Chpt. 7.*

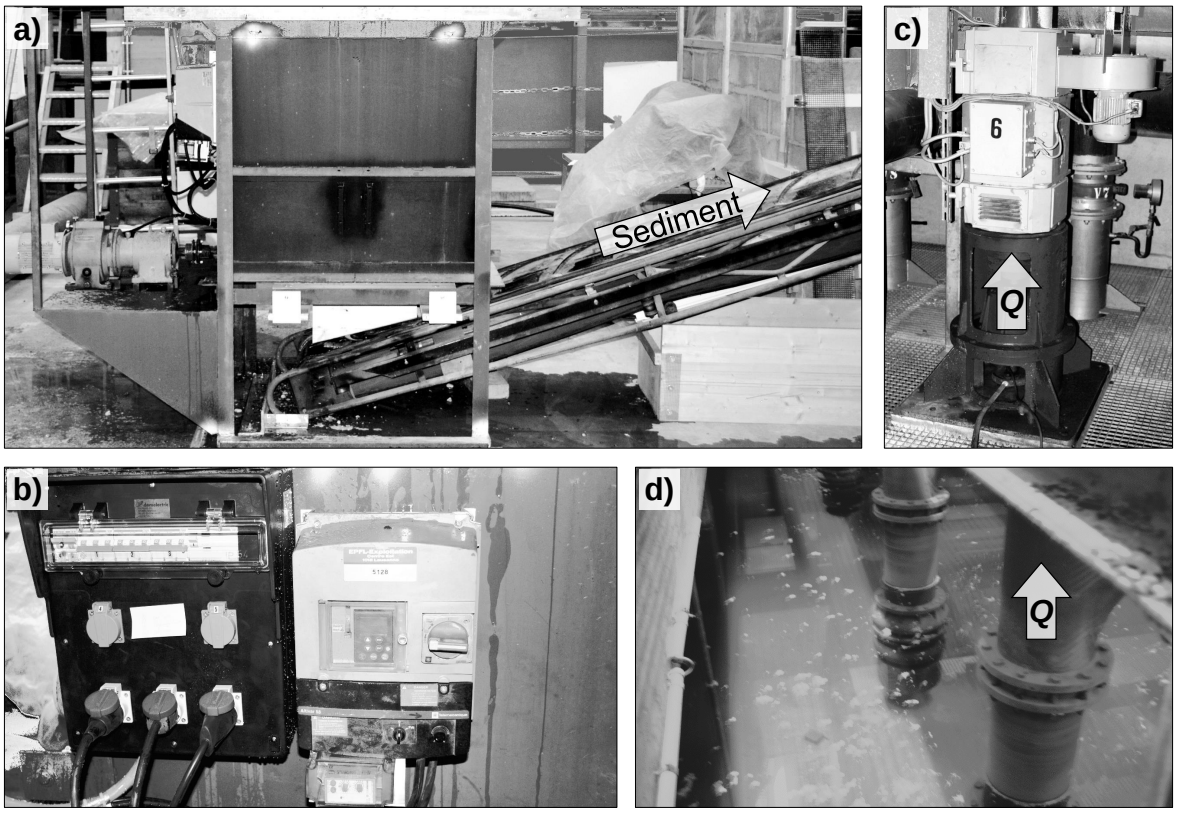

Figure A.5 – *Picture a) shows a longitudinal view of the sediment container releasing the sediments on the system of conveyor belts, with b) the control unit of the drive speed for the manipulation of the sediment supply. Picture c) shows the pump above d) the principle basin (pump well) with the pump inlet sides.*

Fig. A.6 illustrates the moving of the sediments: a) and b) show the manipulation with the overhead crane; and c) shows details of the upper part of the system of conveyor belts with indication of the upper water basin.

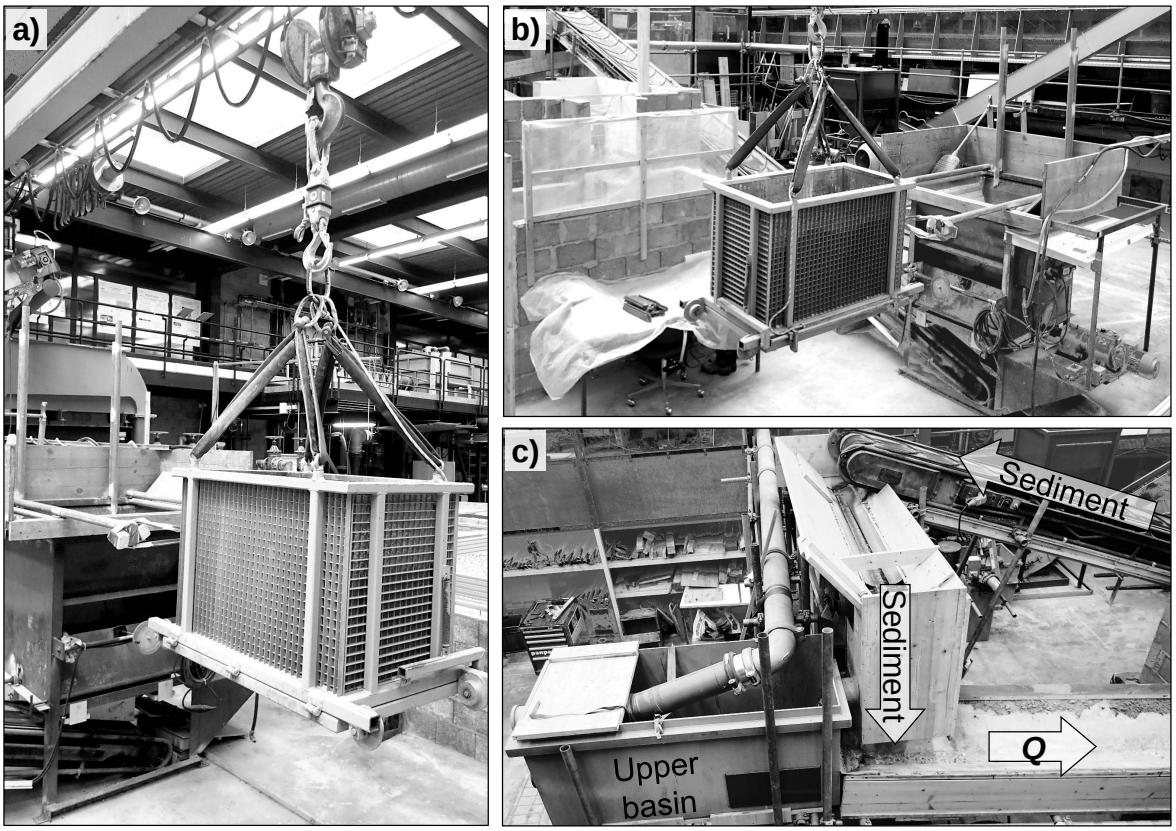

Figure A.6 – *Pictures illustrating the sediment supply system: a) moving of sediments in the filter basket with the overhead crane; b) positioning of the filter basket on top of the sediment container for the emptying of the filter basket through its bottom; and c) the upper water basin with the upper part of the system of conveyor belts delivering the sediments.*

A.3.2 Sediment supply calibration

The sediment release for a modulation frequency of 0.55 Hz is illustrated in Fig. A.7. The inaccuracy of the rating curves is approximately 5 % within a 68 % confidence interval.

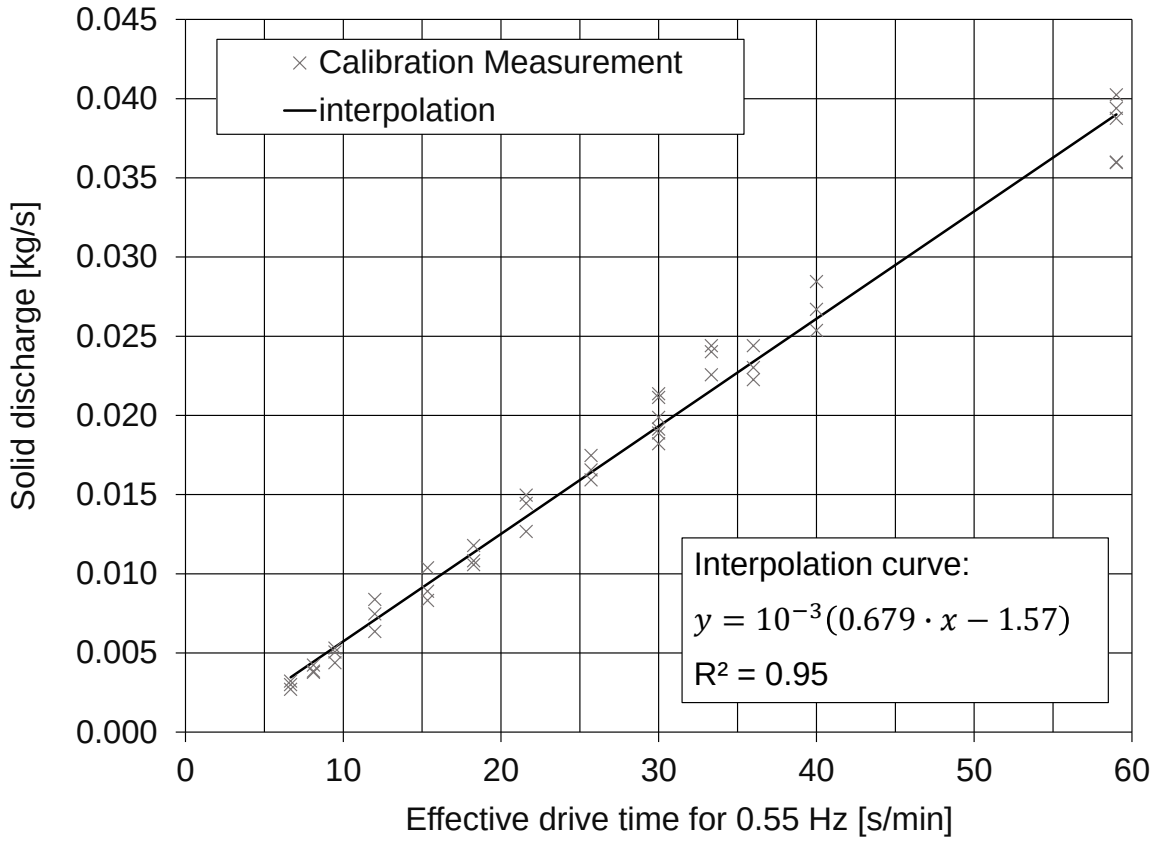

Figure A.7 – *Sediment release rating curve for a modulation frequency of 0.55 Hz.*

A.3.3 Application of the motion sensing camera

The technical basis for the application of the motion sensing camera (type Microsoft Kinect V2) was established by Sandro Düblin in spring 2016. The measurements on the model were primarily done by Alessandro Reffo, in the framework of his Master's thesis from October to December 2016. The following technical instructions for the application of the motion sensing camera refers to the reports from Sandro Düblin and Alessandro Reffo.

The distortion effects of the motion sensing camera are minimum within a frame size of 350 x 300 mm, when the objective has a distance of 650 ± 150 mm to the camera lens. The scanning of larger frames requires an assembly of several pictures, which need to include some uniquely identifiable marker. Multiple markers need to be placed on large surfaces, to overlay neighboring pictures later on. An adequate marker was found in checked squares as shown in Fig. A.8.

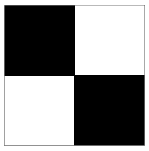

Figure A.8 – *Example for a marker for the superposition of multiple pictures taken with the motion sensing camera.*

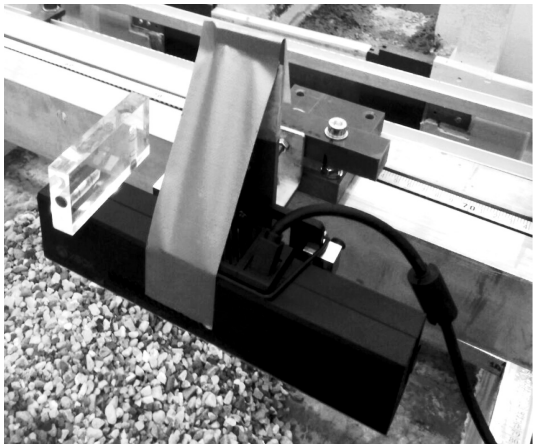

Figure A.9 – *Fixation of the motion sensing (Kinect V2) camera on the rail and verification of its position using a spirit level. © Alessandro Reffo.*

The camera was attached to a slide on a rail crossing over the model. The position of every picture was determined based on the model x-y-z-coordinate system as introduced in Chpt. 7. Thus, the camera was moved on the rail in equidistant steps, for taking a series of pictures along the model y-axis, starting at the upstream model end. Then, the rail was moved in downstream direction (negative x-direction) for shooting a subsequent series of pictures along the y-axis. This procedure was repeated until the entire observation area was captured (15 to 17 pictures overall). The distance between the basin bottom and the camera was imposed by the rail and therefore identical for every measurement series. The vertical alignment of the camera was verified with a spirit level (Fig. A.9).

An example picture (*.png*–format) of the model without and with sediment deposits is shown in Fig. A.10, with gray scales (originally: green-scale), corresponding to the differences in the vertical position (z-axis) of the closest object.

In-house Matlab codes were used to derive spatial coordinates from the pixel size and the shading intensity of the assembled *.png*–file. The position and size of the checked markers was used to transform the pixel size and green intensity of the pictures to spatial coordinates. This results in a series of 15 to 17 spatial matrices (depending on the deposit extents) that were subsequently assembled into one spatial matrix of the model.
CAD software was used to transform the spatial matrix in solid bodies for the definition of 3D

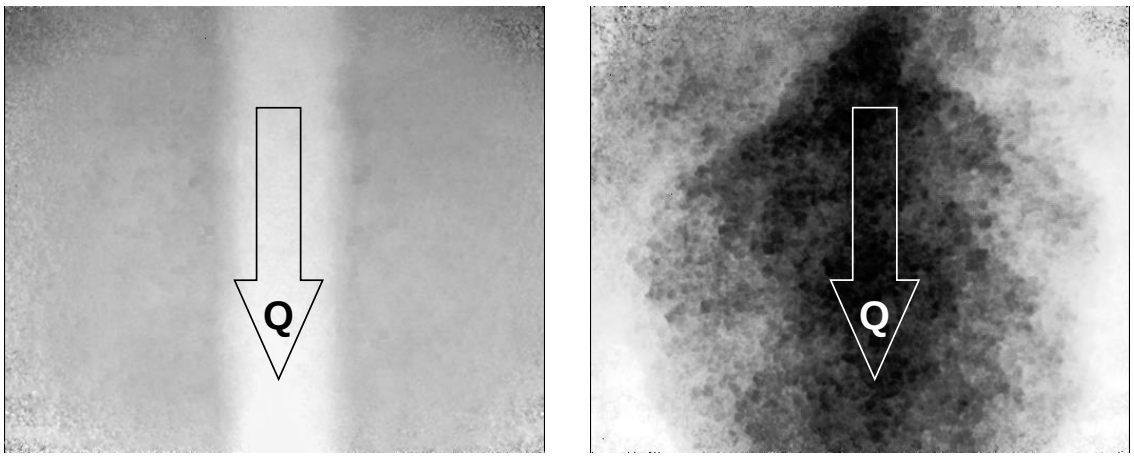

Figure A.10 – *Assembled gray scale pictures of the model without (left hand side) and with (right hand side) sediment deposits.*

objects with volume attributes. The subtraction of spatial matrices with sediment deposits in the basin from a reference matrix based on pictures of the model without sediment deposits, was used to compute net deposit volumes (in m^3). An example of a solid representing the sediment deposit after a test-run, with a hydraulic constriction of height a = 0.040 m and width b = 0.150 m, is shown in Fig. A.11.

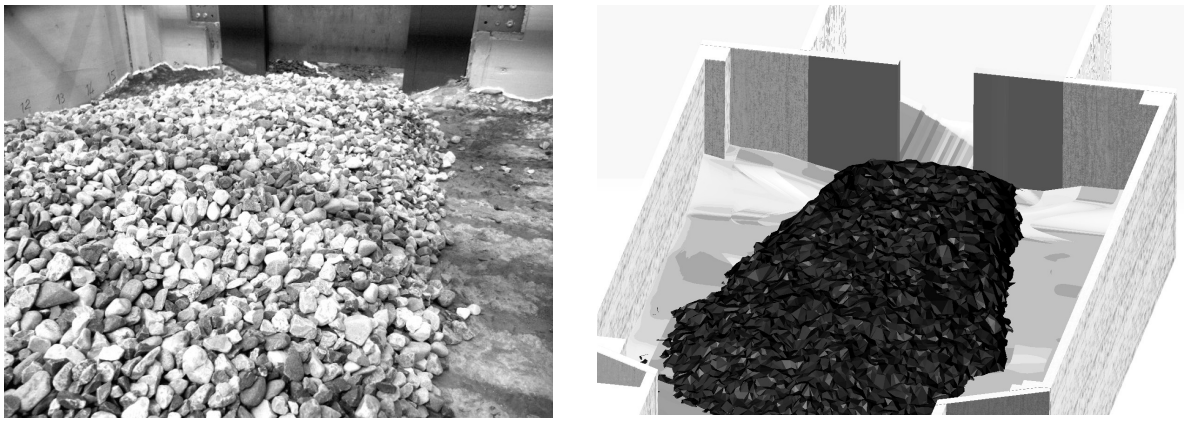

Figure A.11 – *Picture of the model with sediment deposit (left hand side), compared with its numerical representation (right hand side) based on pictures from the motion sensing camera, after a hydrograph test run with overflown hydraulic constriction of height a = 0.040 m and width b = 0.15 m, and superposed upstream mechanical barrier.*

A.3.4 Supplementary evaluation of discharge coefficients

The analysis in Chpt. 5 refers to the discharge-related critical flow depth in the non-constricted channel, using Eq. A.14 for free surface and Eq. A.15 for pressurized orifice flow.

$$Q_{\mathrm{c,\,f}} = \mu_f \; b \; \sqrt{2\,g} \; H_0^{\frac{3}{2}} \tag{A.14}$$

$$Q_{\mathrm{c,\,p}} = \mu_p \; b \; \sqrt{2\,g} \; \frac{2}{3} \left[H_0^{\frac{3}{2}} - (H_0 - a)^{\frac{3}{2}} \right] \tag{A.15}$$

The supplementary evaluations of the corresponding discharge coefficients μ_f (free surface) and μ_p (pressurized) are shown in Fig. A.12 as a function of the upstream Froude number, following the dimensional considerations in Chpt. 4.

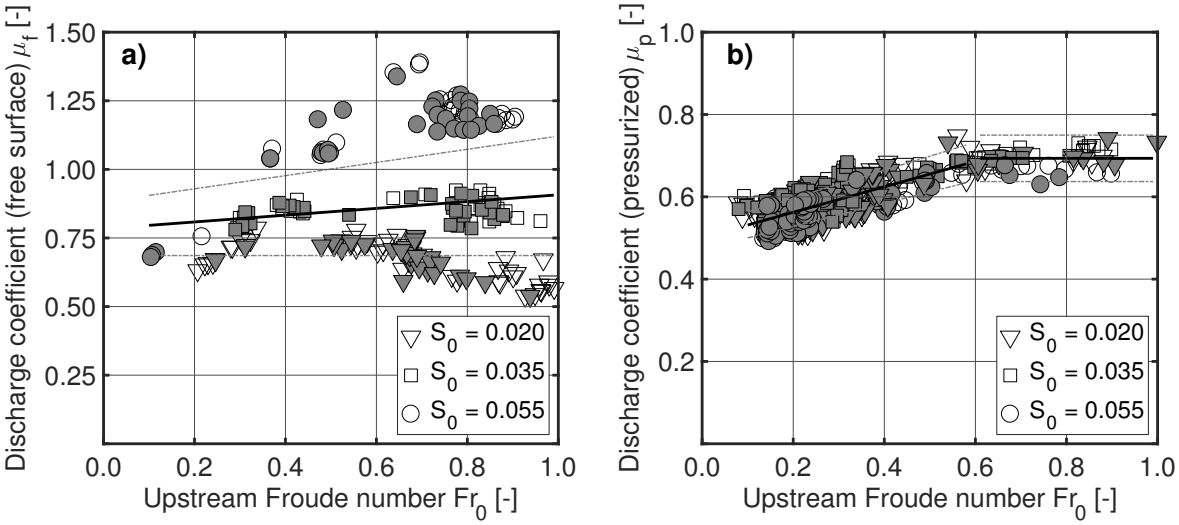

Figure A.12 – *Evaluation of the discharge coefficients a) μ_f for free surface flow according to Eq. A.14 and b) μ_p for pressurized flow according to Eq. A.15, as a function of the upstream Froude number Fr_0 for three channel slopes S_0. The regression curves are shown with indication of the 68 % confidence intervals. The filled symbols indicate measurements with bed load.*

The regression curves indicated in Fig. A.12 are given by:

$$mu_f\,(Fr_0 < 1.0) = 0.124 \cdot Fr_0 \; + \; 0.784 \qquad R^2 = 0.01 \tag{A.16}$$

$$mu_p\,(Fr_0 < 0.6) = 0.245 \cdot Fr_0 \; + \; 0.517 \qquad R^2 = 0.76 \tag{A.17}$$

$$mu_p\,(Fr_0 \geq 0.6) = \qquad 0.70 \; \pm \; 0.04 \qquad R^2 = 0.74 \tag{A.18}$$

The data in Fig. A.12 a) can be grouped by the channel slope values of $S_0 \in [0.020, 0.035, 0.055]$. These data groups can be collapsed using a channel slope-dependent regression curve as follows ($R^2 = 0.87$):

$$mu_f\,(Fr_0 < 1.0) \; = \; (20 \cdot S_0 \; - \; 0.8) \cdot Fr_0 \; + \; 0.93 \tag{A.19}$$

A.4 Experimental data

A.4.1 Hydraulic control analysis (to Chpts. 4 and 5)

The following tables contain data based on the measurements performed in the non-constricted and hydraulically constricted channel (Chpts. 4 and 5). The data are classed by parameter and the three channel slopes of 0.020, 0.035 and 0.055. Empty cells refer to invalid measurements due to perturbations. The columns refer to the following variables:

Latin letters		
a	m	constriction height
b	m	constriction width
h_0	m	flow depth upstream of flow constrictions
Q	$m^3\ s^{-1}$	pump (water) discharge
S_0	$m\ m^{-1}$	channel slope

NON-CONSTRICTED CHANNEL															
$			*[m³/s]*			*[kg/s]*			*[kg/s]*			*[kg/s]*		
h 0 (Sensor 4)			***Q***			***Qb***			***Qb (Rickenmann)***			***Qb (Smart-Jaeggi)***		
0.020	**0.035**	**0.055**	**0.020**	**0.035**	**0.055**	**0.020**	**0.035**	**0.055**	**0.020**	**0.035**	**0.055**	**0.020**	**0.035**	**0.055**
0.045	0.037	0.035	0.005	0.005	0.005	0.003	0.036	0.204		0.050	0.225	0.011	0.058	0.243
0.046	0.037	0.035	0.006	0.005	0.005	0.004	0.049	0.193		0.053	0.231	0.011	0.060	0.251
0.048	0.039	0.037	0.006	0.005	0.006	0.005	0.064	0.250		0.055	0.238	0.012	0.062	0.258
0.047	0.040	0.039	0.006	0.006	0.006	0.006	0.069	0.291		0.058	0.244	0.012	0.063	0.265
0.047	0.040	0.039	0.006	0.006	0.006	0.006	0.076	0.322		0.060	0.250	0.013	0.065	0.272
0.048	0.042	0.039	0.007	0.007	0.006	0.006	0.097	0.295		0.063	0.257	0.013	0.067	0.279
0.051	0.042	0.040	0.008	0.006	0.007	0.007	0.084	0.335		0.065	0.263	0.014	0.069	0.287
0.049	0.041	0.041	0.007	0.007	0.007	0.007	0.097	0.366		0.068	0.270	0.014	0.070	0.294
0.047	0.043	0.041	0.006	0.007	0.007	0.007	0.099	0.363		0.070	0.276	0.015	0.072	0.302
0.051	0.043	0.040	0.008	0.007	0.007	0.008	0.114	0.344		0.073	0.283	0.015	0.074	0.309
0.045	0.043	0.041	0.005	0.007	0.007	0.008	0.123	0.404		0.076	0.289	0.016	0.076	0.317
0.050	0.044	0.041	0.007	0.008	0.008	0.009	0.127	0.423		0.078	0.296	0.017	0.078	0.324
0.052	0.044	0.041	0.008	0.008	0.008	0.011	0.128	0.444		0.081	0.303	0.017	0.080	0.332
0.048	0.045	0.042	0.007	0.008	0.008	0.012	0.131	0.461		0.084	0.309	0.018	0.082	0.339
0.052	0.046	0.043	0.008	0.008	0.008	0.015	0.133	0.470		0.087	0.316	0.018	0.083	0.347
0.052	0.050	0.043	0.008	0.008	0.008	0.017		0.474		0.089	0.323	0.019	0.085	0.355
0.053	0.046	0.043	0.008	0.008	0.008	0.019	0.159	0.474		0.092	0.329	0.019	0.087	0.363
0.051	0.047	0.044	0.008	0.009	0.008	0.020	0.194	0.482		0.095	0.336	0.020	0.089	0.371
0.053	0.049	0.044	0.008	0.009	0.009	0.020		0.500		0.098	0.343	0.021	0.091	0.379
0.052	0.051	0.046	0.008	0.009	0.009	0.021		0.511		0.101	0.350	0.021	0.093	0.386
0.052	0.048	0.046	0.008	0.009	0.009	0.022	0.239	0.526		0.104	0.357	0.022	0.095	0.394
0.053	0.049	0.046	0.009	0.010	0.009	0.022	0.242	0.541		0.107	0.364	0.022	0.098	0.402
0.054	0.050	0.047	0.009	0.010	0.010	0.026	0.253	0.545		0.110	0.371	0.023	0.101	0.411
0.054	0.050	0.047	0.009	0.010	0.010	0.026	0.271	0.556		0.113	0.378	0.024	0.104	0.419
0.051	0.051	0.047	0.008	0.010	0.010	0.027		0.558			0.385	0.024		0.427
0.056	0.050	0.032	0.010	0.010	0.005	0.031					0.392			
0.054	0.056	0.032	0.009	0.009	0.005	0.031					0.399			
0.054	0.053	0.033	0.009	0.005	0.006	0.034					0.406			
0.055	0.036	0.035	0.010	0.005	0.006	0.035					0.413			
0.055	0.037	0.036	0.009	0.005	0.006	0.036					0.420			
0.056	0.037	0.035	0.009	0.006	0.006	0.037					0.427			
0.056	0.038	0.037	0.010	0.006	0.007	0.040					0.434			
0.058	0.040	0.038	0.010	0.007	0.007	0.046					0.441			
0.057	0.038	0.038	0.010	0.006	0.007	0.048					0.448			
0.045	0.039	0.036	0.005	0.007	0.007						0.456			
0.045	0.040	0.041	0.005	0.007	0.007						0.463			
0.047	0.041	0.038	0.006	0.007	0.008						0.470			
0.049	0.041	0.039	0.007	0.007	0.008						0.477			
0.045	0.042	0.039	0.005	0.008	0.008						0.484			
0.045	0.042	0.040	0.005	0.008	0.008						0.492			
0.045	0.043	0.039	0.005	0.008	0.008						0.499			
0.045	0.043	0.040	0.005	0.008	0.008						0.506			
0.052	0.043	0.041	0.008	0.008	0.008						0.514			
0.055	0.043	0.041	0.010	0.008	0.009						0.521			
0.056	0.044	0.042	0.010	0.009	0.009						0.528			
0.045	0.045	0.043	0.005	0.009	0.009						0.536			
0.046	0.046	0.043	0.006	0.009	0.009						0.543			
0.046	0.045	0.043	0.006	0.009	0.010						0.551			
0.046	0.046	0.045	0.006	0.010	0.010						0.558			
0.048	0.047	0.044	0.006	0.010	0.010						0.565			
0.047	0.047		0.006	0.010							0.573			
0.048	0.048		0.007	0.010										
0.048	0.047		0.007	0.010										
0.049	0.045		0.007	0.009										

NON-CONSTRICTED CHANNEL														
$			*[m³/s]*			*[kg/s]*			*[kg/s]*			*[kg/s]*		
h 0 (Sensor 4)			***Q***			***Qb***			***Qb (Rickenmann)***			***Qb (Smart-Jaeggi)***		
0.020	**0.035**	**0.055**	**0.020**	**0.035**	**0.055**	**0.020**	**0.035**	**0.055**	**0.020**	**0.035**	**0.055**	**0.020**	**0.035**	**0.055**
0.050	0.050		0.007	0.011										
0.050			0.007											
0.050			0.008											
0.051			0.008											
0.051			0.008											
0.051			0.008											
0.052			0.008											
0.052			0.008											
0.052			0.008											
0.052			0.008											
0.053			0.009											
0.053			0.009											
0.053			0.009											
0.054			0.009											
0.055			0.009											
0.055			0.010											
0.056			0.010											
0.056			0.010											
0.057			0.010											
0.046			0.006											
0.046			0.006											
0.047			0.006											
0.047			0.006											
0.048			0.006											
0.048			0.006											
0.048			0.007											
0.048			0.007											
0.049			0.007											
0.049			0.007											
0.049			0.007											
0.050			0.007											
0.050			0.008											
0.051			0.008											
0.051			0.008											
0.052			0.008											
0.052			0.008											
0.053			0.009											
0.053			0.009											
0.054			0.009											
0.054			0.009											
0.055			0.010											
0.055			0.010											
0.056			0.010											

PRESSURIZED VERTICAL FLOW CONSTRICTION															
[m]			[not applicable]			[m]			[m³/s]			[kg/s]			
a			b			h_0			Q			Q_b			
S_o=2.0%	S_o=3.5%	S_o=5.5%	S_o=2.0%	S_o=3.5%	S_o=5.5%	S_o=2.0%	S_o=3.5%	S_o=5.5%	S_o=2.0%	S_o=3.5%	S_o=5.5%	S_o=2.0%	S_o=3.5%	S_o=5.5%	
0.03867	0.03363	0.04290				0.08245	0.14385	0.07989	0.00557	0.00534	0.00569	0.00008	0.00023	0.03073	
0.03967	0.03812	0.04290				0.07348	0.09247	0.07670	0.00553	0.00538	0.00538	0.00007	0.00047	0.02719	
0.04466	0.04232	0.04290				0.04936	0.06873	0.07705	0.00557	0.00533	0.00552	0.00233	0.00364	0.02454	
0.03967	0.04232	0.04290				0.09674	0.08955	0.07813	0.00608	0.00575	0.00566	0.00016	0.00080	0.02168	
0.04266	0.04412	0.04290				0.04789	0.07026	0.08127	0.00605	0.00589	0.00584	0.00354	0.00942	0.01988	
0.04266	0.04412	0.04290				0.09431	0.06810	0.10961	0.00702	0.00599	0.00614	0.00045	0.00567	0.01325	
0.04765	0.04412	0.04290				0.05184	0.06702	0.11723	0.00705	0.00591	0.00641	0.00748	0.00571	0.00222	
0.04765	0.04412	0.04290				0.10612	0.07529	0.12428	0.00836	0.00596	0.00682	0.00166	0.00388	0.00155	
0.05065	0.04412	0.04290				0.05551	0.09189	0.14122	0.00824	0.00631	0.00707	0.01378	0.00085	0.00012	
0.05065	0.04412	0.04590				0.05858	0.09221	0.05803	0.00868	0.00635	0.00588	0.01369	0.00086	0.05406	
0.04865	0.04412	0.04590				0.11281	0.09389	0.05878	0.00870	0.00652	0.00572	0.00134	0.00117	0.06569	
0.05563	0.04412	0.04590				0.06597	0.09573	0.06424	0.00906	0.00656	0.00625	0.01376	0.00119	0.07125	
0.05164	0.04412	0.04590				0.07289	0.10609	0.08268	0.00846	0.00681	0.00646	0.00793	0.00053	0.05000	
0.05164	0.04412	0.04590				0.09805	0.10243	0.08675	0.00905	0.00694	0.00674	0.00334	0.00034	0.04248	
0.05763	0.04412	0.04590				0.06582	0.11450	0.12029	0.00950	0.00714	0.00701	0.01613	0.00016	0.00325	
0.05763	0.04412	0.04590				0.06978	0.11892	0.12443	0.00987	0.00723	0.00750	0.01812	0.00025	0.00301	
0.05464	0.04662	0.04590				0.11585	0.07640	0.14407	0.01021	0.00653	0.00765	0.00288	0.00922	0.00025	
0.05464	0.04662	0.04940				0.10149	0.09217	0.11886	0.00980	0.00671	0.00781	0.00525	0.00118	0.00839	
0.05563	0.04662	0.04940				0.07597	0.07176	0.08042	0.00936	0.00670	0.00726	0.00794	0.00838	0.07986	
0.05563	0.04662	0.04940				0.07532	0.09144	0.08018	0.00934	0.00678	0.00743	0.00845	0.00283	0.06509	
0.05563	0.04662	0.04940				0.06030	0.09371	0.08897	0.00922	0.00683	0.00768	0.02163	0.00162	0.05584	
0.04865	0.04662	0.04940				0.06508	0.09459	0.11867	0.00743	0.00700	0.00796	0.00481	0.00190	0.01327	
0.04865	0.04662	0.04940				0.09774	0.09796	0.12310	0.00806	0.00726	0.00820	0.00233	0.00234	0.00803	
0.04865	0.04662	0.04940				0.05471	0.10823	0.12557	0.00749	0.00744	0.00842	0.00716	0.00065	0.00837	
0.04865	0.04662	0.04940				0.08466	0.11131	0.12901	0.00774	0.00747	0.00876	0.00124	0.00069	0.00802	
0.04366	0.04662	0.04940				0.08765	0.11929	0.15383	0.00689	0.00780	0.00893	0.00167	0.00050	0.00062	
0.04366	0.04662	0.05290				0.05271	0.12344	0.08955	0.00621	0.00792	0.00923	0.00346	0.00059	0.10793	
0.04067	0.04662	0.05290				0.08635	0.12924	0.11868	0.00580	0.00815	0.00914	0.00022	0.00040	0.02675	
0.05065	0.04662	0.05290				0.06831	0.13323	0.12023	0.00785	0.00828	0.00949	0.00545	0.00034	0.02423	
0.05065	0.04662	0.05290				0.09204	0.14384	0.13408	0.00828	0.00851	0.01016	0.00220	0.00003	0.00491	
0.03967	0.04882	0.05290				0.07793	0.06829	0.15885	0.00528	0.00710	0.01030	0.00000	0.02216	0.00009	
0.03967	0.04882	0.05040				0.10500	0.06564	0.07251	0.00586	0.00694	0.00793	0.00000	0.02321	0.06954	
0.03967	0.04882	0.05040				0.12687	0.06668	0.08426	0.00656	0.00699	0.00807	0.00000	0.02032	0.07495	
0.03967	0.04882	0.05040				0.12827	0.07396	0.08463	0.00662	0.00727	0.00810	0.00000	0.01737	0.06272	
0.03967	0.04882	0.05040				0.16142	0.09638	0.11640	0.00756	0.00741	0.00829	0.00000	0.00581	0.00822	
0.03967	0.04882	0.05040				0.17889	0.09675	0.12060	0.00811	0.00765	0.00846	0.00000	0.00467	0.00495	
0.03967	0.04882	0.05040				0.19530	0.10259	0.12282	0.00857	0.00788	0.00854	0.00000	0.00278	0.00355	
0.04266	0.04882	0.05040				0.18657	0.11130	0.12382	0.00867	0.00809	0.00865	0.00000	0.00144	0.00343	
0.04266	0.04882	0.05040				0.15971	0.12008	0.12627	0.00798	0.00830	0.00879	0.00000	0.00073	0.00421	
0.04266	0.04882	0.05040				0.14894	0.12704	0.12815	0.00756	0.00857	0.00902	0.00000	0.00029	0.00352	
0.04266	0.04882	0.05040				0.12845	0.13195	0.15098	0.00665	0.00882	0.00911	0.00000	0.00231	0.00010	
0.04266	0.05312	0.04290				0.11095	0.07486	0.07504	0.00621	0.00831	0.00554	0.00000	0.02692	0.00000	
0.04266	0.05312	0.04290				0.09410	0.08520	0.07579	0.00608	0.00862	0.00550	0.00000	0.02409	0.00000	
0.04266	0.05312	0.04290				0.07928	0.09969	0.07389	0.00542	0.00876	0.00554	0.00000	0.01068	0.00000	
0.04466	0.05312	0.04290				0.04514	0.10170	0.07777	0.00541	0.00904	0.00566	0.00000	0.00600	0.00000	
0.04466	0.05312	0.04290				0.04689	0.11667	0.07969	0.00598	0.00936	0.00579	0.00000	0.00159	0.00000	
0.04466	0.05312	0.04290				0.08657	0.12328	0.08391	0.00680	0.00965	0.00617	0.00000	0.00126	0.00000	
0.04466	0.05312	0.04290				0.09615	0.12800	0.11913	0.00699	0.00974	0.00655	0.00000	0.00106	0.00000	
0.04466	0.05512	0.04290				0.11125	0.08909	0.12464	0.00755	0.00937	0.00687	0.00000	0.02709	0.00000	
0.04466	0.05512	0.04290				0.12312	0.10084	0.14079	0.00814	0.00956	0.00705	0.00000	0.01198	0.00000	
0.04466	0.05512	0.04590				0.13405	0.10334	0.05396	0.00844	0.00990	0.00581	0.00000	0.00721	0.00000	
0.04665	0.05512	0.04590				0.11076	0.11287	0.05533	0.00810	0.01012	0.00590	0.00000	0.00219	0.00000	
0.04665	0.04112	0.04590				0.10573	0.06443	0.05876	0.00788	0.00495	0.00614	0.00000	0.00438	0.00000	
0.04665	0.04112	0.04590				0.09214	0.06014	0.06362	0.00750	0.00496	0.00648	0.00000	0.00613	0.00000	
0.04665	0.04112	0.04590				0.06763	0.05549	0.08426	0.00697	0.00495	0.00678	0.00000	0.01103	0.00000	
0.04665	0.04112	0.04590				0.05587	0.09528	0.12027	0.00650	0.00586	0.00717	0.00000	0.00169	0.00000	
0.04965	0.04112	0.04590				0.05933	0.10381	0.12475	0.00716	0.00592	0.00745	0.00000	0.00031	0.00000	
0.04965	0.04112	0.04590				0.06008	0.10997	0.14299	0.00760	0.00621	0.00777	0.00000	0.00035	0.00000	
0.04965	0.04112	0.04940				0.07598	0.12130	0.08850	0.00845	0.00653	0.00789	0.00000	0.00016	0.00000	
0.04965	0.04112	0.04940				0.09499	0.13849	0.06539	0.00798	0.00700	0.00730	0.00000	0.00004	0.00000	
0.05264	0.03363	0.04940				0.06079	0.14520	0.07083	0.00788	0.00537	0.00747	0.00000	0.00000	0.00000	
0.05264	0.03812	0.04940				0.06409	0.09053	0.08323	0.00864	0.00539	0.00776	0.00000	0.00000	0.00000	
0.05264	0.04232	0.04940				0.07598	0.06340	0.11715	0.00910	0.00541	0.00791	0.00000	0.00000	0.00000	
0.05264	0.04232	0.04940				0.08873	0.07204	0.12416	0.00925	0.00577	0.00818	0.00000	0.00000	0.00000	
0.05563	0.04412	0.04940				0.05990	0.05858	0.12671	0.00920	0.00572	0.00850	0.00000	0.00000	0.00000	
0.05563	0.04412	0.04940				0.06228	0.06443	0.12952	0.01013	0.00592	0.00873	0.00000	0.00000	0.00000	
0.05563	0.04412	0.04940				0.06462	0.06252	0.15697	0.00913	0.00586	0.00898	0.00000	0.00000	0.00000	
	0.04412	0.05290					0.06553	0.08433		0.00595	0.00926		0.00000	0.00000	
	0.04412	0.05290					0.09068	0.11964		0.00617	0.00922		0.00000	0.00000	
	0.04412	0.05290					0.09185	0.11787		0.00636	0.00933		0.00000	0.00000	
	0.04412	0.05290					0.09401	0.13236		0.00649	0.01020		0.00000	0.00000	
	0.04412	0.05290					0.09532	0.16066		0.00656	0.01050		0.00000	0.00000	
	0.04412	0.05040					0.10671	0.07000		0.00674	0.00776		0.00000	0.00000	
	0.04412	0.05040					0.11212	0.07455		0.00696	0.00803		0.00000	0.00000	
	0.04412	0.05040					0.11450	0.07780		0.00718	0.00791		0.00000	0.00000	
	0.04412	0.05040					0.11859	0.08038		0.00727	0.00812		0.00000	0.00000	
	0.04662	0.05040					0.06663	0.11888		0.00654	0.00836		0.00000	0.00000	
	0.04662	0.05040					0.08800	0.12239		0.00680	0.00851		0.00000	0.00000	
	0.04662	0.05040					0.07973	0.12449		0.00652	0.00864		0.00000	0.00000	
	0.04662	0.05040					0.09191	0.12647		0.00678	0.00877		0.00000	0.00000	
	0.04662	0.05040					0.09208	0.12830		0.00671	0.00899		0.00000	0.00000	
	0.04662	0.05040					0.09495	0.13595		0.00718	0.00920		0.00000	0.00000	
	0.04662						0.09700			0.00707			0.00000		
	0.04662						0.10161			0.00733			0.00000		
	0.04662						0.11129			0.00740			0.00000		
	0.04662						0.11828			0.00794			0.00000		

PRESSURIZED VERTICAL FLOW CONSTRICTION															
[m]			*[not applicable]*			*[m]*			*[m³/s]*			*[kg/s]*			
a			***b***			***h_0***			***Q***			***Q_b***			
S_o=2.0%	***S_o=3.5%***	***S_o=5.5%***	***S_o=2.0%***	***S_o=3.5%***	***S_o=5.5%***	***S_o=2.0%***	***S_o=3.5%***	***S_o=5.5%***	***S_o=2.0%***	***S_o=3.5%***	***S_o=5.5%***	***S_o=2.0%***	***S_o=3.5%***	***S_o=5.5%***	
	0.04662						0.12462			0.00790			0.00000		
	0.04662						0.13023			0.00799			0.00000		
	0.04662						0.13349			0.00835			0.00000		
	0.04662						0.14271			0.00853			0.00000		
	0.04882						0.05993			0.00709			0.00000		
	0.04882						0.05796			0.00691			0.00000		
	0.04882						0.06012			0.00693			0.00000		
	0.04882						0.06826			0.00719			0.00000		
	0.04882						0.09421			0.00744			0.00000		
	0.04882						0.09802			0.00771			0.00000		
	0.04882						0.10203			0.00783			0.00000		
	0.04882						0.11292			0.00803			0.00000		
	0.04882						0.11998			0.00830			0.00000		
	0.04882						0.12759			0.00853			0.00000		
	0.04882						0.13250			0.00882			0.00000		
	0.05312						0.06549			0.00840			0.00000		
	0.05312						0.06697			0.00856			0.00000		
	0.05312						0.09762			0.00881			0.00000		
	0.05312						0.10105			0.00909			0.00000		
	0.05312						0.11554			0.00944			0.00000		
	0.05312						0.12542			0.00965			0.00000		
	0.05312						0.12928			0.00966			0.00000		
	0.05512						0.07567			0.00935			0.00000		
	0.05512						0.09921			0.00960			0.00000		
	0.05512						0.10464			0.00986			0.00000		
	0.05512						0.11064			0.01008			0.00000		
	0.04112						0.05834			0.00495			0.00000		
	0.04112						0.05996			0.00495			0.00000		
	0.04112						0.05135			0.00485			0.00000		
	0.04112						0.09255			0.00579			0.00000		
	0.04112						0.10410			0.00591			0.00000		
	0.04112						0.11145			0.00613			0.00000		
	0.04112						0.12228			0.00662			0.00000		
	0.04112						0.13696			0.00691			0.00000		

PRESSURIZED COMBINED FLOW CONSTRICTION															
[m]			[m]			[m]			[m³/s]			[kg/s]			
a			b			h_0			Q			Q_b			
S_o=2.0%	S_o=3.5%	S_o=5.5%	S_o=2.0%	S_o=3.5%	S_o=5.5%	S_o=2.0%	S_o=3.5%	S_o=5.5%	S_o=2.0%	S_o=3.5%	S_o=5.5%	S_o=2.0%	S_o=3.5%	S_o=5.5%	
0.04601	0.04822	0.07005	0.18700	0.18700	0.13670	0.10016	0.10036	0.12076	0.00566	0.00646	0.00686	0.00026	0.00052	0.00434	
0.04900	0.04822	0.07005	0.18700	0.18700	0.13670	0.09628	0.09822	0.12154	0.00567	0.00643	0.00696	0.00050	0.00129	0.00288	
0.05150	0.04822	0.07005	0.18700	0.18700	0.13670	0.08006	0.10498	0.13937	0.00570	0.00650	0.00709	0.00066	0.00052	0.00031	
0.09090	0.04822	0.07740	0.10000	0.18700	0.13670	0.09851	0.11029	0.11562	0.00570	0.00667	0.00753	0.00073	0.00051	0.00248	
0.08691	0.04822	0.07740	0.10000	0.18700	0.13670	0.10249	0.11930	0.12016	0.00559	0.00690	0.00762	0.00003	0.00036	0.00347	
0.05898	0.04822	0.07740	0.15000	0.18700	0.13670	0.08516	0.12872	0.12183	0.00557	0.00711	0.00785	0.00012	0.00038	0.00407	
0.06097	0.04822	0.07740	0.15000	0.18700	0.13670	0.07826	0.13597	0.12288	0.00561	0.00733	0.00793	0.00059	0.00006	0.00552	
0.05599	0.04822	0.07740	0.15000	0.18700	0.13670	0.07453	0.14456	0.14390	0.00557	0.00750	0.00819	0.00061	0.00003	0.00054	
0.08890	0.05312	0.09525	0.10000	0.18700	0.13670	0.09690	0.09405	0.11823	0.00563	0.00675	0.00834	0.00007	0.00277	0.00808	
0.04501	0.05312	0.09525	0.20000	0.18700	0.13670	0.06094	0.09445	0.12167	0.00560	0.00659	0.00856	0.00113	0.00192	0.00826	
0.04501	0.05312	0.09525	0.20000	0.18700	0.13670	0.08017	0.09640	0.12502	0.00557	0.00697	0.00888	0.00014	0.00275	0.00582	
0.04302	0.05312	0.09525	0.20000	0.18700	0.13670	0.08478	0.11416	0.12734	0.00589	0.00728	0.00908	0.00034	0.00124	0.00732	
0.05200	0.05312	0.09525	0.20000	0.18700	0.13670	0.08757	0.12271	0.15497	0.00642	0.00752	0.00925	0.00131	0.00079	0.00039	
0.05050	0.05312	0.05745	0.20000	0.18700	0.15000	0.09855	0.12540	0.08707	0.00649	0.00767	0.00598	0.00017	0.00072	0.02341	
0.06347	0.05312	0.05745	0.15000	0.18700	0.15000	0.10502	0.13180	0.12160	0.00647	0.00788	0.00600	0.00008	0.00025	0.00039	
0.06646	0.04692	0.05745	0.15000	0.15000	0.15000	0.08819	0.08783	0.12076	0.00643	0.00481	0.00584	0.00107	0.00027	0.00111	
0.06845	0.04692	0.06480	0.15000	0.15000	0.15000	0.08323	0.10236	0.10295	0.00652	0.00509	0.00602	0.00077	0.00006	0.00195	
0.05299	0.04692	0.06480	0.18700	0.15000	0.15000	0.09727	0.11155	0.10998	0.00654	0.00520	0.00614	0.00030	0.00002	0.00180	
0.05599	0.05821	0.06480	0.18700	0.15000	0.15000	0.08677	0.11551	0.11693	0.00658	0.00660	0.00648	0.00131	0.00027	0.00140	
0.05798	0.05821	0.06480	0.18700	0.15000	0.15000	0.08824	0.12429	0.11791	0.00655	0.00693	0.00663	0.00086	0.00031	0.00117	
0.05948	0.05821	0.06480	0.18700	0.15000	0.15000	0.09852	0.14277	0.11859	0.00736	0.00737	0.00677	0.00093	0.00002	0.00131	
0.06217	0.04862	0.06480	0.18700	0.20000	0.15000	0.08576	0.03793	0.12290	0.00732	0.00567	0.00699	0.00102		0.00175	
0.05818	0.04862	0.06480	0.18700	0.20000	0.15000	0.11289	0.05679	0.13974	0.00730	0.00613	0.00720	0.00031	0.01571	0.00018	
0.05818	0.04862	0.07110	0.20000	0.20000	0.15000	0.08475	0.09465	0.11209	0.00726	0.00641	0.00713	0.00180	0.00308	0.00354	
0.05698	0.04862	0.07110	0.20000	0.20000	0.15000	0.11315	0.09508	0.11781	0.00781	0.00625	0.00730	0.00007	0.00329	0.00377	
0.07893	0.04862	0.07110	0.15000	0.20000	0.15000	0.07466	0.10617	0.12006	0.00748	0.00656	0.00749	0.00406	0.00069	0.00344	
0.07444	0.04862	0.07110	0.15000	0.20000	0.15000	0.08949	0.11951	0.12131	0.00752	0.00686	0.00770	0.00272	0.00025	0.00326	
0.07294	0.04862	0.07110	0.15000	0.20000	0.15000	0.10172	0.13395	0.12407	0.00755	0.00725	0.00779	0.00069	0.00016	0.00246	
0.06925	0.05292	0.07110	0.15000	0.20000	0.15000	0.11939	0.12019	0.14304	0.00753	0.00766	0.00798	0.00023	0.00049	0.00038	
0.07494	0.05292	0.07530	0.15000	0.20000	0.15000	0.12350	0.12559	0.11844	0.00832	0.00782	0.00771	0.00010	0.00035	0.00433	
0.08142	0.05292	0.07530	0.15000	0.20000	0.15000	0.09400	0.13348	0.11593	0.00831	0.00816	0.00774	0.00139	0.00034	0.00334	
0.07843	0.05292	0.07530	0.15000	0.20000	0.15000	0.12826	0.14547	0.11925	0.00837	0.00833	0.00792	0.00061	0.00006	0.00389	
0.06446	0.05721	0.07530	0.20000	0.20000	0.15000	0.08876	0.09841	0.11892	0.00805	0.00792	0.00793	0.00171	0.00491	0.00413	
0.06197	0.05721	0.07530	0.20000	0.20000	0.15000	0.10058	0.10034	0.12111	0.00809	0.00812	0.00815	0.00069	0.00524	0.00432	
0.05848	0.05721	0.07530	0.20000	0.20000	0.15000	0.12121	0.11913	0.12460	0.00804	0.00828	0.00847	0.00009	0.00091	0.00372	
0.06197	0.05721	0.07530	0.18700	0.20000	0.15000	0.12337	0.12667	0.12406	0.00815	0.00851	0.00849	0.00010	0.00066	0.00502	
0.06716	0.05721	0.07530	0.18700	0.20000	0.15000	0.07327	0.12890	0.15270	0.00809	0.00862	0.00880	0.00297	0.00062	0.00044	
0.06496	0.05721	0.08055	0.18700	0.20000	0.15000	0.10425	0.13260	0.11589	0.00806	0.00875	0.00877	0.00061	0.00050	0.00964	
0.06496	0.05721	0.08055	0.18700	0.20000	0.15000	0.12941	0.13771	0.12305	0.00894	0.00900	0.00898	0.00003	0.00029	0.00712	
0.07015	0.05721	0.08055	0.18700	0.20000	0.15000	0.09668	0.13974	0.12240	0.00893	0.00901	0.00913	0.00253	0.00019	0.00723	
0.07115	0.06481	0.08055	0.18700	0.13700	0.15000	0.09531	0.12860	0.12482	0.00889	0.00732	0.00925	0.00313	0.00020	0.00954	
0.08511	0.06481	0.08055	0.15000	0.13700	0.15000	0.09963	0.11864	0.12697	0.00893	0.00720	0.00936	0.00141	0.00036	0.00550	
0.08242	0.06481	0.08055	0.15000	0.13700	0.15000	0.11322	0.11757	0.15666	0.00898	0.00701	0.00960	0.00070	0.00038	0.00022	
0.08092	0.06481	0.08580	0.15000	0.13700	0.10000	0.12495	0.11462	0.09976	0.00899	0.00696	0.00527	0.00013	0.00042	0.00026	
0.08392	0.06481	0.08580	0.15000	0.13700	0.10000	0.13397	0.11082	0.10514	0.00909	0.00684	0.00542	0.00002	0.00041	0.00008	
0.06845	0.06481	0.11730	0.20000	0.13700	0.10000	0.08644	0.10751	0.15026	0.00910	0.00666	0.00899	0.00317	0.00056	0.00025	
0.06646	0.06481	0.11730	0.20000	0.13700	0.10000	0.10891	0.09522	0.15079	0.00920	0.00655	0.00901	0.00150	0.00216	0.00027	
0.06397	0.06481	0.11730	0.20000	0.13700	0.10000	0.12307	0.09352	0.15645	0.00916	0.00652	0.00927	0.00033	0.00252	0.00005	
0.06247	0.06481	0.07005	0.20000	0.13700	0.13670	0.13164	0.09238	0.11976	0.00929	0.00635	0.00686	0.00008	0.00237	0.00000	
0.04601	0.06481	0.07005	0.18700	0.13700	0.13670	0.10056	0.14616	0.12048	0.00572	0.00759	0.00683	0.00000	0.00017	0.00000	
0.04900	0.07381	0.07005	0.18700	0.13700	0.13670	0.09810	0.09931	0.14007	0.00564	0.00759	0.00706	0.00000	0.00415	0.00000	
0.05150	0.07381	0.07740	0.18700	0.13700	0.13670	0.08018	0.10007	0.11795	0.00562	0.00778	0.00730	0.00000	0.00375	0.00000	
0.09090	0.07381	0.07740	0.10000	0.13700	0.13670	0.11916	0.12080	0.11928	0.00570	0.00801	0.00756	0.00000	0.00175	0.00000	
0.08691	0.07381	0.07740	0.10000	0.13700	0.13670	0.10295	0.13318	0.12150	0.00553	0.00833	0.00773	0.00000	0.00029	0.00000	
0.05898	0.07381	0.07740	0.15000	0.13700	0.13670	0.08585	0.13647	0.12252	0.00556	0.00854	0.00789	0.00000	0.00017	0.00000	
0.06097	0.07381	0.07740	0.15000	0.13700	0.13670	0.07862	0.15543	0.12659	0.00552	0.00909	0.00821	0.00000	0.00003	0.00000	
0.05599	0.05262	0.09525	0.15000	0.13700	0.13670	0.07450	0.10783	0.11940	0.00564	0.00541	0.00838	0.00000	0.00007	0.00000	
0.08890	0.05262	0.09525	0.10000	0.13700	0.13670	0.09650	0.09909	0.12084	0.00557	0.00512	0.00855	0.00000	0.00025	0.00000	
0.04501	0.05262	0.09525	0.20000	0.13700	0.13670	0.06000	0.13926	0.12349	0.00558	0.00616	0.00883	0.00000	0.00011	0.00000	
0.04501	0.05262	0.09525	0.20000	0.13700	0.13670	0.08000	0.17756	0.12583	0.00561	0.00708	0.00903	0.00000	0.00002	0.00000	
0.04302	0.04822	0.09525	0.20000	0.18700	0.13670	0.08000	0.09977	0.12786	0.00595	0.00646	0.00930	0.00000	0.00000	0.00000	
0.05200	0.04822	0.05745	0.20000	0.18700	0.15000	0.08500	0.10107	0.08825	0.00640	0.00639	0.00591	0.00000	0.00000	0.00000	
0.05050	0.04822	0.05745	0.20000	0.18700	0.15000	0.09850	0.10668	0.12191	0.00651	0.00648	0.00588	0.00000	0.00000	0.00000	
0.06347	0.04822	0.05745	0.15000	0.18700	0.15000	0.10500	0.11215	0.12158	0.00661	0.00666	0.00580	0.00000	0.00000	0.00000	
0.06646	0.04822	0.06480	0.15000	0.18700	0.15000	0.08600	0.12002	0.10460	0.00648	0.00684	0.00610	0.00000	0.00000	0.00000	
0.06845	0.04822	0.06480	0.15000	0.18700	0.15000	0.07766	0.12782	0.11061	0.00662	0.00713	0.00630	0.00000	0.00000	0.00000	
0.05299	0.04822	0.06480	0.18700	0.18700	0.15000	0.09700	0.13599	0.11583	0.00660	0.00735	0.00646	0.00000	0.00000	0.00000	
0.05599	0.04822	0.06480	0.18700	0.18700	0.15000	0.08600	0.14501	0.11856	0.00653	0.00745	0.00659	0.00000	0.00000	0.00000	
0.05798	0.05312	0.06480	0.18700	0.18700	0.15000	0.09926	0.09429	0.11960	0.00666	0.00670	0.00654	0.00000	0.00000	0.00000	
0.05948	0.05312	0.06480	0.18700	0.18700	0.15000	0.09869	0.09395	0.12300	0.00741	0.00668	0.00698	0.00000	0.00000	0.00000	
0.06217	0.05312	0.06480	0.18700	0.18700	0.15000	0.08677	0.09737	0.14336	0.00730	0.00687	0.00714	0.00000	0.00000	0.00000	
0.05818	0.05312	0.07110	0.18700	0.18700	0.15000	0.10893	0.11420	0.11550	0.00717	0.00734	0.00712	0.00000	0.00000	0.00000	
0.05818	0.05312	0.07110	0.20000	0.18700	0.15000	0.08559	0.12115	0.12060	0.00723	0.00760	0.00727	0.00000	0.00000	0.00000	
0.05698	0.05312	0.07110	0.20000	0.18700	0.15000	0.11644	0.12735	0.12111	0.00767	0.00777	0.00752	0.00000	0.00000	0.00000	
0.07893	0.05312	0.07110	0.15000	0.18700	0.15000	0.07400	0.13173	0.12117	0.00764	0.00782	0.00753	0.00000	0.00000	0.00000	
0.07444	0.04692	0.07110	0.15000	0.15000	0.15000	0.08850	0.08764	0.12382	0.00758	0.00461	0.00776	0.00000	0.00000	0.00000	
0.07294	0.04692	0.07110	0.15000	0.15000	0.15000	0.09900	0.10410	0.14499	0.00759	0.00508	0.00794	0.00000	0.00000	0.00000	
0.06925	0.04692	0.07530	0.15000	0.15000	0.15000	0.11800	0.11305	0.11648	0.00761	0.00531	0.00768	0.00000	0.00000	0.00000	
0.07494	0.05821	0.07530	0.15000	0.15000	0.15000	0.12350	0.11351	0.11684	0.00843	0.00664	0.00773	0.00000	0.00000	0.00000	
0.08142	0.05821	0.07530	0.15000	0.15000	0.15000	0.09400	0.12438	0.11790	0.00830	0.00686	0.00794	0.00000	0.00000	0.00000	
0.07843	0.05821	0.07530	0.15000	0.15000	0.15000	0.11400	0.13999	0.11998	0.00840	0.00746	0.00800	0.00000	0.00000	0.00000	
0.06446	0.04862	0.07530	0.20000	0.20000	0.15000	0.07450	0.04380	0.12432	0.00801	0.00568	0.00822	0.00000	0.00000	0.00000	
0.06197	0.04862	0.07530	0.20000	0.20000	0.15000	0.10000	0.05708	0.12420	0.00818	0.00633	0.00845	0.00000	0.00000	0.00000	
0.05848	0.04862	0.07530	0.20000	0.20000	0.15000	0.12000	0.09496	0.12591	0.00812	0.00647	0.00854	0.00000	0.00000	0.00000	
0.06197	0.04862	0.07530	0.18700	0.20000	0.15000	0.12250	0.09461	0.15275	0.00822	0.00624	0.00883	0.00000	0.00000	0.00000	
0.06716	0.04862	0.08055	0.18700	0.20000	0.15000	0.07300	0.11021	0.11820	0.00814	0.00644	0.00874	0.00000	0.00000	0.00000	

PRESSURIZED COMBINED FLOW CONSTRICTION															
[m]			*[m]*			*[m]*			*[m³/s]*			*[kg/s]*			
a			***b***			***h_0***			***Q***			***Q_b***			
S_o=2.0%	***S_o=3.5%***	***S_o=5.5%***	***S_o=2.0%***	***S_o=3.5%***	***S_o=5.5%***	***S_o=2.0%***	***S_o=3.5%***	***S_o=5.5%***	***S_o=2.0%***	***S_o=3.5%***	***S_o=5.5%***	***S_o=2.0%***	***S_o=3.5%***	***S_o=5.5%***	
0.06496	0.04862	0.08055	0.18700	0.20000	0.15000	0.09734	0.11834	0.12236	0.00815	0.00681	0.00891	0.00000	0.00000	0.00000	
0.06496	0.04862	0.08055	0.18700	0.20000	0.15000	0.12921	0.13476	0.12173	0.00895	0.00732	0.00904	0.00000	0.00000	0.00000	
0.07015	0.05292	0.08055	0.18700	0.20000	0.15000	0.09449	0.11894	0.12411	0.00896	0.00756	0.00923	0.00000	0.00000	0.00000	
0.07115	0.05292	0.08055	0.18700	0.20000	0.15000	0.08436	0.12586	0.12683	0.00893	0.00791	0.00934	0.00000	0.00000	0.00000	
0.08511	0.05292	0.08055	0.15000	0.20000	0.15000	0.09787	0.13354	0.13086	0.00895	0.00816	0.00966	0.00000	0.00000	0.00000	
0.08242	0.05292	0.08580	0.15000	0.20000	0.10000	0.10865	0.14512	0.10068	0.00903	0.00848	0.00527	0.00000	0.00000	0.00000	
0.08092	0.05721	0.08580	0.15000	0.20000	0.10000	0.12499	0.09882	0.10532	0.00900	0.00802	0.00537	0.00000	0.00000	0.00000	
0.08392	0.05721	0.11730	0.15000	0.20000	0.10000	0.13359	0.10308	0.14752	0.00912	0.00810	0.00911	0.00000	0.00000	0.00000	
0.06845	0.05721	0.11730	0.20000	0.20000	0.10000	0.09428	0.11768	0.14931	0.00902	0.00824	0.00910	0.00000	0.00000	0.00000	
0.06646	0.05721	0.11730	0.20000	0.20000	0.10000	0.10391	0.12336	0.15533	0.00916	0.00846	0.00936	0.00000	0.00000	0.00000	
0.06397	0.05721		0.20000	0.20000		0.12228	0.12876		0.00919	0.00858		0.00000	0.00000		
0.06247	0.05721		0.20000	0.20000		0.13147	0.13159		0.00922	0.00871		0.00000	0.00000		
	0.05721			0.20000			0.13583			0.00897			0.00000		
	0.05721			0.20000			0.14099			0.00900			0.00000		
	0.06481			0.13700			0.13038			0.00731			0.00000		
	0.06481			0.13700			0.12230			0.00702			0.00000		
	0.06481			0.13700			0.11931			0.00689			0.00000		
	0.06481			0.13700			0.11529			0.00684			0.00000		
	0.06481			0.13700			0.11224			0.00683			0.00000		
	0.06481			0.13700			0.10987			0.00676			0.00000		
	0.06481			0.13700			0.10543			0.00653			0.00000		
	0.06481			0.13700			0.09365			0.00635			0.00000		
	0.06481			0.13700			0.09319			0.00634			0.00000		
	0.06481			0.13700			0.14064			0.00758			0.00000		
	0.07381			0.13700			0.09847			0.00759			0.00000		
	0.07381			0.13700			0.10041			0.00764			0.00000		
	0.07381			0.13700			0.12071			0.00800			0.00000		
	0.07381			0.13700			0.13134			0.00833			0.00000		
	0.07381			0.13700			0.13785			0.00847			0.00000		
	0.07381			0.13700			0.15523			0.00896			0.00000		
	0.05262			0.13700			0.11058			0.00547			0.00000		
	0.05262			0.13700			0.10372			0.00516			0.00000		
	0.05262			0.13700			0.13640			0.00622			0.00000		
	0.05262			0.13700			0.16911			0.00727			0.00000		

FREE SURFACE LATERAL FLOW CONSTRICTION														
[not applicable]			*[m]*			*[m]*			*[m³/s]*			*[kg/s]*		
a			***b***			***h_0***			***Q***			***Q_b***		
S_o= 2.0%	***S_o=3.5%***	***S_o=5.5%***	***S_o=2.0%***	***S_o=3.5%***	***S_o=5.5%***	***S_o=2.0%***	***S_o=3.5%***	***S_o=5.5%***	***S_o=2.0%***	***S_o=3.5%***	***S_o=5.5%***	***S_o=2.0%***	***S_o=3.5%***	***S_o=5.5%***
			0.10000	0.20000	0.15000	0.10643	0.03392	0.02732	0.00703	0.00504	0.00522	0.00062	0.03148	0.19469
			0.10000	0.15000	0.15000	0.08316	0.04205	0.02674	0.00531	0.00500	0.00535	0.00022	0.01842	0.22165
			0.15000	0.10000	0.15000	0.07589	0.07043	0.02853	0.00741	0.00509	0.00541	0.00340	0.00215	0.22152
			0.15000	0.18640	0.15000	0.06987	0.03465	0.02343	0.00688	0.00508	0.00546	0.00207	0.03378	0.22892
			0.15000	0.13640	0.15000	0.05812	0.05359	0.02581	0.00528	0.00510	0.00561	0.00083	0.01081	0.25000
			0.17000	0.13640	0.15000	0.07152	0.05511	0.02748	0.00834	0.00529	0.00597	0.00637	0.01081	0.26136
			0.15000	0.18640	0.15000	0.08223	0.03699	0.02846	0.00845	0.00534	0.00605	0.00385	0.03304	0.29891
			0.17000	0.20000	0.15000	0.05938	0.03555	0.02930	0.00586	0.00535	0.00655	0.00166	0.04553	0.32609
			0.15000	0.15000	0.15000	0.07723	0.04393	0.03113	0.00661	0.00530	0.00676	0.00150	0.02174	0.34409
			0.18700	0.10000	0.15000	0.06182	0.07257	0.03230	0.00669	0.00540	0.00710	0.00362	0.00244	0.34146
			0.18700	0.10000	0.15000	0.06018	0.07833	0.03303	0.00587	0.00603	0.00749	0.00125	0.00625	0.41954
			0.15000	0.15000	0.15000	0.07747	0.04958	0.03370	0.00803	0.00602	0.00754	0.00504	0.03302	0.41758
			0.17000	0.20000	0.15000	0.06478	0.04022	0.03744	0.00693	0.00598	0.00775	0.00329	0.06118	0.41667
			0.15000	0.18640	0.15000	0.08616	0.03713	0.03560	0.00925	0.00599	0.00795	0.00441	0.04779	0.42771
			0.18700	0.13640	0.15000	0.06602	0.05731	0.03819	0.00742	0.00595	0.00817	0.00470	0.02427	0.44304
			0.15000	0.13640	0.15000	0.08866	0.05895	0.03677	0.00932	0.00633	0.00837	0.00638	0.04620	0.44253
			0.17000	0.18640	0.15000	0.06723	0.03735	0.03956	0.00739	0.00637	0.00874	0.00406	0.06771	0.44382
			0.17000	0.20000	0.15000	0.07059	0.03790	0.03998	0.00800	0.00640	0.00874	0.00535	0.06931	0.47727
			0.18700	0.15000	0.15000	0.07042	0.04726	0.04076	0.00876	0.00645	0.00893	0.00904	0.04032	0.50000
			0.20000	0.10000	0.15000	0.05204	0.08150	0.04150	0.00562	0.00642	0.00908	0.00249	0.00520	0.50676
			0.20000	0.10000	0.15000	0.06021	0.08539	0.04230	0.00698	0.00683	0.00913	0.00422	0.00263	0.51515
			0.18700	0.15000	0.15000	0.06778	0.06010	0.04400	0.00810	0.00670	0.00929	0.00477	0.04167	0.51899
			0.17000	0.20000	0.15000	0.07599	0.03908	0.04496	0.00974	0.00687	0.00966	0.01399	0.08733	0.51471
			0.17000	0.18640	0.15000	0.07396	0.04077	0.04281	0.00919	0.00684	0.00980	0.00893	0.07407	0.51899
			0.23400	0.13640	0.10000	0.04882	0.06265	0.09300	0.00660	0.00693	0.00972	0.00551	0.02660	0.07576
			0.20000	0.13640	0.10000	0.06689	0.06460	0.09167	0.00798	0.00737	0.00950	0.00613	0.03091	0.08667
			0.23400	0.18640	0.10000	0.05471	0.04108	0.09053	0.00693	0.00744	0.00946	0.00394	0.08696	0.09483
			0.18700	0.20000	0.10000	0.07484	0.04509	0.08850	0.00947	0.00748	0.00903	0.00786	0.08500	0.08661
			0.22000	0.15000	0.10000	0.06867	0.06147	0.07325	0.00923	0.00746	0.00890	0.00819	0.04505	0.09292
			0.23400	0.10000	0.10000	0.05785	0.08952	0.06991	0.00869	0.00742	0.00867	0.01633	0.00041	0.10753
			0.20000	0.10000	0.10000	0.07315	0.09931	0.07179	0.00974	0.00777	0.00844	0.01064	0.00059	0.13107
			0.23400	0.15000	0.10000	0.06026	0.06245	0.06775	0.00936	0.00788	0.00812	0.01845	0.03629	0.12500
			0.17000	0.20000	0.10000	0.05769	0.04159	0.06584	0.00538	0.00785	0.00784	0.00000	0.11616	0.09524
			0.10000	0.18640	0.10000	0.08364	0.04526	0.06765	0.00540	0.00772	0.00757	0.00000	0.10000	0.08889
			0.20000	0.13640	0.10000	0.05001	0.06504	0.06910	0.00541	0.00791	0.00743	0.00000	0.03140	0.08335
			0.23400	0.13640	0.10000	0.04101	0.06782	0.06344	0.00543	0.00837	0.00726	0.00000	0.03361	0.07817
			0.15000	0.18640	0.10000	0.05998	0.04323	0.06446	0.00544	0.00835	0.00702	0.00000	0.12288	0.06969
			0.23400	0.20000	0.10000	0.04490	0.04497	0.06109	0.00545	0.00828	0.00668	0.00000	0.13235	0.05947
			0.15000	0.15000	0.10000	0.06074	0.06524	0.05823	0.00546	0.00834	0.00642	0.00000	0.06383	0.05753
			0.10000	0.10000	0.10000	0.08287	0.10529	0.06163	0.00547	0.00834	0.00624	0.00000	0.00225	0.05271
			0.22000	0.10000	0.10000	0.04880	0.11021	0.05934	0.00549	0.00875	0.00606	0.00000	0.00387	0.05192
			0.20000	0.15000	0.10000	0.05107	0.06772	0.05715	0.00561	0.00883	0.00576	0.00000	0.04455	0.05187
			0.22000	0.20000	0.10000	0.04449	0.04560	0.05597	0.00562	0.00886	0.00575	0.00000	0.13699	0.05336
			0.22000	0.23600	0.10000	0.05088	0.04306	0.05432	0.00618	0.00881	0.00563	0.00000	0.16484	0.05053
			0.17000	0.18600	0.10000	0.06121	0.04699	0.05589	0.00618	0.00893	0.00562	0.00000	0.13333	0.05106
			0.20000	0.13600	0.05000	0.05271	0.07266	0.12801	0.00619	0.00885	0.00474	0.00000	0.02817	0.00021
			0.10000	0.13600	0.05000	0.08630	0.07626	0.13808	0.00619	0.00920	0.00523	0.00000	0.02206	0.00002
			0.15000	0.18600	0.05000	0.06423	0.04669	0.14101	0.00622	0.00917	0.00534	0.00000	0.15534	0.00003
			0.23400	0.23600	0.07670	0.04769	0.04660	0.05996	0.00623	0.00919	0.00518	0.00000	0.18421	0.01040
			0.20000	0.20000	0.07670	0.05711	0.04645	0.06651	0.00624	0.00926	0.00524	0.00000	0.16667	0.00799
			0.22000	0.15000	0.07670	0.05147	0.07145	0.07389	0.00631	0.00920	0.00585	0.00000	0.06707	0.00799
			0.23400	0.10000	0.07670	0.04836	0.10834	0.08521	0.00635	0.00926	0.00617	0.00000	0.00410	0.02470
			0.15000	0.10000	0.13670	0.06499	0.11208	0.02465	0.00649	0.00976	0.00532	0.00000	0.00347	0.21311
			0.10000	0.15000	0.13670	0.09635	0.07019	0.04485	0.00655	0.00976	0.00870	0.00000	0.07364	0.36486
			0.10000	0.20000	0.13670	0.09364	0.04855	0.04549	0.00657	0.00977	0.00903	0.00000	0.17089	0.40000
			0.22000	0.23600	0.13670	0.05191	0.04665	0.04878	0.00661	0.00987	0.00927	0.00000	0.19412	0.41667
			0.17000	0.18600	0.13670	0.06209	0.05534	0.04880	0.00664	0.00972	0.00936	0.00000	0.14646	0.40741
			0.23400	0.13600	0.13670	0.04909	0.08700	0.05487	0.00665	0.00974	0.00970	0.00000	0.05870	0.32653
			0.20000	0.20000	0.13670	0.05452	0.03359	0.04960	0.00666	0.00500	0.00962	0.00000	0.00000	0.34444
			0.23400	0.15000	0.15000	0.05029	0.03717	0.02433	0.00673	0.00505	0.00536	0.00000	0.00000	0.00000
			0.10000	0.10000	0.15000	0.09836	0.07013	0.02417	0.00677	0.00501	0.00525	0.00000	0.00000	0.00000
			0.15000	0.18640	0.15000	0.06551	0.03416	0.02444	0.00679	0.00499	0.00533	0.00000	0.00000	0.00000
			0.15000	0.13640	0.15000	0.07073	0.05122	0.02481	0.00682	0.00507	0.00549	0.00000	0.00000	0.00000
			0.22000	0.13640	0.15000	0.05173	0.05388	0.02535	0.00682	0.00535	0.00560	0.00000	0.00000	0.00000
			0.20000	0.18640	0.15000	0.04968	0.03487	0.02688	0.00690	0.00531	0.00587	0.00000	0.00000	0.00000
			0.10000	0.20000	0.15000	0.10795	0.03478	0.02636	0.00707	0.00539	0.00610	0.00000	0.00000	0.00000
			0.20000	0.15000	0.15000	0.06140	0.04014	0.02764	0.00709	0.00526	0.00645	0.00000	0.00000	0.00000
			0.20000	0.10000	0.15000	0.05689	0.07262	0.02956	0.00710	0.00530	0.00672	0.00000	0.00000	0.00000
			0.17000	0.10000	0.15000	0.06548	0.07815	0.03074	0.00713	0.00589	0.00703	0.00000	0.00000	0.00000
			0.22000	0.15000	0.15000	0.05442	0.04411	0.03091	0.00716	0.00608	0.00742	0.00000	0.00000	0.00000
			0.15000	0.20000	0.15000	0.07096	0.03649	0.03155	0.00717	0.00597	0.00757	0.00000	0.00000	0.00000
			0.23400	0.18640	0.15000	0.05077	0.03624	0.03208	0.00718	0.00602	0.00770	0.00000	0.00000	0.00000
			0.15000	0.13640	0.15000	0.07250	0.04581	0.03379	0.00720	0.00592	0.00795	0.00000	0.00000	0.00000
			0.22000	0.13640	0.15000	0.05522	0.05850	0.03507	0.00721	0.00640	0.00809	0.00000	0.00000	0.00000
			0.23400	0.18640	0.15000	0.05560	0.03679	0.03602	0.00723	0.00648	0.00833	0.00000	0.00000	0.00000
			0.10000	0.20000	0.15000	0.10839	0.03632	0.03680	0.00727	0.00636	0.00867	0.00000	0.00000	0.00000
			0.20000	0.15000	0.15000	0.05980	0.04656	0.03695	0.00762	0.00637	0.00873	0.00000	0.00000	0.00000
			0.15000	0.10000	0.15000	0.07577	0.08039	0.03755	0.00767	0.00648	0.00889	0.00000	0.00000	0.00000
			0.17000	0.10000	0.15000	0.06845	0.08461	0.03864	0.00772	0.00668	0.00911	0.00000	0.00000	0.00000
			0.23400	0.15000	0.15000	0.05266	0.05586	0.03999	0.00774	0.00685	0.00944	0.00000	0.00000	0.00000
			0.22000	0.20000	0.15000	0.05671	0.03772	0.04030	0.00775	0.00684	0.00941	0.00000	0.00000	0.00000
			0.10000	0.18640	0.15000	0.11538	0.03844	0.04110	0.00778	0.00676	0.00967	0.00000	0.00000	0.00000
			0.15000	0.13640	0.15000	0.07881	0.05954	0.04163	0.00806	0.00674	0.00982	0.00000	0.00000	0.00000
			0.17000	0.13640	0.10000	0.06972	0.06180	0.09302	0.00807	0.00743	0.00982	0.00000	0.00000	0.00000
			0.22000	0.18640	0.10000	0.05669	0.04005	0.08992	0.00812	0.00737	0.00966	0.00000	0.00000	0.00000
			0.10000	0.20000	0.10000	0.11932	0.03905	0.09184	0.00812	0.00737	0.00944	0.00000	0.00000	0.00000

FREE SURFACE LATERAL FLOW CONSTRICTION														
[not applicable]			*[m]*			*[m]*			*[m³/s]*			*[kg/s]*		
a			***b***			***h_0***			***Q***			***Q_b***		
S_o= 2.0%	***S_o=3.5%***	***S_o=5.5%***	***S_o=2.0%***	***S_o=3.5%***	***S_o=5.5%***	***S_o=2.0%***	***S_o=3.5%***	***S_o=5.5%***	***S_o=2.0%***	***S_o=3.5%***	***S_o=5.5%***	***S_o=2.0%***	***S_o=3.5%***	***S_o=5.5%***
			0.20000	0.15000	0.10000	0.05615	0.05945	0.08826	0.00817	0.00737	0.00904	0.00000	0.00000	0.00000
			0.23400	0.10000	0.10000	0.05592	0.09001	0.07263	0.00821	0.00739	0.00885	0.00000	0.00000	0.00000
			0.17000	0.10000	0.10000	0.07215	0.10089	0.07034	0.00854	0.00781	0.00869	0.00000	0.00000	0.00000
			0.10000	0.15000	0.10000	0.12656	0.06189	0.06988	0.00855	0.00773	0.00843	0.00000	0.00000	0.00000
			0.23400	0.20000	0.10000	0.05752	0.04046	0.06785	0.00855	0.00781	0.00820	0.00000	0.00000	0.00000
			0.20000	0.18640	0.10000	0.05795	0.04141	0.06734	0.00857	0.00793	0.00785	0.00000	0.00000	0.00000
			0.15000	0.13640	0.10000	0.07987	0.06349	0.06632	0.00858	0.00787	0.00765	0.00000	0.00000	0.00000
			0.22000	0.13640	0.10000	0.05612	0.06626	0.06634	0.00859	0.00840	0.00754	0.00000	0.00000	0.00000
			0.23400	0.18640	0.10000	0.05778	0.04384	0.06448	0.00870	0.00837	0.00730	0.00000	0.00000	0.00000
			0.10000	0.20000	0.10000	0.12988	0.04222	0.06299	0.00871	0.00839	0.00706	0.00000	0.00000	0.00000
			0.22000	0.15000	0.10000	0.05671	0.06392	0.06158	0.00873	0.00832	0.00672	0.00000	0.00000	0.00000
			0.15000	0.10000	0.10000	0.08251	0.10517	0.06024	0.00875	0.00839	0.00652	0.00000	0.00000	0.00000
			0.20000	0.10000	0.10000	0.06073	0.10946	0.05646	0.00876	0.00873	0.00621	0.00000	0.00000	0.00000
			0.17000	0.15000	0.10000	0.07284	0.06614	0.05567	0.00889	0.00875	0.00598	0.00000	0.00000	0.00000
			0.23400	0.20000	0.10000	0.05725	0.04348	0.05380	0.00939	0.00894	0.00582	0.00000	0.00000	0.00000
			0.15000	0.23600	0.10000	0.08286	0.04252	0.05384	0.00941	0.00874	0.00570	0.00000	0.00000	0.00000
			0.10000	0.18600	0.10000	0.13853	0.04492	0.05320	0.00941	0.00896	0.00565	0.00000	0.00000	0.00000
			0.22000	0.13600	0.10000	0.05892	0.06990	0.05387	0.00943	0.00878	0.00558	0.00000	0.00000	0.00000
			0.20000	0.13600	0.05000	0.06598	0.07418	0.12776	0.00944	0.00909	0.00487	0.00000	0.00000	0.00000
			0.17000	0.18600	0.05000	0.07483	0.04628	0.13895	0.00945	0.00915	0.00530	0.00000	0.00000	0.00000
				0.23600	0.05000		0.04345	0.14398		0.00930	0.00542		0.00000	0.00000
				0.20000	0.07670		0.04499	0.05796		0.00944	0.00519		0.00000	0.00000
				0.15000	0.07670		0.06865	0.05831		0.00938	0.00527		0.00000	0.00000
				0.10000	0.07670		0.10993	0.06211		0.00926	0.00550		0.00000	0.00000
				0.10000	0.07670		0.11384	0.08511		0.00971	0.00615		0.00000	0.00000
				0.15000	0.07670		0.07029	0.08841		0.00977	0.00675		0.00000	0.00000
				0.20000	0.07670		0.04650	0.11059		0.00972	0.00641		0.00000	0.00000
				0.23600	0.13670		0.04549	0.02400		0.00985	0.00519		0.00000	0.00000
				0.18600	0.13670		0.04921	0.04013		0.00973	0.00867		0.00000	0.00000
				0.13600	0.13670		0.08064	0.04202		0.00977	0.00914		0.00000	0.00000
					0.13670			0.04383			0.00929			0.00000
					0.13670			0.04549			0.00948			0.00000
					0.13670			0.04545			0.00963			0.00000
					0.13670			0.04584			0.00973			0.00000

A.4.2 Data tables of hydraulic and mechanical control barriers (to Chpt. 6)

The following tables contain the measurement data of the experiments for the analysis of the clogging of overflown barriers for the hydraulic and mechanical deposition controls shown in Chpt. 6. The following variables are listed:

Latin letters		
a	m	constriction height
a_{*D}	–	grain-related relative constriction height
b	m	constriction width
b_{*D}	–	grain related relative constriction width
F_*	–	flow intensity
h_0	m	flow depth upstream of permeable barriers
h_{nc}	m	flow depth, non-constricted channel
Q	$m^3\ s^{-1}$	pump (water) discharge
$Q_{b,o}$	$kg\ s^{-1}$	bed load outflow rate
S_0	$m\ m^{-1}$	channel slope
t	s	time, duration

Greek letters		
Φ	–	bed load transport intensity (outflow)
θ	–	relative reduction of the bed load transport capacity

a [m]	b [m]	S_0 [-]	HY non-overflown (1)
0.0685	0.1367	0.055	

[s]	[m³/s]	[kg/s]	[m]	[m]	[-]
t	**Q**	**Q_{bo}**	**h_0**	**h_{nc} (theo.)**	**Φ**
0	0.00747	0.0000	0.120	0.038	0.00000
30	0.00758	0.0035	0.120	0.038	0.00151
60	0.00745	0.0023	0.119	0.038	0.00101
90	0.00758	0.0045	0.122	0.038	0.00190
120	0.00752	0.0026	0.124	0.038	0.00109
150	0.00743	0.0041	0.128	0.038	0.00168
180	0.00745	0.0026	0.129	0.038	0.00104
210	0.00739	0.0017	0.132	0.038	0.00068
240	0.00750	0.0018	0.137	0.038	0.00071
270	0.00747	0.0000	0.139	0.038	0.00000
300	0.00757	0.0000	0.140	0.038	0.00000
330	0.00747	0.0003	0.141	0.038	0.00013
360	0.00746	0.0030	0.138	0.037	0.00118
0	0.00570	0.0000	0.115	0.034	0.00000
30	0.00589	0.0000	0.094	0.034	0.00000
60	0.00588	0.0040	0.090	0.034	0.00213
90	0.00583	0.0062	0.090	0.034	0.00330
120	0.00580	0.0136	0.089	0.034	0.00718
150	0.00588	0.0160	0.092	0.034	0.00829
180	0.00579	0.0141	0.088	0.034	0.00758
210	0.00564	0.0113	0.082	0.034	0.00635
240	0.00581	0.0167	0.070	0.034	0.01036
270	0.00583	0.0219	0.058	0.034	0.01524
300	0.00596	0.0974	0.041	0.034	0.08095
330	0.00567	0.0218	0.040	0.034	0.01844
360	0.00577	0.0163	0.037	0.034	0.01430
390	0.00574	0.0094	0.037	0.034	0.00827

a [m]	b [m]	S_0 [-]	HY non-overflown (2)
0.0835	0.1367	0.055	

[s]	[m³/s]	[kg/s]	[m]	[m]	[-]
t	**Q**	**Q_{bo}**	**h_0**	**h_{nc} (theo.)**	**Φ**
0	0.00999	0.0000	0.155	0.044	0.00000
30	0.00995	0.0000	0.154	0.044	0.00000
60	0.01008	0.0013	0.154	0.044	0.00045
90	0.00983	0.0003	0.153	0.044	0.00010
120	0.01009	0.0003	0.154	0.045	0.00011
150	0.01003	0.0001	0.156	0.044	0.00005
0	0.00807	0.0002	0.158	0.042	0.00007
30	0.00819	0.0000	0.162	0.040	0.00000
60	0.00801	0.0001	0.161	0.039	0.00002
90	0.00818	0.0000	0.142	0.040	0.00000
120	0.00815	0.0001	0.133	0.040	0.00003
150	0.00815	0.0002	0.133	0.040	0.00008
180	0.00824	0.0001	0.134	0.040	0.00003
210	0.00796	0.0007	0.134	0.039	0.00029
0	0.00755	0.0013	0.133	0.038	0.00052
30	0.00769	0.0011	0.134	0.039	0.00042
60	0.00756	0.0023	0.127	0.038	0.00093
90	0.00756	0.0028	0.123	0.038	0.00117
120	0.00763	0.0078	0.122	0.039	0.00331
150	0.00773	0.0071	0.122	0.036	0.00303
0	0.00572	0.0100	0.122	0.034	0.00423
30	0.00589	0.0061	0.123	0.034	0.00256
60	0.00575	0.0064	0.105	0.034	0.00305
90	0.00587	0.0156	0.079	0.034	0.00901
120	0.00576	0.0572	0.066	0.034	0.03692
150	0.00602	0.0678	0.054	0.035	0.04891
180	0.00582	0.0851	0.044	0.034	0.06823
210	0.00578	0.0168	0.043	0.034	0.01366

a [m]	b [m]	S_0 [-]	HY non-overflown (3)
0.0825	0.100	0.055	

[s]	[m³/s]	[kg/s]	[m]	[m]	[-]
t	**Q**	**Q_{bo}**	**h_0**	**h_{nc} (theo.)**	**Φ**
0	0.00696	0.0000	0.136	0.037	0.00000
30	0.00699	0.0000	0.134	0.037	0.00000
60	0.00705	0.0003	0.133	0.037	0.00013
90	0.00695	0.0020	0.138	0.037	0.00076
120	0.00706	0.0003	0.140	0.037	0.00010
150	0.00706	0.0000	0.142	0.037	0.00000
180	0.00702	0.0000	0.144	0.037	0.00000
210	0.00705	0.0000	0.145	0.037	0.00000
240	0.00698	0.0000	0.147	0.037	0.00000
270	0.00707	0.0000	0.148	0.037	0.00000
300	0.00708	0.0000	0.150	0.037	0.00000
330	0.00700	0.0000	0.151	0.037	0.00000
360	0.00694	0.0000	0.151	0.037	0.00000
390	0.00706	0.0000	0.152	0.037	0.00000
420	0.00703	0.0000	0.153	0.037	0.00000
450	0.00699	0.0000	0.155	0.037	0.00000
480	0.00681	0.0000	0.155	0.037	0.00000
510	0.00714	0.0000	0.155	0.037	0.00000
540	0.00717	0.0000	0.155	0.037	0.00000
570	0.00699	0.0000	0.155	0.037	0.00000
600	0.00704	0.0000	0.153	0.037	0.00000
630	0.00721	0.0000	0.153	0.038	0.00000
660	0.00707	0.0000	0.153	0.037	0.00000
690	0.00720	0.0000	0.154	0.037	0.00000
720	0.00711	0.0000	0.155	0.037	0.00000
750	0.00704	0.0000	0.155	0.037	0.00000
780	0.00694	0.0000	0.155	0.037	0.00000
810	0.00703	0.0000	0.155	0.037	0.00000
840	0.00694	0.0000	0.156	0.037	0.00000
870	0.00695	0.0000	0.154	0.037	0.00000

a [m]	b [m]	S_0 [-]	HY non-overflown (4) - arb. variations
0.0825	0.100	0.055	

[s]	[m³/s]	[kg/s]	[m]	[m]	[-]
t	**Q**	**Q_{bo}**	**h_0**	**h_{nc} (theo.)**	**Φ**
0	0.00549	0.0000	0.154	0.033	0.00000
30	0.00564	0.0000	0.155	0.034	0.00000
60	0.00577	0.0000	0.141	0.034	0.00000
90	0.00576	0.0000	0.121	0.034	0.00000
120	0.00556	0.0000	0.117	0.034	0.00000
150	0.00563	0.0000	0.116	0.034	0.00000
180	0.00566	0.0000	0.116	0.034	0.00000
210	0.00552	0.0000	0.117	0.033	0.00000
240	0.00562	0.0000	0.116	0.034	0.00000
270	0.00559	0.0000	0.115	0.034	0.00000
300	0.00545	0.0000	0.114	0.033	0.00000
330	0.00547	0.0000	0.111	0.033	0.00000
0	0.00520	0.0000	0.109	0.033	0.00000
30	0.00523	0.0000	0.105	0.033	0.00000
60	0.00517	0.0000	0.103	0.033	0.00000
90	0.00512	0.0000	0.095	0.032	0.00000
120	0.00512	0.0000	0.090	0.032	0.00000
150	0.00497	0.0001	0.092	0.032	0.00005
0	0.00473	0.0002	0.087	0.032	0.00011
30	0.00464	0.0000	0.084	0.031	0.00000
60	0.00452	0.0017	0.080	0.031	0.00098
90	0.00453	0.0012	0.080	0.031	0.00068
0	0.00419	0.0000	0.080	0.030	0.00000
30	0.00419	0.0000	0.078	0.030	0.00000
60	0.00409	0.0002	0.074	0.030	0.00012
90	0.00392	0.0000	0.074	0.030	0.00000
0	0.00357	0.0000	0.074	0.029	0.00000
30	0.00366	0.0000	0.073	0.029	0.00000
60	0.00361	0.0000	0.073	0.024	0.00000
0	0.00074	0.0002	0.066	0.022	0.00011
30	0.00100	0.0000	0.059	0.022	0.00000
60	0.00070	0.0013	0.048	0.022	0.00100
90	0.00001	0.0005	0.043	0.020	0.00038
120	0.00002	0.0000	0.043	0.020	0.00000
150	0.00002	0.0000	0.039	0.020	0.00000
180	0.00001	0.0007	0.030	0.020	0.00064
210	0.00003	0.0000	0.027	0.020	0.00000
240	0.00233	0.0000	0.026	0.026	0.00000
0	0.00542	0.0000	0.022	0.033	0.00000
30	0.00538	0.0000	0.019	0.033	0.00000
60	0.00534	0.0000	0.049	0.033	0.00000
90	0.00536	0.0058	0.088	0.033	0.00312
120	0.00597	0.0000	0.093	0.035	0.00000
150	0.00684	0.0000	0.093	0.037	0.00000

a [m]	b [m]	S_0 [-]	HY non-overflown (5)
0.125	0.100	0.055	

[s]	[m³/s]	[kg/s]	[m]	[m]	[-]
t	**Q**	**Q_{bo}**	**h_0**	**h_{nc} (theo.)**	**Φ**
0	0.00662	0.0000	0.089	0.036	0.00000
30	0.00656	0.0000	0.109	0.036	0.00000
60	0.00677	0.0000	0.116	0.036	0.00000
90	0.00693	0.0007	0.117	0.037	0.00032
120	0.00657	0.0000	0.117	0.036	0.00000
150	0.00685	0.0000	0.108	0.037	0.00000
180	0.00671	0.0069	0.091	0.036	0.00359
210	0.00678	0.0195	0.087	0.036	0.01053
240	0.00691	0.0495	0.086	0.037	0.02687
270	0.00675	0.0992	0.068	0.036	0.06271
300	0.00675	0.1059	0.075	0.036	0.06282
330	0.00693	0.1214	0.084	0.037	0.06691
360	0.00693	0.0729	0.093	0.037	0.03762
390	0.00674	0.0273	0.088	0.036	0.01458
420	0.00696	0.0352	0.099	0.037	0.01734
450	0.00691	0.0263	0.097	0.037	0.01314
480	0.00677	0.0359	0.093	0.036	0.01843
510	0.00682	0.0354	0.092	0.037	0.01834
540	0.00684	0.0451	0.087	0.037	0.02431
570	0.00670	0.0466	0.082	0.036	0.02606
600	0.00690	0.0310	0.087	0.037	0.01664
630	0.00684	0.0359	0.083	0.037	0.01994
660	0.00679	0.0378	0.082	0.036	0.02109
690	0.00694	0.0083	0.071	0.037	0.00511
720	0.00675	0.0245	0.064	0.036	0.01597
750	0.00679	0.0432	0.061	0.037	0.02920
780	0.00668	0.0151	0.061	0.036	0.01019
810	0.00675	0.0069	0.063	0.036	0.00454
840	0.00689	0.0019	0.064	0.037	0.00124
870	0.00682	0.0030	0.063	0.037	0.00198
900	0.00674	0.0013		0.036	
930	0.00684	0.0012		0.037	

HY (overflown) ONLY										
[m³/s]	*[kg/s]*	*[m]*	*[m]*	*[m]*	*[-]*	*[-]*	*[-]*	*[-]*	*[-]*	*[-]*
Q	**Q_{bo}**	**h_0**	**a**	**b**	**a_{*D}**	**b_{*D}**	**Φ**	**ϑ**	**F_***	**a_{*D}/h_{*D}**
0.00825	0.1023	0.112	0.0395	0.15	2.887	10.965	0.0463	0.2226	0.5929	0.3535
0.00798	0.1140	0.104	0.0395	0.15	2.887	10.965	0.0544	0.2581	0.6505	0.3804
0.00848	0.1140	0.112	0.0395	0.15	2.887	10.965	0.0516	0.2404	0.6100	0.3538
0.00924	0.1567	0.118	0.0395	0.15	2.887	10.965	0.0681	0.3014	0.6027	0.3343
0.00961	0.1976	0.114	0.0395	0.15	2.887	10.965	0.0882	0.3655	0.6679	0.3467
0.00763	0.0849	0.111	0.0395	0.15	2.887	10.965	0.0387	0.2037	0.5563	0.3566
0.00712	0.0794	0.105	0.0395	0.15	2.887	10.965	0.0377	0.2093	0.5735	0.3778
0.00640	0.0594	0.106	0.0395	0.15	2.887	10.965	0.0279	0.1855	0.5027	0.3723
0.00610	0.0485	0.107	0.043	0.15	3.143	10.965	0.0226	0.1655	0.4699	0.4009
0.00689	0.0876	0.107	0.043	0.15	3.143	10.965	0.0409	0.2425	0.5341	0.4022
0.00757	0.1058	0.104	0.043	0.15	3.143	10.965	0.0503	0.2561	0.6118	0.4120
0.00829	0.1403	0.110	0.043	0.15	3.143	10.965	0.0642	0.3040	0.6102	0.3904
0.00864	0.1649	0.112	0.043	0.15	3.143	10.965	0.0744	0.3406	0.6166	0.3833
0.00906	0.1740	0.110	0.043	0.15	3.143	10.965	0.0799	0.3414	0.6733	0.3924
0.00957	0.1794	0.107	0.043	0.15	3.143	10.965	0.0835	0.3333	0.7348	0.4000
0.01002	0.1903	0.113	0.043	0.15	3.143	10.965	0.0853	0.3385	0.7019	0.3793
0.00648	0.0485	0.109	0.047	0.15	3.436	10.965	0.0223	0.1482	0.4847	0.4305
0.00709	0.0767	0.101	0.047	0.15	3.436	10.965	0.0373	0.2033	0.6063	0.4655
0.00765	0.1176	0.097	0.047	0.15	3.436	10.965	0.0590	0.2811	0.7028	0.4858
0.00820	0.1194	0.102	0.047	0.15	3.436	10.965	0.0577	0.2618	0.6888	0.4607
0.00870	0.1740	0.109	0.047	0.15	3.436	10.965	0.0802	0.3568	0.6529	0.4315
0.00883	0.1703	0.112	0.047	0.15	3.436	10.965	0.0770	0.3435	0.6316	0.4195
0.00941	0.1885	0.113	0.047	0.15	3.436	10.965	0.0845	0.3560	0.6604	0.4149
0.00978	0.2303	0.113	0.047	0.15	3.436	10.965	0.1033	0.4190	0.6877	0.4155
0.01233	0.3156	0.111	0.047	0.15	3.436	10.965	0.1435	0.4710	0.8949	0.4230

[m³/s]	[kg/s]	[m]	[-]	[-]	[-]	[-]	
Q	Q_{bo}	h_0	a_{*D}	b_{*D}	ϑ	F_*	
0.00352	0.0083	0.0372	3.436	10.965	0.059	1.467	HY(a = 0.047m, b=0.150m) + MEC
0.00354	0.0183	0.0370	3.436	10.965	0.129	1.484	
0.00350	0.0275	0.0371	3.436	10.965	0.196	1.466	
0.00360	0.0367	0.0375	3.436	10.965	0.252	1.480	
0.00356	0.0479	0.0373	3.436	10.965	0.334	1.480	
0.00348	0.0575	0.0359	3.436	10.965	0.413	1.527	
0.00345	0.0700	0.0358	3.436	10.965	0.510	1.518	
0.00365	0.0800	0.0378	3.436	10.965	0.540	1.484	
0.00347	0.1000	0.0359	3.436	10.965	0.722	1.523	
0.00358	0.1200	0.0374	3.436	10.965	0.832	1.479	
0.00360	0.1149	0.0375	3.436	10.965	0.789	1.482	
0.00363	0.0534	0.0376	3.436	10.965	0.363	1.491	
0.00405	0.0574	0.0402	3.436	10.965	0.336	1.507	
0.00400	0.0479	0.0400	3.436	10.965	0.286	1.496	
0.00400	0.0575	0.0401	3.436	10.965	0.343	1.491	
0.00382	0.0700	0.0384	3.436	10.965	0.443	1.519	
0.00396	0.0700	0.0400	3.436	10.965	0.423	1.484	
0.00394	0.0800	0.0400	3.436	10.965	0.486	1.477	
0.00397	0.0799	0.0399	3.436	10.965	0.482	1.491	
0.00397	0.0800	0.0399	3.436	10.965	0.481	1.490	
0.00393	0.0876	0.0398	3.436	10.965	0.534	1.485	
0.00389	0.1000	0.0382	3.436	10.965	0.618	1.562	
0.00393	0.1000	0.0396	3.436	10.965	0.611	1.491	
0.00363	0.0689	0.0378	3.436	10.965	0.468	1.478	
0.00398	0.1200	0.0398	3.436	10.965	0.719	1.503	
0.00393	0.1200	0.0397	3.436	10.965	0.734	1.484	
0.00400	0.1318	0.0400	3.436	10.965	0.785	1.498	
0.00398	0.1319	0.0400	3.436	10.965	0.792	1.490	
0.00400	0.0600	0.0402	3.436	10.965	0.357	1.488	
0.00455	0.1085	0.0469	3.436	10.965	0.543	1.339	
0.00447	0.1200	0.0468	3.436	10.965	0.615	1.321	
0.00460	0.1199	0.0479	3.436	10.965	0.591	1.314	
0.00435	0.1162	0.0457	3.436	10.965	0.618	1.332	
0.00445	0.1253	0.0464	3.436	10.965	0.646	1.335	
0.00445	0.0587	0.0464	3.436	10.965	0.303	1.331	
0.00488	0.0818		3.436	10.965	0.373		
0.00446	0.0917	0.0467	3.436	10.965	0.472	1.322	
0.00474	0.0999	0.0471	3.436	10.965	0.474	1.385	
0.00462	0.0799	0.0471	3.436	10.965	0.391	1.354	
0.00449	0.0800	0.0465	3.436	10.965	0.408	1.341	
0.00451	0.0800	0.0470	3.436	10.965	0.406	1.322	
0.00469	0.0574	0.0479	3.436	10.965	0.276	1.337	
0.00447	0.0366	0.0468	3.436	10.965	0.188	1.321	
0.00480	0.0366		3.436	10.965	0.170		

[m³/s]	*[kg/s]*	*[m]*	*[-]*	*[-]*	*[-]*	*[-]*	
Q	Q_{bo}	h_0	a_{*D}	b_{*D}	ϑ	F_*	
0.00453	0.0367	0.0470	3.436	10.965	0.185	1.331	HY(a = 0.047m, b=0.150m) + MEC
0.00459	0.0183	0.0470	3.436	10.965	0.091	1.348	
0.00452	0.0183	0.0472	3.436	10.965	0.093	1.316	
0.00448	0.0183	0.0467	3.436	10.965	0.094	1.327	
0.00551	0.1197	0.0480	3.436	10.965	0.463	1.567	
0.00538	0.1198	0.0479	3.436	10.965	0.478	1.536	
0.00553	0.1318	0.0485	3.436	10.965	0.507	1.547	
0.00555	0.1851	0.0486	3.436	10.965	0.708	1.550	
0.00552	0.0366	0.0488	3.436	10.965	0.141	1.534	
0.00536	0.0183	0.0483	3.436	10.965	0.073	1.513	
0.00830	0.0802	0.0981	3.436	10.965	0.178	0.745	
0.00860	0.0592	0.0990	3.436	10.965	0.125	0.759	
0.00337	0.1019	0.0345			0.766	1.565	MEC ONLY
0.00302	0.0688	0.0320			0.600	1.568	
0.00331	0.0769	0.0341			0.592	1.568	
0.00338	0.0769	0.0347			0.577	1.558	
0.00331	0.0769	0.0339			0.592	1.579	
0.00396	0.0769	0.0388			0.464	1.551	
0.00390	0.0962	0.0387			0.592	1.534	
0.00404	0.1154	0.0402			0.679	1.499	
0.00390	0.1346	0.0393			0.830	1.498	
0.00388	0.1346	0.0388			0.837	1.517	
0.00393	0.1346	0.0391			0.823	1.523	
0.00505	0.1346	0.0482			0.585	1.427	
0.00510	0.1154	0.0490			0.494	1.408	
0.00529	0.1154	0.0494			0.471	1.437	
0.00496	0.0577	0.0480			0.257	1.410	
0.00500	0.0769	0.0484			0.339	1.401	
0.00509	0.0769	0.0483			0.331	1.435	
0.00483	0.0769	0.0476			0.355	1.390	
0.00487	0.1538	0.0476			0.702	1.403	
0.00546	0.0769	0.0501			0.300	1.458	
0.00552	0.1631	0.0500			0.628	1.476	
0.00559	0.1726	0.0503			0.653	1.481	
0.00562	0.2412	0.0504			0.907	1.481	
0.00567	0.2566	0.0511			0.952	1.466	
0.00577	0.2614	0.0517			0.949	1.463	
0.00795	0.2660	0.0771			0.624	1.066	

[m³/s]	[kg/s]	[m]	[-]	[-]	[-]	[-]	
Q	Q_{bo}	h_0	a_{*D}	b_{*D}	ϑ	F_*	
0.00360	0.0230	0.0731	2.887426901	10.96491	0.158	0.527	HY (a = 0.0395m, b=0.150m) + MEC
0.00380	0.0328	0.0733	2.887426901	10.96491	0.210	0.554	
0.00412	0.0098	0.0746	2.887426901	10.96491	0.056	0.583	
0.00414	0.0098	0.0741	2.887426901	10.96491	0.056	0.593	
0.00398	0.0097	0.0731	2.887426901	10.96491	0.058	0.583	
0.00410	0.0179	0.0744	2.887426901	10.96491	0.103	0.583	
0.00403	0.0278	0.0739	2.887426901	10.96491	0.164	0.579	
0.00324	0.0392	0.0434	2.887426901	10.96491	0.311	1.075	
0.00328	0.0784	0.0455	2.887426901	10.96491	0.612	1.012	
0.00343	0.0980	0.0506	2.887426901	10.96491	0.719	0.902	
0.00315	0.0350	0.0426	2.887426901	10.96491	0.289	1.073	
0.00368	0.0328	0.0581	2.887426901	10.96491	0.219	0.777	
0.00378	0.0497	0.0594	2.887426901	10.96491	0.320	0.772	
0.00505	0.0040	0.0995	2.887426901	10.96491	0.017	0.442	
0.00339	0.0882	0.0357	3.143274854	10.96491	0.659	1.500	HY(a = 0.043m, b=0.150m) + MEC
0.00345	0.1176	0.0361	3.143274854	10.96491	0.859	1.497	
0.00351	0.0248	0.0367	3.143274854	10.96491	0.176	1.491	
0.00345	0.0980	0.0366	3.143274854	10.96491	0.715	1.468	
0.00370	0.0293	0.0480	3.143274854	10.96491	0.194	1.052	
0.00373	0.0784	0.0480	3.143274854	10.96491	0.515	1.061	
0.00355	0.1078	0.0424	3.143274854	10.96491	0.756	1.218	
0.00374	0.0875	0.0485	3.143274854	10.96491	0.571	1.048	
0.00400	0.0530	0.0641	3.143274854	10.96491	0.316	0.724	
0.00406	0.0751	0.0646	3.143274854	10.96491	0.439	0.725	
0.00424	0.0588	0.0654	3.143274854	10.96491	0.324	0.743	
0.00505	0.0242	0.0770	3.143274854	10.96491	0.105	0.680	
0.00501	0.0129	0.0761	3.143274854	10.96491	0.057	0.685	
0.00529	0.0175	0.0925	3.143274854	10.96491	0.072	0.524	
0.00535	0.0163	0.0969	3.143274854	10.96491	0.065	0.490	

A.4.3 Data tables of the time variation of sediment outflow (to Chpt. 7)

The data tables shown in this section refer to the following variables and acronyms:

Latin letters		
a	m	hydraulic opening height
a_1 / a_2 a_3	m	hydraulic opening heights of combined barriers
b	m	hydraulic opening width
D_{84}	m	characteristic grain diameter
Q	$m^3\ s^{-1}$	pump (water) discharge
$Q_{b,i}$	$kg\ s^{-1}$	bed load supply rate
$Q_{b,o}$	$kg\ s^{-1}$	bed load outflow rate

Greek letters		
α	var.	first test run
β	var.	repetitive (redundant), second test run

Acronyms	
Hy	barrier aiming at hydraulically controlled sediment deposition
HyMec	barrier combining hydraulically and mechanically controlled sediment deposition
Mec	barrier aiming at mechanically controlled sediment deposition
no	non-overflown
o	overflown

The following table contains the measurements of the outflowing sediments during the hydrograph experiments shown in Chpt. 7.

a [m]	0.152		0.0395	--		0.0395		0.043		0.047	
b [m]	0.076		0.150	--		0.150		0.150		0.150	
mec. [-]	--		--	1.75 · D84		1.75 · D84		1.75 · D84		1.75 · D84	
[hh:mm:ss]	$Q_{b,o}$[kg/s]	$Q_{b,o}$[kg/s]	$Q_{b,o}$[kg/s]	$Q_{b,o}$[kg/s]	$Q_{b,o}$[kg/s]	$Q_{b,o}$[kg/s]	$Q_{b,o}$[kg/s]	$Q_{b,o}$[kg/s]	$Q_{b,o}$[kg/s]	$Q_{b,o}$[kg/s]	$Q_{b,o}$[kg/s]
time	**Hy - no α**	**Hy - no β**	**Hy - o**	**Mec α**	**Mec β**	**HyMec.a_1 α**	**HyMec.a_1 β**	**HyMec.a_2 α**	**HyMec.a_2 β**	**HyMec.a_3 α**	**HyMec.a_3 β**
00:01:00	0.0417	0.0542	0.0408	0.0773	0.0550	0.0000	0.0000	0.0008	0.0005	0.0546	0.0504
00:02:00	0.0417	0.0492	0.0000	0.0723	0.0575	0.0000	0.0000	0.0000	0.0005	0.0453	0.0522
00:03:00	0.0383	0.0342	0.0000	0.0489	0.0600	0.0000	0.0000	0.0000	0.0008	0.0543	0.0473
00:04:00	0.0383	0.0542	0.0023	0.0589	0.0595	0.0086	0.0000	0.0058	0.0025	0.0485	0.0063
00:05:00	0.0417	0.0308	0.0140	0.0723	0.0590	0.0093	0.0117	0.0058	0.0042	0.0077	0.0000
00:06:00	0.0333	0.0425	0.0017	0.0606	0.0698	0.0000	0.0033	0.0000	0.0002	0.0022	0.0000
00:07:00	0.0283	0.0375	0.0084	0.0523	0.0806	0.0000	0.0001	0.0000	0.0000	0.0000	0.0000
00:08:00	0.0417	0.0575	0.0105	0.0623	0.0798	0.0000	0.0000	0.0005	0.0000	0.0000	0.0000
00:09:00	0.0183	0.0208	0.0420	0.0639	0.0789	0.0000	0.0100	0.0125	0.0002	0.0000	0.0000
00:10:00	0.0083	0.0575	0.0324	0.0656	0.0834	0.0083	0.0183	0.0142	0.0002	0.0000	0.0053
00:11:00	0.0050	0.0058	0.0350	0.0656	0.0878	0.0169	0.0233	0.0108	0.0000	0.0082	0.0044
00:12:00	0.0200	0.0175	0.0604	0.0523	0.0923	0.0357	0.0433	0.0458	0.0000	0.0238	0.0099
00:13:00	0.0117	0.0175	0.0949	0.0839	0.0973	0.0518	0.0500	0.0583	0.0000	0.0385	0.0435
00:14:00	0.0083	0.0225	0.0702	0.0706	0.1023	0.0731	0.0533	0.0708	0.0000	0.0458	0.0452
00:15:00	0.0050	0.0258	0.0972	0.0656	0.0773	0.0731	0.0700	0.0808	0.0000	0.0399	0.0468
00:16:00	0.0083	0.0158	0.1243	0.0623	0.0884	0.0732	0.1150	0.0908	0.0000	0.0530	0.0742
00:17:00	0.0050	0.0042	0.1306	0.1089	0.0995	0.0732	0.0967	0.0953	0.0000	0.0653	0.0819
00:18:00	0.0025	0.0017	0.1369	0.0823	0.1106	0.0982	0.1250	0.0997	0.0000	0.0811	0.0896
00:19:00	0.0025	0.0008	0.1515	0.1189	0.1212	0.1232	0.1233	0.1042	0.0000	0.0853	0.1172
00:20:00	0.0017	0.0008	0.1662	0.0639	0.1317	0.1346	0.1433	0.1047	0.0000	0.0894	0.1449
00:21:00	0.0008	0.0008	0.1809	0.0523	0.0789	0.1459	0.1450	0.1053	0.0000	0.0936	0.1342
00:22:00	0.0008	0.0008	0.1963	0.0146	0.1037	0.1442	0.1467	0.1058	0.0000	0.1072	0.1236
00:23:00	0.0008	0.0008	0.2116	0.0168	0.1285	0.1424	0.1350	0.1136	0.0002	0.1207	0.1129
00:24:00	0.0008	0.0005	0.1349	0.0324	0.0046	0.1281	0.1233	0.1214	0.0000	0.1111	0.1009
00:25:00	0.0008	0.0000	0.1519	0.0320	0.0327	0.1139	0.1242	0.1292	0.0002	0.1015	0.0889
00:26:00	0.0008	0.0000	0.1690	0.0280	0.0608	0.0976	0.1250	0.1197	0.0000	0.0921	0.0939
00:27:00	0.0000	0.0000	0.1861	0.0399	0.0889	0.0813	0.1233	0.1103	0.0000	0.0828	0.0990
00:28:00	0.0000	0.0000	0.2273	0.0387	0.0668	0.0650	0.1217	0.1008	0.0000	0.0778	0.0814
00:29:00	0.0000	0.0000	0.2087	0.0563	0.0632	0.0752	0.1192	0.1003	0.0000	0.0729	0.0639
00:30:00	0.0000	0.0000	0.1148	0.0527	0.0597	0.0853	0.1167	0.0997	0.0000	0.0667	0.0702
00:31:00	0.0000	0.0000	0.0208	0.0773	0.0561	0.0614	0.1042	0.0992	0.0000	0.0605	0.0766

a [m]	0.152		0.0395	--		0.0395		0.043		0.047	
b [m]	0.076		0.150	--		0.150		0.150		0.150	
mec. [-]	--		--	1.75 · D84		1.75 · D84		1.75 · D84		1.75 · D84	
[hh:mm:ss]	$Q_{b,o}$[kg/s]	$Q_{b,o}$[kg/s]	$Q_{b,o}$[kg/s]	$Q_{b,o}$[kg/s]	$Q_{b,o}$[kg/s]	$Q_{b,o}$[kg/s]	$Q_{b,o}$[kg/s]	$Q_{b,o}$[kg/s]	$Q_{b,o}$[kg/s]	$Q_{b,o}$[kg/s]	$Q_{b,o}$[kg/s]
time	**Hy - no α**	**Hy - no β**	**Hy - o**	**Mec α**	**Mec β**	**HyMec.a_1 α**	**HyMec.a_1 β**	**HyMec.a_2 α**	**HyMec.a_2 β**	**HyMec.a_3 α**	**HyMec.a_3 β**
00:32:00	0.0000	0.0000	--	0.0517	0.0540	0.0375	0.0917	0.0942	0.0003	0.0753	0.0624
00:33:00	0.0000	0.0000	--	0.0429	0.0518	0.0195	0.0842	0.0892	0.0000	0.0697	0.0483
00:34:00	0.0000	0.0000	--	0.0371	0.0497	0.0015	0.0767	0.0842	0.0000	0.0683	0.0465
00:35:00	0.0000	0.0000	--	0.0198	0.0332	0.0000	0.0717	0.0747	0.0000	0.0567	0.0300
00:36:00	0.0000	0.0000	--	0.0019	0.0168	0.0000	0.0667	0.0653	0.0000	0.0483	0.0034
00:37:00	0.0000	0.0000	--	0.0000	0.0003	0.0000	0.0658	0.0558	0.0000	0.0345	0.0000
00:38:00	0.0000	0.0000	--	0.0000	0.0003	0.0000	0.0650	0.0492	0.0242	0.0338	0.0000
00:39:00	0.0000	0.0000	--	0.0000	0.0002	0.0000	0.0558	0.0425	0.0175	0.0028	0.0000
00:40:00	0.0000	0.0000	--	0.0000	0.0002	0.0000	0.0467	0.0358	0.0017	0.0018	0.0000
00:41:00	0.0000	0.0000	--	0.0000	0.0002	0.0000	0.0258	0.0239	0.0008	0.0000	0.0000
00:42:00	0.0000	0.0000	--	0.0000	0.0002	0.0000	0.0050	0.0121	0.0017	0.0000	0.0000
00:43:00	0.0000	0.0000	--	0.0000	0.0002	0.0000	0.0001	0.0002	0.0003	0.0000	0.0000
00:44:00	0.0000	0.0000	--	0.0000	0.0001	0.0000	0.0001	0.0001	0.0000	0.0000	0.0000
00:45:00	0.0000	0.0000	--	0.0000	0.0000	0.0000	0.0001	0.0001	0.0002	0.0000	0.0000
00:46:00	0.0000	0.0000	--	0.0000	0.0000	0.0000	0.0000	0.0001	0.0002	0.0000	0.0000
00:47:00	0.0000	0.0000	--	0.0000	0.0000	0.0000	0.0000	0.0000	0.0002	0.0000	0.0000
00:48:00	0.0000	0.0000	--	0.0016	0.0000	0.0000	0.0000	0.0000	0.0003	0.0000	0.0000
00:49:00	0.0000	0.0000	--	0.0001	0.0002	0.0000	0.0000	0.0000	0.0003	0.0000	0.0000
00:50:00	0.0000	0.0000	--	0.0000	0.0000	0.0000	0.0000	0.0000	0.0002	0.0000	0.0000
00:51:00	0.0000	0.0000	--	0.0000	0.0000	0.0000	0.0000	0.0000	0.0000	0.0000	0.0000
00:52:00	0.0000	0.0000	--	0.0000	0.0000	0.0000	0.0000	0.0000	0.0000	0.0000	0.0000
00:53:00	0.0000	0.0000	--	0.0000	0.0000	0.0000	0.0000	0.0000	0.0000	0.0000	0.0000
00:54:00	0.0000	0.0000	--	0.0000	0.0000	0.0000	0.0000	0.0000	0.0000	0.0000	0.0000
00:55:00	0.0000	0.0000	--	0.0000	0.0000	0.0000	0.0000	0.0000	0.0000	0.0000	0.0000

The following table contains the measurements of the outflowing sediments during the flushing experiments shown in Chpt. 7.

	SEDIMENT OUTFLOW $Q_{b,o}$				SEDIMENT SUPPLY $Q_{b,i}$			DISCHARGE Q	
a [m]	0.152		0.043						
b [m]	0.076		0.150						
mec. [-]	--		1.75 · D84						
[hh:mm:ss]	[kg/s]	[kg/s]	[kg/s]	[kg/s]	[kg/s]	[kg/s]	[kg/s]	[m³/s]	[m³/s]
time	**Hy-no α**	**Hy-no β**	**HyMec.a_2 α**	**HyMec.a_2 β**	**Hy-no α_**	**Hy-no β_**	**HyMec α/β**	**Hy-no α__**	**Hy-no β__**
00:01:00	0.0008	0.0000	0.0000	0.0158	0.0000	0.0588	NONE	0.00533	0.00647
00:02:00	0.0042	0.0000	0.0014	0.0108	0.0000	0.1176	--	0.00523	0.01097
00:03:00	0.0000	0.0000	0.0000	0.0075	0.0000	0.1176	--	0.00602	0.01168
00:04:00	0.0000	0.0000	0.0000	0.0125	0.0000	0.1176	--	0.00795	0.01232
00:05:00	0.0000	0.0025	0.0008	0.0058	0.0000	0.1176	--	0.00796	0.01219
00:06:00	0.0000	0.0092	0.0008	0.0058	0.0000	0.1176	--	0.00804	0.01249
00:07:00	0.0000	0.0000	0.0008	0.0058	0.0000	0.1176	--	0.00789	0.01235
00:08:00	0.0000	0.0000	0.0000	0.0042	0.0000	0.1176	--	0.00787	0.01251
00:09:00	0.0000	0.0000	0.0000	0.0000	0.0000	0.1176	--	0.00956	0.01240
00:10:00	0.0000	0.0000	0.0000	0.0000	0.0000	0.1176	--	0.01144	0.01239
00:11:00	0.0000	0.0000	0.0000	--	0.0000	0.1176	--	0.01210	0.01256
00:12:00	0.0000	0.0000	0.0002	--	0.0000	0.1176	--	0.01215	0.01243
00:13:00	0.0000	0.0000	0.0002	--	0.0000	0.1176	--	0.01208	0.01263
00:14:00	0.0000	0.0000	0.0002	--	0.0000	0.1176	--	0.01215	0.01250
00:15:00	0.0000	0.0000	0.0002	--	0.0000	0.1176	--	0.01204	0.01248
00:16:00	0.0000	0.0000	0.0002	--	0.1176	0.1176	--	0.01207	0.01247
00:17:00	0.0000	0.0000	0.0000	--	0.1176	0.1176	--	0.01212	0.01248
00:18:00	0.0000	0.0000	0.0000	--	0.1176	0.1176	--	0.01217	0.01248
00:19:00	0.0000	0.0000	0.0000	--	0.1176	0.1176	--	0.01206	0.01248
00:20:00	0.0000	0.0000	0.0000	--	0.1176	0.1176	--	0.01223	0.01250
00:21:00	0.0000	0.0000	0.0000	--	0.1176	0.1176	--	0.01224	0.01248
00:22:00	0.0000	0.0000	0.0000	--	0.1176	0.1176	--	0.01205	0.01254
00:23:00	0.0000	0.0000	0.0000	--	0.1176	0.1176	--	0.01202	0.01266
00:24:00	0.0000	0.0000	0.0000	--	0.1176	0.1176	--	0.01222	0.01257
00:25:00	0.0000	0.0000	0.0004	--	0.1176	0.1176	--	0.01211	0.01249
00:26:00	0.0000	0.0000	0.0000	--	0.1176	0.1176	--	0.01209	0.01251
00:27:00	0.0000	0.0000	0.0000	--	0.1176	0.1176	--	0.01223	0.01245
00:28:00	0.0000	0.0000	0.0004	--	0.1176	0.1176	--	0.01219	0.01249
00:29:00	0.0000	0.0000	0.0002	--	0.1176	0.1176	--	0.01216	0.01255
00:30:00	0.0000	0.0000	0.0000	--	0.1176	0.1176	--	0.01208	0.01252
00:31:00	0.0000	0.0000	0.0000	--	0.1176	0.1176	--	0.01214	0.01258
00:32:00	0.0000	0.0000	0.0000	--	0.1176	0.1176	--	0.01210	0.01247
00:33:00	0.0000	0.0000	0.0011	--	0.1176	0.1176	--	0.01224	0.01251
00:34:00	0.0000	0.0000	0.0000	--	0.1176	0.1176	--	0.01205	0.01248
00:35:00	0.0000	0.0000	0.0000	--	0.1176	0.1176	--	0.01202	0.01247
00:36:00	0.0000	0.0000	0.0000	--	0.1176	0.1176	--	0.01225	0.01253
00:37:00	0.0000	0.0000	0.0000	--	0.1176	0.1176	--	0.01216	0.01258
00:38:00	0.0000	0.0000	0.0009	--	0.1176	0.1176	--	0.01215	0.01251
00:39:00	0.0000	0.0058	0.0000	--	0.1176	0.1176	--	0.01210	0.01253
00:40:00	0.0000	0.0075	0.0000	--	0.1176	0.1176	--	0.01217	0.01261
00:41:00	0.0000	0.0192	0.0000	--	0.1176	0.1176	--	0.01225	0.01272
00:42:00	0.0000	0.0158	0.0000	--	0.1176	0.1176	--	0.01223	0.01261
00:43:00	0.0000	0.0225	0.0006	--	0.1176	0.1176	--	0.01220	0.01262
00:44:00	0.0000	0.0358	0.0000	--	0.1176	0.1176	--	0.01208	0.01262
00:45:00	0.0000	0.0408	0.0000	--	0.1176	0.1176	--	0.01081	0.01256
00:46:00	0.0000	0.0375	0.0000	--	0.1176	0.1176	--	0.00836	0.01257
00:47:00	0.0425	0.0342	0.0000	--	0.1176	0.1176	--	0.00801	0.01252
00:48:00	0.0342	0.0275	0.0000	--	0.1176	0.1176	--	0.00811	0.01250
00:49:00	0.0000	0.0275	0.0006	--	0.1176	0.1176	--	0.00814	0.01259

	SEDIMENT OUTFLOW $Q_{b,o}$				SEDIMENT SUPPLY $Q_{b,i}$			DISCHARGE Q	
a [m]	0.152		0.043						
b [m]	0.076		0.150						
mec. [-]	--		1.75 · D84						
[hh:mm:ss]	[kg/s]	[kg/s]	[kg/s]	[kg/s]	[kg/s]	[kg/s]	[kg/s]	[m³/s]	[m³/s]
time	**Hy-no α**	**Hy-no β**	**HyMec.a_2 α**	**HyMec.a_2 β**	**Hy-no α_**	**Hy-no β_**	**HyMec α/β**	**Hy-no α__**	**Hy-no β__**
00:50:00	0.0292	0.0142	0.0000	--	0.1176	0.1176	--	0.00813	0.01255
00:51:00	0.0292	0.0075	0.0000	--	0.1176	0.1176	--	0.00802	0.01252
00:52:00	0.0358	0.0025	0.0000	--	0.1176	0.1176	--	0.00828	0.01263
00:53:00	0.0000	0.0008	0.0000	--	0.1176	0.0588	--	0.00809	0.01268
00:54:00	0.0000	0.0008	0.0000	--	0.1176	0.0000	--	0.00809	0.01257
00:55:00	0.0000	0.0000	0.0001	--	0.1176	0.0000	--	0.00699	0.01265
00:56:00	0.0442	0.0000	0.0001	--	0.1176	0.0000	--	0.00634	0.01245
00:57:00	0.0558	0.0000	0.0001	--	0.1176	0.0000	--	0.00634	0.01241
00:58:00	0.0242	0.0000	0.0001	--	0.1176	0.0000	--	0.00646	0.01246
00:59:00	0.0125	0.0000	0.0001	--	0.1176	0.0000	--	0.00647	0.01255
01:00:00	0.0292	0.0000	0.0001	--	0.1176	0.0000	--	0.00640	0.01263
01:01:00	0.0000	0.0000	0.0000	--	0.1176	0.0000	--	0.00623	0.01270
01:02:00	0.0358	0.0000	0.0000	--	0.1176	0.0000	--	0.00647	0.01265
01:03:00	0.0000	0.0000	0.0000	--	0.1176	0.0000	--	0.00655	0.01260
01:04:00	0.0000	0.0000	0.0000	--	0.1176	0.0000	--	0.00639	0.01260
01:05:00	0.0000	0.0000	0.0000	--	0.1176	0.0000	--	0.00636	0.01266
01:06:00	0.0000	0.0000	0.0000	--	0.1176	0.0000	--	0.00642	0.01258
01:07:00	0.0333	0.0000	0.0000	--	0.1176	0.0000	--	0.00648	0.01262
01:08:00	0.0000	0.0000	0.0000	--	0.1176	0.0000	--	0.00636	0.01249
01:09:00	0.0000	0.0000	0.0000	--	0.1176	0.0000	--	0.00648	0.01272
01:10:00	0.0000	0.0000	0.0000	--	0.1176	0.0000	--	0.00649	0.01259
01:11:00	0.0000	0.0000	0.0000	--	0.1176	0.0000	--	0.00641	0.01251
01:12:00	0.0000	0.0000	0.0000	--	0.1176	0.0000	--	0.00633	0.01259
01:13:00	0.0000	0.0000	0.0000	--	0.0000	0.0000	--	0.00636	0.01263
01:14:00	0.0000	0.0000	0.0000	--	0.0000	0.0000	--	0.00639	0.01246
01:15:00	0.0000	0.0000	0.0000	--	0.0000	0.0000	--	0.00641	0.01238
01:16:00	0.0000	0.0000	0.0000	--	0.0000	0.0000	--	0.00643	0.01255
01:17:00	0.0000	0.0000	0.0000	--	0.0000	0.0000	--	0.00650	0.01240
01:18:00	0.0000	0.0000	--	--	0.0000	0.0000	--	0.00638	0.01250
01:19:00	0.0000	0.0000	--	--	0.0000	0.0000	--	0.00650	0.01260
01:20:00	0.0000	0.0000	--	--	0.0000	0.0000	--	0.00642	0.01251
01:21:00	0.0000	0.0000	--	--	0.0000	0.0000	--	0.00648	0.01255
01:22:00	0.0000	0.0000	--	--	0.0000	0.0000	--	0.00650	0.01241
01:23:00	0.0000	0.0000	--	--	0.0000	0.0000	--	0.00640	0.01253
01:24:00	0.0000	0.0000	--	--	0.0000	0.0000	--	0.00648	0.01261
01:25:00	0.0000	0.0000	--	--	0.0000	0.0000	--	0.00645	0.01248
01:26:00	0.0000	0.0000	--	--	0.0000	0.0000	--	0.00642	0.01258
01:27:00	0.0000	0.0000	--	--	0.0000	0.0000	--	0.00649	0.01233
01:28:00	0.0000	0.0000	--	--	0.0000	0.0000	--	0.00645	0.01262
01:29:00	0.0000	0.0000	--	--	0.0000	0.0000	--	0.00641	0.01248
01:30:00	0.0000	0.0000	--	--	0.0000	0.0000	--	0.00645	0.01260
01:31:00	0.0000	0.0000	--	--	0.0000	0.0000	--	0.00630	0.01242
01:32:00	0.0000	0.0000	--	--	0.0000	0.0000	--	0.00646	0.01252
01:33:00	0.0000	0.0000	--	--	0.0000	0.0000	--	0.00646	0.01235
01:34:00	0.0000	0.0000	--	--	0.0000	0.0000	--	0.00640	0.01247
01:35:00	0.0000	0.0000	--	--	0.0000	0.0000	--	0.00656	0.01251
01:36:00	0.0000	0.0000	--	--	0.0000	0.0000	--	0.00644	0.01253
01:37:00	0.0000	0.0000	--	--	0.0000	0.0000	--	0.00635	0.01249
01:38:00	0.0000	0.0000	--	--	0.0000	0.0000	--	0.00641	0.01245

	SEDIMENT OUTFLOW $Q_{b,o}$				SEDIMENT SUPPLY $Q_{b,i}$			DISCHARGE Q	
a [m]	0.152		0.043						
b [m]	0.076		0.150						
mec. [-]	--		1.75 · D84						
[hh:mm:ss]	[kg/s]	[kg/s]	[kg/s]	[kg/s]	[kg/s]	[kg/s]	[kg/s]	[m³/s]	[m³/s]
time	**Hy-no α**	**Hy-no β**	**HyMec.a_2 α**	**HyMec.a_2 β**	**Hy-no α_**	**Hy-no β_**	**HyMec α/β**	**Hy-no α__**	**Hy-no β__**
01:39:00	0.0000	0.0000	--	--	0.0000	0.0000	--	0.00640	0.01244
01:40:00	0.0000	0.0000	--	--	0.0000	0.0000	--	0.00641	0.01245
01:41:00	0.0000	0.0000	--	--	0.0000	0.0000	--	0.00647	0.01256
01:42:00	0.0000	0.0000	--	--	0.0000	0.0000	--	0.00639	0.01239
01:43:00	0.0000	0.0000	--	--	0.0000	0.0000	--	0.00637	0.01243
01:44:00	0.0000	0.0000	--	--	0.0000	0.0000	--	0.00629	0.01250
01:45:00	0.0000	0.0000	--	--	0.0000	0.0000	--	0.00636	0.01229
01:46:00	0.0000	0.0000	--	--	0.0000	0.0000	--	0.00639	0.01245
01:47:00	0.0000	0.0000	--	--	0.0000	0.0000	--	0.00632	0.01253
01:48:00	0.0000	0.0000	--	--	0.0000	0.0000	--	0.00626	0.01253
01:49:00	0.0000	0.0000	--	--	0.0000	0.0000	--	0.00644	0.01264
01:50:00	0.0000	0.0000	--	--	0.0000	0.0000	--	0.00639	0.01252
01:51:00	0.0000	0.0000	--	--	0.0000	0.0000	--	0.00637	0.01253
01:52:00	0.0000	0.0000	--	--	0.0000	0.0000	--	0.00634	0.01252
01:53:00	0.0000	0.0000	--	--	0.0000	0.0000	--	0.00622	0.01251
01:54:00	0.0000	0.0000	--	--	0.0000	0.0000	--	0.00647	0.01242
01:55:00	0.0000	0.0000	--	--	0.0000	0.0000	--	0.00640	0.01250
01:56:00	0.0000	0.0000	--	--	0.0000	0.0000	--	0.00635	0.01256
01:57:00	0.0000	0.0000	--	--	0.0000	0.0000	--	0.00635	0.01249
01:58:00	0.0000	0.0000	--	--	0.0000	0.0000	--	0.00640	0.01231
01:59:00	0.0000	0.0000	--	--	0.0000	0.0000	--	0.00634	0.01258
02:00:00	0.0000	0.0000	--	--	0.0000	0.0000	--	0.00638	0.01251
02:01:00	0.0000	0.0000	--	--	0.0000	0.0000	--	0.00639	0.01240
02:02:00	0.0000	0.0000	--	--	0.0000	0.0000	--	0.00630	0.01250
02:03:00	0.0000	0.0000	--	--	0.0000	0.0000	--	0.00647	0.01240
02:04:00	0.0000	0.0000	--	--	0.0000	0.0000	--	0.00639	0.01254
02:05:00	0.0000	0.0000	--	--	0.0000	0.0000	--	0.00640	0.01243
02:06:00	0.0000	0.0000	--	--	0.0000	0.0000	--	0.00633	0.01237
02:07:00	0.0000	0.0000	--	--	0.0000	0.0000	--	0.00624	0.01257
02:08:00	0.0000	0.0000	--	--	0.0000	0.0000	--	0.00629	0.01238
02:09:00	0.0000	0.0000	--	--	0.0000	0.0000	--	0.00642	0.01249
02:10:00	0.0000	0.0000	--	--	0.0000	0.0000	--	0.00652	0.01249
02:11:00	0.0000	0.0000	--	--	0.0000	0.0000	--	0.00636	0.01243
02:12:00	0.0000	0.0000	--	--	0.0000	0.0000	--	0.00621	0.01249
02:13:00	0.0000	0.0000	--	--	0.0000	0.0000	--	0.00642	0.01242
02:14:00	0.0000	0.0258	--	--	0.0000	0.0000	--	0.00637	0.01016
02:15:00	0.0000	0.0225	--	--	0.0000	0.0000	--	0.00645	0.01006
02:16:00	0.0000	0.0075	--	--	0.0000	0.0000	--	0.00641	0.00930
02:17:00	0.0000	0.0275	--	--	0.0000	0.0000	--	0.00639	0.00617
02:18:00	0.0000	0.0442	--	--	0.0000	0.0000	--	0.00646	0.00617
02:19:00	0.0000	0.0225	--	--	0.0000	0.0000	--	0.00629	0.00620
02:20:00	0.0000	0.0058	--	--	0.0000	0.0000	--	0.00645	0.00626
02:21:00	0.0000	0.0042	--	--	0.0000	0.0000	--	0.00636	0.00624
02:22:00	0.0000	0.0058	--	--	0.0000	0.0000	--	0.00633	0.00610
02:23:00	0.0000	0.0005	--	--	0.0000	0.0000	--	0.00622	0.00622
02:24:00	0.0000	0.0058	--	--	0.0000	0.0000	--	0.00629	0.00607
02:25:00	0.0000	0.0005	--	--	0.0000	0.0000	--	0.00627	0.00944
02:26:00	0.0000	0.0192	--	--	0.0000	0.0000	--	0.00633	0.01139
02:27:00	0.0000	0.0042	--	--	0.0000	0.0000	--	0.00632	0.01149

	SEDIMENT OUTFLOW $Q_{b,o}$				SEDIMENT SUPPLY $Q_{b,i}$			DISCHARGE Q	
a [m]	0.152		0.043						
b [m]	0.076		0.150						
mec. [-]	--		1.75 · D84						
[hh:mm:ss]	[kg/s]	[kg/s]	[kg/s]	[kg/s]	[kg/s]	[kg/s]	[kg/s]	[m³/s]	[m³/s]
time	**Hy-no α**	**Hy-no β**	**HyMec.a_2 α**	**HyMec.a_2 β**	**Hy-no α_**	**Hy-no β_**	**HyMec α/β**	**Hy-no α__**	**Hy-no β__**
02:28:00	0.0000	0.0005	--	--	0.0000	0.0000	--	0.00642	0.01146
02:29:00	0.0000	0.0005	--	--	0.0000	0.0000	--	0.00630	0.01077
02:30:00	0.0000	0.0005	--	--	0.0000	0.0000	--	0.00640	0.01050
02:31:00	0.0000	0.0005	--	--	0.0000	0.0000	--	0.00631	0.00748
02:32:00	0.0000	0.0058	--	--	0.0000	0.0000	--	0.00630	0.00718
02:33:00	0.0000	0.0075	--	--	0.0000	0.0000	--	0.00635	0.00725
02:34:00	0.0000	0.0042	--	--	0.0000	0.0000	--	0.00653	0.00722
02:35:00	0.0000	0.0042	--	--	0.0000	0.0000	--	0.00639	0.00720
02:36:00	0.0000	0.0058	--	--	0.0000	0.0000	--	0.00636	0.00719
02:37:00	0.0000	0.0042	--	--	0.0000	0.0000	--	0.00637	0.00719
02:38:00	0.0000	0.0092	--	--	0.0000	0.0000	--	0.00632	0.00725
02:39:00	0.0000	0.0005	--	--	0.0000	0.0000	--	0.00637	0.00723
02:40:00	0.0000	0.0005	--	--	0.0000	0.0000	--	0.00643	0.00721
02:41:00	0.0000	0.0005	--	--	0.0000	0.0000	--	0.00629	0.00727
02:42:00	0.0000	0.0005	--	--	0.0000	0.0000	--	0.00646	0.00721
02:43:00	0.0000	0.0005	--	--	0.0000	0.0000	--	0.00647	0.00721
02:44:00	0.0000	0.0005	--	--	0.0000	0.0000	--	0.00631	0.00710
02:45:00	0.0000	0.0005	--	--	0.0000	0.0000	--	0.00637	0.00719
02:46:00	0.0000	0.0005	--	--	0.0000	0.0000	--	0.00648	0.00718
02:47:00	0.0000	0.0005	--	--	0.0000	0.0000	--	0.00643	0.00727
02:48:00	0.0000	0.0005	--	--	0.0000	0.0000	--	0.00633	0.00727
02:49:00	0.0000	0.0005	--	--	0.0000	0.0000	--	0.00649	0.00720
02:50:00	0.0000	0.0005	--	--	0.0000	0.0000	--	0.00646	0.00719
02:51:00	0.0000	0.0005	--	--	0.0000	0.0000	--	0.00640	0.00724
02:52:00	0.0000	0.0005	--	--	0.0000	0.0000	--	0.00630	0.00729
02:53:00	0.0000	0.0005	--	--	0.0000	0.0000	--	0.00636	0.00735
02:54:00	0.0000	0.0005	--	--	0.0000	0.0000	--	0.00631	0.00720
02:55:00	0.0000	0.0005	--	--	0.0000	0.0000	--	0.00637	0.00738
02:56:00	0.0000	0.0005	--	--	0.0000	0.0000	--	0.00634	0.00725
02:57:00	0.0000	0.0005	--	--	0.0000	0.0000	--	0.00630	0.00720
02:58:00	0.0000	0.0005	--	--	0.0000	0.0000	--	0.00632	0.00717
02:59:00	0.0000	0.0005	--	--	0.0000	0.0000	--	0.00635	0.00719
03:00:00	0.0000	0.0005	--	--	0.0000	0.0000	--	0.00630	0.00732
03:01:00	0.0000	0.0005	--	--	0.0000	0.0000	--	0.00642	0.00726
03:02:00	0.0000	0.0005	--	--	0.0000	0.0000	--	0.00630	0.00719
03:03:00	0.0000	0.0005	--	--	0.0000	0.0000	--	0.00640	0.00725
03:04:00	0.0000	0.0005	--	--	0.0000	0.0000	--	0.00634	0.00723
03:05:00	0.0000	0.0005	--	--	0.0000	0.0000	--	0.00640	0.00717
03:06:00	0.0000	0.0005	--	--	0.0000	0.0000	--	0.00643	0.00721
03:07:00	0.0000	0.0005	--	--	0.0000	0.0000	--	0.00637	0.00713
03:08:00	0.0000	0.0005	--	--	0.0000	0.0000	--	0.00640	0.00716
03:09:00	0.0000	0.0005	--	--	0.0000	0.0000	--	0.00636	0.00726
03:10:00	0.0000	0.0005	--	--	0.0000	0.0000	--	0.00633	0.00729
03:11:00	0.0000	0.0005	--	--	0.0000	0.0000	--	0.00647	0.00724
03:12:00	0.0000	0.0005	--	--	0.0000	0.0000	--	0.00645	0.00731
03:13:00	0.0000	0.0005	--	--	0.0000	0.0000	--	0.00608	0.00726
03:14:00	0.0000	0.0005	--	--	0.0000	0.0000	--	0.00589	0.00738
03:15:00	0.0000	0.0005	--	--	0.0000	0.0000	--	0.00569	0.00726
03:16:00	0.0000	0.0005	--	--	0.0000	0.0000	--	0.01385	0.00729

	SEDIMENT OUTFLOW $Q_{b,o}$				SEDIMENT SUPPLY $Q_{b,i}$			DISCHARGE Q	
a [m]	0.152		0.043						
b [m]	0.076		0.150						
mec. [-]	--		1.75 · D84						
[hh:mm:ss]	[kg/s]	[kg/s]	[kg/s]	[kg/s]	[kg/s]	[kg/s]	[kg/s]	[m³/s]	[m³/s]
time	**Hy-no α**	**Hy-no β**	**HyMec.a_2 α**	**HyMec.a_2 β**	**Hy-no α_**	**Hy-no β_**	**HyMec α/β**	**Hy-no α__**	**Hy-no β__**
03:17:00	0.0000	0.0005	--	--	0.0000	0.0000	--	0.01395	0.00727
03:18:00	0.0000	0.0005	--	--	0.0000	0.0000	--	0.01401	0.00729
03:19:00	0.0000	0.0005	--	--	0.0000	0.0000	--	0.01205	0.00718
03:20:00	0.0000	0.0005	--	--	0.0000	0.0000	--	0.00783	0.00731
03:21:00	0.0000	0.0005	--	--	0.0000	0.0000	--	0.00751	0.00724
03:22:00	0.0000	0.0005	--	--	0.0000	0.0000	--	0.00800	0.00721
03:23:00	0.0000	0.0005	--	--	0.0000	0.0000	--	0.00818	0.00727
03:24:00	0.0008	0.0005	--	--	0.0000	0.0000	--	0.00821	0.00728
03:25:00	0.0000	0.0005	--	--	0.0000	0.0000	--	0.00003	0.00724
03:26:00	--	0.0005	--	--	--	0.0000	--	--	0.00722
03:27:00	--	0.0005	--	--	--	0.0000	--	--	0.00723
03:28:00	--	0.0005	--	--	--	0.0000	--	--	0.00722
03:29:00	--	0.0005	--	--	--	0.0000	--	--	0.00717
03:30:00	--	0.0005	--	--	--	0.0000	--	--	0.00730
03:31:00	--	0.0005	--	--	--	0.0000	--	--	0.00723
03:32:00	--	0.0005	--	--	--	0.0000	--	--	0.00728
03:33:00	--	0.0005	--	--	--	0.0000	--	--	0.00723
03:34:00	--	0.0005	--	--	--	0.0000	--	--	0.00728
03:35:00	--	0.0005	--	--	--	0.0000	--	--	0.00727
03:36:00	--	0.0005	--	--	--	0.0000	--	--	0.00718
03:37:00	--	0.0005	--	--	--	0.0000	--	--	0.00719
03:38:00	--	0.0005	--	--	--	0.0000	--	--	0.00732
03:39:00	--	0.0005	--	--	--	0.0000	--	--	0.00732
03:40:00	--	0.0005	--	--	--	0.0000	--	--	0.00724
03:41:00	--	0.0005	--	--	--	0.0000	--	--	0.00732
03:42:00	--	0.0005	--	--	--	0.0000	--	--	0.00737
03:43:00	--	0.0005	--	--	--	0.0000	--	--	0.00733
03:44:00	--	0.0005	--	--	--	0.0000	--	--	0.00727
03:45:00	--	0.0005	--	--	--	0.0000	--	--	0.00724
03:46:00	--	0.0005	--	--	--	0.0000	--	--	0.00729
03:47:00	--	0.0005	--	--	--	0.0000	--	--	0.00733
03:48:00	--	0.0005	--	--	--	0.0000	--	--	0.00734
03:49:00	--	0.0005	--	--	--	0.0000	--	--	0.00739
03:50:00	--	0.0005	--	--	--	0.0000	--	--	0.00731
03:51:00	--	0.0005	--	--	--	0.0000	--	--	0.00729
03:52:00	--	0.0005	--	--	--	0.0000	--	--	0.00742
03:53:00	--	0.0005	--	--	--	0.0000	--	--	0.00728
03:54:00	--	0.0005	--	--	--	0.0000	--	--	0.00728
03:55:00	--	0.0005	--	--	--	0.0000	--	--	0.00742
03:56:00	--	0.0005	--	--	--	0.0000	--	--	0.00736
03:57:00	--	0.0005	--	--	--	0.0000	--	--	0.00743
03:58:00	--	0.0005	--	--	--	0.0000	--	--	0.00735
03:59:00	--	0.0005	--	--	--	0.0000	--	--	0.01103
04:00:00	--	0.0008	--	--	--	0.0000	--	--	0.01246
04:01:00	--	0.0005	--	--	--	0.0000	--	--	0.01243
04:02:00	--	0.0005	--	--	--	0.0000	--	--	0.01241
04:03:00	--	0.0005	--	--	--	0.0000	--	--	0.01250
04:04:00	--	0.0005	--	--	--	0.0000	--	--	0.01245
04:05:00	--	0.0005	--	--	--	0.0000	--	--	0.01249

	SEDIMENT OUTFLOW $Q_{b,o}$				SEDIMENT SUPPLY $Q_{b,i}$			DISCHARGE Q	
a [m]	0.152		0.043						
b [m]	0.076		0.150						
mec. [-]	--		1.75 · D84						
[hh:mm:ss]	[kg/s]	[kg/s]	[kg/s]	[kg/s]	[kg/s]	[kg/s]	[kg/s]	[m³/s]	[m³/s]
time	**Hy-no α**	**Hy-no β**	**HyMec.a_2 α**	**HyMec.a_2 β**	**Hy-no α_**	**Hy-no β_**	**HyMec α/β**	**Hy-no α__**	**Hy-no β__**
04:06:00	--	0.0005	--	--	--	0.0000	--	--	0.01255
04:07:00	--	0.0005	--	--	--	0.0000	--	--	0.01239
04:08:00	--	0.0005	--	--	--	0.0000	--	--	0.01237
04:09:00	--	0.0005	--	--	--	0.0000	--	--	0.01239
04:10:00	--	0.0005	--	--	--	0.0000	--	--	0.01245
04:11:00	--	0.0005	--	--	--	0.0000	--	--	0.01255
04:12:00	--	0.0005	--	--	--	0.0000	--	--	0.01233
04:13:00	--	0.0005	--	--	--	0.0000	--	--	0.01233
04:14:00	--	0.0005	--	--	--	0.0000	--	--	0.01256
04:15:00	--	0.0005	--	--	--	0.0000	--	--	0.01235
04:16:00	--	0.0005	--	--	--	0.0000	--	--	0.01248
04:17:00	--	0.0005	--	--	--	0.0000	--	--	0.01246
04:18:00	--	0.0005	--	--	--	0.0000	--	--	0.01236
04:19:00	--	0.0005	--	--	--	0.0000	--	--	0.01237
04:20:00	--	0.0005	--	--	--	0.0000	--	--	0.01244
04:21:00	--	0.0005	--	--	--	0.0000	--	--	0.01238
04:22:00	--	0.0005	--	--	--	0.0000	--	--	0.01237
04:23:00	--	0.0005	--	--	--	0.0000	--	--	0.01248
04:24:00	--	0.0005	--	--	--	0.0000	--	--	0.01245
04:25:00	--	0.0005	--	--	--	0.0000	--	--	0.01230
04:26:00	--	0.0005	--	--	--	0.0000	--	--	0.01238
04:27:00	--	0.0005	--	--	--	0.0000	--	--	0.01237
04:28:00	--	0.0005	--	--	--	0.0000	--	--	0.01231
04:29:00	--	0.0005	--	--	--	0.0000	--	--	0.01245
04:30:00	--	0.0005	--	--	--	0.0000	--	--	0.01251
04:31:00	--	0.0005	--	--	--	0.0000	--	--	0.01247
04:32:00	--	0.0005	--	--	--	0.0000	--	--	0.01229
04:33:00	--	0.0005	--	--	--	0.0000	--	--	0.01227
04:34:00	--	0.0005	--	--	--	0.0000	--	--	0.01253
04:35:00	--	0.0005	--	--	--	0.0000	--	--	0.01247
04:36:00	--	0.0005	--	--	--	0.0000	--	--	0.01244
04:37:00	--	0.0005	--	--	--	0.0000	--	--	0.01243
04:38:00	--	0.0005	--	--	--	0.0000	--	--	0.01242
04:39:00	--	0.0008	--	--	--	0.0000	--	--	0.01210
04:40:00	--	0.0808	--	--	--	0.0000	--	--	0.00605
04:41:00	--	0.0492	--	--	--	0.0000	--	--	0.00607
04:42:00	--	0.0475	--	--	--	0.0000	--	--	0.00619
04:43:00	--	0.0108	--	--	--	0.0000	--	--	0.00605
04:44:00	--	0.0242	--	--	--	0.0000	--	--	0.00609
04:45:00	--	0.0208	--	--	--	0.0000	--	--	0.00626
04:46:00	--	0.0208	--	--	--	0.0000	--	--	0.00604
04:47:00	--	0.0242	--	--	--	0.0000	--	--	0.00602
04:48:00	--	0.0175	--	--	--	0.0000	--	--	0.00624
04:49:00	--	0.0092	--	--	--	0.0000	--	--	0.00608
04:50:00	--	0.0005	--	--	--	0.0000	--	--	0.00617
04:51:00	--	0.0005	--	--	--	0.0000	--	--	0.00608
04:52:00	--	0.0005	--	--	--	0.0000	--	--	0.00612
04:53:00	--	0.0005	--	--	--	0.0000	--	--	0.00691
04:54:00	--	0.0005	--	--	--	0.0000	--	--	0.00750

	SEDIMENT OUTFLOW $Q_{b,o}$				SEDIMENT SUPPLY $Q_{b,i}$			DISCHARGE Q	
a [m]	0.152		0.043						
b [m]	0.076		0.150						
mec. [-]	--		1.75 · D84						
[hh:mm:ss]	[kg/s]	[kg/s]	[kg/s]	[kg/s]	[kg/s]	[kg/s]	[kg/s]	[m³/s]	[m³/s]
time	**Hy-no α**	**Hy-no β**	**HyMec.a_2 α**	**HyMec.a_2 β**	**Hy-no α_**	**Hy-no β_**	**HyMec α/β**	**Hy-no α__**	**Hy-no β__**
04:55:00	--	0.0005	--	--	--	0.0000	--	--	0.00735
04:56:00	--	0.0005	--	--	--	0.0000	--	--	0.00925
04:57:00	--	0.0005	--	--	--	0.0000	--	--	0.00995
04:58:00	--	0.0005	--	--	--	0.0000	--	--	0.01184
04:59:00	--	0.0005	--	--	--	0.0000	--	--	0.01272
05:00:00	--	0.0005	--	--	--	0.0000	--	--	0.01273
05:01:00	--	0.0005	--	--	--	0.0000	--	--	0.01269
05:02:00	--	0.0005	--	--	--	0.0000	--	--	0.01277
05:03:00	--	0.0005	--	--	--	0.0000	--	--	0.01257
05:04:00	--	0.0005	--	--	--	0.0000	--	--	0.01274
05:05:00	--	0.0005	--	--	--	0.0000	--	--	0.01265
05:06:00	--	0.0005	--	--	--	0.0000	--	--	0.01267
05:07:00	--	0.0005	--	--	--	0.0000	--	--	0.01272
05:08:00	--	0.0005	--	--	--	0.0000	--	--	0.01266
05:09:00	--	0.0005	--	--	--	0.0000	--	--	0.01287
05:10:00	--	0.0005	--	--	--	0.0000	--	--	0.01266
05:11:00	--	0.0005	--	--	--	0.0000	--	--	0.01261
05:12:00	--	0.0005	--	--	--	0.0000	--	--	0.01269
05:13:00	--	0.0005	--	--	--	0.0000	--	--	0.01279
05:14:00	--	0.0005	--	--	--	0.0000	--	--	0.01263
05:15:00	--	0.0005	--	--	--	0.0000	--	--	0.01278
05:16:00	--	0.0005	--	--	--	0.0000	--	--	0.01272
05:17:00	--	0.0005	--	--	--	0.0000	--	--	0.01258
05:18:00	--	0.0005	--	--	--	0.0000	--	--	0.01284
05:19:00	--	0.0005	--	--	--	0.0000	--	--	0.01267
05:20:00	--	0.0005	--	--	--	0.0000	--	--	0.01268
05:21:00	--	0.0005	--	--	--	0.0000	--	--	0.01277
05:22:00	--	0.0005	--	--	--	0.0000	--	--	0.01272
05:23:00	--	0.0005	--	--	--	0.0000	--	--	0.01264
05:24:00	--	0.0005	--	--	--	0.0000	--	--	0.01281
05:25:00	--	0.0005	--	--	--	0.0000	--	--	0.01259
05:26:00	--	0.0005	--	--	--	0.0000	--	--	0.01254
05:27:00	--	0.0005	--	--	--	0.0000	--	--	0.01271
05:28:00	--	0.0005	--	--	--	0.0000	--	--	0.01279
05:29:00	--	0.0005	--	--	--	0.0000	--	--	0.01278
05:30:00	--	0.0005	--	--	--	0.0000	--	--	0.01272
05:31:00	--	0.0005	--	--	--	0.0000	--	--	0.01264
05:32:00	--	0.0005	--	--	--	0.0000	--	--	0.01273
05:33:00	--	0.0005	--	--	--	0.0000	--	--	0.01248
05:34:00	--	0.0005	--	--	--	0.0000	--	--	0.01258
05:35:00	--	0.0005	--	--	--	0.0000	--	--	0.01276
05:36:00	--	0.0005	--	--	--	0.0000	--	--	0.01278
05:37:00	--	0.0005	--	--	--	0.0000	--	--	0.01265
05:38:00	--	0.0005	--	--	--	0.0000	--	--	0.01253
05:39:00	--	0.0005	--	--	--	0.0000	--	--	0.00941
05:40:00	--	0.1292	--	--	--	0.0000	--	--	0.00690
05:41:00	--	0.0775	--	--	--	0.0000	--	--	0.00675
05:42:00	--	0.0075	--	--	--	0.0000	--	--	0.00675
05:43:00	--	0.0025	--	--	--	0.0000	--	--	0.00672

	SEDIMENT OUTFLOW $Q_{b,o}$				SEDIMENT SUPPLY $Q_{b,i}$			DISCHARGE Q	
a [m]	0.152		0.043						
b [m]	0.076		0.150						
mec. [-]	--		1.75 · D84						
[hh:mm:ss]	[kg/s]	[kg/s]	[kg/s]	[kg/s]	[kg/s]	[kg/s]	[kg/s]	[m³/s]	[m³/s]
time	**Hy-no α**	**Hy-no β**	**HyMec.a_2 α**	**HyMec.a_2 β**	**Hy-no α_**	**Hy-no β_**	**HyMec α/β**	**Hy-no α__**	**Hy-no β__**
05:44:00	--	0.0005	--	--	--	0.0000	--	--	0.00592
05:45:00	--	0.0005	--	--	--	0.0000	--	--	0.00592
05:46:00	--	0.0005	--	--	--	0.0000	--	--	0.00753
05:47:00	--	0.0258	--	--	--	0.0000	--	--	0.01180
05:48:00	--	0.0008	--	--	--	0.0000	--	--	0.01236
05:49:00	--	0.0005	--	--	--	0.0000	--	--	0.01244
05:50:00	--	0.0005	--	--	--	0.0000	--	--	0.01221
05:51:00	--	0.0005	--	--	--	0.0000	--	--	0.01240
05:52:00	--	0.0005	--	--	--	0.0000	--	--	0.01245
05:53:00	--	0.0005	--	--	--	0.0000	--	--	0.01236
05:54:00	--	0.0005	--	--	--	0.0000	--	--	0.01237
05:55:00	--	0.0005	--	--	--	0.0000	--	--	0.01237
05:56:00	--	0.0005	--	--	--	0.0000	--	--	0.01235
05:57:00	--	0.0005	--	--	--	0.0000	--	--	0.01227
05:58:00	--	0.0005	--	--	--	0.0000	--	--	0.01240
05:59:00	--	0.0005	--	--	--	0.0000	--	--	0.01236
06:00:00	--	0.0005	--	--	--	0.0000	--	--	0.01229
06:01:00	--	0.0005	--	--	--	0.0000	--	--	0.01230
06:02:00	--	0.0005	--	--	--	0.0000	--	--	0.01239
06:03:00	--	0.0005	--	--	--	0.0000	--	--	0.01231
06:04:00	--	0.0005	--	--	--	0.0000	--	--	0.01226
06:05:00	--	0.0005	--	--	--	0.0000	--	--	0.01237
06:06:00	--	0.0005	--	--	--	0.0000	--	--	0.01237
06:07:00	--	0.0005	--	--	--	0.0000	--	--	0.01233
06:08:00	--	0.0005	--	--	--	0.0000	--	--	0.01700
06:09:00	--	0.0005	--	--	--	0.0000	--	--	0.01317
06:10:00	--	0.0005	--	--	--	0.0000	--	--	0.00623
06:11:00	--	0.1142	--	--	--	0.0000	--	--	0.00629
06:12:00	--	0.0125	--	--	--	0.0000	--	--	0.00636
06:13:00	--	0.0325	--	--	--	0.0000	--	--	0.00624
06:14:00	--	0.0325	--	--	--	0.0000	--	--	0.00634
06:15:00	--	0.0225	--	--	--	0.0000	--	--	0.00627
06:16:00	--	0.0058	--	--	--	0.0000	--	--	0.00620
06:17:00	--	0.0005	--	--	--	0.0000	--	--	0.00750
06:18:00	--	0.0025	--	--	--	0.0000	--	--	0.01356
06:19:00	--	0.0005	--	--	--	0.0000	--	--	0.01255
06:20:00	--	0.0005	--	--	--	0.0000	--	--	0.01252
06:21:00	--	0.0005	--	--	--	0.0000	--	--	0.01255
06:22:00	--	0.0005	--	--	--	0.0000	--	--	0.01257
06:23:00	--	0.0005	--	--	--	0.0000	--	--	0.01250
06:24:00	--	0.0005	--	--	--	0.0000	--	--	0.01244
06:25:00	--	0.0005	--	--	--	0.0000	--	--	0.01252
06:26:00	--	0.0005	--	--	--	0.0000	--	--	0.01247
06:27:00	--	0.0005	--	--	--	0.0000	--	--	0.01244
06:28:00	--	0.0000	--	--	--	0.0000	--	--	0.01249
06:29:00	--	0.0000	--	--	--	0.0000	--	--	0.01258
06:30:00	--	0.0000	--	--	--	0.0000	--	--	0.01260
06:31:00	--	0.0000	--	--	--	0.0000	--	--	0.01263
06:32:00	--	0.0000	--	--	--	0.0000	--	--	0.01258

	SEDIMENT OUTFLOW $Q_{b,o}$				SEDIMENT SUPPLY $Q_{b,i}$			DISCHARGE Q	
a [m]	0.152		0.043						
b [m]	0.076		0.150						
mec. [-]	--		1.75 · D84						
[hh:mm:ss]	[kg/s]	[kg/s]	[kg/s]	[kg/s]	[kg/s]	[kg/s]	[kg/s]	[m³/s]	[m³/s]
time	**Hy-no α**	**Hy-no β**	**HyMec.a_2 α**	**HyMec.a_2 β**	**Hy-no α_**	**Hy-no β_**	**HyMec α/β**	**Hy-no α__**	**Hy-no β__**
06:33:00	--	0.0000	--	--	--	0.0000	--	--	0.01252
06:34:00	--	0.0000	--	--	--	0.0000	--	--	0.01243
06:35:00	--	0.0000	--	--	--	0.0000	--	--	0.01258
06:36:00	--	0.0000	--	--	--	0.0000	--	--	0.01264
06:37:00	--	0.0000	--	--	--	0.0000	--	--	0.01256
06:38:00	--	0.0000	--	--	--	0.0000	--	--	0.01268
06:39:00	--	0.0000	--	--	--	0.0000	--	--	0.01246
06:40:00	--	0.0000	--	--	--	0.0000	--	--	0.01259
06:41:00	--	0.0000	--	--	--	0.0000	--	--	0.01258
06:42:00	--	0.0000	--	--	--	0.0000	--	--	0.01256
06:43:00	--	0.0000	--	--	--	0.0000	--	--	0.01265
06:44:00	--	0.0000	--	--	--	0.0000	--	--	0.01259
06:45:00	--	0.0000	--	--	--	0.0000	--	--	0.01248
06:46:00	--	0.0000	--	--	--	0.0000	--	--	0.01259
06:47:00	--	0.0000	--	--	--	0.0000	--	--	0.01253
06:48:00	--	0.0000	--	--	--	0.0000	--	--	0.01254
06:49:00	--	0.0000	--	--	--	0.0000	--	--	0.01237
06:50:00	--	0.0000	--	--	--	0.0000	--	--	0.01249
06:51:00	--	0.0000	--	--	--	0.0000	--	--	0.01246
06:52:00	--	0.0000	--	--	--	0.0000	--	--	0.01246
06:53:00	--	0.0000	--	--	--	0.0000	--	--	0.01240
06:54:00	--	0.0000	--	--	--	0.0000	--	--	0.01254
06:55:00	--	0.0000	--	--	--	0.0000	--	--	0.01257
06:56:00	--	0.0000	--	--	--	0.0000	--	--	0.01246
06:57:00	--	0.0000	--	--	--	0.0000	--	--	0.01247
06:58:00	--	0.0000	--	--	--	0.0000	--	--	0.01250
06:59:00	--	0.0000	--	--	--	0.0000	--	--	0.01237
07:00:00	--	0.0000	--	--	--	0.0000	--	--	0.01250
07:01:00	--	0.0000	--	--	--	0.0000	--	--	0.01258
07:02:00	--	0.0000	--	--	--	0.0000	--	--	0.01241
07:03:00	--	0.0000	--	--	--	0.0000	--	--	0.01255
07:04:00	--	0.0000	--	--	--	0.0000	--	--	0.01264
07:05:00	--	0.0000	--	--	--	0.0000	--	--	0.01266
07:06:00	--	0.0000	--	--	--	0.0000	--	--	0.01248
07:07:00	--	0.0000	--	--	--	0.0000	--	--	0.01253
07:08:00	--	0.0000	--	--	--	0.0000	--	--	0.01254
07:09:00	--	0.0000	--	--	--	0.0000	--	--	0.01245
07:10:00	--	0.0000	--	--	--	0.0000	--	--	0.01257
07:11:00	--	0.0000	--	--	--	0.0000	--	--	0.01251
07:12:00	--	0.0000	--	--	--	0.0000	--	--	0.01250
07:13:00	--	0.0000	--	--	--	0.0000	--	--	0.01251
07:14:00	--	0.0000	--	--	--	0.0000	--	--	0.01247
07:15:00	--	0.0000	--	--	--	0.0000	--	--	0.01239
07:16:00	--	0.0000	--	--	--	0.0000	--	--	0.01242
07:17:00	--	0.0000	--	--	--	0.0000	--	--	0.01258
07:18:00	--	0.0000	--	--	--	0.0000	--	--	0.01249
07:19:00	--	0.0000	--	--	--	0.0000	--	--	0.01242
07:20:00	--	0.0000	--	--	--	0.0000	--	--	0.01239
07:21:00	--	0.0005	--	--	--	0.0000	--	--	0.01247

	SEDIMENT OUTFLOW $Q_{b,o}$				SEDIMENT SUPPLY $Q_{b,i}$			DISCHARGE Q	
a [m]	0.152		0.043						
b [m]	0.076		0.150						
mec. [-]	--		1.75 · D84						
[hh:mm:ss]	[kg/s]	[kg/s]	[kg/s]	[kg/s]	[kg/s]	[kg/s]	[kg/s]	[m³/s]	[m³/s]
time	**Hy-no α**	**Hy-no β**	**HyMec.a_2 α**	**HyMec.a_2 β**	**Hy-no α_**	**Hy-no β_**	**HyMec α/β**	**Hy-no α__**	**Hy-no β__**
07:22:00	--	0.0005	--	--	--	0.0000	--	--	0.01241
07:23:00	--	0.0005	--	--	--	0.0000	--	--	0.01240
07:24:00	--	0.0005	--	--	--	0.0000	--	--	0.01238
07:25:00	--	0.0005	--	--	--	0.0000	--	--	0.01233
07:26:00	--	0.0005	--	--	--	0.0000	--	--	0.01223
07:27:00	--	0.0005	--	--	--	0.0000	--	--	0.01212
07:28:00	--	0.0005	--	--	--	0.0000	--	--	0.01221
07:29:00	--	0.0005	--	--	--	0.0000	--	--	0.01220
07:30:00	--	0.0005	--	--	--	0.0000	--	--	0.01231
07:31:00	--	0.0005	--	--	--	0.0000	--	--	0.01216
07:32:00	--	0.0005	--	--	--	0.0000	--	--	0.01218
07:33:00	--	0.0005	--	--	--	0.0000	--	--	0.01220
07:34:00	--	0.0005	--	--	--	0.0000	--	--	0.01153
07:35:00	--	0.0408	--	--	--	0.0000	--	--	0.00656
07:36:00	--	0.0392	--	--	--	0.0000	--	--	0.00657
07:37:00	--	0.0075	--	--	--	0.0000	--	--	0.00650
07:38:00	--	0.0125	--	--	--	0.0000	--	--	0.00658
07:39:00	--	0.0005	--	--	--	0.0000	--	--	0.00655
07:40:00	--	0.0005	--	--	--	0.0000	--	--	0.00648
07:41:00	--	0.0005	--	--	--	0.0000	--	--	0.00654
07:42:00	--	0.0005	--	--	--	0.0000	--	--	0.00659
07:43:00	--	0.0108	--	--	--	0.0000	--	--	0.00647
07:44:00	--	0.0158	--	--	--	0.0000	--	--	0.00645
07:45:00	--	0.0005	--	--	--	0.0000	--	--	0.00655
07:46:00	--	0.0005	--	--	--	0.0000	--	--	0.00648
07:47:00	--	0.0005	--	--	--	0.0000	--	--	0.00650
07:48:00	--	0.0625	--	--	--	0.0000	--	--	0.00648
07:49:00	--	0.1008	--	--	--	0.0000	--	--	0.00650
07:50:00	--	0.1225	--	--	--	0.0000	--	--	0.00645
07:51:00	--	0.0775	--	--	--	0.0000	--	--	0.00657
07:52:00	--	0.0975	--	--	--	0.0000	--	--	0.00655
07:53:00	--	0.0742	--	--	--	0.0000	--	--	0.00648
07:54:00	--	0.0925	--	--	--	0.0000	--	--	0.00666
07:55:00	--	0.0592	--	--	--	0.0000	--	--	0.00659
07:56:00	--	0.0442	--	--	--	0.0000	--	--	0.00657
07:57:00	--	0.0425	--	--	--	0.0000	--	--	0.00658
07:58:00	--	0.0308	--	--	--	0.0000	--	--	0.00658
07:59:00	--	0.0658	--	--	--	0.0000	--	--	0.00657
08:00:00	--	0.0442	--	--	--	0.0000	--	--	0.00648
08:01:00	--	0.0425	--	--	--	0.0000	--	--	0.00642
08:02:00	--	0.0492	--	--	--	0.0000	--	--	0.00662
08:03:00	--	0.0125	--	--	--	0.0000	--	--	0.00653
08:04:00	--	0.0025	--	--	--	0.0000	--	--	0.00649
08:05:00	--	0.0005	--	--	--	0.0000	--	--	0.00661
08:06:00	--	0.0005	--	--	--	0.0000	--	--	0.00654
08:07:00	--	0.0000	--	--	--	0.0000	--	--	0.00655
08:08:00	--	0.0000	--	--	--	0.0000	--	--	0.00656
08:09:00	--	0.0000	--	--	--	0.0000	--	--	0.00083

Typeset July 18, 2017

Communications du Laboratoire de Constructions Hydrauliques ISSN 1661-1179
Ecole Polytechnique Fédérale de Lausanne
Editeur: Prof. Dr A. Schleiss

N°	58	2014	T. Ghilardi Sediment transport and flow conditions in steep rivers with large immobile boulders
N°	59	2014	R. Duarte Influence of air entrainment on rock scour development and block stability in plunge pools
N°	60	2014	J. P. Matos Hydraulic-hydrologic model for the Zambezi River using satellite data and artificial intelligence techniques
N°	61	2015	S. Guillén Ludeña Hydro-morphodynamics of open-channel confluences with low discharge ratio and dominant tributary sediment supply
N°	62	2016	M. Jafarnejad Chaghooshi Time-dependent failure analysis of large block size riprap as bank protection in mountain rivers
N°	63	2016	S. Terrier Hydraulic performance of stepped spillway aerators and related downstream flow features
N°	64	2016	M. Ostad Mirza Experimental study on the influence of abrupt slope changes on flow characteristics over stepped spillways
N°	65	2016	I. Almeida Samora Optimization of low-head hydropower recovery in water supply networks
N°	66	2016	D. Ferràs Segura Fluid-structure interaction during hydraulic transients in pressurized pipes: experimental and numerical analyses
N°	67	2016	E. Battisacco Replenishment of sediment downstream of dams: Erosion and transport processes
N°	68	2017	F. Zeimetz Development of a methodology for extreme flood estimations in alpine catchments for the verification of dam safety
N°	69	2017	A. J. Pachoud Influence of geometrical imperfections and flaws at welds of steel liners on fatigue behavior of pressure tunnels and shafts in anisotropic rock
N°	70	2017	F. Oberrauch Hydropower design under uncertainties
N°	71	2017	S. Schwindt Hydro-morphological processes through permeable sediment traps at mountain rivers

ISSN 1661-1179

DOI: 10.5075/epfl-lchcomm-71

Prof. Dr A. Schleiss
Laboratoire de constructions hydrauliques - LCH
EPFL, Bât. GC, Station 18, CH-1015 Lausanne
http://lch.epfl.ch
e-mail: secretariat.lch@epfl.ch